AQUEOUS PHASE CATALYTIC HYDROGENATION AND DEUTERIUM EXCHANGE OF α-SUBSTITUTED ORGANIC ACIDS USING Ru/C

By

Jennifer Elizabeth Jacobs

A DISSERTATION

Submitted to
Michigan State University
in partial fulfillment of the requirements
for the degree of

DOCTOR OF PHILOSOPHY

Chemistry

2009

ABSTRACT

AQUEOUS PHASE CATALYTIC HYDROGENATION AND DEUTERIUM EXCHANGE OF α-SUBSTITUTED ORGANIC ACIDS USING Ru/C

By

Jennifer Elizabeth Jacobs

The biomass refinery of the future will require a wide range of catalytic conversions, largely aqueous phase reductions. This dissertation explores the use of a 5% ruthenium on carbon catalyst in hydrogenation and C-H activation studies of carboxylic acids, a significant class of biogenic feedstocks. Several two- and three-carbon organic acid substrates were studied to probe (a) the effects of α- substituents on hydrogenation and H/D exchange reactions and (b) the relationship between these two processes. Substrates included the following groups: -H, $-CH_3$, -OH, $-N^+H_3$, $-OCH_3$, $-N^+H_2CH_3$, $-N^+H(CH_3)_2$, and $-N^+(CH_3)_3$. Most reactions were performed at 100 °C or 130 °C in D_2O solution but ranged from 50 °C to 150 °C and 1000 psi H_2 or D_2. As expected, both catalyst and H_2 gas are required to convert organic acids to the corresponding alcohols. Simple alkanoic acids (acetic, propanoic, and isobutyric) and betaine, $((CH_3)_3N^+CH_2COOH{\bullet}Cl^-)$, a quaternized glycine, are very unreactive. For the other methylated glycines, the rate of hydrogenation falls off by a factor of three with each additional methyl, and reduction requires acid, as found earlier by Jere. Use of water as reaction medium appears optimal; addition of organic co-solvents such as ethanol, ethylene glycol, THF, or ethyl lactate led to reduced hydrogenation rates. This apparent inhibition by organic additives may reflect their tendency to tie up catalytic sites via metal insertion into C-H bonds, especially those neighboring heteroatoms. Another feature of both the solvents and the substituents is their capacity for hydrogen bonding, which may play a role in modulating hydrogenation

rates. Similarly, steric crowding may also affect the substrates' ability to access the surface in productive orientations. To explore this issue, activation of C-H bonds next door to amine N sites was probed via H/D exchange studies performed on the N-methylated glycine series.

Reactions run in D_2O with either H_2 or D_2 and catalyst were effective at exchanging deuterium into the CH_2 and CH_3 sites of the amino acids. The Ru catalyst also exchanges H (from H_2) for D (from D_2O) to form HOD and HD, independent of substrate. Analysis by internal standard-calibrated ^1H NMR allowed complete isotopomer-specific inventory of H concentration in substrates and water. Simple sequential replacements of H by D were observed in the amino acids. Two kinetic models were developed to determine the rate constants for H/D exchange at both the methylene and methyl positions. Both included possible time delays due gas/liquid isotopic equilibration (k_H) and/or a catalyst induction (k_{turn_on}) period; ultimately the latter was discarded as redundant. The first model treated each isotope replacement step as a process unrelated to the others. Thus, between forward and reverse replacements in CH_2 and CH_3 sites and k_H, eleven rate constants were freely varied in the fitting. The second model used a single rate constant for each site, further modified by primary and secondary isotope effect values, resulting in six values + k_H for this fitting. The latter, more economical and interpretive model gave fits nearly as good as those from the eleven-variable one. Somewhat surprisingly, these analyses found H/D exchange rates to decrease in the following order: D_2O > sarcosine ($CH_3NH_2^+CH_2CO_2^-$) > glycine (CH_2 site) > N,N-dimethylglycine.

TABLE OF CONTENTS

LIST OF TABLES

LIST OF FIGURES

LIST OF SCHEMES

LIST OF EQUATIONS

Chapter 1. INTRODUCTION

1.1 Background

The Jackson/Miller group at Michigan State University is focused on emerging plant/crop-based renewables technology, where these renewables can serve to replace or complement conventional feedstocks to meet the ever-growing need for chemicals and other materials. The group is working in an interdisciplinary and collaborative effort using mechanistic organic chemistry and chemical reaction engineering. The studies described in this dissertation explore the aqueous phase catalytic hydrogenation reaction of organic acids and their derivatives to alcohols. In addition a detailed H/D exchange study was conducted on glycine and its N-methylated derivatives. Though several effective procedures have been developed, the mechanistic details of such reactions are far from understood. By examining the effects of structure and medium on organic acid reductions and H/D exchange, an improved understanding of some of the mechanisms involved in heterogeneous catalysis can be obtained. This knowledge will prove to be far reaching in that it helps map out the chemical transformations that will be needed for the renewables-based "refinery of the future".

1.2 Significance

Green chemistry, also known as sustainable chemistry, is an umbrella concept that has grown substantially since it fully emerged in 1990. By definition, green chemistry is the design, development, and implementation of chemical products and processes to reduce or eliminate the use and generation of substances hazardous to human health and the environment. Many of the concerns green chemistry is trying to address are not

laboratory curiosities or individual research projects,[1] but global issues such as climate change, energy consumption, pollution, and management of water resources. Green chemistries can be used to help reduce our dependence on petroleum and natural gas.

The supply of petroleum is limited and finding an alternative to crude oil is increasingly important.[2] Petroleum has been the most used energy source due to automobiles since the 1950's due to its energy content, ease of transport, and abundance (albeit finite). It is used as a raw material for nearly all organic chemical products, including pharmaceuticals, solvents, fertilizers, etc. Identifying renewable feedstocks and green pathways to producing the same high-valued chemicals is required to ensure a sustainable future. Use of renewable feedstocks also has the potential to dramatically reduce U.S. dependence on foreign oil and allow for domestic growth of a bio-based chemical industry.

Research at Michigan State University seeks non-fossil based alternative pathways for the production of a variety of commodity and specialty chemicals. The research presented in this dissertation is aimed at the development and characterization of novel pathways to produce high-valued chemicals using a "green chemistry" approach. Central to this objective is the need for insight into the reactions' mechanisms as well as a broad descriptive knowledge of their variability as a function of input variables such as substituents, solvent, pH, temperature and reaction pressure. In this work, the main tools employed to probe the hydrogenation pathways of organic acids have been isotopic deuterium exchange and kinetic modeling. The ability to successfully and selectively

hydrogenate biomass derived organic acids will open pathways to the use of renewable starting materials in polymers, foods, and pharmaceutical applications, all at costs competitive with existing petroleum based routes.

In evaluating the possible renewable "green" feedstocks, it is evident that carbohydrate polymers (starch, cellulose) and monomers (glucose, fructose, mannose, etc.) and sugar alcohols will be major contributors. Currently, bioconversion (fermentation) of carbohydrates can selectively produce a large variety of products. The direct chemical conversion of these downstream fermentation products can in turn result in a plethora of high-valued products. The combination of chemical- and bio-processing, to date, offers the most promising and flexible strategy for the development of renewable resource refining. Such a partnership is illustrated in Scheme 1 for the net transformation of glucose to propylene glycol, a commodity chemical with US production of ca. 5 x 10^8 kg/yr.

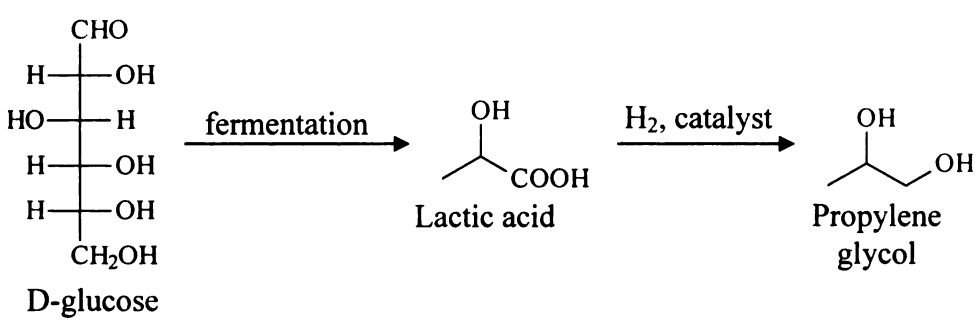

Scheme 1. Biomass based organic acids in the production of commodity chemicals

An additional advantage of this "environmentally friendly" approach is the domestically centered economic potential of converting simple sugars to high-valued and large volume commodities. In the US in 2006, 9178 thousand tonnes of oil equivalent ethanol were

produced, up 24% from 2005 (7389).[2] A tonne of oil equivalent is equivalent to the amount of energy given off by burning one tonne of crude oil (~ 42GJ). The U.S. Departments of Energy and Agriculture determined that 1.3 billion tons of U.S. biomass feedstocks are potentially available for the production of biofuels. Thus, there is no shortage of bio-based raw materials for chemicals production. The development of low-cost, high efficiency hydrogenation routes to exploit this opportunity is a major goal of the work described herein. In addition, a series of methylated amino acids was evaluated in terms of H/D exchange to better understand the mechanism of hydrogenation and possibly build on the opportunity for stereoretentive reduction to high-valued amino-substituted alcohols.

1.3 Literature Review

1.3.1 Hydrogenation/Dehydrogenation

Hydrogenation refers to a general chemical reaction that results in the addition of H_2 to either double or triple bonds. Hydrogenolysis (to be discussed later, section 1.3.7) refers to a general chemical reaction that involves breaking bonds and the addition of hydrogen. In the work described here, the hydrogenation reactions that are being considered are mostly the reduction of X=Y double bonds. The exact ways in which the hydrogen atoms are delivered are varied depending on how polar the substrate is, etc. The largest and best studied class of hydrogenation includes hydrogenation of hydrocarbons. The first paper described below discusses the effect of hydrogen pressure in a reaction with 1-methylcyclohexene and following this is a brief discussion of the effect of hydrogen pressure on the hydrogenation rate of organic acids (our research).

Hydrogen pressure is a critical parameter in catalytic hydrocarbon-refining processes, controlling reaction rates and selectivity. Traditionally the rate of dehydrogenation and fragmentation of hydrocarbons is slowed by the presence of hydrogen adsorbed on a catalyst surface. Surprisingly, Yang et al. found that in the presence of excess hydrogen at 0.3-0.7 psi (reported as 15-40 Torr) and at temperatures between 290-480 K, dehydrogenation of 1-methylcyclohexene on Pt(111) to form toluene dominates over hydrogenation to form methylcyclohexane (Scheme 2).

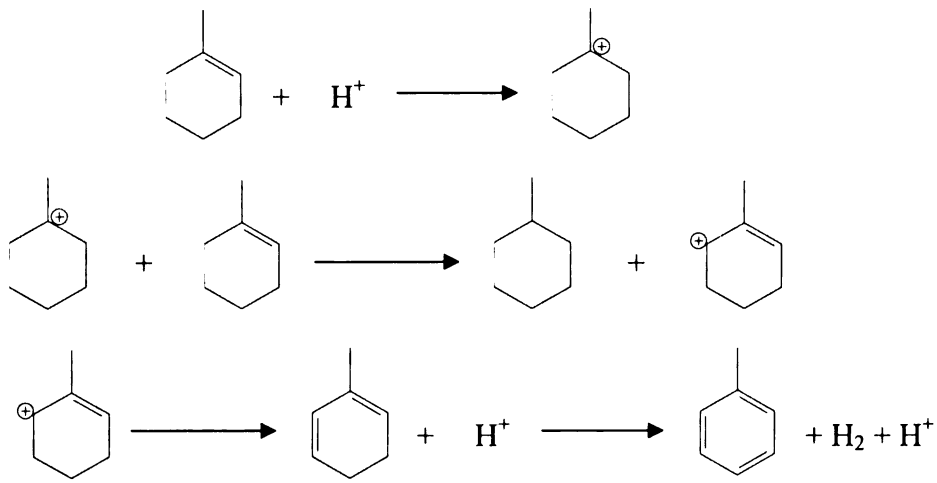

Scheme 2. Dehydrogenation of 1-methylcyclohexene onto Pt(111) surface

The authors acknowledge that this dehydrogenation is somewhat counterintuitive and suggest that perhaps the excess hydrogen might assist in displacing adsorbed hydrocarbon fragments, which inhibit the chemisorption of the reactant. Hydrogenation to 1-methylcyclohexane is temperature dependent reaching a maximum at 370 K, whereas dehydrogenation to form toluene increases, starting around 350 K. In general, as temperature increases, π-bonded alkenes, which are weakly bonded to the surface, easily desorb, or they are converted into strongly di-σ-bonded species.

Taking a SFG (sum frequency generation) spectrum of 1-methylcyclohexene at 403 K in 0.03 psi (reported as 1.5 Torr) of substrate and 0.3 psi (reported as 15 Torr) of hydrogen pressure and again at 300 K and below 9.7×10^{-11} psi (reported as 5×10^{-9} Torr), Yang et al. found no change in the SFG spectrum (two bands at 2845 and 2925 cm^{-1}). SFG spectroscopy is a second-order nonlinear optical process for analyzing surfaces and from the output, structural information regarding the molecules on the surface can be determined. The process involves an infrared laser beam combined with a visible laser beam to generate a sum frequency output. Other surface analytical techniques exist, such as thermal desorption spectroscopy (TDS), high-resolution electron energy loss spectroscopy (HREELS), and reflection absorption infrared spectroscopy (RAIRS).

The results from Yang indicated that the species responsible for the spectrum was σ-bonded to the surface (Scheme 3).

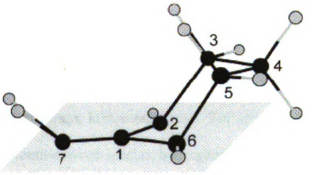

Scheme 3. Suggested molecular structure of methylcyclohexenyl species (C_7H_{10})

They suggest that excess strongly chemisorbed hydrogen molecules react with weakly π-bonded 1-methylcyclohexene to form the hydrogenated methylcyclohexyl, C_7H_{13} which is σ-bonded to the surface. The methylcyclohexyl intermediate can undergo a

disproportionation reaction with a weakly π-bonded 1-methylcyclohexene to form methylcyclohexane, and a dehydrogenated species C_7H_{11}, which can continue losing hydrogen to form toluene, C_7H_8.[3]

The effect of pressure has been studied in our research group on the hydrogenation of organic acids (X=Y). Jere et al. the Jackson/Miller group determined the kinetics of aqueous-phase hydrogenation of L-alanine to L-alaninol over 5 wt% Ru/C. Reaction temperatures were between 353-398 K with 0.22-0.46 M feed concentration, 0-1.2 M phosphoric acid concentrations and hydrogen pressure between 1.7-13.8 MPa (6.9 MPa = 1000 psi). Results indicated only a mild pressure dependence of the hydrogenation rate above 1000 psi H_2 partial pressure. Jere et al. found that at pressures above 1000 psi H_2, the rate was independent of the hydrogen concentration concluding that the surface was saturated with hydrogen.[4]

Literature describing hydrogenation of organic acids to high-valued chemicals exists; however, the fundamental chemistry involved at the catalyst surface has been little discussed, especially for processes in aqueous phase. For producing chemicals that replace traditional petroleum-derived species, hydrogenation or other reductions must play a key role to reduce the overall oxidation state of the oxygenated feed material. The ability to successfully and selectively hydrogenate organic acids will open pathways to the use of biomass-derived materials in polymers, foods, and pharmaceuticals applications. The development of low-cost, high-efficiency hydrogenation routes is the goal of our research group.

Research conducted on hydrogenation of organic acids to alcohols will be discussed first, followed by a discussion on the research conducted on hydrogenation of esters and aldehydes.

Somewhat recently (1998), Antons et al. described the preparation of optically active alcohols from optically active carboxylic acids using a ruthenium catalyst. For the hydrogenation of lactic acid the enantiomeric excess of propylene glycol dropped with increasing temperatures (from 383 K to 413 K).[5,6] Recent patents describing heterogeneous catalysis for the hydrogenation of carboxylic acids to alcohols provide yields and selectivities, but do not go into the mechanistic aspects of the chemistry involved.

Carnahan and co-workers examined hydrogenation of carboxylic acids using a ruthenium catalyst. They used both ruthenium dioxide and ruthenium-on-carbon at temperatures of about 423 K (reported as 150 °C); platinum and palladium under similar conditions were not successful. They obtained an 80% yield of ethylene glycol from 20 wt% glycolic acid (hydroxyacetic acid) after a reaction time of 1 hour using 10 g of 10% Ru on carbon and extremely high pressures. The hydrogenation was performed at a temperature of 418-423 K (reported as 145-150 °C) and 9,500-10,400 psi (reported as 650-710 atm) in water (Scheme 4).

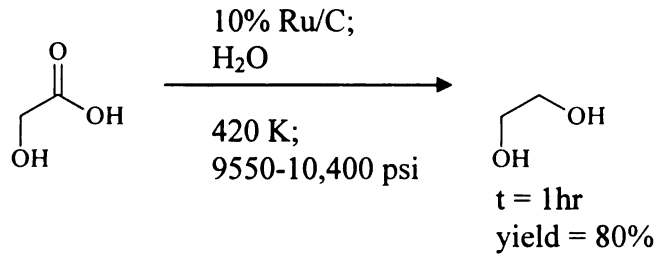

Scheme 4. Hydrogenation of glycolic acid

The yield was reduced to 68% ethylene glycol when using 3 g of 10% Ru on carbon at the same reaction conditions. In an experiment with glycolic acid and 10% Ru on carbon at 523-528 K (reported as 250-255 °C) and 7,900-10,300 psi (reported as 540-700 atm), Carnahan et al. analyzed the gas in the head space using mass spectrometry and reported the following distribution: 78.3 mole % hydrogen; 1.8 mole % methane; 0.8 mole % ethane; 0.04 mole % carbon dioxide; 0.8 mole % oxygen; 0.09 mole % argon; 18.2 mole % nitrogen (they mention that the last three constituents may have resulted from contamination of the sample with air and with nitrogen used to purge the sample lines). The yield of ethylene glycol from this reaction was 32% with side products methane and ethane, lower than the 80% obtained at the conditions in scheme 4. The lower yield was a result of reducing the catalyst amount from 10 to 3 g and increasing the reaction temperature from 420 K to 523 K. The yield of 32% was obtained after 15 minutes compared to the yield of 80% after a reaction time of 1 hour.[7]

Behr et al. reported homogenous bi-metallic catalyzed reduction of carboxylic acids to alcohols with hydrogen. One drawback of traditional heterogeneous hydrogenations using metal catalysts is the use of high pressure, namely ~2900-4300 psi and expensive high pressure reactors. Thus, homogeneous catalysis can often be advantageous in that it

can be performed at more moderate reaction temperatures and hydrogen pressures. Both homogeneous and heterogeneous catalysis were investigated in the reduction of 2-ethylheptanoic acid to 2-ethylheptanol. Catalysts included $[Mo(CO)_6]$, $[Rh(acac)(CO)_2]$, $[Ru(acac)_3]$, Rh/C, Rh/Al_2O_3, and Ru/C (Scheme 5).

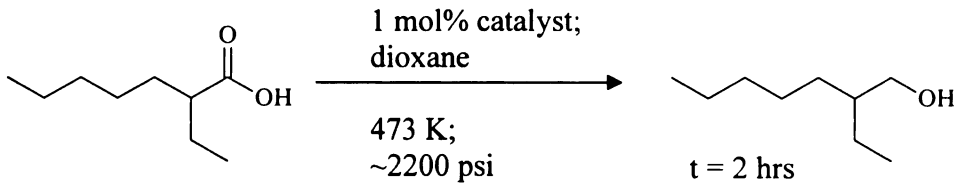

Scheme 5. Hydrogenation of 2-ethylheptanoic acid

Yields of 10% (for the heterogeneous case of 1 mol% Ru/C) or less were obtained for all catalysts, however, nearly quantitative yields were possible with homogeneous bimetallic catalysts. An alcohol yield of 99% was found with $Mo(CO)_6$, a group 6 early transition-metal carbonyl, and $Rh(acac)(CO)_2$, a group 8 late transition-metal complex, at 473 K (reported as 200 °C), 2200 psi (reported as 150 bar) H_2 pressure in dioxane for 4 hours. They suggest that the acetylacetate anion, $C_5H_7O^-$ (acac) oxygen-donor ligands in general show the highest activity for the reduction of carboxylic acids.

Behr and co-workers also looked at the reduction of 2-ethylheptanoic acid with homogeneous/heterogeneous bimetallic catalysts. A yield of 69% alcohol was achieved using the homogeneously dissolved $Mo(CO)_6$ and heterogeneous Ru/C at 473 K (reported as 200 °C), 2200 psi (reported as 150 bar) H_2 pressure in dioxane for 2 hours.

Although the yields are not as high as in the case of the homogeneous bi-metallic catalysis, there seems to be a collaborative effect. In the case of $Mo(CO)_6$ or Ru/C alone

yields of only 2 and 10%, respectively were reported after 2 hours. It may be that the main catalytic reaction is occurring on the Ru surface because in the case of reduction of 2-ethylheptan-5-olide to 2-ethyl-1,5-heptanediol (Scheme 6) with $Mo(CO)_6$ and $[Rh(acac)(CO)_2]$ reducing the amount of rhodium (reduction of ~66%) leads to a greater loss of activity (from 92% to 19% yield), however, less molybdenum (reduction of ~66%) has less of an effect on the reaction (from 92% to 53% yield) (Scheme 6).

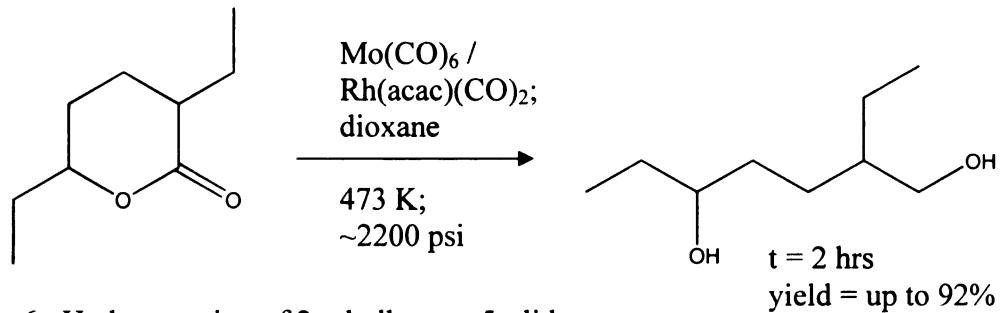

Scheme 6. Hydrogenation of 2-ethylheptan-5-olide

Behr also expanded the work to evaluate reduction of commercially available lactones with the rhodium/molybdenum catalyst. They found that the reduction of lactones was more difficult if the compound was branched in the α-position to the carboxylic acid and suggested perhaps it is because the compound is more sterically hindered.[8] A disadvantage of this chemistry is that homogeneous bimetallic catalysts can be difficult to prepare and often cannot be reused because they are not separated from the substrate, etc.

Mao and co-workers found that a magnesia-supported poly-γ-aminopropylsiloxane-Ru complex ($MgO\text{-}NH_2\text{-}Ru$) was extremely effective in the aqueous catalytic hydrogenation of several carboxylic acids (acetic, propanoic, lactic, and isobutyric acid). Optimal reaction conditions included 513 K (reported as 240 °C), 725 psi (reported as 5.0 MPa)

H_2 in 5 mL of water for 18 h. Upon examination of the hydrogenation of 0.1 mL (1.35 mmol) propanoic acid, results revealed that the amount of Ru in the MgO-NH_2-Ru complex, reaction temperature, and the amount of water significantly affected the yield of desired alcohol. An increasing Ru content up to 0.12 mmol/g (from 0.048 mmol/g) increased the yield of propanol formed. As the temperature increased from 433 K to 523 K (reported as 160 °C to 250 °C), the yield of propanol went from 0% to 95%. Increasing the water amount from 1 to 5 mL increased the yield of propanol to 100% (from 5%), however, more than 5 mL (up to 8 mL) reduced the yield of propanol (to 28%). In summary, the optimal conditions for 0.1 mL of propanoic acid in water is 513 K, 725 psi H_2 pressure, 5 mL of water, and a Ru content of 0.12 mmol/g in the MgO-NH_2-Ru complex.[9]

Fuchikami and co-workers discussed transition-metal catalyzed hydrogenation of pentadecanoic acid using 1.0 mL of dimethoxyethane as a solvent. Optimum reaction conditions included 1.0 mmol substrate and 0.01 eq. 5% [Rh/Al_2O_3] and [$Mo(CO)_6$] at 423 K (reported as 150 °C), 1470 psi (reported as 100 atm) H_2 pressure for 16 h. The reaction in the presence of only $Mo(CO)_6$ resulted in no conversion to the desired alcohol indicating that bimetallic catalysts consisting of Group 8 to 10 late transition-metal compounds and Group 6 or 7 early transition-metal carbonyls were extremely effective in the hydrogenation of organic acids.[10]

Summarizing the hydrogenation of organic acid reactions, Antons et al. found that with a ruthenium catalyst the enantiomeric excess of propylene glycol from hydrogenation of

optically active lactic dropped with increasing temperature (similar to results observed by our research group, to be discussed later). Carnahan obtained yields of 80% ethylene glycol from glycolic acid after 1 hour using Ru/C but at high H_2 pressures (~10000 psi). Research in this paper presents yields up to 50% for ethylene glycol from glycolic acid using Ru/C at similar conditions except for lower H_2 pressures (1000 psi) and 1/3 the catalyst : substrate amount. Behr reported low yields (less than 10%) for hydrogenation of 2-ethylheptanoic acid to the desired alcohol using 1 mol% Ru/C at conditions similar to what our research used, but again Behr used higher pressures (~3000-4300 psi) compared with our research at 1000 psi H_2.

Behr expanded his work to lactones and found they were more difficult to hydrogenate than organic acids. Expanding the use of ruthenium to a magnesia-supported poly-γ-aminopropylsiloxane-Ru complex (MgO-NH_2-Ru), Mao et al. found this catalyst very effective in hydrogenating several carboxylic acids in water. Reaction temperatures were about 100 °C higher than what we used in our research (to be discussed later). Fuchikami et al. found that bimetallic catalysts (similar to the results from Behr) exhibited extremely powerful reducing ability for the hydrogenation of organic acids focusing mostly on [Rh/Al_2O_3] and [$Mo(CO)_6$]. It may be suggested to expand the use of heterogeneous Ru/C hydrogenations to include bimetallic catalysts.

Hydrogenation of esters and aldehydes has also been studied. Adkins et al. looked at optically active esters, the effect of free acids on the hydrogenation of esters, and also α- and β-oxygen substituted esters. Vaidya et al. looked at hydrogenation of n-

valeraldehyde and fit a power law model to the experimental data in order to generate a rate expression for the reaction. We will first consider the hydrogenation of esters then follow this discussion with Vaidya's work with aldehydes.

Adkins and Bowden described the hydrogenation of optically active esters to alcohols using copper-chromium oxide at a temperature of 523 K (reported as 250 °C) and pressures of 2200-2900 psi (reported as 150-200 atm). A yield of 81% 1,2-propanediol from butyl lactate (91% conversion) was obtained after 2 hours at these conditions.[11]

Earlier (1932) studies by Adkins and coworkers also showed that hydrogenation of esters over copper-chromium oxide at 523 K (reported as 250 °C), 2900-4400 psi (reported as 200-300 atm) H_2 in ethanol is inhibited in the presence of free acids, presumably due to competitive adsorption resulting in less desired product formation.[12,13]

In 1947, Adkins and Pavlic studied alpha amino ester hydrogenation over Raney nickel in a non-aqueous solvent, namely dry ethanol, using lower temperatures (25-75 °C) and high pressures (150-200 atm or 2200-2900 psi). The reaction was carried out in a 96 5 M stainless steel reactor with about 20 to 35 mL of solution. The hydrogenated products were isolated by fractional distillation. Yields of desired alcohol were as high as 98% for hydrogenation of α-ethylpiperdinoacetate.[14]

Adkins and Billica reported effective hydrogenations of esters to alcohols at modest temperatures (298-423 K reported as 25-150 °C), yet with the requirement of higher

catalyst loadings. They suggest using similar mass amounts or greater of catalyst compared with the mass used of ester. In most cases, they used 10 g of the ester substrate (roughly 0.085 moles for the case of ethyl lactate) and 15 g of catalyst. When using an excess of Raney nickel the hydrogenation at 373 K (reported as 100 °C) and 5000 psi of α-amino esters was quantitative and reasonably rapid (e.g. ethyl piperidinoacetate was complete in 1.7 hrs). One limitation with Raney nickel is that hydrogenation of phenyl substituted esters unavoidably results in benzene ring reduction to form the cyclohexyl substituted amino alcohol.

Raney nickel was also used for the hydrogenation of α and β-oxygen substituted esters. A quantitative yield of 1,2-propanediol from ethyl lactate in dry ethanol at 423 K (150 °C) and 5000 psi was obtained after 1.5 hrs. The research presented in this thesis includes α-oxygen substituted organic acids and found an enhanced hydrogenation rate with these substrates compared with the unsubstituted substrates (to be discussed later).

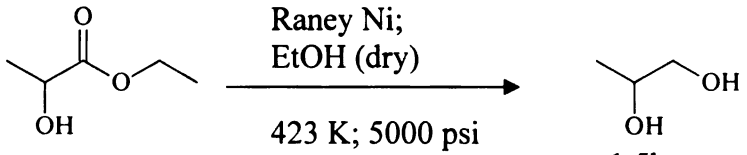

Scheme 7. Hydrogenation of ethyl lactate

Adkins et al. report that for most of the substrates examined as good or better yields can be obtained from the esters using copper chromium oxide as opposed to Raney nickel. They suggest using copper chromium oxide unless hydrogenation is being performed at temperatures below 100 °C, in which case Raney nickel is preferred. An added benefit of

running reactions at increased catalyst loadings and lower temperatures, is that undesired hydrogenolysis of 1,3-glycols is avoided.[15]

Vaidya et al. report kinetic data from liquid phase hydrogenation of *n*-valeraldehyde to *n*-amyl alcohol over a 5% Ru/Al_2O_3 catalyst. Reaction conditions included temperatures and pressures between 323-348 K (50-75 °C), 0.69-2.76 MPa (100-400 psi), and 2-propanol as the solvent (Scheme 8). The Ru/Al_2O_3 catalyst (size 25-60 μm; diameter 46.6 μm; BET surface area 598 m^2g^{-1}; pore volume 0.17 cm^3g^{-1}; pore diameter 10.1 nm) could be used three times before any loss in activity.

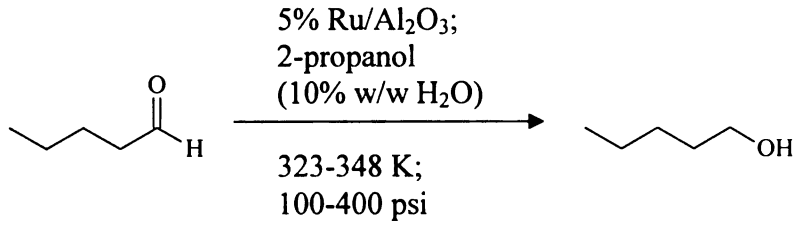

Scheme 8. Hydrogenation of *n*-valeraldehyde

Reduction of the catalyst was carried out at 648 K (375 °C) under pure hydrogen. They comment that, "our experience is that heterogeneous Ru catalyst works better in the presence of water." To support this claim they present a finding in which hydrogenation of 0.3 $kmol/m^3$ *n*-valeraldehyde was carried out in 2-propanol containing water (10% w/w) at 323 K, and a hydrogen pressure of 400 psi (1.29 kg/m^3 catalyst loading). At 10, 20, and 30 minute intervals samples were collected and analyzed. Results indicate the conversion rate is nearly doubled in the presence of water at 10 minutes, but the enhancement drops off over time with only about a 5% increase in conversion at 30

minutes (for the case with water added). Examining the mass transfer limitations, the gas phase mass transfer resistance is neglected due to the gas phase being almost all pure hydrogen (attributed to the low vapor pressure of the solvent under these conditions). The speed of agitation controls the liquid phase mass transfer resistance and transfer of dissolved hydrogen and valeraldehyde to the external surface of the catalyst particle. They found an impeller speed of 20 rps was enough to overcome all mass transfer resistances (gas-liquid, liquid-solid, and intraparticle diffusion).

There results also indicated that initial rates increased linearly with catalyst loading (between 0.26 – 1.29 kg/m^3). The initial rate of hydrogenation was also increased with both an increased hydrogen pressure (between 100 - 400 psi reported as 0.69 – 2.76 MPa) and increased initial valeraldehyde concentration (between 0.075 – 0.3 $kmol/m^3$).

They fit a power law model to the experimental data and the resulting rate expression was: $r = 69.9 \exp(-2587/T)[A]^{0.44}[B]^{0.46}$ ([A] = conc. of hydrogen in bulk liquid phase, M; [B] = conc. of *n*-valeraldehyde in liquid phase, M). Thus the order of the reaction with respect to *n*-valeraldehyde and hydrogen is 0.46 and 0.44, respectively. They also examined using Langmuir-Hinshelwood type models for both single and dual site mechanisms as well as dissociative and non-dissociative adsorption of hydrogen. There results supported a single site mechanism and dissociative adsorption of hydrogen.

The final model derived was represented as: $r = \{k_3 K_A K_B [A][B]\} / \{1 + (K_A[A])^{1/2} + (K_B[B])\}^3$ (k_3 = surface reaction rate constant, kmol/kg cat/min; K_A and K_B = adsorption

equilibrium constant for A and B, m^3/kmol). The product term, [P], in the denominator was omitted based on an experiment at 348 K in which the addition of *n*-amyl alcohol (10% w/w of *n*-valeraldehyde) to the beginning reaction mixture had no effect on the rate of reaction. The surface reaction step activation energy, 38.5 kJ/mol was calculated from the temperature dependence of k_3. Using the van't Hoff equation and from the temperature dependence of K_A and K_B, the heats of adsorption of hydrogen and valeraldehyde were found to be 48.6 and 29.1 kJ/mol, respectively (no measure of the uncertainties was provided).[16]

1.3.2 H/D Exchange

Deuterium-labeled compounds are used in many different facets of research, from biological to environmental, and organic synthesis. In the catalytic hydrogenation of double and triple bonds, ring-opening of epoxides, etc., the use of H/D exchange using either D_2O and/or D_2 gas offers an efficient route to deuterium-labeled compounds.

Deuterium gas is quite expensive, so the development of a method for preparing D_2 gas in-situ could be valuable. Sajiki et al. used 1.0 mL (55 mmol) of D_2O and 10 mg of 10% Pd/C (0.0094 mmol of Pd metal) in the presence of ~2.0 L (~83 mmol) H_2 gas at room temperature to study the amount of D_2 produced. Using ^1H NMR, the signal intensity of HOD was monitored and continued to increase over time. The reaction they monitored is presented in Scheme 9.

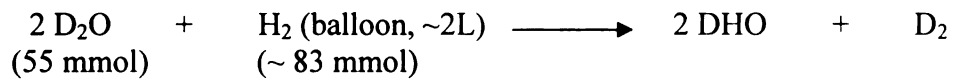

Scheme 9. Reaction scheme for generation of D_2 gas

After 48 hours, 87 mL of D_2 gas was generated from 1.0 mL of D_2O (TON = 829). In the absence of 10% Pd/C or H_2 gas (under Ar) results indicated a negligible increase in the HOD signal over time.

Sajiki et al. expanded this work and examined the amount of deuterium exchange into organic substrates in a closed system, in the presence of a limited amount of H_2 gas. After 24 h of stirring, deuterium was incorporated via reduction of 0.5 mmol cinnamic acid ($C_6H_5CHCHCOOH$) into both methylene positions of dihydrocinnamic (3-phenylpropanoic) acid. The reaction consisted of 7.4 mg of 10% Pd/C in 5.0 mL or 3.0 mL (277 mmol or 166 mmol) of D_2O in a 100 mL hydrogen-charged sealed flask at room temperature. The actual internal volume of the hydrogen-charged sealed flask (100 mL) was 160 mL. They also found that the efficiency of incorporation was greatly reduced in reactions which used a larger flask. The mechanism of D_2 gas generation is unclear. However, Sajiki et al. propose oxidative insertion of Pd(0) activated by H_2 or HD as a ligand into D_2O to give Pd(II) species followed by the key step, a ligand exchange between H_2-D_2O, in the catalytic isotope exchange reaction. Subsequent reductive elimination gives the corresponding Pd(0)-HD or D_2 complex. At the end of the reaction D_2 gas is liberated.[17]

Performing the reaction under an atmosphere of D_2 and in dry EtOAc as an inert solvent as opposed to H_2 and D_2O, resulted in significantly less deuterium exchange, even at a temperature of 180 °C. Thus, Sajiki, et al. concluded that D_2O is required for efficient isotopic exchange.

Deuterium-labeled organic compounds can be prepared using two main strategies: (a) a multistep synthetic method starting from deuterium-labeled synthons and (b) selective catalytic replacement of carbon-bound hydrogen with deuterium. Both homogeneous and heterogeneous catalytic conditions have been employed, with a wide variety of catalytically active metals (e.g. Ir[18], Rh[19], Co[20], Pt[21], Ru[22], and Mn[23]). However, because they are easily separated from reaction mixtures by filtration, heterogeneous catalysts are most convenient, where they work for these applications. The work described (later) in this thesis discusses aqueous-phase heterogeneous catalytic H/D exchange.

Sajiki et al. using heterogeneous catalytic H/D exchange evaluated the effect of temperature and also described the H/D exchange observed at carbons alpha to an acid, phenyl ring, primary alcohol or ether. The work discussed in this thesis centers around the H/D exchange at the alpha carbon of glycine and its derivatives. A maximum amount of deuterium incorporation into 5-phenylvaleric acid occurred at a temperature of 160 °C. Deuterium incorporation decreased with increasing distance from the benzene ring. Over the time course of the reaction, rapid exchange was observed at the benzylic carbon (C_1) as well as at the beta carbon (C_2) and also at position C_3 with respect to the phenyl ring, however, the carbon alpha to the acid (C_4) and the aromatic carbons show only a gradual

increase of deuterium exchange (Scheme 10). At a temperature of 110 °C, there was no measurable incorporation at the carbon alpha (C_4) to the acid.

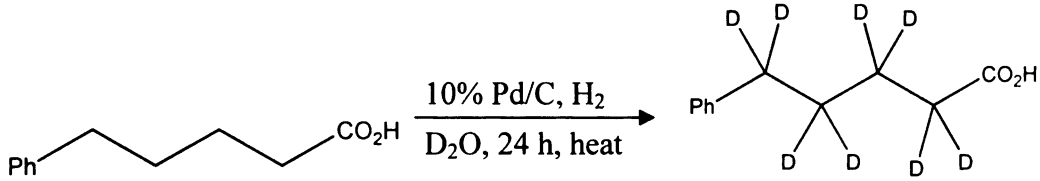

Scheme 10. 10% Pd/C H/D exchange on 5-phenyl-1-valeric acid

Sajiki et al. found that the hydrogens on the alpha carbon adjacent to a primary alcohol or ether as a substrate exchanged with deuterium to a lesser extent as compared with the methylenes closer to the phenyl ring. Reactions with substrates which lacked an aromatic ring, such as octanoic acid, led to almost no deuterium incorporation (at reaction temperatures ranging from 110-160 °C). In addition, substrates with an oxygen between the phenyl ring and the alkyl chain, such as 5-phenoxyvaleric acid underwent almost no deuterium incorporation. Thus there is apparently a need for an aromatic ring to be directly connected to the alkyl chain for H/D exchange using 10% Pd/C. The exact mechanism of the exchange is not clear, but the authors proposed that the reaction goes via Pd/C-catalyzed C-H bond activation combined with deuteration from D_2O. The results presented provide a deuterium gas-free, totally catalytic and postsynthetic deuterium labeling method in D_2O.[24]

Our research group, specifically Jere et al. report aqueous stereoretentive hydrogenation of L-alanine to L-alaninol using a 5% Ru/C catalyst at 100 °C and 1000 psi in the presence of added acid (Scheme 11). Alanine had become a compound of interest because an enhanced rate of hydrogenation of α-substituted organic acids such as alanine

and lactic acid (to be discussed in section 1.4 summary of previous work) had been noted. A slight excess, 0.29 M H_3PO_4 (pK_a = 2.15) was added to protonate 0.22 M alanine (pK_a = 2.34) and afford a 91% yield of alaninol after 6 hrs.

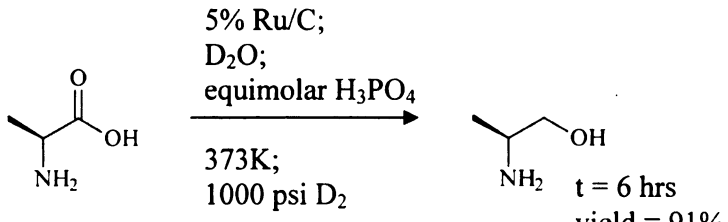

Scheme 11. Hydrogenation of L-alanine

To track the reaction's stereochemistry, D_2O was used as the solvent at 1000 psi D_2 and 100 °C. Surprisingly, although rapid deuterium incorporation at the α-carbon was observed for alanine and alaninol, little or no racemization was seen.

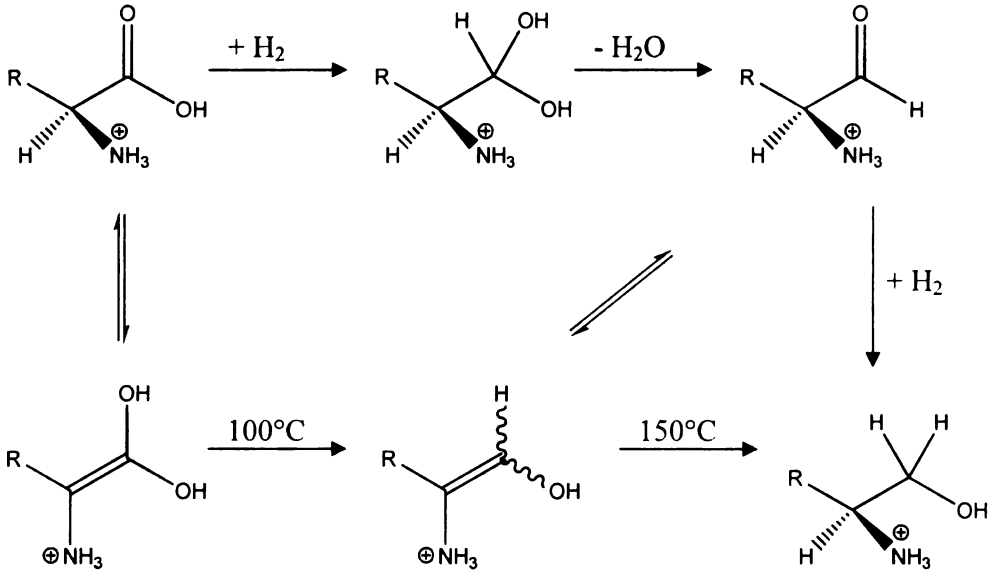

Scheme 12. Generalized amino acid hydrogenation sequence

Scheme 12 shows a generalized amino acid hydrogenation sequence which includes an aldehyde and two potential enols as intermediates. Jere et al. suggest that the enhanced rate of hydrogenation with lactic acid and protonated alanine is due to the electron withdrawing α-OH and α-N^+H_3, enhancing the carbonyl group's preference for sp^3 hybridization.[25]

Looking again at enolization, Frey et al. using 2-acetylthiamin pyrophosphate (AcTPP, **1**) and 2-acetyl-3,4-dimethylthiazolium (**2**) performed an H/D exchange kinetic analysis of sequential reactions. Frey et al. found that an electrophilic thiazolium ring enhances the ionization rate and that the acetyl methyl hydrogens of AcTPP, **1** and **2** ion exchange with water at a pD of ~4.0 (Scheme 13).

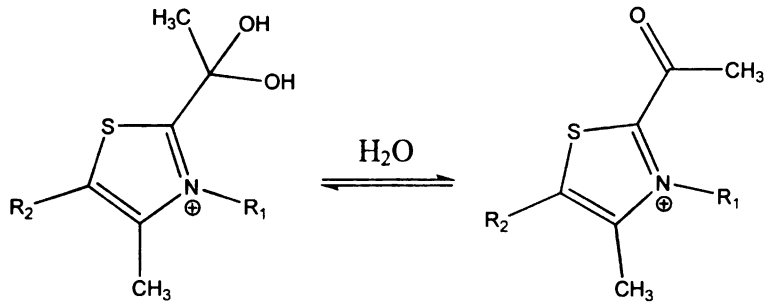

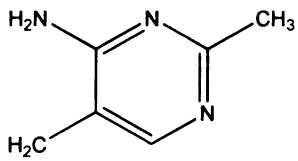

1: R_1 = $R_2 = CH_2CH_2OP_2O_6^{3-}$

2: $R_1 = CH_3$ $R_2 = H$

Scheme 13. Ion exchange with water of 2-acetylthiamin pyrophosphate and 2-acetyl-3,4-dimethylthiazolium

The rate of ionization for AcTPP is on the order of 10^7 faster than acetone. The following kinetics were employed to describe the exchange of the acetyl methyl hydrogens (R-CH_3):

$$R-CH_3 \rightarrow R-CDH_2 \rightarrow R-CD_2H$$

Defining a = [R-CH_3] and b = [R-CDH_2], at time t = 0, $a = a_0 = [R\text{-}CH_3]_0$, and $b = b_0 = 0$. Describing consecutive (pseudo) first-order reactions the differential equations and solutions are given by:

$$\frac{-da}{dt} = k_1 * a = k_1 * a_0 * \exp(-k_1 * t) \qquad a = a_0 * \exp(-k_1 * t)$$

$$\frac{db}{dt} = k_1 * a_0 * \exp(-k_1 * t) - k_2 * b \qquad b = \frac{k_1 * a_0}{(k_2 - k_1)} * [\exp(-k_1 * t) - \exp(-k_2 * t)]$$

The rate constant k is defined for exchange of a single proton, thus the values of k_1 and k_2 are $3k$ and $2k$, respectively. The substitution of these variables into the above equations can be expressed as:

$$a = a_0 * \exp(-3 * k * t) \text{ and } b = 3 * a_0 * [\exp(-2 * k * t) - \exp(-3 * k * t)]$$

From these equations, the following ratios can be expressed.

$$\frac{a}{\left(\frac{3a+b}{3}\right)} = \exp(-k * t), \text{ thus } \frac{[R-CH_3]}{\left[\frac{[3*(R\text{-}CH_3)+R-CDH_2]}{3}\right]} = \exp(-k * t)$$

Using ^{1}H NMR, normalized integral ratios were measured as a function of time to the extent of 70-80% exchange of one proton. Frey et al. found that the rates of exchange with water were the same (within error) for the hydrate and ketone forms and thus the interconversion between them is fast compared with the exchange reactions. The rate of exchange was not observed at pD $\leq$ 2, thus the reaction is not acid catalyzed but base

catalyzed and presumably occurs via an enolization mechanism. Using the iodine scavenging method, rate constants for the uncatalyzed and base catalyzed enolization were determined (k_0^E = (3.8 x 0.5) x 10^{-6} s^{-1} and (6.73 ± 0.22) x 10^{-5} s^{-1} at pD 4.17 (46 mM Na oxalate)).

Frey et al. suggest that the exchange reaction occurs via the rate-limiting loss of a proton to produce an enolate, which then can be rapidly deuterated in the presence of D_2O. The rate of enolate formation from a carbonyl compound is related to the carbon acidity. In the case of AcTPP, Frey et al. believe the largest contributor to the fast enolization is due to through-space electrostatic effects of the positively charged thiazolium ring. Fast rates of enolization have been reported for other cationic ketones, namely $PhCOCH_2N^+C_5H_5$ (k_{OH}^E = 1.8 x 10^5 $M^{-1}s^{-1}$). The rate enhancement in the ionization of carbon acids and the enolization of carbonyl compounds is poorly understood, but Frey et al. suggest that rates of base-catalyzed enolization are accelerated by the through-space electrostatic effect of a nearby positive charge.[26]

Proteins have stereochemical integrity due to the weakly acidic nature of the α-protons on the repeating amino-acid monomers. Richard et al. calculated aqueous carbon acidities for the zwitterions of glycine and its derivatives: $H_3N^+CH_2COO^-$, pK_a = 28.9 ± 0.5; $H_3N^+CH_2CO_2Me$, pK_a = 21.0 ± 1.0; $Me_3N^+CH_2CO_2Me$, pK_a = 18.0 ± 1.0; $Me_3N^+CH_2CO_2^-$, pK_a = 27.3 ± 1.2 (Scheme 14).

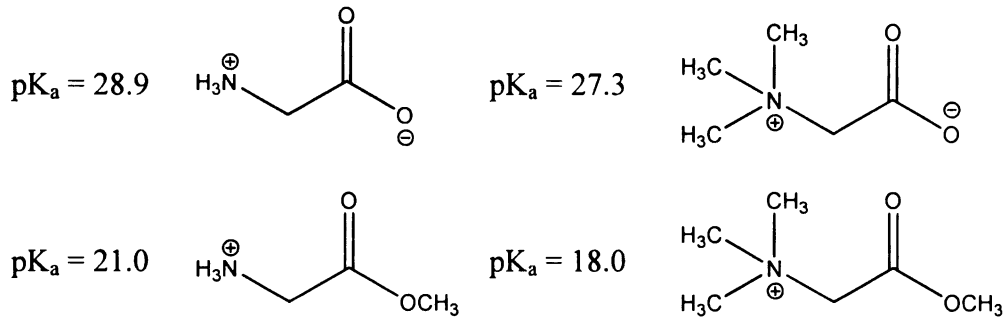

Scheme 14. Calculated acidities for the zwitterions of glycine and its derivatives

The ionization state of the amino acid relates to the acidity of the α-proton. A decrease in pH results in protonation of glycine and an increased reactivity towards enolization, whereas enolization of the anionic form of glycine is far less favorable. The pH is mathematically related to pKa by the following general equations. The acid dissociation constant, Ka, is a quantitative measure which defines the equilibrium for a chemical reaction. It can be written in terms of equilibrium concentrations, Ka = [H+][A-]/[HA]. Thus, [H+] = Ka[HA]/[A-] and due to the large orders of magnitude spanned by Ka values, the log is of Ka is commonly used. The logarithmic measure of the acid dissociation constant is written as, log[H+] = log Ka + log[HA] - log[A-]. Since pH = -log[H+] the equation can be rewritten in the form of the Henderson-hasselbalch equation, pH = pKa + log[A-]/[HA].

In glycine and its derivatives, Richard et al.[28,29] found that modifying the α-substituent from N^+H_3 to NH_2 increases the pK_a values of the α-proton by 5 pK_a units, and changing the α-substituent from COO^- to $COOCH_3$ decreases the pK_a of the α-proton by 8 pK_a units. Malthouse and co-workers used the above values and estimated the pK_a values and

tryptophan-synthase-catalyzed exchange rates of α-protons of alanine, serine, aminobutyrate, norvaline, norleucine, and tryptophan. They assumed a linear relationship and estimated that $\Delta pK_a = -\alpha\Delta\sigma^*$, where α=1.6-2.2 and σ^* represents the appropriate Taft substituent constant. From the calculations, the pK_a values of alanine, aminobutyrate, norvaline, norleucine, and tryptophan are all raised by about 1 pK_a unit, namely ~35, relative to glycine and serine, ~34.[27]

Richard et al. performed kinetic studies in D_2O at 25 °C using a substrate concentration of 20 or 40 mM glycine with a constant ionic strength of 1.0, maintained with potassium chloride. In the ^1H NMR spectra, they monitored the replacement of the α-CH_2 group's singlet resonance with the triplet due to α-CHD sites. This mono-deuterated product signal exhibited an upfield shift of 0.014 ppm for glycine and its derivatives or 0.016 ppm for betaine and its derivatives (J_{HD} = 2.5 Hz). To quantify the progress of deuterium exchange, values of R, reaction progress, were calculated: $R = (A_{CH2}/(A_{CH2}+A_{CHD}))$. Note: There is a mistake in this journal in that there is a two missing in front of the A_{CHD} term to represent the fact that for CH_2 there are two hydrogens available for exchange and for CHD there is only one hydrogen. A_{CH2} and A_{CHD} are the integrated areas of the singlet due to the α-CH_2 of the substrate and triplet due to the α-CHD of the monodeuterated product.

They did not account for the α-CD_2 group, because it was their assumption that no dideuterated glycine was formed. For the early reaction time samples, the ^{13}C satellite of the signal due to the α-CH_2 group was not resolved from the most downfield peak of the

triplet due to the α-CHD group. Due to this, the total integrated area of the triplet due to the α-CHD group, A_{CHD} was calculated by multiplying the integrated area of the most upfield peak of the triplet by three. The area of the singlet due to the α-CH_2 group, A_{CH2}, was calculated by subtracting the calculated value of A_{CHD} from the total integrated area of all signals due to the α-protons. Semi logarithmic plots ($\ln R = -k_{obsd}t$) of R vs time were linear with negative slopes equal to k_{obsd} (s^{-1}), which is the rate constant for exchange of a single proton of the α-CH_2 group. The fraction of deuterated glycine, f_D, was calculated: $f_D = 2A_{CHD}/(A_{CH2} + 2A_{CHD})$. Their assumption was that there was essentially no formation of dideuterated glycine, α-CD_2 during the hydrolysis of glycine methyl ester in D_2O. They suggested a mechanism whereby the zwitterionic glycine enolizes to form the anionic intermediate which they believe is not stabilized via protonation of the substrate carbonyl oxygen ($pK_a < 7.0$). This intermediate quickly forms the carboxylate compound and undergoes deuteration at the α-carbon (Scheme 15).

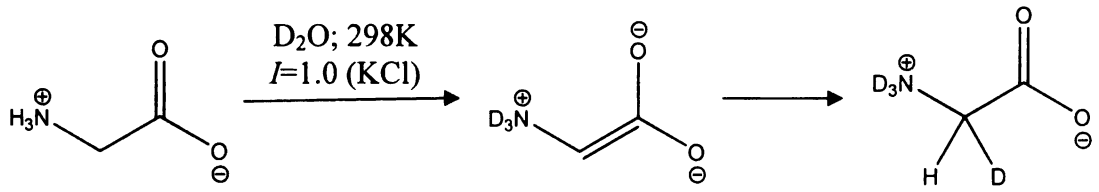

Scheme 15. H/D exchange at the α-carbon on glycine

Calculating rate constants, Richard et al. found that simple amino acid zwitterions (glycine and betaine) are weaker carbon acids than the simple oxygen ester ethyl acetate ($pK_a = 25.6$). In addition, there is about a 2-3 unit increase in acidifying effect of an α-N^+Me_3 as compared to an α-N^+H_3 substituent on the carbon acidity, corresponding to the difference in polar effects of these substituents. There is more of a polar effect with the

N^+Me_3 due to the formation of hydrogen bonds between the α-N^+H_3 and the solvent, which moves the positive charge away from the nitrogen and onto the solvent, increasing the effective separation between the interacting cationic and anionic centers at the enolate. There is greater stabilization of negative charge by electrostatic intramolecular interactions with the α-N^+Me_3, wherein the methyl groups reduce the effective dielectric constant of the local medium.[28]

Richard et al. found that hydrolysis of N-protonated glycine methyl ester is 10-times faster than deuterium exchange of the first α-hydrogen at a neutral pD (pD = 7.4). The glycine obtained after the completion of the hydrolysis reaction (>10 half-times) is enriched with 0.10 atom of deuterium (Scheme 16). N-protonated glycine methyl ester has a second-order rate constant of $k_{DO} = 6.0\ M^{-1}s^{-1}$ for DO^- catalyzed exchange of the first α-proton, whereas the rate constant for H/D exchange of acetone is $k_{DO} = 0.3\ M^{-1}s^{-1}$ (20-fold difference).

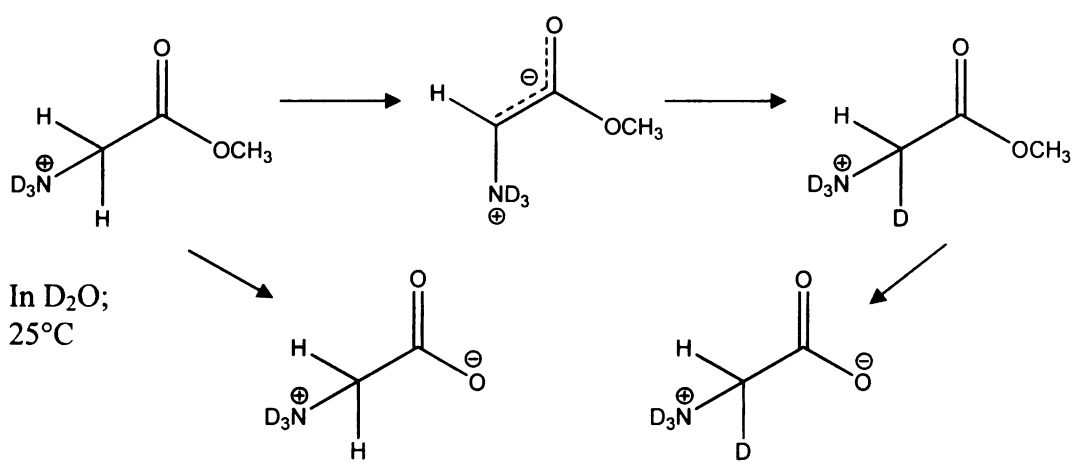

Scheme 16. Hydrolysis of N-protonated glycine methyl ester

The fast H/D exchange of N-protonated glycine methyl ester is presumably due to polar stabilization by interactions between the α-NH_3^+ group and the developing enol's partially negative carbon next door. The α-protons of N-protonated glycine methyl ester (pKa $\approx$ 21) show roughly the same acidity as the corresponding protons for the thiol ester and mandelic acid.[29]

In general, the extent of H/D exchange for a given species increases with the basicity of the exchange reagent. Cox et al., using an external ion source 7-T FTICR (Fourier transform ion cyclotron resonance) mass spectrometer, found that charge-solvated sodiated glycine oligomers (Gly_1Na^+ see Scheme 18 to Gly_5Na^+) are of the lowest energy (gas phase). Both experimental and computational methods were employed. An FTICR is one of the highest performance mass spectrometers and measures the mass-to-charge ratio of ions based on the cyclotron frequency of the ions in a fixed magnetic field with excellent resolution and mass accuracy. Using a low level of theory calculations, 3-21G, and comparing and confirming with higher theory calculations (Jensen used 6-31G* see JACS 1992, 114, 9533, Moison and Armentrout used MP2/6-31G* see J. Phys. Chem. A. 2002, 106, 10350, and Wyttenbach et al. used B3LYP/6-311++G** see JACS 1998, 120, 5098) in the literature, the most stable structure was the one in which the glycine was not in the zwitterionic form but rather when the sodium cation was bound to both the nitrogen and the carbonyl oxygen (Scheme 17).

CS $C_2H_5NO_2Na^+$ ZW $C_2H_5NO_2Na^+$

Scheme 17. Sodiated glycine in the charge-solvated (CS) and zwitterionic (ZW) forms

Experimentally, sodiated peptide ions were generated by matrix-assisted laser desorption/ionization (MALDI) and samples were deposited onto a stainless steel probe tip. The MALDI solutions consisted of a mix (6:3:2) of 1 M 2,5-dihydroxybenzoic acid in ethanol, 0.03 M peptide in water/acetonitrile (3:7 v/v), and 1 M D-fructose in water. A static pressure of the H/D exchange gas, ND_3 (7×10^{-8} Torr) was maintained. In the gas phase for sodiated pentaglycine they experimentally found the rate constants for deuterium exchange with ND_3 were 3.0×10^{-10}, 2.5×10^{-10}, and 1.5×10^{-10} cm^3 $molecule^{-1}$ s^{-1} for the three observed hydrogen exchanges (nitrogen and oxygen hydrogens). The exchange rate ratios were about 3:2:1, thus three equivalent hydrogens are presumed to be exchanging with ND_3. They also suggest that the mechanism requires a carboxylic acid hydrogen due to the fact that no exchange occurs with methyl esters of glycine oligomers.[30]

Matsubara et al. examined deuterium exchange of cyclododecene in hydrothermal or subcritical water (523 K reported as 250 °C, 5 MPa ≈ 725 psi), in the absence of hydrogen. At these conditions the pK_w of water is lower (ca. 11) and thus the water ionizes more to form OH^- and H_3O^+ than water at ambient conditions. They propose that

in these conditions the Pd(0) might oxidatively insert into O-H bonds of water to form the Pd(II) species, H-Pd-OH. The key species is the palladium hydride that exchanges with the solvent water's hydrogens. Using cyclododecene (5.0 mmol), 10 wt% Pd on active carbon (100 mg, 0.1 mmol Pd) and deuterium oxide (20 g) in a 30 mL Teflon vessel under hydrothermal conditions for 12 h, cyclododecene was converted into the fully deuterated product (E/Z = 72:28) (Scheme 18).

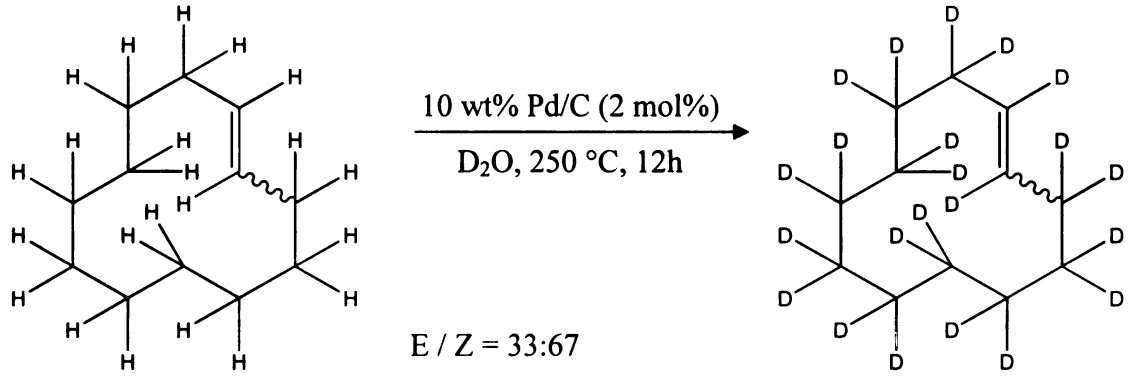

Scheme 18. H/D exchange on cyclododecene

The product was extracted with hexane and analyzed by GC, ^{1}H NMR, ^{2}H NMR, and mass spectra. Matsubara et al. explain the deuteration of alkene containing compounds via an interaction of the alkene and the palladium hydride. However, they also report full deuteration of saturated hydrocarbons, and in this case suggest that direct C-H activation may be the probable route to forming the fully deuterated alkanes. *Tert*-butyl benzene was subjected to the above conditions and no exchange was observed at the sterically hindered ortho positions, however full deuteration occurred at the meta- and para-positions. Nearly 45% of the C-H bonds on the tertiary butyl group were exchanged with deuterium after 10 h (10 wt% Pd/C (2 mol%), D_2O , 250 °C). Using the same conditions, biphenyl was fully deuterated. Mechanistic studies have not yet been examined. It is

worth noting that hydrogen gas was needed for the 10% Pd/C-catalyzed deuterium exchange reaction below 180 °C.[31]

1.3.3 Alkynylation of sp^3 C-H Bonds Adjacent to a Nitrogen Atom

A challenging, yet attractive organic synthesis reaction is C-C bond formation via C-H bond activation. The possibility of enantioselective catalytic C-C bond formation via this method could enhance asymmetric synthesis both theoretically and practically. In order to construct a chiral carbon center, a prochiral sp^2 carbon center is generally necessary as the precursor; however, Li et al. discuss the synthesis of enantioselective C-C bond formation based on activation of a sp^3 C-H bond.

Three papers by Li et al. will be discussed, starting with alkynylation of sp^3 C-H bonds adjacent to a nitrogen atom followed by enantioselective alkynylation of prochiral sp^3 C-H bonds adjacent to a nitrogen atom, and finally cross-dehydrogenative coupling between sp^3 C-H bonds and sp^3 C-H bonds. In the first paper, Li et al. report a copper-catalyzed (5 mol%) oxidative cross-coupling of amines with various alkynes via a direct sp^3 C-H bond alkynylation in the presence of *tert*-butyl hydroperoxide (2:1:1 ratio, respectively) at 100 °C for 3h with yields as high as 74%. The reaction did not take place in the absence of the *tert*-butyl hydroperoxide. There was less desired product formed in reactions with aliphatic amines, as opposed to aryl amines. Interesting to note is that N,N-dimethylbenzylamine produced alkynylation of the methyl group rather than the benzyl position.

Li et al. propose a tentative mechanism for the direct oxidative coupling suggesting the formation of an imine-type intermediate (coordinated to copper) through activation of sp^3 C-H adjacent to nitrogen. Copper also activated the terminal alkyne and coupling of the two intermediates resulted in the desired product and regenerated the copper catalyst.[32]

Li et al. expanded on this work to include tetrahydroisoquinoline alkaloids which exist widely in nature and are of biological and pharmacological interest. Specifically, they discuss the development of a novel catalytic asymmetric 1-alkynylation of tetrahydroisoquinoline derivatives via activation of the sp^3 C-H bonds of prochiral CH_2, yielding optically active C-1-substituted tetrahydroisoquinoline derivatives.

Li et al. found that the optimal conditions were with CuOTf (as opposed to CuBr seen in their previous work), at 50 °C (as opposed to 80 °C) in THF with a chiral ligand, yielding 63% of the desired product. Asymmetric alkynylation also proceeds in water or without solvent but the yields are lower. Aromatic substituted alkynes provided good yields and enantiomeric excess in most cases, whereas aliphatic substituted alkynes resulted in fair or low enantiomeric excesses. The factors which influence the enantioselectivities of the reaction are still being investigated.[33]

Vicinal diamines are found in biologically active natural products and are used in medicinal chemistry as well as in chiral ligands for asymmetric catalysis. Li et al. previously discussed both alkynylation of sp^3 C-H bonds adjacent to a nitrogen atom and enantioselective alkynylation of prochiral sp^3 C-H bonds adjacent to a nitrogen atom.

They expand on this work and discuss what they consider to be the first simple and efficient cross-dehydrogenative-coupling reaction between two sp^3 C-Hs. Due to the importance of vicinal diamines they explore an alternative approach to these compounds. Typically a nitro-Mannich (aza-Henry) reaction to afford the new C-C bond β-nitroamine derivative might be employed. Following the formation of the β-nitroamine derivative, reduction of the nitro group to give vicinal diamines can be obtained. Using tetrahydroisoquinoline and nitromethane, Li et al. report a 90% yield of the C-C coupled product at room temperature with 2 mol% of CuBr catalyst with 1.0-1.2 equivalents of *tert*-butyl hydroperoxide, 0.1 mmol tetrahydroisoquinoline, and 1.0 mL of nitromethane. The exact mechanism of this coupling is unknown. However, Li et al. propose three possible intermediates: 1) an imine-type intermediate formed via coordination to copper through H-abstraction of the sp^3 C-H adjacent to nitrogen. 2) In addition to the previous intermediate, the copper catalyst activates the nitroalkanes to form an oxygen coordinated copper species which couples with the previous intermediate to form the product, while regenerating the copper catalyst. Lastly, 3) an intermediate, in which *tert*-butyl hydroperoxide is involved, which further is converted into the cross-coupling products catalyzed by CuBr.[34] The mechanism of this reaction is still under investigation.

1.3.4 Secondary Deuterium Isotope Effects for Enolization Reactions

Murray et al. report α- and β-deuterium isotope effects for the enolization reaction and equilibria for acetone or acetophenone in deuterium oxide using ^1H NMR spectroscopy, triton exchange kinetics, and ab initio calculations. For the C-H,D bond adjacent to the carbonyl in the ionization of protonated acetone, an inverse secondary isotope effect of

0.97/D was calculated. This isotope effect is consistent with the decrease in hyperconjugation upon ionization. Upon further loss of hyperconjugation in the out-of-plane CH in the enolization reaction, a secondary α-deuterium kinetic isotope effect of 1.06 ± 0.02 was calculated. Murray et al. described the kinetics according to the following first order equations for α-CH_3 singlet (P), triplet α-CH_2D (Q), and quintet α-CHD_2 (R):

$$P = P_0 * \exp(-\lambda_1 * t)$$

$$Q = \left[\frac{\lambda_1}{(\lambda_2 - \lambda_1)}\right] * P_0 * \exp(-\lambda_1 * t) + \left[\frac{\lambda_1 * P_0}{(\lambda_1 - \lambda_2)} + Q_0\right] * \exp(-\lambda_2 * t)$$

$$R = \left[\frac{\lambda_1 * \lambda_2 * P_0}{(\lambda_2 - \lambda_1) * (\lambda_3 - \lambda_1)}\right] * \exp(-\lambda_1 * t) + \left[\left[\frac{\lambda_1 * \lambda_2 * P_0}{(\lambda_1 - \lambda_2) * (\lambda_3 - \lambda_2)}\right] + \frac{\lambda_2 * Q_0}{(\lambda_3 - \lambda_2)}\right] * \exp(-\lambda_2 * t)$$

$$+ \left[\left[\left[\frac{\lambda_1 * \lambda_2 * P_0}{(\lambda_1 - \lambda_3) * (\lambda_2 - \lambda_3)}\right] + \frac{\lambda_2 * Q_0}{(\lambda_2 - \lambda_3)}\right] + R_0\right] * \exp(-\lambda_3 * t)$$

P_0, Q_0, and R_0 correspond to the initial peak area, and λ_1, λ_2, and λ_3 are the pseudo-first-order rate constants for deuteroxide ion catalyzed exchange of protons. Murray et al. display the ^1H NMR spectra for acetophenone illustrating the incomplete resolution of the multiplets for the α-CH_2D and α-CHD_2 signals (J= 2.2 Hz for both). The data were fit to first-order consecutive process equations with rate constants $3k_H^{HH}$ [OD-] = 4.20 x 10^{-4} s^{-1}, $2k_H^{HD}$[OD-] = 2.52 x 10^{-4} s^{-1}, and k_H^{DD}[OD-] = 1.25 x 10^{-4} s^{-1}. A secondary isotope effect of k_H^{HH}/k_H^{HD} = 1.11 and k_H^{HD}/k_H^{DD} = 1.01 was calculated. (k_L^{ij} where L is the primary hydron, hydron meaning hydrogen cation, that is cleaved and i and j refer to the remaining secondary hydron sites). The isotope effects determined by ^1H NMR for proton exchange of CHH and CHD are not significantly different from one another. Murray et al. examined several methods of accounting for the lack of complete resolution

of the multiplets including adding 0.1 Hz of line broadening, Gaussian weighting of the FIDs, and using peak heights instead of integrals.[35]

1.3.5 Catalytic Hydrogenation of α-Amino and α-Hydroxy Esters

Carboxylic acids and esters are among the least reactive functional groups in catalytic hydrogenation reactions. They usually require higher temperatures (>200 °C) and higher pressures, and thus can result in racemization of stereogenic centers. However, Broadbent *et al.* demonstrated with rhenium heptoxide reduced *in situ* as catalyst, propylene glycol yields as high as 84% from ethyl lactate at 150 °C, 250 atm, and neat.[36] Studer et al. report using 10% Rh/Pt oxide (Nishimura catalyst 45.9% Rh, 19.9% Pt) for the mild reduction of various α-amino and α-hydroxy esters in methanol at 100 bar (1450 psi) hydrogen pressure and 25 °C while maintaining the integrity of the α-stereogenic center. Antons et al. report using Ru oxide to hydrogenate alanine at 100 °C and 200 bar with moderate to good yields and some racemization (93-98.5% ee).[37]

In looking at the available catalyst systems for the hydrogenation of acids and esters, many of them are not commercially available, catalyst loading can be high, and racemization can be a problem at higher temperatures. Studer et al. found that the Nishimura catalyst was the only catalyst effective (compared with Ru and Pt oxide which showed weak activity; and Rh, Pd, Ir, and Re oxide as well as 2% Pt, 4% Rh/C were completely inactive) in the reduction of α-substituted esters at room temperature, and methanol and ethanol as solvents yielded the highest amount of desired product. Monomethylation of the amino group resulted in ~17-25% reduction in yield of

hydrogenated product. In addition, the alanine derivatives, N(*n*-Pr)2 or an NH-BOC group did not react at all.

Studer et al. also found that Nishimura catalyst can selectively reduce an activated ester in the presence of an unactivated ester, as is the case with the dimethyl ester of glutamic acid. The non-activated ester forms a lactam, while the α-functionalized carboxylic acid derivative is hydrogenated to the corresponding alcohol. Studer et al. also found that α-methoxy and β-hydroxy esters did not react over the Nishimura catalyst at these conditions. In preparative-scale experiments with alanine methyl ester and methyl lactate (2 g substrate and 6 g substrate; 10:30 catalyst to substrate ratio) yields of greater than 80 and 90%, respectively were obtained and a distinct induction period of 4 minutes was observed after hydrogen saturation. The ease of ester reduction decreased in the order of α-NH_2 > α-OH, NH-alkyl > β-NH_2 using these mild reaction conditions and the oxidic, bimetallic Nishimura catalyst. The addition of acid lowered the hydrogenation rate and deactivation of the catalyst was observed at higher temperatures.

Studer et al. propose that pre-hydrogenation of the catalyst in the absence of substrate reduces the catalytic activity. They suggest a working hypothesis of a multi-functional active center, both basic and multi-metallic sites in which the substrate is adsorbed, then transformed in several steps, and the desired product is desorbed. Studer et al. think the α-NH_2, α-NHR, or α-OH functionalities serve to interact with the basic (oxidic) sites, thus anchoring the activated ester near the metallic centers. This interaction would not be possible with the OR or NR_2 groups and less favored with β-functionalities.

A drawback of this research is that the Nishimura catalysts are very expensive and these reactions require high catalyst loadings.[38] In terms of direct relevance to green chemistry goals, the use of esters as substrates and alcohols as solvents imply additional steps and disposal requirements for any practical implementation of these processes.

1.3.6 Catalytic Properties of Ru/C

Ruiz and co-workers explored the interactions between Ru nanoparticles and carbon support.[39] Carbon materials for support in heterogeneous catalytic reactions such as hydrogenations (and hydroprocessing of petroleum fractions) have several advantages. They are chemically inert, stable (in the absence of oxygen), have high surface area and optimum porosity. In addition to a large surface area, the carbon-support surface must also be chemically accessible so that active sites (unsaturated valences) must be present. Ruiz et al. discuss that the narrow microporosity of activated carbons can hardly participate in the adsorption process of the metallic precursors from solution, so there is no simple relationship between the surface area of the activated carbon and the final metal dispersion of the carbon-supported catalysts.

They prepared Ru catalysts with three different carbon material supports to evaluate how the physical and chemical properties of the support and the Ru precursor on the surface affect the Ru nanoparticles generated after reduction using hydrogen. The three carbon materials were 1) powdered carbon black (S_{BET} = 135 m^2/g); 2) mesoporous high surface area graphite (S_{BET} = 297 m^2/g); and 3) microporous carbon molecular sieves (S_{BET}=1500 m^2/g). All were prepared using the incipient wetness impregnation technique, using

metal precursor solutions with the proper precursor quantity in order to obtain a 2wt% Ru in the final catalyst. The reduction of Ru is from Ru(III) to Ru^0 via a continuous flow of 20 cm^3/min of a H_2/He gas mixture (10% H_2) with 200-300 mg of prepared sample. The reduction started at room temperature and continued to 800 K at 2 K /min. In the presence of chlorine, a higher reduction (470 K as compared to 400 K and 440 K for RuS and RuNH, respectively) temperature was used due to the chlorine chemisorbing on the metal particles decreasing their reducibility. Furthermore, Ruiz and co-workers found that residual chloride species reduce absorption capacity of the sample by poisoning the surface of the Ru particles.

1.3.7 Hydrogenolysis of Glycerol to Propylene Glycol

About 1 kg of crude glycerol by-product is produced for every 9 kg of biodiesel produced. Nearly 1 billion pounds of propylene glycol is generated annually in the United States[40] and retails for about $0.71 per pound.[41] The commercial route of preparing propylene glycol is the hydration of propylene oxide derived from propylene by either the chlorohydrin process or the hydroperoxide process. Dasari et al. discuss the selective hydrogenolysis of concentrated glycerol to propylene glycol at lower temperatures and pressures using various catalysts. All catalysts were pre-reduced at 300 °C for four hours under a constant stream of hydrogen.[42]

Shanks et al. discuss the kinetics in the hydrogenolysis of glycerol to form either propylene glycol or ethylene glycol. Looking first at the degradation rate of the products, they found the rate was zero order (independent of initial concentration) for the

concentration levels of 2.5 – 10 wt% (0.3-1.5 M) in water. The catalyst is saturated with the glycols even at very low concentrations. The calculated degradation rates for ethylene glycol and propylene glycol were 40 and 50 mol/(kg of catalyst)•s, respectively. Therefore, the degradation of products needs to be included in the model for glycerol hydrogenolysis.

Shanks et al. also examined the competitive adsorption of ethylene glycol and propylene glycol. Results indicated that even though propylene glycol degraded slightly faster than ethylene glycol, it was less competitive for active sites. Previous work suggested that the polyols adsorb to the ruthenium through oxygen, thus the non-oxygenated end of propylene glycol may be responsible for a lower binding energy compared with ethylene glycol.[43] The following model (Scheme 19) was used for ethylene glycol (EG):

$$EG + S \rightleftharpoons EG{\bullet}S \text{ (fast)}$$

$$EG{\bullet}S \rightleftharpoons EG'{\bullet}S \text{ (slow)}$$

$$EG'{\bullet}S \rightleftharpoons EG' + S \text{ (fast)}$$

$$EG' \longrightarrow X \text{ (pH dependent)}$$

Scheme 19. Proposed model for adsorption of ethylene glycol

A similar model was proposed for propylene glycol, where S is the catalytic site, EG′ is the aldehyde formed via dehydrogenation in the first step, and X is the degradation products. From Gibbs free energy data, the equilibrium concentration of glycol is strongly favored over the formation of the aldehyde (second step) under these conditions.

Assuming Langmuir-Hinshelwood kinetics, and assuming competitive adsorption between the glycols, the following rate equation (Scheme 20) was initially derived:

$$-r'_{iG} = \frac{k'_{iG} * (iG)}{(k_{EG} * EG + k_{PG} * PG + 1)}$$

Scheme 20. Langmuir-Hinshelwood kinetic expression for competitive degradation of ethylene glycol or propylene glycol

where i = E for ethylene glycol and P for propylene glycol, k'_{iG} is the degradation rate constant, iG is the respective concentrations of the glycols, and k_{EG} and k_{PG} are the adsoption constants. Experiments were conducted at two pH levels, 11.7 and 8.0. The glycols had about twice the degradation at the higher pH, even though, the adsorption constants did not vary significantly. Another observation was that as the pH increased, the amount of product degradation increased, but presumably due to ethylene glycol degradation. At the higher pH, a 5-fold increase in the glycerol reaction correlated to a 5 times higher production in propylene glycol, but less than two times higher production in ethylene glycol. Including glycerol in the competitive adsorption, it was found that ethylene glycol had an inhibitory effect, whereas propylene glycol did not. Fitting experimental data to the proposed reaction rate model, a modified equation was obtained which included a reaction order of 1.5 for the glycerol. The mechanistic reason for this 1.5 order is not clear, but may be explained by a reaction intermediate. The modified equation (Scheme 21) is shown as:

$$-r'_{iG} = \frac{k_{iG} * (iG) - s_{iG} * k'_G * \left(G^{1.5}\right)}{\left(k_G * G + k_{EG} * EG + k_{PG} * PG + 1\right)}$$

Scheme 21. Langmuir-Hinshelwood kinetic expression for hydrogenolysis of glycerol

They performed the reactions at 500 rpm, although data was also obtained at 1000 rpm. No difference in reaction rates was found between the two mixing speeds, confirming that the system is not limited by external diffusion.

1.3.8 Deuterium NMR

There are several differences between ^1H and ^2H including spin, natural abundance, frequency, shape, quadrupolar relaxation, isotope shift, and conventional coupling. Unlike the familiar spin ½ proton (^1H), deuterium (^2H) with its extra neutron has a nuclear spin of 1 and a natural abundance of 0.015% (proton 99.985%), and an NMR frequency (at 7.05T) of 46.05 (as compared to the proton NMR frequency of 300).

When I=1, as in ^2H, there are three stable nucleus orientations in the magnetic field. The orientations are parallel, orthogonal, and antiparallel. The mechanism is distinguished from dipole-dipole relaxation in two ways. First, it does not require a second nucleus in motion; the quadrupolar nucleus experiences its own fluctuating field due to its motion in the unsymmetrical electron cloud. Second, because the mechanism is extremely effective when the quadrupolar moment of the nucleus is large, T_1 can become very short (milliseconds or less, in contrast to multisecond T_1 values typically seen for ^1H). When the lifetime of the spin state, as measured by the relaxation time, is very short, the larger

uncertainty in energies implies a larger range of resonant frequencies, or a broader signal in the NMR spectrum.

Deuterium has a very weak quadrupole moment, with the result that neighboring protons exhibit normal couplings to ^2H. Thus nitromethane with one deuterium (CH_2DNO_2) shows a 1:1:1 triplet because the protons are influenced by the three spin states (+1, 0, -1) of deuterium. Nitromethane with two deuteriums (CHD_2NO_2) shows a 1:2:3:2:1 quintet from coupling to the various combinations of the three spin states (++; +0, 0+; +-, 00, -+; -0, 0-; --).[44]

Lambert et al. summarized the general isotopic shift observed for hydrogen exchanged with deuterium. As the number of bonds increases between the perturbing and resonating nuclei, the magnitude of the isotopic shift decreases. Typical shifts for hydrogen perturbed by deuterium are on the order of 0.04 ppm, 0.015, and 0.01 for 1, 2, and 3 bonds between the participating nuclei.[45] Isotopic proton shifts have been observed in several pairs of compounds. Gutowsky reports an upfield proton shift for CH_2D in Ph-CH_2D of $0.015 \pm 0.002 \times 10^{-6}$ with respect to CH_3 in Ph-CH_3. Gutowsky suggests that differences in vibrational amplitudes of D and H atoms are the primary causes of such isotopic shifts. The difference between the electronic wave functions of the isotopic compounds shift the protons in CHD upfield relative to CH_2. Since C-D has a smaller vibrational amplitude, it is closer to the nucleus and imparts an enhanced shielding effect.[46]

A coupling interaction between a spin ½ and spin >½, as in the case of a deuterium, may lead to broadening of the individual components of both multiplets assuming a relatively slow rate of relaxation. If the rate of relaxation becomes fast enough it may lead to a broadening that results in a merging of broad signals. Pople discusses the theory behind broadening of a component with spin ½ coupled to a nucleus with a spin of $I = 1$. His results revealed that for slow quadrupole relaxation there is individual and unequal line broadening and as the lines continue to broaden, the outer peaks move inward until they merge with the center to become a single signal.[47]

1.4 Summary of Previous Work

Over the past several years, the Jackson/Miller group has probed the Ru/C-catalyzed aqueous-phase reductions of several organic acids, focusing on lactic acid hydrogenation to propylene glycol and amino acid hydrogenation to the corresponding amino alcohols. Related aqueous hydrogenolysis reactions of glycerol and higher sugar alcohols to high-valued polyols have also been studied, providing valuable additional insights.

In 2001, Zhang et al. examined several factors including catalyst, effect of pressure and temperature, feed concentration, and catalyst loading in the aqueous-phase hydrogenation of lactic acid to propylene glycol.[48] Reactions were carried out in a 300 ml stirred batch reactor (Parr Instruments) with a typical reaction time of 5 hours. Zhang found that the Ru/C catalyst achieved nearly 100% conversion of 0.55 M lactic acid at 423 K (reported as 150 °C), 2100 psi (reported as 14.5 MPa) H_2, and 1.0 g of catalyst within 5 hours. In comparison at the same conditions, Ru/Al_2O_3 achieved ~60 % conversion, Ru/TiO_2

achieved ~38 %, Raney Nickel achieved ~20 %, and CuCrOx, Pd/C, and Ni/Al_2O_3 achieved conversions all less than ~5%. Zhang also characterized the product mixture from hydrogenation of lactic acid using Ru/C < 170 °C the major byproducts at < 170 °C are light hydrocarbons (methane, ethane, and propane). For reactions at temperatures > 170 °C the byproducts are 1-propanol and ethanol, with trace amounts of 2-propanol. An optimum reaction temperature of 150 °C was determined; at higher temperatures (170 °C) cracking and excessive byproduct formations become an issue.

Due to low solubility of hydrogen in water, higher pressures are required to increase the hydrogen concentration in the liquid. Pressures between 500 psi and 2,000 psi (reported as 3.5 MPa and 13.8 MPa) were evaluated. Higher pressures resulted in an increased yield of propylene glycol. Zhang calculated the absolute reaction rate (moles lactic acid/h/g catalyst) for three different feed concentrations (0.55, 1.15, and 3.6 M) and found that the reaction rate increases at higher lactic acid concentrations, but leads to a lower conversion. These results suggest that the reaction may not be first-order in lactic acid and a Langmuir-Hinshelwood rate expression might better describe the reaction kinetics.

Zhang compared three different catalyst loadings and found that with higher catalyst loadings, conversion rates increased, yet selectivity to propylene glycol slightly decreases due to the increased exposure of propylene glycol to the catalyst. Zhang also looked at the addition of potassium and calcium salts on the effect of lactic acid hydrogenation. Typically calcium lactate is the usual product of fermentation and Zhang found that it can

be easily converted to propylene glycol by adding a stoichiometric quantity of sulfuric acid followed by hydrogenation of the free acid. Zhang et al's achieved 90-95 % lactic acid conversion to propylene glycol at optimal conditions (423 K and ~2100 psi). Zhang et al. continued with this work and determined the kinetics of aqueous-phase hydrogenation of lactic acid to propylene glycol (423 K, 2,000 psi, 1.5 g of catalyst, and 1.15 M lactic acid in water).[49] Mass transfer was considered in a three-phase reaction.

For the hydrogenation reaction to occur several physical and chemical steps need to occur: (1) transport of hydrogen from the gas phase to the liquid phase; (2) mass transfer of both hydrogen and lactic acid from the liquid phase to the catalyst surface; (3) diffusion of both hydrogen and lactic acid within the porous catalyst to the metal surface sites; and (4) hydrogenation of the acid to the desired alcohol via a sequence of surface chemical reaction steps. To calculate the reaction rate of lactic acid hydrogenation to propylene glycol, a fourth order polynomial was fit to lactic acid conversion vs time data. The equation was then differentiated and evaluated at various times during the reaction. Using stirring rates between 400 and 1200 rpm, Zhang et al. evaluated the influence of gas-liquid mass transfer on the rate. They found a weak dependence of reaction rate on hydrogen concentration. And although at lower stirring speeds (400 rpm) there is a reduced concentration, as the reaction proceeds, the reaction rate declines and mass transfer has less effect and the result is no observable influence of stirring speed on the reaction rate over the course of the conversion.

Zhang et al. used Langmuir-Hinshelwood kinetics and described the hydrogenation of lactic acid by the following steps (Scheme 22), where lactic acid (LA) and hydrogen (H_2) adsorb on the catalyst surface (S) and react to form propylene glycol (PG). The exact mechanism of the surface reactions are unknown.

(1) LA + S = LA•S (fast)

(2) H_2 + S = H_2•S (fast)

(3) H_2•S + LA•S ⟶ P_1•S + S (slow)

(4) P_1•S + H_2•S = PG•S (fast)

(5) PG•S = PG + S (fast)

Scheme 22. Langmuir-Hinshelwood model of hydrogenation of lactic acid

Zhang et al. found that the above model which suggests molecular adsorption of both lactic acid and hydrogen (as opposed to dissociative adsorption), the rate-limiting surface reaction step between lactic acid and hydrogen, and desorption of propylene glycol gave all positive kinetic and adsorption constants with the correct temperature dependence. The rate-limiting step was found to be irreversible. The effect of propylene glycol on the reaction kinetics was evaluated by adding propylene glycol in the amount of 2.5 times that of lactic acid feed concentration and the rate was unaffected. So, propylene glycol was not used in the final Langmuir-Hinshelwood model. The final form of the kinetic expression is given in Scheme 23.

$$-R_{G,LA}(\text{kmol/kg of cat/s}) = \frac{kC_{LA}P_{H2}}{\left(1+K_{H2}P_{H2}+K_{LA}C_{LA}\right)^2}$$

Scheme 23. Langmuir-Hinshelwood kinetic expression of hydrogenation of lactic acid

Also, when Zhang et al. used only the initial rate data, the Langmuir-Hinshelwood model gave similar regression coefficients thus the catalyst deactivation was not a major factor at these experimental conditions. This work was later re-visited by Chen (2007, discussed later). Chen found that using a multivariable regression on the initial rate data resulted in error from an unrealized interdependence of the kinetic parameters. But, when using the initial rate data from Zhang et al, an activation energy of 46 kJ mol was calculated which agreed with later results. From the model, heats of adsorption of lactic acid and hydrogen were estimated based on the adsorption constants (K_{LA} and K_{H2}) at the two temperatures. Lactic acid had a $\triangle H_{LA}$ = 47 kJ/mol and hydrogen had a $\triangle H_{H2}$ = 79 kJ/mol. They also looked at the relative surface concentrations of hydrogen and lactic acid on the catalyst. They found the ratio of empty, hydrogen-occupied ($K_{H2}P_{H2}$), and lactic acid-occupied ($K_{LA}C_{LA}$) sites is 1 : 0.05 : 0.6 at ~2000 psi hydrogen pressure, 403 K and 1.13 M lactic acid. This supports the finding that increased hydrogen pressure increases the reaction rate. There is significant lactic acid adsorbed but relatively little hydrogen. In summary, Zhang developed a useful kinetic model which could be used a tool for further investigation into the mechanism of hydrogenation of lactic acid to propylene glycol.

Jere et al. expanded on this work by including hydrogenation of the amino acid L-alanine ((*S*)-2-aminopropanoic acid) to L-alaninol (*S*-(+)-2-amino-1-propanol).[25] This simple chiral amino acid was chosen to further probe the mechanism and stereochemistry of the hydrogenation by using isotopic labeling and reaction rate data. It was found that the addition of phosphoric acid (slight excess) is required to pronate alanine (pKa = 2.34)

enabling the carboxylic acid functionality to be undissociated. Jere et al. found that with sufficient acid (0.29 M), hydrogenation of protonated L-alanine (0.22 M) to protonated L-alaninol at 398 K (reported as 125 °C) and 1800 psi D_2 in D_2O occurred with more than 95% selectivity and 99% enantiomeric excess (ee). At 448K (reported as 150 °C) and 1000 psi hydrogen pressure, the product L-alaninol was found to racemize to D-alaninol, however, at no point during the hydrogenation reaction was D-alanine detected. At lower reaction temperatures, less racemization is observed with essentially no product racemization detected at 100 °C. Also at 100 °C they found incorporation of deuterium at C2 without loss of optical purity for both alanine and alaninol (greater than 90% D incorporation at six hours reaction time). At higher temperatures (150 °C), H/D exchange is observed at the C3 positions with racemization of alaninol (65% D incorporation; 81% ee alaninol) (Scheme 24).

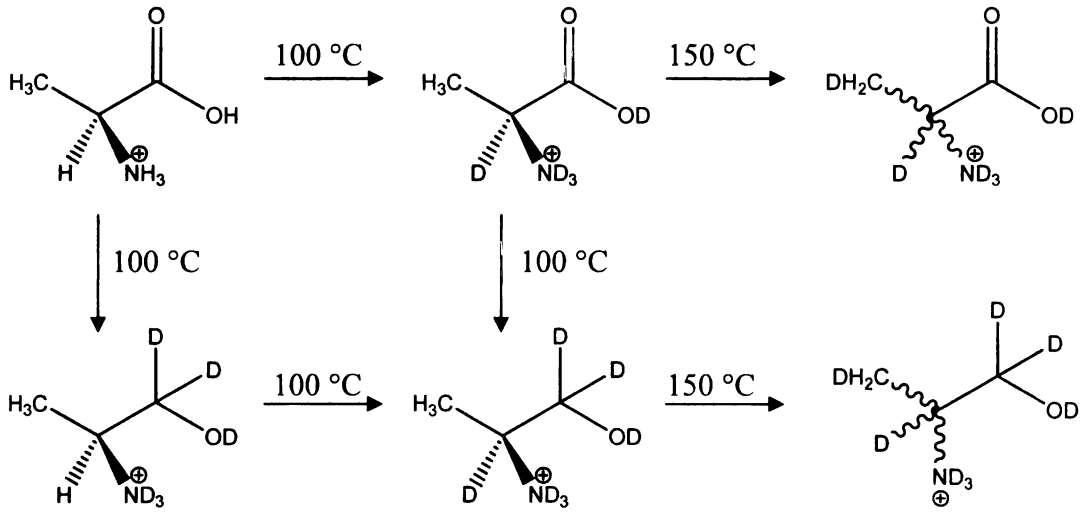

Scheme 24. Deuterium incorporation in D_2/D_2O using Ru/C

Jere et al. also found that the catalyst binding sites were saturated with hydrogen above 1000 psi and that at pressures at or above this neither hydrogen nor substrate

concentrations limit the reaction rate. From their results, they postulate a general amino acid hydrogenation sequence (Scheme 12). The scheme does not explicitly represent the role of the catalyst.

It is expected that hydrogenation of amino acid is fast relative to dehydration of the 1,1-diol and reduction of the aldehyde. The aldehyde has not been detected but it is postulated that the hydrogenation reaction does go through this intermediate as opposed to enol which is catalyst-independent and not seen in the conditions investigated (Scheme 12). The H/D exchange reaction presumably occurs separately from hydrogenation. One reason for this is that in the H/D exchange reaction there is little or no loss of chirality at C2, despite exchange. So, a free enol, sp^2 hybridized at C2 cannot play a role in this reaction. Also, in the absence of additional acid, hydrogenation does not occur but H/D exchange at C2 occurs rapidly.

These results suggest that deuterium is incorporated via the catalyst directly removing hydrogen from the amine-bearing carbon yielding a surface-bound intermediate that retains the original C2 configuration. Jere et al. continued with this work and developed a Langmuir-Hinshelwood kinetic model for predicting alanine conversion over Ru/C catalyst.[50] Reaction conditions included alanine concentrations between 0.22 to 0.46 M, phosphoric acid concentrations between 0 and 1.2 M, 80 °C to 125 °C (reported as 353 K to 398 K), and hydrogen pressures from 250 psi to 2,000 psi (reported as 1.7 MPa to 13.8 MPa). Jere et al. made some new assumptions than what Zhang had previous proposed. Jere modeled hydrogen as dissociatively adsorbing on the Ru metal surface and also

suggested that the hydrogen and the acids (protonated alanine and phosphoric acid) absorb on different sites. The hypothesis that protonated alanine and phosphoric acid compete for the same sites is based on experimental data. The reaction rate of hydrogenation of protonated alanine starts to decrease upon excess phosphoric acid addition, which can not be explained unless competitive adsorption is at work. The assumption that hydrogen dissociatively adsorbs comes from recent work done by both Vannice and Neurock.[51,52] Jere et al. proposed the following series of elementary reactions to model the hydrogenation of alanine (Scheme 25).

$$(1)\ A^+ + S_1 = A^+\bullet S_1 \quad \text{(fast)}$$

$$(2)\ P + S_1 = P\bullet S_1 \quad \text{(fast)}$$

$$(3)\ H_2 + 2S_2 = 2H\bullet S_2 \quad \text{(fast)}$$

$$(4)\ 2H\bullet S_2 + A^+\bullet S_1 \longrightarrow A_1^+\bullet S_1 + 2S_2 \quad \text{(slow)}$$

$$(5)\ 2H\bullet S_2 + A_1^+\bullet S_1 = Alol^+\bullet S_1 + 2S_2 \quad \text{(fast)}$$

$$(6)\ Alol^+\bullet S_1 = Alol^+ + S_1 \quad \text{(fast)}$$

Scheme 25. Langmuir-Hinshelwood model of hydrogenation of protonated alanine

Earlier research in the Jackson/Miller group looked at aqueous-phase catalytic hydrogenolysis of glycerol to propylene glycol.[53,54,55,56,25,57,58] Glycerol is a by-product of biodiesel formation, however, there is more of an industrial demand for propylene glycol than glycerol. Propylene glycol is used as a solvent, coolant, moisturizer in medicines and cosmetics, and chemical intermediate. Peereboom et al. sought to gain a deeper understanding of glycerol hydrogenolysis by studying the activated carbon support used in the catalytic reaction.[59] Two carbon supports were used, a 0.8 mm extrudate activated

carbon referred to as ROX and a power activated carbon designated as 3310. The properties of the carbon supports are presented in Table 1.

Table 1. Carbon characterization by N_2 adsorption at 78 K

Carbon type	**3310**	**ROX**
BET surface area (m^2/g)	716	834
Micropore area (m^2/g)	375	586
Total pore volume (cm^3/g)	0.654	0.536
Micropore volume (cm^3/g)	0.173	0.272

Typically there are local concentrations of the substrate and product (glycerol and propylene glycol) in the activated carbon micropores. These concentrations are presumably different than those in the bulk solution phase. In an effort to gain a bigger picture regarding the reaction kinetics it is necessary to try and understand the difference in concentration between solution and pore. Typically only the concentration in the bulk solution is being measured and used for the chemical kinetics. Peereboom et al. performed carbon adsorption experiments using propylene glycol and glycerol (0.01 M to 2.0 M each) at room temperature (298 K reported as 25 °C) and modeled the results using both Freundlich and Langmuir isotherms. Both models are relatively simple and describe non-competitive adsorption. The Freundlich is based on a least-squares linear regression of experimental data from $\ln(C_{AS})$ vs $\ln(C_A)$, where C_{AS} is the concentration of A adsorbed onto the activated carbon and C_A is the observed A concentration in solution in equilibrium with carbon. The data is fit to the equation $C_{AS} = K_F C^n_A$ to give slope, n, and intercept $\ln(K_F)$. The Langmuir is based on a plot of (C_A/C_{AS}) vs C_A and fit to the

equation $C_{AS} = K_A C_A C_{TA}/(1+K_A C_A)$. This gives a slope of $1/C_{TA}$ and intercept, $(1/K_A C_{TA})$, where C_{TA} is the maximum concentration of A in activated carbon absorbent.

In general for ROX, the Langmuir isotherm gave the best fit of the data and the indicated a similar value for the maximum concentration of absorbed glycerol and propylene glycol (C_{TA} = 1.77 and 1.64 mol/kg, respectively). However, at concentrations below the Langmuir maximum, the quantity of propylene glycol adsorbed is greater than that of glycerol. This is deduced from the equilibrium constants for each, K_A is 0.0163 M^{-1} for propylene glycol and 0.00475 M^{-1} for glycerol (3.5 times more for propylene glycol). The enhanced adsorption for propylene glycol is due to the less hydrophilic nature of propylene glycol favoring it presence in the carbon micropores rather than the bulk solution. There is also a lower extent of solvation of propylene glycol via hydrogen bonding.

Peereboom et al. also studied elevated temperature adsorption (313 to 433 K) with substrate concentrations of 0.1 to 0.5 M using the assumption that all adsorption sites have equal binding energies. The Van't Hoff equation is described as $\ln(K_A) = -(\Delta H/R)*(1/T)+\ln(K_0)$ and the heat of adsorption (ΔH) is the slope calculated from a plot of $\ln(K_A)$ vs 1/T. The heats of adsorption for glycerol and propylene glycol were calculated to be about 15 kJ/mol each (3.6 kcal/mol), suggesting similar van der Waal's type forces and weak hydrogen bonding.

They also studied two-component adsorption and used the extended Langmuir model to describe the adsorption of the two species into the activated carbon micropores. Aqueous solutions of propylene glycol and glycerol with a total species concentration of 0.05 to 0.5 M were evaluated. From the data, the results show a clear preference for propylene glycol adsorption, by about a factor of about 3.5 times. Using a total species concentration of 0.5 M, the heat of adsorption was calculated and verified to be constant at 353 K, 393 K, and 433 K (reported as 80 °C, 120 °C, and 160 °C). Using the measured micropore volume at a temperature of 353 K for different bulk glycerol and propylene glycol concentrations it was found that the glycerol solution concentration is not very different than the pore concentration, however, the pore concentration of propylene glycol is about five times larger than the corresponding glycerol solution concentration. The presence of propylene glycol lowers the glycerol pore concentration significantly. In conclusion, they found that the pore concentrations for both propylene glycol and glycerol deviate from the bulk solution concentrations enough that they should be accounted for in the kinetic modeling of catalytic glycerol hydrogenolysis.

Dalavoy et al. recognized the importance of the commodity chemical propylene glycol and decided to explore electrocatalytic hydrogenation (ECH) as a mild alternative to the traditional chemical catalytic method (involving higher temperatures 423 K, and pressures 1200 psi H_2).[60] In this method, the acid is reduced by hydrogen formed from electrolytic acid decomposition at the surface of a catalytic metal electrode. The hydrogen is produced in situ on the catalyst surface and this presents some challenges. Due to the low hydrogen gas solubility, there is a need for high pressures in order to

achieve adequate concentrations of the gas. Also mass transport and the splitting of hydrogen atoms on the catalyst surface can be a challenge.

A series of ECH experiments using lactic acid and a RVC electrode suffused with 5% Ru/C powder catalyst (same catalyst as used in the chemical catalytic hydrogenation studies) were conducted. Using a two-compartment cell, the anode and cathode compartment were separated by a glass frit preventing the diffusion of gaseous products. The electrode was an Ag/AgCl and the counter electrode was Pt wire. Depending on the electrolyte and the temperature, the potential of the electrolyte was -100 to -400 mV (vs Ag/AgCl). The final concentration of lactic acid in solution was 11.1 mmol (0.1 wt%) and the total volume was 75 mL. The final electrolyte concentration was about 0.01 M and argon gas was bubbled through the solution to remove oxygen and other dissolved gases. Water was circulated through a glass ATR cell (~20 mL in volume) to help maintain a constant temperature.

At a temperature of 363 K (reported as 90 °C), yields of 5.7% and 9.8% lactaldehyde and propylene glycol were achieved by ECH in 0.01 M H_2SO_4 after 9 h and current = 40 mA. Increased yields of lactaldehyde were achieved using HCl instead of H_2SO_4. Again using 11.1 mmol of lactic acid but at 343 K (reported as 70 °C), 0.01 M HCl and with a current = 100 mA a yield of 80.3% lactaldehyde was achieved. Only 2.9% of propylene glycol was formed at these conditions. The G3 composite ab initio method (in Gaussian 98 code) was performed to determine the heats of formation calculated from atomization enthalpies (Scheme 26).

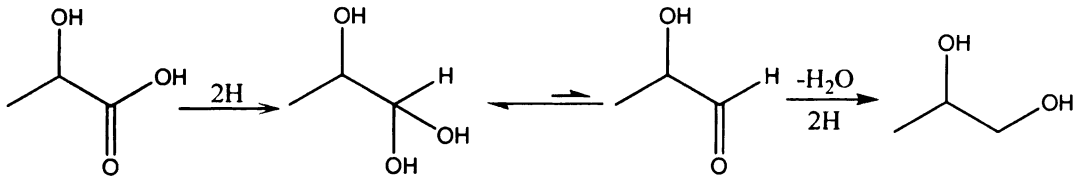

lactic acid	1,1,2-propanetriol (lactaldehyde hydrate)	lactaldehyde	1,2-propanediol
Gas Phase -147.9	-151.5	-142.8	-161.0
Liq. phase -158.8	-163.5	-156.7	-177.3

Scheme 26. Heats of formation (kcal/mol) for lactic acid hydrogenation

To confirm the formation of the intermediate aldehyde, glyceric acid, glycolic acid, and alanine were subjected to the same conditions and were all converted to the intermediate aldehyde (glyceraldehydes, glycolic aldehyde, and 2-amino propanol, respectively). The confirmation of the aldehyde intermediate was an interesting discovery because it was a proposed intermediate in the catalytic hydrogenation experiments and proposed reaction mechanism but was not confirmed.

Dalavoy et al. looked at several reaction conditions to try and optimize the efficiency of the reaction. Results indicated that with increasing temperature, yield of lactaldehyde and propylene glycol increased. Using identical conditions (11.1 mmol lactic acid in 0.01 M H_2SO_4 for 9 h at 363 K) currents between 10 and 100 mA were examined. They found that with increasing current, the propylene glycol yield increases and the lactaldehyde yield decreases, while the total conversion remains nearly constant. A simple interpretation of this based on scheme G is that propylene glycol is formed by two

discrete intermediates (lactaldehyde hydrate and lactaldehyde). At low currents, the lactaldehyde hydrate is weakly bound and easily replaced by the lactic acid substrate. The replacement occurs faster than the dehydration and capture by surface hydrogens. However, at higher currents the lactaldehyde would more quickly be converted to propylene glycol due to the availability of surface hydrogens. In addition, the increased amount of propylene glycol formed at higher currents may be due to the fact that there is higher electrode surface energy at more negative potential, this results in a higher mobility of H atoms. Three different electrolytes at concentrations of either 0.01 or 0.1 M were studied, HCl, $HClO_4$, H_2SO_4, using 11.1 mmol of lactic acid, 343 K and 100 mA current. In general, the rate of formation for lactaldehyde was found to decrease in the order HCl > $HClO_4$ > H_2SO_4. The differences in ECH reaction rates are correlated to the extent of surface poisoning by the anions of the electrolyte.

Chen et al. took the aqueous phase Ru/C catalytic hydrogenation reactions a step further by looking at competitive reactions with lactic acid and propanoic acid to their respective alcohol products, propylene glycol and 1-propanol.[61] The reactions were carried out using several feed concentrations (0.05 to 5 M), temperatures (343 to 423 K), and hydrogen pressures (500 to 1500 psi reported as 3.4 to 10.3 MPa). However, for most reactions a pressure of 1000 psi and temperature of 403 K were used for most experiments. Catalyst loading was 0.5 g (dry basis) in 50 mL of aqueous solution. Scheme 27 shows the general hydrogenation reaction, conditions, and products.

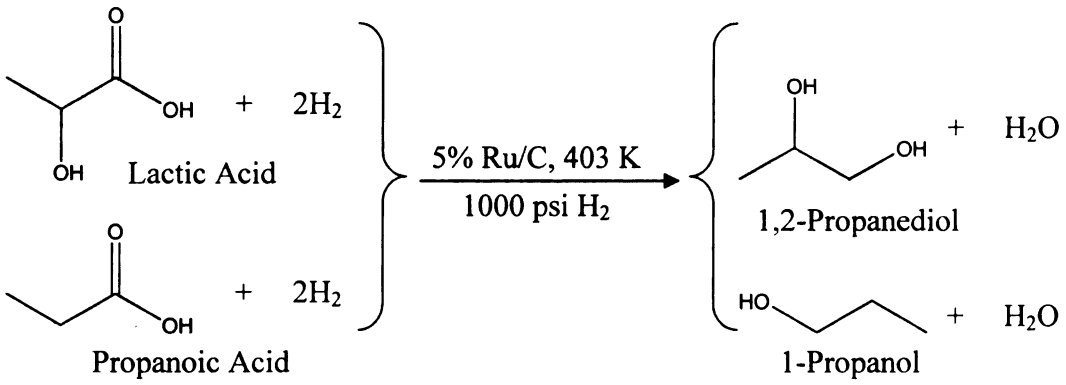

Scheme 27. Catalytic hydrogenation of lactic acid and propanoic acid

Chen et al. found that the reaction rate of lactic acid was nearly 4x faster than that of propanoic acid and that the conversion rates of both increased dramatically with temperature. These results support previous findings (discussed earlier) in our research group. In addition the selectivity to propylene glycol from lactic acid ranged from 80 to 99%, while selectivity to 1-propanol from propanoic acid was less than 60% for most conditions. The lower selectivity to 1-propanol is due to a faster degradation rate of 1-propanol and also the slow hydrogenation rate of propanoic acid. Also, it was found that 1-propanol adsorbs more strongly than propylene glycol on the catalyst Ru metal and carbon support, creating locally high pore concentrations of 1-propanol near the Ru sites which contribute to its elevated degradation rate.

At four feed concentrations (0.1, 0.5, 2, and 5 M) and otherwise identical concentrations, initial lactic acid and propanoic acid hydrogenation rates were calculated. A nonlinear dependence of the initial rate on the initial concentration indicates that the reactions are not first order and as previously found in our research group, suggests that a Langmuir-

Hinshelwood rate expression would best describe the kinetics. Activation energies were also calculated from plot of the natural log of the initial rate vs 1/T. The average activation energy for lactic acid was 52 kJ/mol and 68 kJ/mol for propanoic acid.

In competition experiments, it was found that the addition of a second acid has an inhibitory effect on the conversion and this effect increases with concentration. However at concentrations over 2 M the catalyst is saturated with acids and thus the inhibitory effect becomes constant. The influence of the product alcohols were also and it was found that the presence of either propylene glycol of 1-propanol in the starting solution had little effect on the lactic acid hydrogenation rate. However, 1-propanol did have an effect on the hydrogenation rate of propylene glycol. Together these results suggest that the kinetic model should include these inhibitory effects in order to properly describe the reaction.

Chen et al. performed a mass transfer analysis on the three-phase catalytic hydrogenation reaction and used these data and experimental reaction data to develop a kinetic model. Again using a Langmuir-Hinshelwood kinetic model and the same assumptions from Jere (discussed previously) a set of elementary reactions were used to describe the lactic acid and propanoic acid hydrogenation reactions. Again the rate limiting step is the irreversible surface reaction of the adsorbed acid and the hydrogen to form a surface bound intermediate. The resulting rate expression for single acid hydrogenation is presented in Scheme 28.

$$-r_{Acid}\,(\text{kmol/kg of catalyst/s}) = \frac{k_{Acid}C_{Acid}P_{H_2}}{(1 + K_{Acid}C_{Acid} + K_{Alcohol}C_{Alcohol})\left(1 + \sqrt{K_{H_2}P_{H_2}}\right)^2}$$

$$k_{Acid} = k_{sA}K_{Acid}K_{H_2}C_{t1}(C_{t2})^2$$

Scheme 28. Rate expressions for single acid hydrogenation

Performing a least squares regression analysis on 35 experiments at 403 K the adsorption constant for lactic acid was slightly more than propanoic acid (1.75 vs 1.36 m^3/kmol) and both significantly more than that of propylene glycol (0.063 m^3/kmol). However, as noted in the competition experiments, the adsorption constant of 1-propanol is much higher (2.41 m^3/kmol) and it's presence in the starting solution decreased the propanoic acid hydrogenation rate. The rate constants for lactic acid and propanoic acid were calculated to be 1.03×10^{-5} and 1.66×10^{-6}, respectively.

The Langmuir-Hinshelwood model was extended to include adsorption of additional species for the mixed acid/alcohol hydrogenation reactions and worked reasonably well. Using the model, it was found for 0.5 M concentrations of lactic acid and propanoic acid at 403 K resulted in site occupancies of 39.1% vacant, 34.3% lactic acid, and 26.6% propanoic acid. However, with 0.5 M 1-propanol added the fractions change to 26.6% vacant, 23.3% lactic acid, 18.1% propanoic acid, and 32% 1-propanol. Propylene glycol was not included in the study due to its weak adsorption. Also, at the typical hydrogen concentration of 1000 psi, the fraction of occupied sites is 60%. These results suggest that at high concentrations (>2 M), the surface is saturated with reactants.

Zhang et al., who originally (2001, discussed above) studied aqueous phase Ru/C catalytic hydrogenation of lactic acid to propylene glycol expanded this work to understand the effect of biogenic fermentation impurities on the hydrogenation reaction.[62] The work done in our research group consisted of using reagent grade lactic acid, which allowed us to study different catalysts and reaction conditions as well as measuring intrinsic reaction kinetics. However, in order for propylene glycol production from lactic acid to compete with existing petroleum-based routes it is necessary to consider the use of lower cost, less pure lactic acid feedstock. The current petroleum-based routes produce propylene glycol from propylene involving either hydroperoxide intermediate of direct hydration of propylene oxide. Conversion of propylene to propylene glycol requires only 0.6 kg propylene/kg propylene glycol compared with 1.25 kg lactic acid/kg propylene glycol using lactic acid as the feedstock. So, in order to compete, the renewable feedstock must be on the order of one-half that of propylene.

Currently, lactic acid is made from glucose via fermentation with *Lactobacillus* microorganisms. The yields obtained are nearly quantitative and the fermentation media has a complex mixture of nutrients, minerals, and base ($Ca(OH)_2$) to neutralize the forming acid. After fermentation lactate is formed and is acidulated with H_2SO_4 to form lactic acid, which is then purified (~88% wt acid in solution). Characterizing the key biogenic impurities present in the fermentation process and their effect on catalyst performance in producing propylene glycol was the key objective in this work.

Three different lactic acid samples from along the purification train of a demonstration-scale lactic acid production facility were studied. The three samples were a fully refined lactic acid (1), lactic acid that was withdrawn after the extraction/back extraction step (light brown color) (2), and lactic acid that was not refined beyond acidulation and filtration (dark brown color) (3). The catalyst used in this studied was 5 wt% Ru/C and was prepared in-house. Experiments were conducted in a three-phase trickle bed reactor using the following general conditions: 403 K (reported as 130 °C), 990 psi (reported as 6.8 MPa), 10 g catalyst bed mass, 1.0 mL/min feed rate, 1.35 M feed concentration, and H_2 : LA molar feed ration of 3.5 : 1.

Results from the refined lactic acid (1) indicated that increased pressure (range studied: 200 to 1200 psi) improves both conversion and selectivity. In addition, a temperature of 373 K (reported as 100 °C) gave the best combination of activity and selectivity (range studied: 353 to 423 K). A long-term catalyst evaluation was performed (conditions: 120 kg refined lactic acid/kg catalyst at 403 K and ~1000 psi H_2) over 370 h of operation and the conversion was found to be nearly constant at 90%. The liquid by-products identified included ethanol, *n*-propanol, and *i*-propanol in decreasing amount and together accounted for 3.5% of the lactic acid fed. The gas by-products identified included methane, ethane, and a small amount of propane in decreasing amounts and together accounted for ~12% of the lactic acid fed.

To study the conversion of the partially refined lactic acids (2 and 3), a steady-state lactic acid conversion was established using the refined lactic acid (1) followed by switching

the feed to one of the partially refined lactic acids (2 or 3). For partially refined lactic acid 2, the conversion drops rapidly from 55% (established steady-state conversion using 1) to 30% for the first 5 h and slowly continues to decrease thereafter. For partially refined lactic acid 3, the conversion drops again from 55% to 10% in the first 5 h then essentially levels off. Switching back to the refined lactic acid feed results in a partial recovery and stabilization of the lactic acid conversion. In order to try and improve the conversion using the partially refined lactic acid (2), both heat treating (273 K at 5 h under helium) and bubbling ozone gas through the sample was tried, but there was no improvement in conversion.

In an effort to model the effect of the impurities, the various impurities (salts, organic acids, extraction solvents, proteins, etc) were added to the purified lactic acid solution and the results interpreted. Three different salts (NaOH, Na_2SO_4, Na_2HPO_4) were added to the refined lactic acid feed. When adding NaOH, conversion of lactic acid decreased by an amount proportional to the amount of sodium lactate formed. These results are supported by previous work in our research group (Zhang et al., 2001). However, when Na_2SO_4 and Na_2HPO_4 were added there was little reduction in lactic acid conversion. So, addition of salts (PO_4^{3-} and SO_4^{2-}) did not appear to poison the Ru/C catalyst. Several organic acids (glucose, sorbitol, succinic acid, or propanoic acid) and extraction solvents (dodecane, 1-octanol, or trioctylamine) were added to the lactic acid feed and the results for each indicated no effect on the conversion of lactic acid.

To study the effect of protein and protein fragments, 0.12 wt% bovine albumin was added to the lactic acid solution. Results indicated a steady decline in conversion before essentially leveling off. The behavior observed partially matches the results from the partially refined lactic acid (2 and 3), indicating that proteins are partially responsible for the decreased activity for those feeds. Using nitrogen adsorption at 78 K the pore volume of the protein deactivated catalyst was studied. Results indicated that the deactivation was partly caused by a combination of pore plugging and sulfur poisoning (sources: cysteine and methionine). The main sources of the sulfide were studied and when adding cysteine or methionine to the feed solution, the conversions declined nearly linearly over time. It was found that both cysteine and methionine strongly adsorb on the Ru/C and it results in poisoning of the catalyst.

Due to previous interest in the substrate alanine, it was chosen to be studied as a non-sulfur-containing amino acid impurity. Results showed a significant drop in lactic acid conversion with the addition of alanine. However, when the feed stream was replaced by pure lactic acid, the conversion returned and remained at its original value. It was postulated that alanine reversibly and more strongly adsorbs on the catalyst surface, blocking the adsorption and reaction of lactic acid. These results are consistent with Jere et al.'s results (discussed earlier). Based on all of the studies, it appears that partial plugging of the pores and reversible amino acid (sulfur containing) adsorption are the main contributors to the reduced catalyst efficiency. Initial design considerations have been identified from this work and depending on purification requirements and cost, a more efficient biorefinery could be pursued.

Most recently published, Pimparker et al. studied the hydrogenation of three amino acids (alanine, serine, and valine) and their mixtures to their respective alcohols.[63] The hydrogenation conditions were at 403 K (reported as 130 °C), 1100 psi (reported as 7.0 MPa H_2), with 0.12 to 0.5 M feed concentration and 5-20% excess H_3PO_4. Results indicated nearly comparable hydrogenation rates for alanine and serine (nearly complete conversion after 3.5 h), with significantly lower reactivity for valine (~10% conversion after 3.5 h). However, a selectivity of ~90% was achieved with both alanine and valine, compared with 70% for serine. A second-order polynomial was fit to the concentration vs time data and differentiation of the curves allowed rate data to be calculated. Initial rate data was used to estimate an activation energy and as seen previously in our research group, a nonlinear dependence on initial concentration was observed. The hydrogenation reactions appear to not be first order with respect to the amino acid concentration. The activation energies were calculated: alanine, E_a = 88.5 kJ/mol; serine, E_s = 83.1 kJ/mol; and valine, E_v = 95.5 kJ/mol and were comparable to values reported earlier by our research group (Jere et al. reported alanine, E_a = 86.4 kJ/mol).

Mixed amino acid studies were conducted and the results indicated that as serine or valine is added to alanine, the alanine conversion decreases. The conversion continued to decrease as the amount of competing amino acid is increased (similar results as Chen et al., discussed earlier). Using an equimolar amount of competing amino acid (either serine or valine), the alanine conversion drops from nearly 100% to ~40% after 5 h of reaction time. A kinetic model was again developed to describe the hydrogenation reactions. Using the model developed by Jere et al. (discussed above) a two-site

Langmuir-Hinshelwood kinetic mechanism was proposed. Again, it was assumed that the protonated amino acids adsorb on one type of surface catalytic site (S_1) and the hydrogen dissociatively adsorbs on a second type of site (S_2). The optimized rate constants at 403 K for serine, alanine, and valine were 0.018, 0.016, and 0.0015 kmol/(kgcat h), respectively. The adsorption coefficients were calculated to be 56, 24, and 124 M^{-1} for serine, alanine, and valine, respectively. The larger adsorption affinity for valine (as evidenced also by its essentially zero-order behavior) is not completely understood. Lastly, the Langmuir-Hinshelwood rate expression allows for insight into the relative surface concentrations of hydrogen and amino acid on the catalyst. For a single amino acid the relative concentrations (conditions: 0.22 M amino acid concentration; 0.3 M H_3PO_4) of vacant, H_3PO_4 occupied, and amino acid-occupied surface sites was 9%, 52%, and 39%. In experiments with two amino acids the site distribution was 4% vacant, 35% H_3PO_4, 15% alanine, and 46% serine. Thus, the amount of active sites occupied by the original amino acid (alanine) decreased from 39% to 15%, resulting in a decreased conversion rate.

Chapter 2. EXPERIMENTAL

2.1 Hydrogenation Studies

The catalytic studies were conducted in water, a "green" solvent, as opposed to the more traditional gas-phase hydrogenation widely used in the petrochemical industry. Advantages of developing aqueous-phase conversion reactions include the following: a) most bio-based feedstocks are produced and readily handled in water solution; b) nonvolatile organic acids can be converted without having to be esterified, as required for vapor-phase conversion; c) energy costs associated with vaporizing and condensing the process streams are reduced; d) feed purity is less critical; e) the low concentration of non-volatile residuals from fermentation need not be removed in liquid-phase processing as they must be in vapor phase conversion; and f) conversion temperatures well below the boiling point of the acid or its ester are possible.

2.1.1 Materials

Several three-carbon and two-carbon organic acid substrates were chosen in order to evaluate the extent to which the alpha substituent affects the hydrogenation rate. Substrates included the following substituents: -H, $-CH_3$, -OH, $-N^+H_3$, $-OCH_3$, $-N^+H_2CH_3$, $-N^+H(CH_3)_2$, and $-N^+(CH_3)_3$ (note: purchased as commercially available HCl salt $(CH_3)_3N^+CH_2COOH$). Feeds were purchased from Aldrich Chemical Co. The acid used in the reaction was ACS grade 85% phosphoric acid (J.T. Baker). Water used was of HPLC grade purity (J.T. Baker, USA). Ultra high purity hydrogen (AGA Gas 99.999%) was used for all runs. One wt% dry 5% Ru/C, pre-reduced under H_2 with 0.25 M substrate and 0.3 M H_3PO_4 in water was used. These quantities corresponds to a 50:1

substrate:Ru ratio (5% x 1 g /101.07 = ~0.5 mmol of total Ru and 100 mL x 0.25 M = 25 mmol of substrate). As detailed by Jere, the acid was needed for successful hydrogenation of the amino acids due to the zwitterionic nature of amino acids and the requirement of a protonated carboxylic acid group for hydrogenation. In order to be consistent, the H_3PO_4 was added to all experiments.

A 5% ruthenium on carbon powder catalyst obtained from PMC, Inc. (Severville, TN) was used for all experiments. The particles had a N_2 BET surface area of 716 m^2/g, porosity of 0.6, a mean diameter of 150 microns, and a bulk density of 800 kg/m^3. The as-received ruthenium metal dispersion was 8.8% (measured by volumetric hydrogen chemisorption in a Micromeritics ASAP 2010 instrument). This corresponds to a metal surface area of 1.6 m^2/g catalyst. Upon receiving the catalyst it was 50.9 wt % slurry in water. For all experiments and associated reaction rates a dry catalyst basis was used.

2.1.2 Batch Reactor System

A 300 mL continuously stirred steady-state batch reactor (Parr Instrument Co, USA) equipped with a gas entraining impeller was used for all of the reactions. The temperature was maintained to ±1 °C using a temperature controller that would either heat or cool the vessel in order to ensure the temperature set point. The reactor was constructed of 316 stainless steel and rated to a maximum pressure of 3000 psi at 350 °C. Analyses were performed during the course of the reaction via a liquid sampling system. The experimental conditions include reaction temperatures between 70 °C and 150 °C with the majority of the experiments conducted at 130 °C, 1000 psi H_2, and six hours

reaction time. Hydrogen was added throughout the reaction, as needed, in order to maintain the pressure. The sample composition was analyzed every 30-60 minutes using high-pressure liquid chromatography, for which ~1-2 mL of solution was removed from the reaction vessel.

2.1.3 Reaction Procedure

The reaction procedure consisted of pre-reducing 1 g dry weight (2.036 g wet) of Ru/C catalyst under 250 psi hydrogen at 250 °C, overnight. The reactor vessel was purged three times with nitrogen to flush out oxygen, then heated to the desired temperature. The impellor was set to ~100 rpm to facilitate a consistent temperature throughout the vessel. Following the reduction the reactor was cooled to room temperature and the hydrogen vented.

A carrier vessel was attached to the reactor and a 0.25 M aqueous organic acid solution was charged into the reactor using hydrogen. After charging the reactor it was again purged three times with hydrogen. After the final purge, the heating and stirring (~1000 rpm) were initiated. When the reactor vessel reached the desired temperature, it was pressurized with hydrogen and a sample was taken. This sample was known as time zero, or the start of the reaction. Reaction temperatures were between 70 and 150 °C. Hydrogen pressure was set to 1000 psi for all reactions. Reaction times usually were six hours with samples being taken and analyzed every 30-60 minutes. At the end of the experiment, the vessel was cooled and the pressure was released.

2.1.4 Organic Acid Analysis

2.1.4.1 HPLC Analysis

High-pressure liquid chromatography (HPLC) was used in the analysis of the hydrogenation reactions. Two analytical methods for each substrate and product set evaluated were required. A meticulous protocol of analytical standards and techniques was used. Internal standards were used for all experiments and the calibration of each compound was verified before and after all samples for a particular experiment. These methods allowed the absolute error of each data point to be assessed. In addition, several control experiments were designed to evaluate both the accuracy and repeatability of the analysis method.

Method 1

A Bio-Rad Aminex HPX-87H column was used for all substrates, excluding the amino acids. The mobile phase consisted of 5 mM H_2SO_4. A Waters 410 Differential Refractometer and Hitachi UV Detector set to a wavelength of 210 were used for the detection. To ensure a constant injection volume a LDC/Milton Roy Autosampler was employed. The pump was a Spectra-Physics SP8810 Precision Isocratic Pump. The sample loop was 10 mL and the flow rate was optimized to 0.6 mL/min. Before each analysis a standard mix was run to evaluate the daily performance of the instrument with respect to the calibration curve. If a measurement error of more than 2-5% was obtained, new calibration standards were prepared and a new calibration was performed. The calibration curves were 3-point curves for all compounds (0.02, 0.06, and 0.1 M). The mobile phase consisted of 5 mM H_2SO_4.

2.1.4.2 pH Analysis

The pH of the liquid samples was measured and recorded using a bench top pH meter. The meter was calibrated before each use using solutions of pH 4, 7, and 10.

2.2 H/D Exchange Studies

Valuable information related to retention of stereochemistry during hydrogenation, has been ascertained by our group using H/D exchange studies. To build upon the knowledge gathered from the hydrogenation of α-substituted organic acids, an extensive H/D exchange study was done with glycine and its N-methylated analogs and will be discussed in this thesis.

2.2.1 Materials

All substrates were reagent-grade, including glycine (crystalline, 99%), sarcosine (98%), N,N-dimethylglycine (99%), betaine (98%), betaine hydrochloride (99%), ethanolamine (99%), N-methylethanolamine (98%), N,N-dimethylethanolamine (98%), choline chloride (98%), and choline bicarbonate (80%) were obtained and used as purchased from Aldrich Chemical Co. HPLC grade purity water was used for all aqueous phase experiments (J.T. Baker, USA). The hydrogen used was ultra high purity (Aga Gas, 99.999%) and the deuterium was ultra high purity (Spectra Gases). For deuterium exchange experiments, deuterium oxide (Sigma Aldrich, 99.9%) was used in place of water.

2.2.2 Batch Reactor System

Paramagnetic broadening was observed in early ^1H NMR studies, presumably caused by solution contact with the stainless steel reactor and its parts. Thus, extensive effort was put forth to minimize the amount of stainless steel exposed to the reaction mixture. The 300 mL stainless steel batch reactor (Parr Instrument Co.) was custom coated with a Teflon based material by Unconventional Solutions (Milford, MI). The stainless steel dip tube used for liquid sample removal was replaced with a glass dip tube. A Teflon tube was placed over the stirring shaft. The stainless steel impellor was replaced with a titanium impellor. The stainless steel cooling loop was removed from the system. This eliminated the opportunity for both heating and cooling; therefore, in order to compensate for the lack of dual-control, the rate of heating was slowed. A glass tube was placed over the stainless steel thermocouple. The glass tube was filled with a small amount of water to facilitate the heat transfer.

2.2.3 Reaction Procedure

The reaction procedure consisted of pre-reducing 1 g dry weight (2.036 g wet) of Ru/C catalyst under 500 psi hydrogen at 150 °C, overnight (although the hydrogenation studies above had used 250 °C, it was necessary to reduce the temperature from 250 °C to 150 °C in order to maintain the integrity of the Teflon lining). The lower temperature of 150 °C proved to be sufficient; however, a longer reduction time (overnight) was used (as opposed to 4 h). Several experiments were conducted using either a catalyst reducing temperature of 250 °C or 150 °C to evaluate whether there was an effect on the hydrogenation reaction. For the substrate glycine (0.25 M) with 0.3 M H_3PO_4 at 130 °C

and 1000 psi H_2, the hydrogenation rate was nearly identical for both reducing conditions. The reactor vessel was purged, heated to the desired temperature, and stirred using the same method as described previously.

The carrier vessel was attached to the reactor and the 0.25 M aqueous (D_2O) solution was charged into the reactor using hydrogen or deuterium. The charged reactor was then again purged three times with hydrogen or deuterium. After the final purge, the heating and stirring (~1000 rpm) were initiated. When the reactor vessel reached the desired temperature, it was pressurized with hydrogen and a sample was taken. This sample was defined as time zero, or the start of the reaction. Reactions were usually conducted at temperatures between 50 and 100 °C. Hydrogen or deuterium pressure was set to 1000 psi. Reaction times usually were six hours with samples being taken and analyzed every 30-60 minutes. At the end of the experiment, the vessel was cooled and the pressure was released.

2.2.4 Amino Acid Analysis

Both HPLC and ^1H NMR were used in the analysis of the H/D exchange studies. Results from the HPLC allowed for quantitation of the various substrates and products for each sample (samples collected every 30-60 min for six hours). Results from the ^1H NMR allowed for individual isotopomer ratios to be calculated for each sample. Using these data, kinetic models were developed in order to model and understand the deuterium exchange behavior.

2.2.4.1 HPLC Analysis

Method 2

A Hewlett Packard Series II 1090 liquid chromatograph instrument with a Waters 410 differential refractometer and Hitachi UV detector model L-4000H was used for the amino acid analyses. The mobile phase was 0.01% acetonitrile in 0.05 M phosphoric acid.

2.2.4.2 ^{1}H NMR

Liquid samples were analyzed using a Varian 500 MHz superconducting NMR-spectrometer operating at 499.738 MHz interfaced with a Sun Microsytems Ultra 5 UNIX console. NMR tubes with an outer diameter of 5 mm were used (Wilmad-Labglass, Buena, NJ). A glass insert (2 mm outer diameter; 1.25 mm inner diameter) filled with 0.25 M acetic acid internal standard was used for all experiments. The chemical shift of the internal standard was set to 1.9008 ppm. The integration area of the internal standard was set to 30 for all experiments and based on calibration curves, the concentrations of the observable amino acid isotopomers were calculated.

Chapter 3. CALCULATIONS

3.1 ^{1}H NMR Peak Fitting and Deconvolution

3.1.1 NMR Calibration Calculations

The slope of the area versus the concentration for all compounds was determined both experimentally and mathematically. Experimentally, three-point calibration curves were constructed for all amino acid and amino alcohol compounds. On average, the slope of the calibration curves was 9. Mathematically, the ratio of outer NMR tube to inner insert tube volume was calculated based on the dimensions of the tubes. Equation 1 below was used for the calculation.

Equation 1. NMR tube ratio: outer-to-insert volume

$$= \frac{\left((OD - wt)^2 - \left(OD_{in}{}^2\right)\right)}{ID_{in}{}^2}, \text{ where}$$

OD = outer diameter (mm) of outer NMR tube

wt = wall thickness (mm) of outer NMR tube

OD = outer diameter (mm) of NMR insert

ID_{in} = inner diameter (mm) of NMR insert

Using the low and high values specified by the manufacturer for the dimensions, an average of 9.008 ± 0.298 was calculated for the volume ratio. The prepared concentration of the internal standard, acetic acid, was 0.249 M. The peak integral for the internal standard, acetic acid, was set to 30. Thus, the peak area per hydrogen for the internal standard was 10.

3.1.2 Peak Fitting Equations

The data from the ^{1}H NMR was exported into Excel and using a Lorentzian function, the peak integrals were determined by fitting the data and using deconvolution. The general equation for a Lorentzian function is found in equation 2:

Equation 2. Lorentzian lineshape

$$= \left(\frac{g}{\pi}\right) * \frac{1}{\left((x - x_0)^2 + g^2\right)}$$, where g = half-width and x_0 = unshifted peak center

The integrated area of this function is unity.

Global values and local values were defined. For each H/D exchange reaction, after Fourier transform and phasing, the NMR spectra were exported into Excel as x,y data where y represented the peak height and x represented the peak position, ppm. The data were then analyzed in parallel as a set. For each such set, the fitting procedure defined quantities that were global (i.e. common to all spectra) and those that were local (i.e. specific to a given spectrum). Global values included isotope shifts, coupling constants, and multiplet proportions, while local values included chemical shift, baseline offset, linewidth, and of course, the individual deconvoluted peaks' intensities. Least-squares fitting to all datapoints was used to align and quantitate the Lorentzian functions. The respective fractional areas were then scaled to molarities using the ratios of measured total substrate peak integral to that of the internal standard. Modeled spectra and their integrals were plotted and compared to the originals to ensure accuracy. In the case of a triplet, a triplet scaling factor was defined. And in the case of a quintet, a quintet outer and inner scaling factor was defined.

The equation used for fitting the data is below (3, 4, 5). It is broken into three parts representing the singlet (CH_2 or CH_3), triplet (CHD or CH_2D) and quintet (CHD_2) resonances. In the case of fitting the data which represented the methylene, only the first two parts of the equation (3 and 4) were used. The portion of the equation used to fit a quintet was omitted due to the fact that for the methylene the singlet represented CH_2, and the triplet represented CHD. However, in the case of the methyl, all three parts of the equation were used (3,4,5). The singlet represented CH_3, the triplet represented CH_2D, and the quintet represented CHD_2.

Equation 3. Singlet peak fit

$$= \text{baseline offset} + \left(\frac{(a1)*\left(\frac{g}{\pi}\right)}{(x - x_0)^2 + g^2} \right)$$

Equation 4. Triplet peak fit

$$+\left(a3*\left(\frac{g}{3\pi}\right)\right)$$

$$+\left[\frac{s3}{\left((x - x_0 + IS + HD)^2 + g^2\right)} + \frac{1}{\left((x - x_0 + IS)^2 + g^2\right)} + \frac{s3}{\left((x - x_0 + IS - HD)^2 + g^2\right)}\right]$$

Equation 5. Quintet peak fit

$$+\left(a5*\left(\frac{g}{9\pi}\right)\right)$$

$$*\left[\begin{array}{l}\dfrac{s5_{out}}{\left(\left(x-x_0+2*IS+2*HD\right)^2+\left(s5_{out}*g\right)^2\right)}+\dfrac{2*s5_{in}}{\left(x-x_0+2*IS+HD\right)^2+\left(s5_{in}*g\right)^2} \\ +\dfrac{3}{\left(\left(x-x_0+2*IS\right)^2+\left(g\right)^2\right)} \\ +\dfrac{2*s5_{in}}{\left(\left(x-x_0+2*IS-HD\right)^2+\left(s5_{in}*g\right)^2\right)}+\dfrac{s5_{out}}{\left(x-x_0+2*IS-2*HD\right)^2+\left(s5_{out}*g\right)^2}\end{array}\right]$$

Samples were analyzed using ^{1}H NMR every 30-60 minutes of the reaction. Using the above models to fit the full time point sets of NMR spectra, the global values described above were optimized for all time points. The local values were individually optimized for a particular time point (i.e. NMR spectrum). The local linewidth was defined by the global linewidth multiplied by the local broadening. The global linewidth for the singlet was usually in the range of 0.0006 to 0.001 ppm. The global linewidth for the triplet was usually slightly larger and in the range of 0.0009 to 0.002 ppm. The global isotope shift was between 0.013-0.015 ppm. The global H-D coupling constant was 0.003 to 0.006. The local values were dependent on the individual experiment.

Starting with a good estimate of the global and local values, the sum of the squares error was minimized for each spectrum using Solver. Once the fits were optimized for individual spectra, Solver was run on all spectra to obtain one set of values for each experiment. The sum of the integrals was calculated for both the actual data and the

fitted data and compared. Using the amplitudes ($a1$, $a3$, and $a5$), the mol% of singlet, triplet, and quintet was calculated.

3.1.3 Peak Integration Calculations

MestReC is a powerful NMR software package used for analyzing high-resolution NMR data (Mestrelab Research, Spain www.mestrec.com). The raw FID data was exported to Excel, then to calculate the individual concentration of isotopomers, the below equations were solved.

Equation 6. Total H concentration for each spectrum at time t

$$[\mathrm{H}] = \frac{[IS]^{*}(\mathrm{area}_{s,t})}{9.008^{*}\left(\frac{\mathrm{area}_{IS,t}}{\#\ \mathrm{of\ H}}\right)}, \text{ where}$$

$[IS]$ = concentration of the internal standard, acetic acid (0.24881)

$\mathrm{area}_{s,t}$ = area of the sample at time t

$\mathrm{area}_{IS,t}$ = area of the internal standard, acetic acid, at time t (set to 30)

# of H = 3, for the 3 methyl hydrogens in acetic acid (internal standard)

The value 9.008 is the slope of the calibration curve for the sample versus the standard (see NMR Calibration Calculations 3.1.1). The area fractions as [H] were determined using the following equations (7,8,9). The variables $a1$, $a3$, and $a5$ represent the mol% of the singlet, triplet, and quintet, respectively. For example, to calculate the singlet mol%, $a1$, for methylene the amplitude of the singlet is divided by 2; divided by the sum of the amplitude of the singlet divided by 2 plus the amplitude of the triplet.

Equation 7. Singlet area fraction

$$= [H]_t * \left(\frac{a1}{a1 + a3 + a5} \right)$$

Equation 8. Triplet area fraction

$$= [H]_t * \left(\frac{a3}{a1 + a3 + a5} \right)$$

Equation 9. Quintet area fraction

$$= [H]_t * \left(\frac{a5}{a1 + a3 + a5} \right)$$

The concentration of isotopomers at each time point can then be calculated using the equations below.

Equation 10. CH_2 concentration

$$[CH_2]_t = \frac{(area)_{CH_2}}{2}$$

Equation 11. CHD concentration

$$[CHD]_t = (area)_{CHD}$$

Equation 12. CD_2 concentration

$$[CD_2]_t = ([CH_2]_{t0} + [CHD]_{t0}) - ([CH_2]_t + [CHD]_t)$$

The equations for the methyl are analogous to the above equations. Next, the peak areas of each of the isotopomers can be derived using the following equation.

Equation 13. Peak area of individual isotopomer

$$(\text{area}_S)_t = \frac{[S]_t * \left(\frac{\text{area}_{IS}}{\#\text{ of H}}\right) * 9.008}{[IS]}$$, where S = individual isotopomer

The conversion, yield and selectivity can be calculated from the concentrations of the individual isotopomers. Equations 14, 15, and 16 were used.

Equation 14. Conversion

$$= \frac{[S]_{t0} - [S]_t}{[S]_{t0}}$$, where S = individual isotopomer and t_0 = time zero

Equation 15. Yield

$$= \frac{[S]_t}{[S]_{t0}}$$

Equation 16. Selectivity

$$= \frac{\text{yield}}{\text{conversion}}$$

3.2 H-D Content Inventory

3.2.1 Percent H in Water

The molecular weight of H_2O is 18.015 g/mol and the molecular weight of D_2O is 20.028 g/mol, and at 25 °C, their respective densities are 0.9971 and 1.104 g/mL. Thus their concentrations are 55.34 and 55.14 M, respectively. Their equivalent hydrogen or deuterium concentrations are 110.68, $[H]_{H2O}$, and 111.28, $[D]_{D2O}$. The internal standard, acetic acid, in the insert had a bench concentration of 0.248 M (at 25 °C), thus the equivalent hydrogen concentration was 0.746 M. The peak area of the internal standard

was set to 30. Using the ratio of the outer-to-insert volume of 9.008, the concentration in the insert was calculated to be 0.083 M (not the true concentration, but would be equivalent to this if it had been in the whole volume). During all calculations the untruncated values were used until the end.

If the water was H_2O (no D_2O or HOD) then the water peak should integrate to 40,173.

Equation 17. Peak area of water in sample

$$\left(\frac{[\mathrm{H}]_{\mathrm{H_2O}}}{[IS]_{\mathrm{in}}}\right) * (\mathrm{area})_{IS} = 40{,}173$$

The acetic acid was prepared in deuterium oxide and the ^{1}H NMR of acetic acid was taken in the outer NMR tube (not the insert). If the water in the internal standard, acetic acid, was composed of H_2O (no D_2O or HOD) then the water peak should integrate to 4,462.

Equation 18. Peak area of water in internal standard

$$\left(\frac{[\mathrm{H}]_{\mathrm{H_2O}}}{[IS]}\right) * (\mathrm{area})_{IS} = 4{,}462$$

When measured, the peak area of the water in the acetic acid was 52.52, thus the %H in the deuterium oxide of the internal standard was taken as 52.52/4,462, thus 1.2%.

3.2.2 Percent H in Sample

The molarity of hydrogen and deuterium could be determined experimentally from the NMR integrals and also mathematically by the following equations.

Mathematical:

The initial liquid volume in the reactor, V_L, was 100 mL. The pressure, P, was 1000 psi (68.046 atm). The temperature, T, was 100 °C (373.15K). The initial gas volume, V_g in the reactor, was 200 mL. Using the below equations, an example calculation for sarcosine will be carried out.

Equation 19. Moles of deuterium in D_2O (l)

$$\text{moles of } D_L = \left(\frac{\rho * V_L}{mw}\right), \text{ where mw = molecular weight}$$

The moles of D_L are 5.55, thus in D_2O there are 11.11 moles of D. In practice, we will assume [H] and [D] are equal to ~111 (used 111.11).

Equation 20. Moles of hydrogen in H_2 (g)

$$\text{moles of } H_g = 2 * \left(\frac{P * V_g}{R * T}\right), \text{ where R = ideal gas constant}$$

The moles of H_g are 0.438, thus in H_2 there are 0.876 moles of H.

Equation 21. Substrate – NH_x contribution

$$\text{moles of } H_N = x * [\text{substrate}] * V_L, \text{ where [substrate] is the prepared bench concentration}$$

The typical bench substrate concentration is 0.25 M, thus for sarcosine the moles of H_N are 0.05 (x=2).

Equation 22. Substrate - methylene (CH_2) and methyl contribution y*(CH_3)

$$\text{moles of } H_C = (2 + y * 3) * [\text{substrate}] * V_L \text{, where y = number of methyls}$$

Again, using the typical bench substrate concentration of 0.25 M, the moles of H_C in sarcosine are 0.125 (y=1). Using equation 19 to calculate the moles of deuterium and equations (20, 21, and 22) for the sum of the moles of H in the different isotopomers, the H-D inventory can be determined.

Equation 23. Time zero H-D inventory

$$\%H_{t0} = \left(\frac{\sum \text{moles of H}}{\sum \text{moles of H} + \sum \text{moles of D}} \right) * 100$$

The sum of the moles of H at time zero is calculated from equations 20, 21, and 22 and equal 1.05 for sarcosine. The sum of the moles of D at time zero was calculated from equation 19 and equal 11.11. Thus, the $\%H_{t0}$ in the sample (sarcosine) is 8.6%.

Equation 24. Molarity of H at time zero

$$[H]_{t0} = [H]_{H_2O} * \left(\frac{\sum \text{moles of H}}{\sum \text{moles of H} + \sum \text{moles of D}} \right)$$

Based on the above calculations, the molarity of H at time zero for sarcosine is 9.602 mol/L (again where $[H]_{H2O} = 111.11$).

Equation 25. Molarity of D at time zero

$$[D]_{t0} = [H]_{H_2O} - [H]_{t0}$$

The molarity of D (for 0.25 M sarcosine in D_2O) at time zero is calculated to be 101.51 mol/L.

Once the reactor has reached the reaction temperature, the vessel is pressurized and the reaction is started. A sample (~2.5 mL, $V_{removed}$, which is equal to 0.14 moles) is removed and is referred to as the "time zero" sample. Then, the hydrogen and deuterium composition of the remaining solution is calculated from the NMR analyses using the below equations.

Equation 26. Moles of D (l) at time zero

$$\text{moles of } D_{t0} = 2 * \left(\frac{V_{removed} * \rho}{mw} \right) * \left(\frac{\sum \text{moles of D}}{(\sum \text{moles of H}) - \text{moles of } H_C + \sum \text{moles of D}} \right)$$

Equation 27. Moles of H (l) at time zero

$$\text{moles of } H_{t0} = 2 * \left(\frac{V_{removed} * \rho}{mw} \right) * \left(\frac{(\sum \text{moles of H}) - \text{moles of } H_C}{(\sum \text{moles of H}) - \text{moles of } H_C + \sum \text{moles of D}} \right)$$

The number of moles of H_C are subtracted out from the total moles of H at time zero because at time zero a negligible amount of methylene and methyl hydrogens are exchanged, thus more deuterium is removed. However, after time zero a H-D equilibrium is assumed. After the sample (~2.5 mL) is removed, the reactor is re-pressurized to 1000 psi. The amount of hydrogen re-introduced to the reactor is ~100 psi. Thus the moles of hydrogen added at that time can be calculated from the equation below.

Equation 28. Moles of H (g) at time zero

$$\text{moles of } H_{g_{t0}} = 2 * \left(\frac{P * V_g}{R * T} \right), \text{ where R = ideal gas constant}$$

From this point, it is an iterative process whereby the composition can be re-calculated after each sample (~2.5 mL) is removed.

Equation 29. Moles of D (l) at time t

$$\text{moles of } D_{tl} = \text{moles of } D_L - \text{moles of } D_{t0}$$

Equation 30. Total moles of H (l) and H (g)

$$\text{moles of } H_{tl} = \left(\sum \text{moles of H}\right) - \text{moles of } H_{t0} + \text{moles of } H_{g,t0}$$

Equation 31. %H at time t

$$\%H_{tl} = \frac{\text{moles of } H_{tl}}{\text{moles of } H_{tl} + \text{moles of } D_{tl}}$$

Equation 32. Molarity of H at time t

$$[H]_{tl} = [H]_{H_2O} * (\%H)_{tl}$$

Equation 33. Molarity of D at time t

$$[D]_{tl} = [H]_{H_2O} - [H]_{tl}$$

After this point, the process repeats. The time 2 sample is taken (~2.5 mL) and the new composition of the solution is calculated. After the reaction is complete, the final sample composition (%H, $[H]_{tf}$, $[D]_{tf}$) can be compared with the experimental values obtained from the NMR integrals. The results from both methods were in agreement.

3.3 Kinetic Rate Data Determination

3.3.1 Concentration Calculations

The peak areas from the ^{1}H NMR fitting are used to calculate the concentration of the individual isotopomers for each sample time. The methylene carbon is referred to as "A" and the methyl carbon is referred to as "C". The concentrations at time zero were determined using the internal standard, acetic acid, and the ratio of area to concentration. Again, the slope was determined to be 9.008, the [IS] = 0.25 M, and the peak area was set to 30. All concentrations after time zero were based on the initial concentration of the individual isotopomer and ratio of the area at time, t, to the area at time zero. However, the total concentration of all isotopomers was verified using HPLC to ensure the starting material was not consumed before time zero (once the reactor has reached reaction temperature and pressure) of the experiment. The below equations were used.

Equation 34. AH_2 concentration at time zero

$$[AH_2]_{t0} = \frac{\left(\frac{\left(\text{area } AH_2/2\right)_{t0}}{\left(\text{area } IS/3\right)_{t0}}\right) * [IS]}{9.008}$$

Equation 35. AH_2 concentration at time t

$$[AH_2]_t = [AH_2]_{t0} * \frac{\left(\text{area } AH_2/2\right)_t}{\left(\text{area } AH_2/2\right)_{t0}}$$

Equation 36. AHD concentration at time t

$$[AHD]_t = [AH_2]_{t0} * \frac{\left(\text{area } AHD/2\right)_t}{\left(\text{area } AHD/2\right)_{t0}}$$

Equation 37. AD_2 concentration at time t

$$[AD2]_t = [AH_2]_{t0} - \left([AH_2]_t + [AHD]_t\right)$$

Equation 38. CH_3 concentration at time zero

$$[CH_3]_{t0} = \frac{\left(\frac{\left(\text{area } CH_3/3\right)_{t0}}{\left(\text{area } IS/3\right)_{t0}}\right) * [IS]}{9.008}$$

Equation 39. CH_3 concentration at time t

$$[CH_3]_t = [CH_3]_{t0} * \frac{\left(\text{area } CH_3/3\right)_t}{\left(\text{area } CH_3/3\right)_{t0}}$$

Equation 40. CH_2D concentration at time t

$$[CH_2D]_t = [CH_3]_{t0} * \frac{\left(\text{area } CH_2D/2\right)_t}{\left(\text{area } CH_3/3\right)_{t0}}$$

Equation 41. CHD_2 concentration at time t

$$[CHD_2]_t = [CH_3]_{t0} * \frac{(\text{area } CHD_2)_t}{\left(\text{area } CH_3/3\right)_{t0}}$$

Equation 42. CD_3 concentration at time t

$$[CD3]_t = [CH_3]_{t0} - \left([CH_3]_t + [CH_2D]_t + [CHD_2]_t\right)$$

Equation 43. Aqueous hydrogen concentration in H_2O and HOD

$$[H]_L = (\text{area } H_L) * \left(\frac{\text{average}([AH_2],[CH_3])}{\text{average}((\text{area } AH_2/2),(\text{area } CH_3/3))} \right),$$

where $\left(\frac{\text{average}([AH_2],[CH_3])}{\text{average}((\text{area } AH_2/2),(\text{area } CH_3/3))} \right)$ is equivalent to a calibration based on the internal standard (IS) acetic acid concentration to area and equals 9.008.

Equation 44. Aqueous deuterium concentration in D_2O

$$[D]_L = \left(\frac{1000}{9.008} \right) - [H]_L$$

The sum of the hydrogen area can be calculated for each time point, and during the course of the reaction the areas for C-H sites decrease as hydrogen is replaced with deuterium.

Equation 45. Sum of the H area

$$\sum H_{area} = (\text{area } AH_2) + (\text{area } AHD) + (\text{area } CH_3) + (\text{area } CH_2D) + (\text{area } CHD_2)$$

The aqueous hydrogen concentration data was fit to the following equation over time.

Equation 46. Aqueous hydrogen concentration equation of fit

$[H]_L = A * \exp(-B * t) + C * t + D$, where A, B, C, and D are fitted variables and t = time

The sum of the squares error is minimized to determine the fitted variables.

3.3.2 Kinetic Model A: 10-variables

The time zero concentrations for the isotopomers of the methylene and methyl sites were determined from the time zero areas for each. The kinetic model assumed that the adsorption/desorption of H_2O (or D_2O) is fast and that the ratio of H:D in the solution represents the H:D on the surface. This assumption proved to be adequate for the experiments with 1000 psi D_2 and D_2O. However, after reviewing the results from the experiments with 1000 psi H_2 and D_2O a modified kinetic model was used (to be described later). Using the original kinetic model, for experiments with 1000 psi H_2, the initial hydrogen on the surface was assumed to be 111.11. The initial deuterium on the surface was assumed to be zero. For experiments with 1000 psi D_2, the initial deuterium on the surface was set to the amount of deuterium in the liquid (usually less than 3%) and the hydrogen was equal to the difference between 111.11 and the amount of deuterium. The hydrogen and the deuterium in the liquid at any time, t, was calculated using the rate equations in 47.

The experiment describing the hydrogen-deuterium exchange on the methylene carbon is depicted by the following two reversible, consecutive first-order reactions. Again the role of the catalyst, including the adsorption/desorption events are represented in the aqueous hydrogen (H_L) and consequently the aqueous deuterium (D_L).

Equation 47. Rate equations for H/D exchange at the methylene position

$$AH_2 + D_s \underset{k\text{-}_{1A}}{\overset{k_{1A}}{\rightleftharpoons}} AHD + H_s$$

$$AHD + D_s \underset{k_{2A}}{\overset{k_{2A}}{\rightleftharpoons}} AD_2 + H_s$$

Hence, doing a numerical step-by-step fit, where the time-step increment (Δt) was 0.5 min, the equations become:

Equation 48. CH_2 concentration at time t

$$[AH_2]_t = [AH_2]_{t-\Delta t} - \left(k_{1A} * [AH_2]_{t-\Delta t} * [D]_{L,t-\Delta t} - k_{-1A} * [AHD]_{t-\Delta t} * [H]_{L,t-\Delta t}\right) * \Delta t$$

Equation 49. CHD concentration at time t

$$[AHD]_t = [AHD]_{t-\Delta t} - \left[\begin{array}{l}\left(k_{-1A} * [AHD]_{t-\Delta t} * [H]_{L,t-\Delta t} + k_{2A} * [AHD]_{t-\Delta t} * [D]_{L,t-\Delta t}\right) \\ -\left(k_{1A} * [AH_2]_{t-\Delta t} * [D]_{L,t-\Delta t} + k_{-2A} * [AD_2]_{t-\Delta t} * [H]_{L,t-\Delta t}\right)\end{array}\right] * \Delta t$$

Equation 50. CD_2 concentration at time t

$$[AD_2]_t = [AD_2]_{t-\Delta t} - \left(k_{-2A} * [AD_2]_{t-\Delta t} * [H]_{L,t-\Delta t} - k_{2A} * [AHD]_{t-\Delta t} * [D]_{L,t-\Delta t}\right) * \Delta t$$

The experiment describing the hydrogen-deuterium exchange on the methyl carbon is depicted by the following three reversible, consecutive first-order reactions.

Equation 51. Rate equations for H/D exchange at the methyl position

$$CH_3 + D_s \underset{k\text{-}_{1C}}{\overset{k_{1C}}{\rightleftharpoons}} CH_2D + H_s$$

$$CH_2D + D_s \underset{k\text{-}_{2C}}{\overset{k_{2C}}{\rightleftharpoons}} CHD_2 + H_s$$

$$CHD_2 + D_s \underset{k\text{-}_{3C}}{\overset{k_{3C}}{\rightleftharpoons}} CD_3 + H_s$$

Hence, doing a numerical step-by-step fit the equations are defined as follows.

Equation 52. CH3 concentration at time t

$$[CH_3]_t = [CH_3]_{t-\Delta t} - \left(k_{1C} * [CH_3]_{t-\Delta t} * [D]_{L,\,t-\Delta t} - k_{-1C} * [CH_2D]_{t-\Delta t} * [H]_{L,\,t-\Delta t}\right) * \Delta t$$

Equation 53. CH_2D concentration

$$[CH_2D]_t = [CH_2D]_{t-\Delta t} - \left[\begin{array}{l}\left(k_{-1C} * [CH_2D]_{t-\Delta t} * [H]_{L,t-\Delta t} + k_{2C} * [CH_2D]_{t-\Delta t} * [D]_{L,t-\Delta t}\right) \\ -\left(k_{1C} * [CH_3]_{t-\Delta t} * [D]_{L,t-\Delta t} + k_{-2C} * [CHD_2]_{t-\Delta t} * [H]_{L,t-\Delta t}\right)\end{array}\right] * \Delta t$$

Equation 54. CHD_2 concentration at time t

$$[CHD_2]_t = [CHD_2]_{t-\Delta t} - \left[\begin{array}{l}\left(k_{-2C} * [CHD_2]_{t-\Delta t} * [H]_{L,t-\Delta t} + k_{3C} * [CHD_2]_{t-\Delta t} * [D]_{L,t-\Delta t}\right) \\ -\left(k_{2C} * [CH_2D]_{t-\Delta t} * [D]_{L,t-\Delta t} + k_{-3C} * [CD_3]_{t-\Delta t} * [H]_{L,t-\Delta t}\right)\end{array}\right] * \Delta t$$

Equation 55. CD_3 concentration at time t

$$[CD_3]_t = [CD_3]_{t-\Delta t} - \left(k_{-3C} * [CD_3]_{t-\Delta t} * [H]_{L,\,t-\Delta t} - k_{3C} * [CHD_2]_{t-\Delta t} * [D]_{L,\,t-\Delta t}\right) * \Delta t$$

The 10-variables: k_{1A}, k_{-1A}, k_{2A}, k_{-2A}, k_{1C}, k_{-1C}, k_{2C}, k_{-2C}, k_{3C}, and k_{-3C} were calculated by minimizing the sum of the squares error between the experimental and the calculated concentrations for all measured time points. To verify that this was a short enough time increment for direct analysis of these multi-hour reactions we confirmed that the resulting k values were not significantly affected by further 2-fold shortening or lengthening of the time increment.

3.3.3 Kinetic Model B – 6 variables

The second kinetic model used to fit the data incorporated primary and secondary isotope effects. All of the rate variables above (Model A) represent the same hydrogen trading

processes except for the isotopes involved. Thus it should be possible to simplify the model. The equations from Model A were used in Model B, but here, the 10 rate variables were re-defined as isotope-perturbed instances of the same events in order to incorporate the possibility of a primary and or secondary isotope effect. The six rate variables used to optimize the data fit were: k_{iA}, p_A, s_A, k_{iC}, p_C, and s_C. The kinetic isotope effect at the methylene carbon and methyl carbon(s) is represented by k_{iA} and k_{iC}, respectively. A primary kinetic isotope effect arises when the bond to the isotopic substitution is broken at or before the rate-limiting step and for the methylene carbon and methyl carbon(s) is represented by p_A and p_C, respectively. When hydrogen-deuterium substitution is not involved in the bond breaking or bond making step, an isotope effect (albeit smaller) may still be observed and is represented by s_A and s_C for the methylene carbon and methyl carbon(s), respectively.

Equation 56. Forward and reverse rate constants for H/D exchange at the methylene position

$$k_{1A} = 2 * k_{iA}$$

$$k_{-1A} = \frac{k_{iA}}{p_A}$$

$$k_{2A} = \frac{k_{iA}}{s_A}$$

$$k_{-2A} = \frac{2 * k_{iA}}{(p_A * s_A)}$$

Equation 57. Forward and reverse rate constants for H/D exchange at the methyl position

$$k_{1C} = 3 * k_{iC}$$

$$k_{-1C} = \frac{k_{iC}}{p_C}$$

$$k_{2C} = \frac{2 * k_{iC}}{s_C}$$

$$k_{-2C} = \frac{2 * k_{iC}}{(p_C * s_C)}$$

$$k_{3C} = \frac{k_{iC}}{(s_C * s_C)}$$

$$k_{-3C} = \frac{3 * k_{iC}}{(p_C * s_C * s_C)}$$

The time step used in calculating the kinetic rate variables was 0.5 min.

Kinetic Model Modification

The kinetic model for isotope exchange was varied to explore the effects of various assumptions with the intent of optimizing the fit to the experimental data. Experiments were conducted with either 1000 psi H_2 or 1000 psi D_2 and for reactions at the same temperature, the calculated rate constants should be the same. Using the kinetic model discussed above, the H/D exchange for the experiments with 1000 psi H_2 and D_2O appeared to be going to fast for some of the early experimental points. This is partly due to the fact that in the kinetic model, the hydrogen and deuterium available for exchange with the substrate was assumed to be in equilibrium with the concentration of hydrogen or deuterium in the liquid. But from the experiments with H_2 and D_2O, it appears that

there is a delay in the substrates' H/D exchange reaction due to the time it takes to reach equilibrium among liquid, gas, and surface hydrogens.

For experiments with 1000 psi D_2, the aqueous hydrogen concentration is almost an order of magnitude lower than the typical 15% or so that is observed with H_2 (Figure 67). This time evolution is important, but also reflects the gas/liquid exchange. To attempt to address this, the hydrogen and deuterium available were defined by equations below. The equations for calculating the hydrogen and deuterium on the surface, assuming the amounts are in equilibrium with the liquid concentrations, at any time are below.

Equation 58. Expression for H on the surface at time t

$$H_{s,t} = [H]_{t-\Delta t} + (2*[AH_2]_{t-\Delta t} + [AHD]_{t-\Delta t} + 3*[CH_3]_{t-\Delta t} + 2*[CH_2D]_{t-\Delta t} + [CHD_2]_{t-\Delta t})$$
$$-(2*[AH_2]_t + [AHD]_t + 3*[CH_3]_t + 2*[CH_2D]_t + [CHD_2]_t)$$
$$-k_H*([D]_{L,t-\Delta t}*H_{s,t-\Delta t} - [H]_{L,t-\Delta t}*D_{s,t-\Delta t})$$

Equation 59. Expression for D on the surface at time t

$$D_{s,t} = 111.11 - H_{s,t}$$

The kinetics for the surface hydrogen incorporate the hydrogen-deuterium surface-liquid exchange represented by k_H. At any point in time, in the solution the sum of hydrogen and deuterium concentrations equals the total concentration [C_t]. During the reaction, we will assume the hydrogen on the surface and the deuterium concentration in solution is in equilibrium with the deuterium on the surface and the hydrogen concentration in solution.

Once the equilibrium between the hydrogen and deuterium is reached, their concentrations in the liquid and their respective amounts on the surface can be expressed by the equilibrium equation below.

Equation 60. Equilibrium expression for hydrogen and deuterium in the liquid and on the surface

$$[D]_L + H_s \rightleftharpoons [H]_L + D_s$$

Let $H_s + D_s = C_t$, the total catalyst site density (C_t) for hydrogen adsorption in the reactor. From this, the rate of deuterium on the surface versus time can be derived.

Equation 61. Rate of deuterium on the surface versus time

$$d(D_s)/dt = k * ([D]_L * H_s - [H]_L * D_s), \text{ thus}$$

$$= k * ([D]_L * (C_t - D_s) - D_s * ([C_t] - [D]_L))$$

Assuming the total concentration in solution is in equilibrium with the surface, then the total catalyst site density for hydrogen adsorption, C_t, equals the concentration of hydrogen and deuterium in the solution, $[C_t]$. Factoring this out of the equation, the effective rate constant can be described as $k*C_t$ and is defined as k_H in the rate equations. D_s is a variable and represents the fraction of total sites occupied by deuterium. This variable can be used in all kinetic expressions recognizing that all the rate constants will then also be effective rate constants with C_t in them, $k_H=k*C_t$.

Chapter 4. RESULTS AND DISCUSSION

4.1 Control Experiments

4.1.1 Hydrogenation Studies

Early research in our group highlighted the need for both catalyst and hydrogen pressure in the hydrogenation of organic acids.[25,48,49,50] Several control experiments have been performed and results confirm that molecular hydrogen and catalyst are required for the hydrogenation reaction. Using otherwise identical procedures, a reaction was performed replacing H_2 with helium. The catalyst was exposed to 1000 psi He pressure. No product formation was observed for the reaction of 0.25 M refluxed lactic acid at these conditions (H_2O, 130 °C, 1000 psi He, 1 g dry 5% Ru/C).

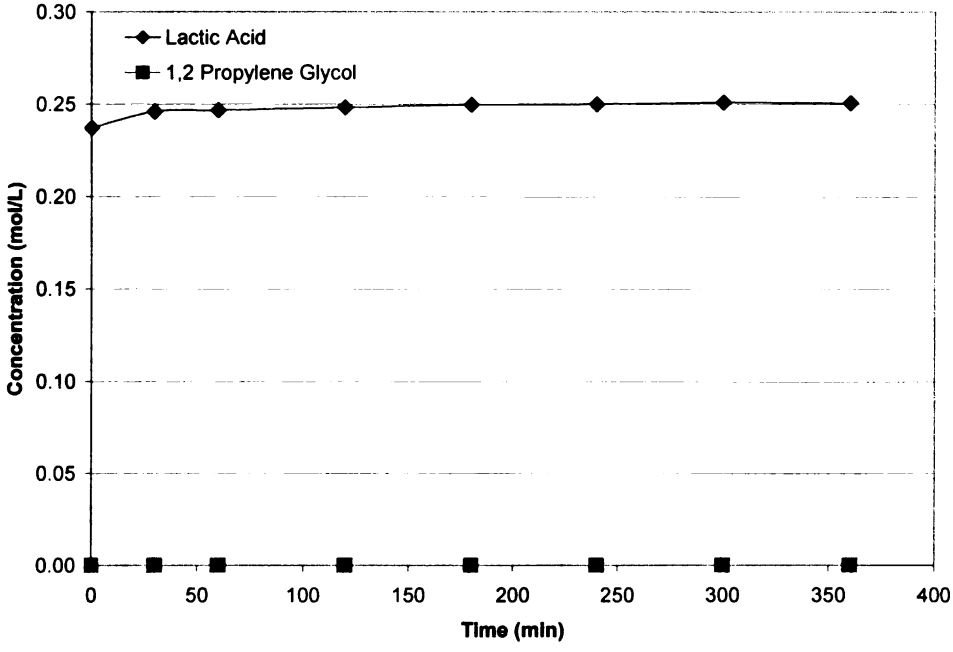

Figure 1. Hydrogenation of 0.25 M refluxed lactic acid (0.3 M H_3PO_4, H_2O, 130 °C, 1000 psi He, 1 g dry 5% Ru/C)

The concentrations of lactic acid and product alcohol, 1,2-propylene glycol, are shown in Figure 1. The purchased (Sigma-Aldrich) lactic acid was 85% (w/w) in H_2O, so before using, the water was removed by refluxing the lactic acid.

A reaction with 0.25 M refluxed lactic acid in the absence of 5% Ru/C catalyst was performed and the results indicated no product formation after six hours (0.3 M H_3PO_4, H_2O, 130 °C, 1000 psi H_2, no catalyst). The concentration data for lactic acid and the desired alcohol product, 1,2-propylene glycol are shown in Figure 2.

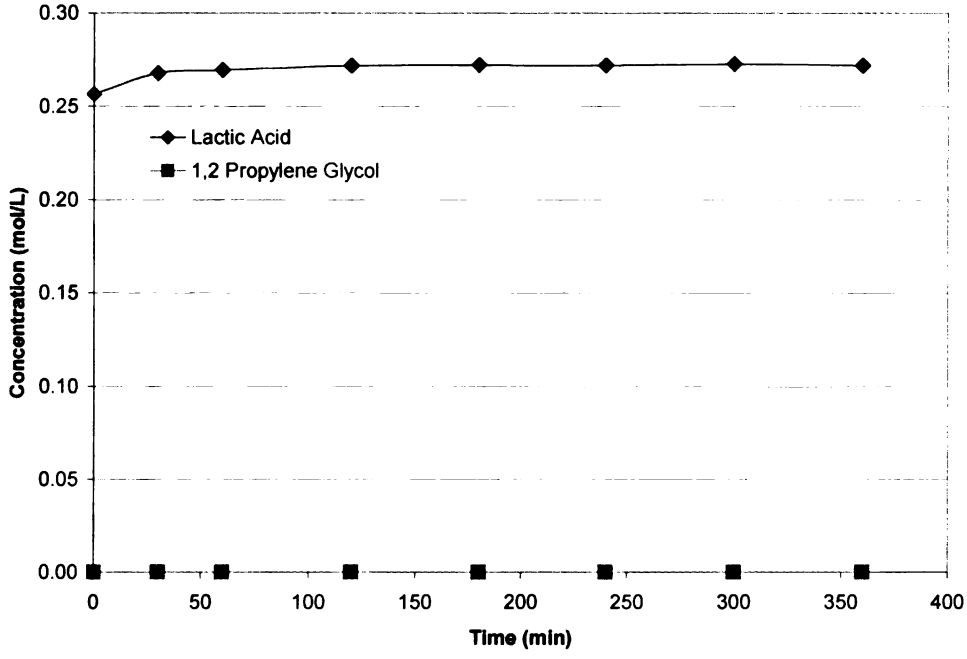

Figure 2. Hydrogenation of 0.25 M refluxed lactic acid (0.3 M H_3PO_4, H_2O, 130 °C, 1000 psi H_2, no catalyst)

For all experiments discussed in this thesis, the reaction procedure involves pre-reducing the 5% Ru/C catalyst under H_2 pressure (150 °C overnight with ~300 psi H_2). The sample is then injected and the reactor is heated to the reaction temperature, 130 °C (one-

step introduction of the solution). One-step introduction involves adding the substrate (0.25 M) at the point in which the reactor has reached the desired temperature. The next step is to immediately pressurize the vessel with H_2. The point when the H_2 is introduced is the point that the reaction is considered to have started (t = 0 min).

In some experiments a small amount of conversion was observed at time zero. So, a control experiment was designed to evaluate the effect of adding the substrate after the reaction vessel was at temperature and pressure. This was done in an effort to avoid any pre-reaction conversion that can occur during the heat up phase of the reactor. The refluxed lactic acid was mixed with 25 mL of water and set to the side. The other 77 mL (all H_2O) of the 102 mL solution was injected into the reactor and allowed to heat to the reaction temperature. Once at the desired temperature, the lactic acid solution was injected (two-step introduction of the solution). Results indicated no significant difference between this and introducing the sample at room temperature and allowing it to heat up (in the absence of H_2) in the reaction vessel to 130 °C (Figure 3). The bench concentration for the two-step was 0.32 M (1.3 M in 25 mL) and slightly higher than the traditional experiment in which the bench concentration is 0.25 M (one-step introduction).

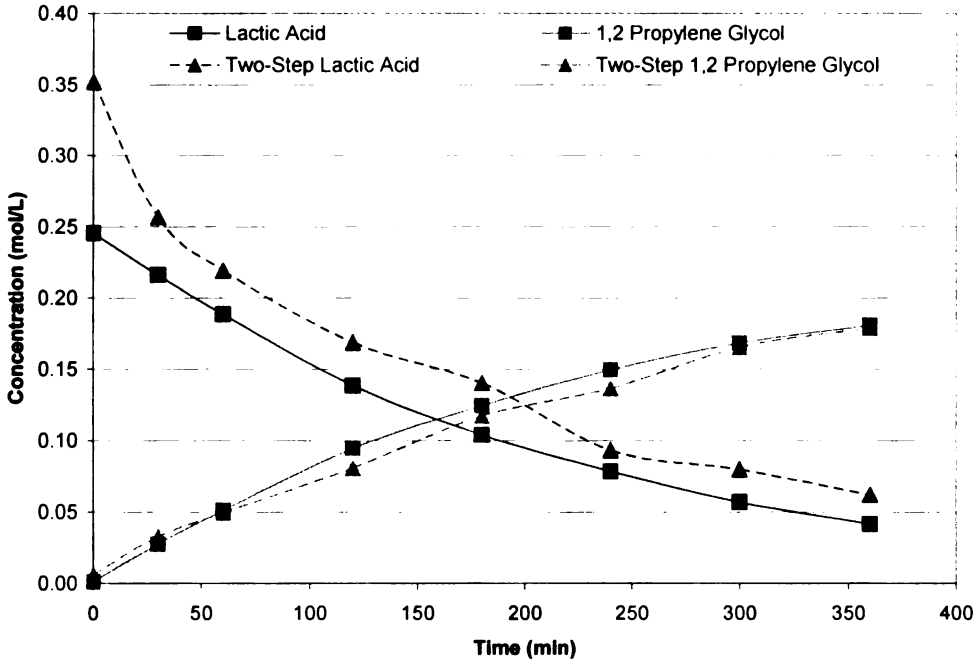

Figure 3. Hydrogenation of refluxed lactic acid (0.3 M H_3PO_4, H_2O, 130 °C, 1000 psi H_2, 1 g dry 5% Ru/C)

All hydrogenation experiments were carried out in aqueous solvent in the presence of 0.3 M H_3PO_4. A control experiment using 0.25 M glycolic acid (GA) in the absence of additional acid was conducted to determine the effect of equimolar H_3PO_4 on the hydrogenation rate. No significant difference in the conversion of glycolic acid and the yield of ethylene glycol (EG) was observed over six hours (H_2O, 130 °C, 1000 psi H_2, 1 g dry 5% Ru/C). The concentrations of glycolic acid and product alcohol, ethylene glycol, are presented in Figure 4.

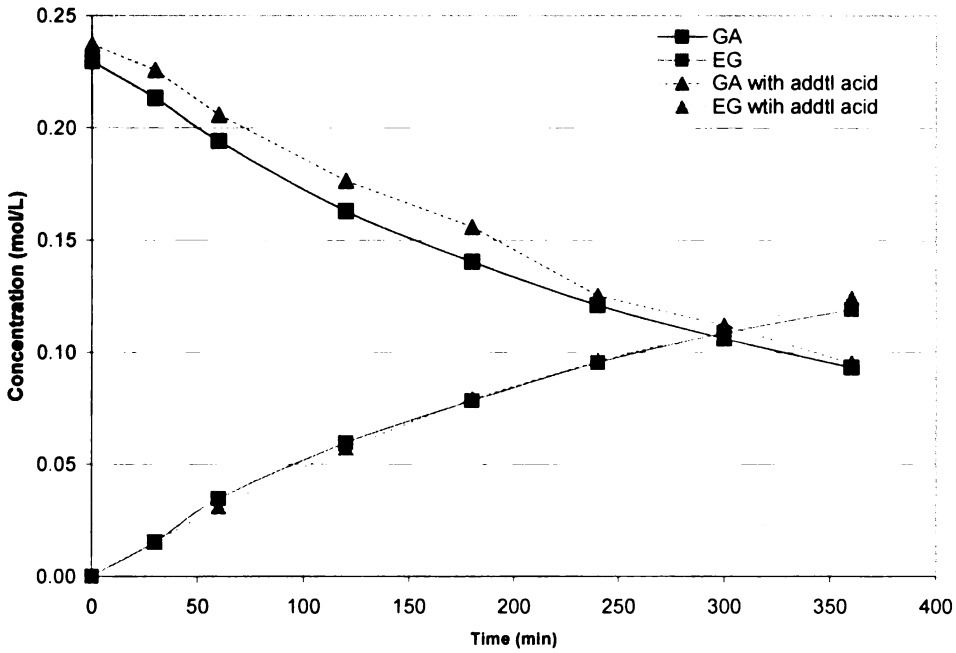

Figure 4. Hydrogenation of 0.25 M glycolic acid in the absence and presence of 0.3 M H_3PO_4 (H_2O, 130 °C, 1000 psi H_2, 1 g dry 5% Ru/C)

It is known from previous research in our group that the catalyst surface interacts with the solvent, substrate, and presumably the acid.[25,59,63] Thus, the presence of additional acid in the case of glycolic acid may not have a significant effect due to a high affinity of the glycolic acid for the catalyst surface, but this may not be true for every substrate and all conditions. The effect of H_3PO_4 on hydrogenation and H/D exchange will be discussed further in section 4.4.

4.1.2 H/D Exchange Studies

Several control experiments were conducted in the absence of the 5% Ru/C catalyst. An experiment with 0.25 M glycine in D_2O at 130 °C and 1000 psi H_2 pressure showed no deuterium incorporation after five hours of reaction. The ^1H NMR specifics for samples

taken at time zero and after five hours are shown below (Figure 5). Based on the ^1H NMR integrations using acetic acid as the internal standard, the concentration, at time zero and after five hours, was essentially unchanged. A very small, but visible amount of deuterium incorporation was observed, partly due to a small amount deprotonation at the α-carbon.

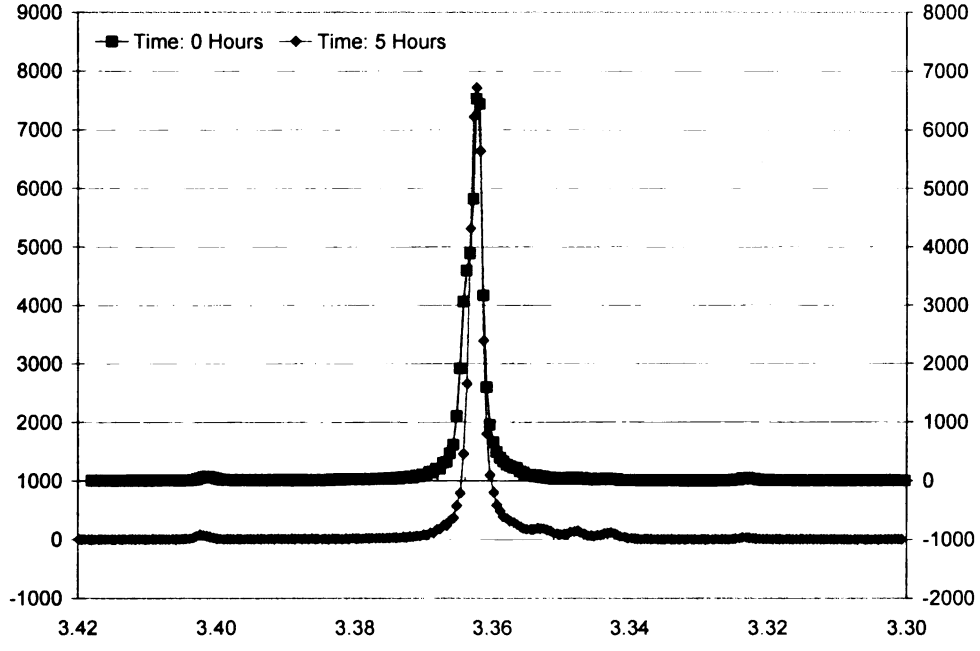

Figure 5. ^1H NMR of H/D exchange at the methylene position of 0.25 M glycine (D_2O, 130 °C, 1000 psi H_2, no catalyst)

An experiment with 0.25 M sarcosine in D_2O at 130 °C and 1000 psi H_2 pressure was allowed to react for six hours in the absence of the 5% Ru/C catalyst. About thirty percent of the methylene was partially deuterated during the reaction. The ^1H NMR of time zero and after six hours is shown in Figure 6. No observable deuterium incorporation was obtained at the N-methyl position on sarcosine after six hours. The ^1H NMR of time zero and after six hours is shown in Figure 7.

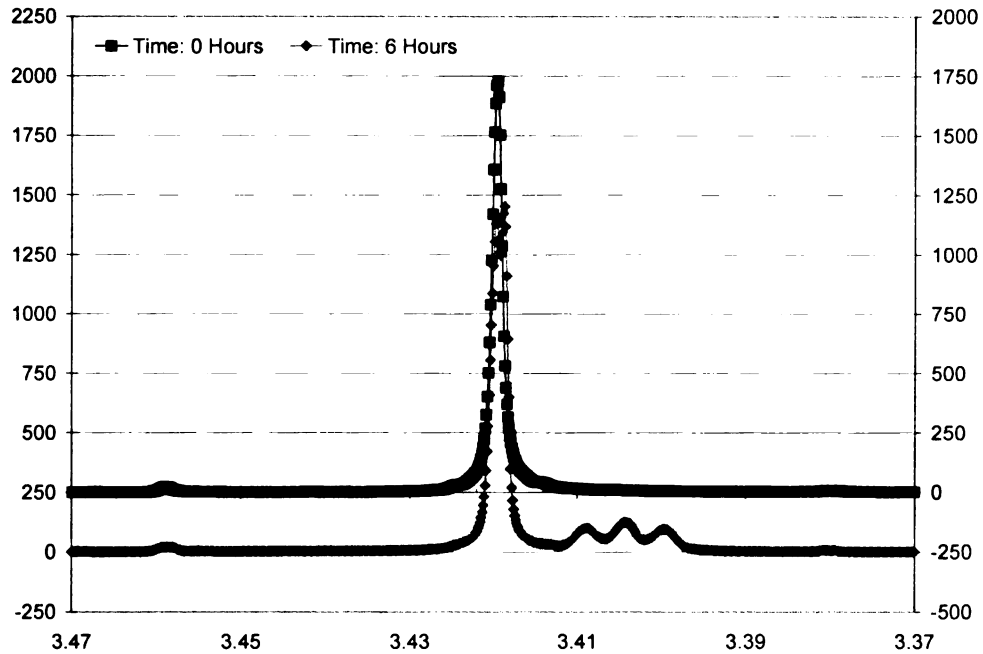

Figure 6. ^{1}H NMR of H/D exchange at the methylene position of 0.25 M sarcosine (D_2O, 130 °C, 1000 psi H_2, no catalyst)

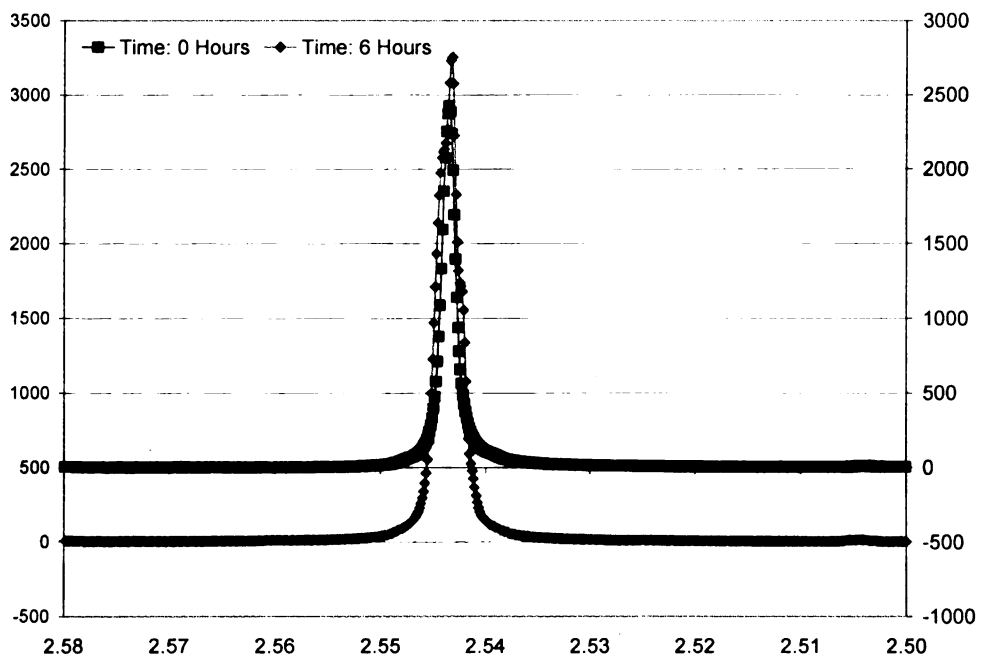

Figure 7. ^{1}H NMR of H/D exchange at the methyl position of 0.25 M sarcosine (D_2O, 130 °C, 1000 psi H_2, no catalyst)

The data were fit to the kinetic models discussed in chapter 3 (Figure 8). The H_2O and HOD experimental (symbols) and fitted (line) data refers to the percent H in water and is on the right y-axis (secondary y-axis). The experimental (symbol) and fitted (line) concentration of CH_2 (referred to as AH_2), CHD (referred to as AHD), and CD_2 (referred to as AD_2) are on the left y-axis (primary y-axis).

The rate constants for the hydrogens on the methylene carbon were calculated using the 10-variable model. The forward rate constant for the first hydrogen exchanged with deuterium was found to be $k_{1A}=9.8\text{x}10^{-6}$ L/mol/min, but the forward rate constant for exchanging the second hydrogen with deuterium was found to be $k_{2A}=0$ (both reverse rate constants were zero $k_{-1A}=0$, $k_{-2A}=0$). All rate constants have the units L/mol/min. There is an appreciable amount of H/D exchange at the methylene position (Figure 8). Results from the H/D exchange studies (to be discussed later) have shown that sarcosine is the most reactive substrate (as compared to glycine and N,N-dimethylglycine). So, the H/D exchange observed in this control experiment (no catalyst) may be partly due to some residual catalyst being present in the reactor lines or reactor wall. However, the majority of the H/D exchange is presumably due to the non-catalytic process of deprotonation of the weakly acidic zwitterion. The compound is most stable in the zwitterionic form. But, again at 130 °C there is a larger population of the higher energy form that can undergo deprotonation.

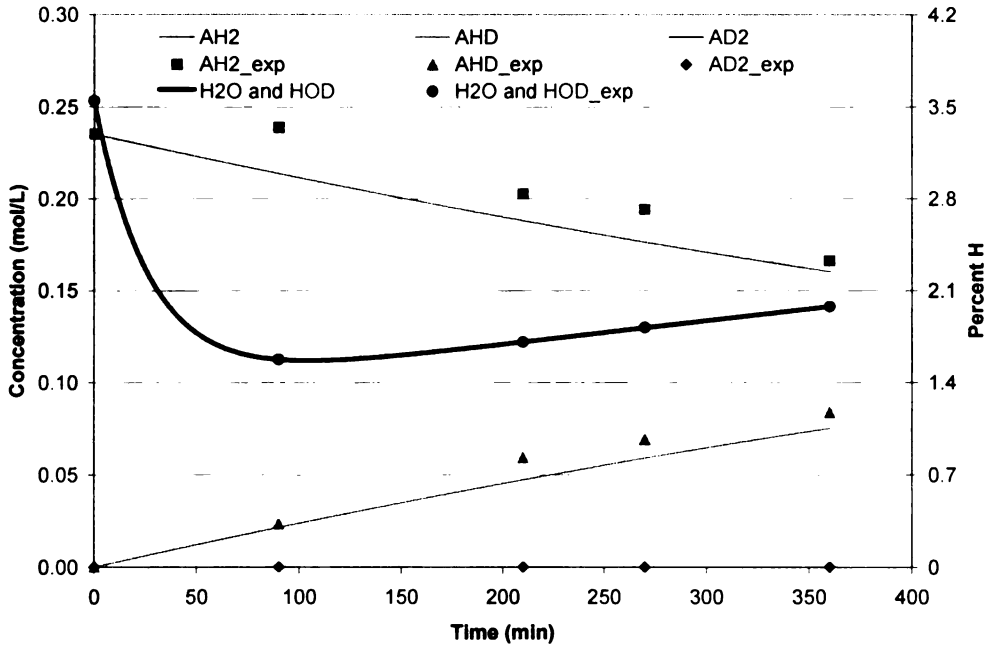

Figure 8. Fit of the kinetic rate data for 0.25 M sarcosine (D_2O, 130 °C, 1000 psi H_2, no catalyst)

A control experiment with 0.25 M choline bicarbonate in D_2O at 130 °C and 1000 psi H_2 was allowed to react for four hours in the absence of 5% Ru/C catalyst. Again, there was no observable deuterium incorporation at either of the two methylenes (3.88 ppm next to -OH and 3.32 ppm next to $-N^+(CH_3)_3$) or on the nitrogen methyl groups (3.02 ppm) (Scheme 29). This is an expected result and differs from the case of the amino acids in that there is not an activating carboxylate group to facilitate non-catalytic H/D exchange.

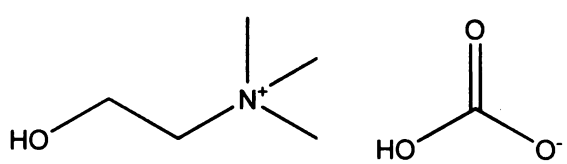

Scheme 29. Structure of choline bicarbonate

The ^{1}H NMR taken at time zero and after four hours for the more downfield methylene position (3.88 ppm) corresponding to the methylene next to the -OH is shown below (Figure 9). The ^{1}H NMR of time zero and after four hours for the more upfield methylene position (3.32 ppm) corresponding to the methylene next to the $-N^+(CH_3)_3$ is shown in Figure 10.

An experiment with choline bicarbonate was performed with 1 g dry 5% Ru/C (D_2O, 130 °C, 1000 psi H_2). Hydrogen exchanged with deuterium at all three positions on choline bicarbonate, however, the ^{1}H NMR peak data was too convoluted to distinguish between the CH_2 and CHD for the two methylene positions and the CH_3, CH_2D, and CHD_2 for the three N-methyl groups. So, the overall integrals were compared. From the results, the methylene hydrogens adjacent to the -OH group exchanged the most quickly reaching a total conversion of 58% after six hours (sum of CH_2 and CHD). The methylene hydrogens adjacent to the $-N^+(CH_3)_3$ and the N-methyl hydrogens exchanged at nearly an identical rate reaching a total conversion of 35% each after six hours. These results confirm that H/D exchange occurs faster at positions adjacent to an oxygen as opposed to a nitrogen. Further evidence for this will be discussed in the H/D exchange of ethanolamine.

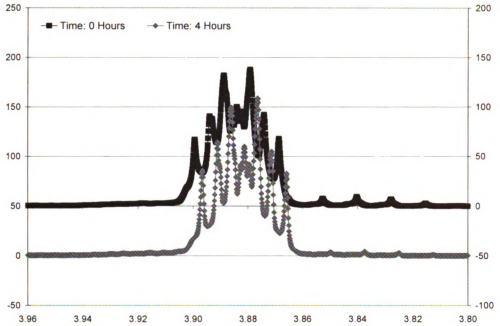

Figure 9. ^{1}H NMR of H/D exchange at the methylene position next to the –OH of 0.25 M choline bicarbonate (D_2O, 130 °C, 1000 psi H_2, no catalyst)

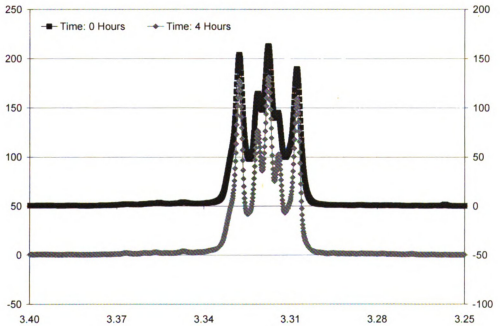

Figure 10. ^{1}H NMR of H/D exchange at the methylene position next to the $-N^{+}(CH_3)_3$ of 0.25 M choline bicarbonate (D_2O, 130 °C, 1000 psi H_2, no catalyst)

A control experiment with 0.25 M betaine ($(CH_3)_3N^+CH_2COO^-$) at 130 °C with 1000 psi H_2 in the absence of catalyst was compared with the identical experiment in the presence of 1 g dry 5% Ru/C. Figure 11 depicts the ^1H NMR for the methylene position at both time zero and after five hours for the experiment conducted in the absence of catalyst. The H/D exchange reaction occurs at a comparable rate in both the presence and absence of catalyst.

Figure 12 shows the ^1H NMR for the methylene position at both time zero and after five hours for the experiment conducted in the presence of catalyst. In the experiment with catalyst, after only three hours nearly 50% of the CH_2 is partially or fully deuterated. After six hours, 86% of the CH_2 is partially or fully deuterated. In contrast, the CH_3 peaks show no evidence of H/D exchange (in either the absence or presence of catalyst). The ^1H NMR of the nitrogen methyls after five hours of reaction time are presented in Figure 13 (no catalyst). The integration area and peak shape is unchanged throughout the course of the reaction.

The ^1H NMR at time zero and after five hours for the methyls on nitrogen for the experiment with betaine in the presence of 1 g dry 5% Ru/C are shown in Figure 14. Again, there is no H/D exchange on the nitrogen methyls even in the case of catalyst. The peak shape is the same for time zero and after five hours.

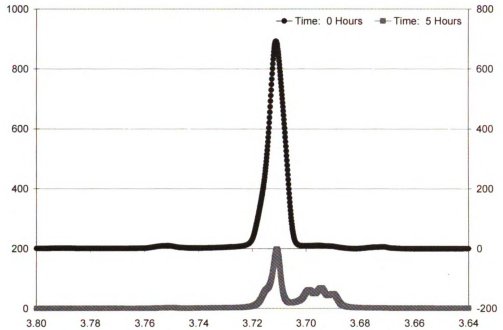

Figure 11. ^{1}H NMR of H/D exchange at the methylene position of 0.25 M betaine (D_2O, 130 °C, 1000 psi H_2, no catalyst)

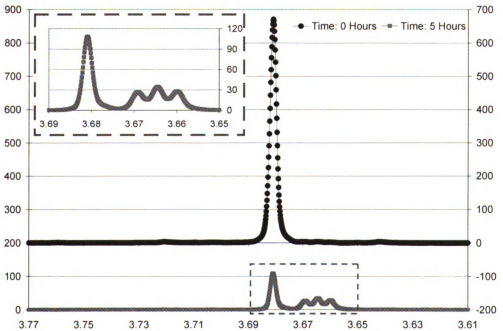

Figure 12. ^{1}H NMR of H/D exchange at the methylene position of 0.25 M betaine (D_2O, 130 °C, 1000 psi H_2, 1g dry 5% Ru/C)

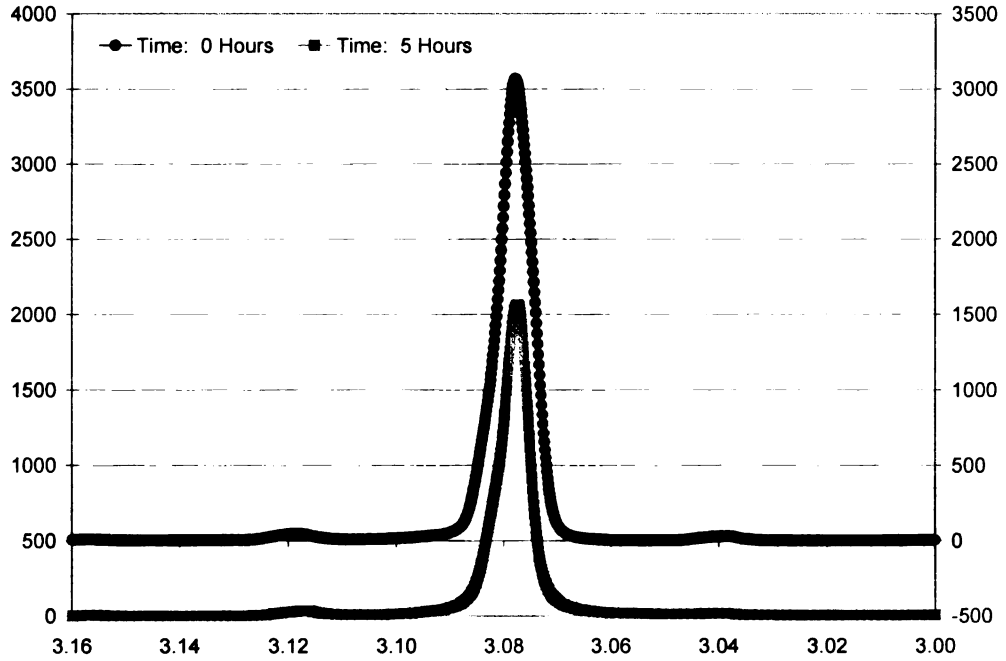

Figure 13. ^{1}H NMR of H/D exchange at the methyl position of 0.25 M betaine (D_2O, 130 °C, 1000 psi H_2, no catalyst)

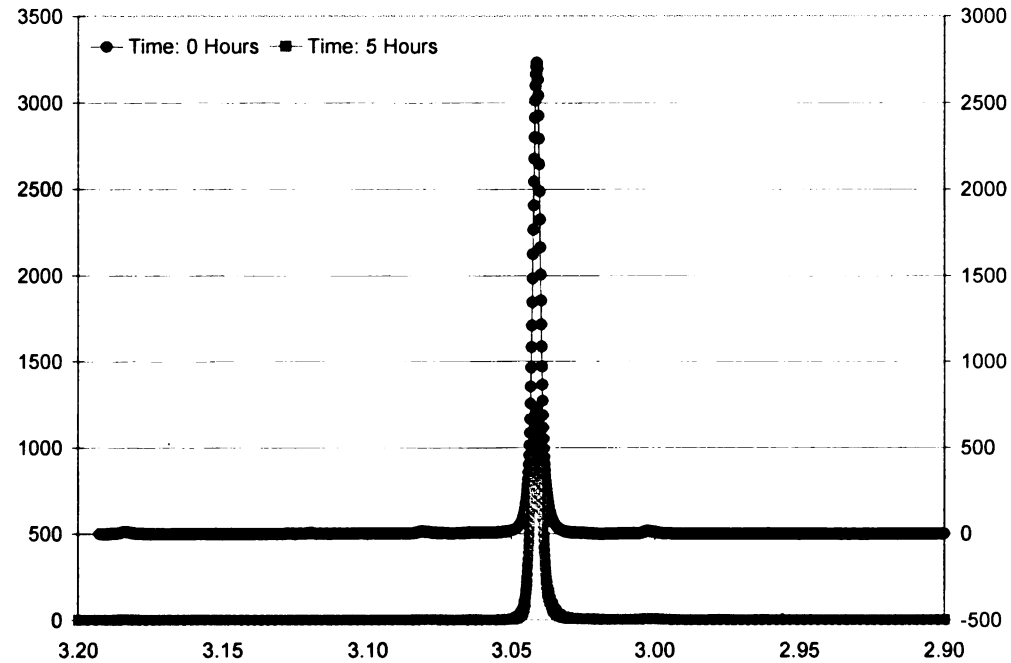

Figure 14. ^{1}H NMR of H/D exchange at the methyl position of 0.25 M betaine (D_2O, 130 °C, 1000 psi H_2, 1g dry 5% Ru/C)

Figure 15 shows the concentrations of CH_2, CHD, CD_2 and the 3 CH_3's over time. The hydrogens on the methyls of the positively charged nitrogen do not exchange. Although the peaks areas not the same height, the peak areas after six hours are about 6% less than the peak areas at time zero. This percentage loss is consistent across all experiments and may represent initial adsorption of the substrate into the catalyst. The rate constants for both experiments were calculated and using kinetic model A (Chapter 3.1.1). The forward rate constants for the experiment with no catalyst were: $k_{1A} = 3.5x10^{-5}$ and $k_{2A} = 2.6x10^{-4}$ L/mol/min. The forward rate constants for the experiment with 1g dry 5% Ru/C catalyst were: $k_{1A} = 4.1x10^{-5}$ and $k_{2A} = 1.6x10^{-2}$ L/mol/min. The rate of k_{1A} is very similar in both reactions suggesting that betaine is undergoing H/D exchange at the same rate irrespective of whether catalyst is present. This suggests that betaine is undergoing a non-catalytic mechanism for H/D exchange. This is supported by the work of Richard et al. They evaluated the acidity of the α-proton of betaine at 25 °C in D_2O and observed nearly 90% of exchange of the first α-proton via deprotonation by the hydroxide ion and formation of the intermediate enol.

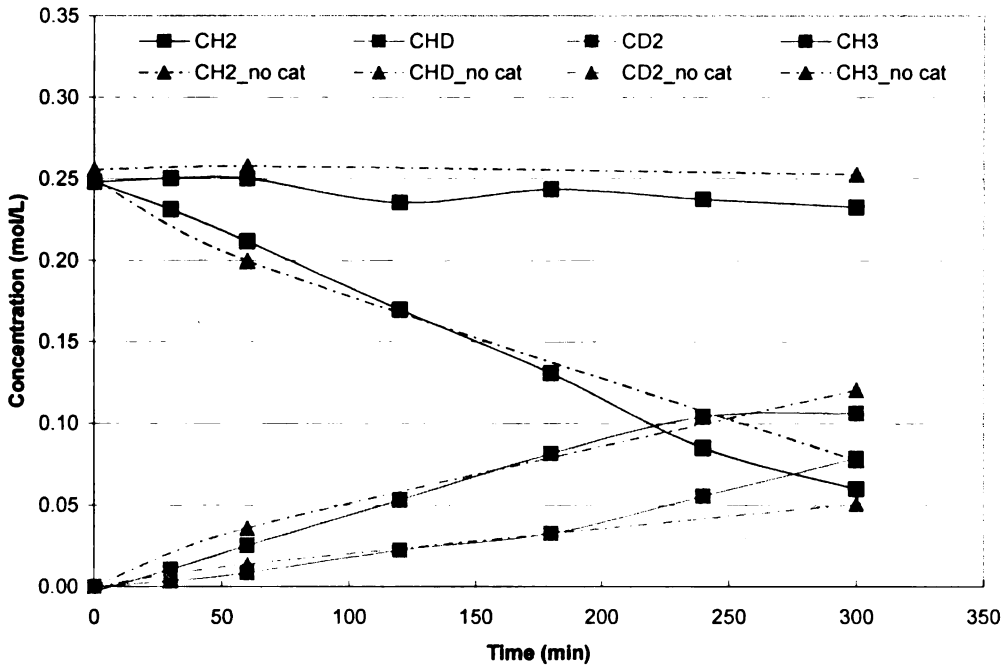

Figure 15. Concentrations of CH_2, CHD, and CD_2 of 0.25 M betaine with and without 1 g dry 5% Ru/C catalyst (D_2O, 130 °C, 1000 psi H_2)

4.2 Substrate Adsorption on the Catalyst/Carbon Support

4.2.1 Adsorption on Ru/C

An early observation in this research was the initial disappearance of substrate in the reaction vessel before reaction conditions were achieved. The concentration of the substrate was measured after preparing the solution on the bench (bench concentration). Again, the concentration was measured after it was exposed to the catalyst (reactor concentration). It was proposed that the substrate was being adsorbed (possibly irreversibly) onto the carbon support. When doubling the catalyst loading using refluxed lactic acid as the substrate, the initial concentration of substrate was reduced by more than half (Figure 16). This provides further evidence that the reaction is kinetically limited by catalyst sites and not by interphase mass transport. In addition, a control was

conducted with no H_2 pressure at room temperature, knowing that the hydrogenation reaction would not be occurring at these conditions, and an initial conversion of about 3.5% was observed, yet no products were detected. The amount "lost" or converted after the bench concentration is exposed to the catalyst is fairly consistent across all experiments.

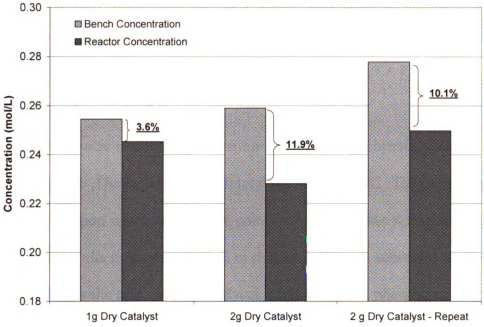

Figure 16. 0.25 M Refluxed lactic acid concentrations measured (bench and reactor)

It is not clear yet, whether all of the initial material adsorbed is desorbed and allowed to react or whether some amount of the substrate is permanently lost on the carbon support. In our research group, Peereboom et al. performed carbon adsorption experiments at room temperature (25 °C) using propylene glycol and glycerol (0.01 M to 2.0 M each) at room temperature and modeled the results using both Freundlich and Langmuir isotherms. Peereboom et al. observed that substrates adsorb on the catalyst and that propylene glycol has a greater preference for the carbon micropores over the bulk

solution than glycerol, due to its less hydrophilic nature. Using the Langmuir model, they found that the bulk glycerol concentration is not very different from the pore concentration. However, the pore concentration of propylene glycol is 5x larger than the glycerol concentration.[59] In general, it appeared that after time the molecules were getting torn apart and did not desorb. In order to further follow up, a Ru-free sample of the carbon support used in our Ru/C catalyst from PMC was obtained and adsorption studies with different substrates were conducted.

4.2.2 Adsorption on Carbon Support

Six substrates were evaluated to determine the amount of substrate adsorbed onto the carbon support. The carbon was 3310 lot #28850 from PMC. The percentage of water in the carbon support was 8.81%. Three-point calibration curves were run for each substrate using the methods described in chapter 2. The six substrates studied were: lactic acid, glycolic acid, propylene glycol, ethylene glycol, phosphoric acid, and *n*-butanol. Normally, in the experiments discussed in this thesis the ratio of moles of substrate to grams of dry catalyst has been 0.025 mol/g dry catalyst. Thus, in this work 5 mL of a concentration of 0.25 M substrate was combined with 0.05 g of dry catalyst resulting in the same ratio as most experiments.

The results indicated that 7% of lactic acid adsorbed onto the carbon support, more than any other substrate. Figure 17 presents all of the substrates (lactic acid = 7.1%, butanol = 5.7%, glycolic acid = 4.8%, propylene glycol = 3.4%, phosphoric acid = 1.0%, ethylene glycol = 0.8%). The error bars represent the measurement error as determined by the

relative standard deviation from the calibration curve for each substrate. The amount of lactic acid adsorbed on the carbon support is similar to the amount of lactic acid lost after being exposed to the 5% Ru/C catalyst. It can thus be assumed that most of the substrate lost is being adsorbed on the carbon support.

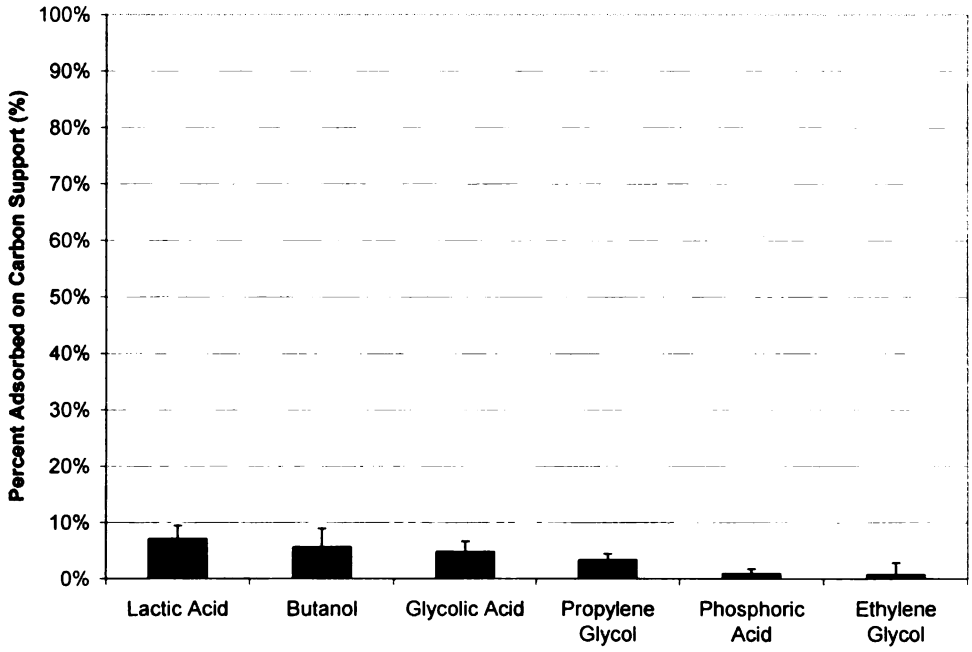

Figure 17. Substrate adsorption on the carbon support

4.3 Effect of HCl

4.3.1 Hydrogenation Studies

A precedent for chloride inhibition has been observed when using a ruthenium catalyst. In our research group, Dalavoy et al. performed electrocatalytic hydrogenation experiments using 11.1 mM lactic acid and a RVC electrode suffused with 5% Ru/C powder catalyst. The electrolytes examined were H_2SO_4, HCl, and $HClO_4$. At 90 °C in 0.01 M H_2SO_4 a yield of 9.8% propylene glycol was achieved after 9 hours and at the same conditions but with 0.01 M HCl instead, only 2.9% of propylene glycol was

achieved. The major product was lactaldehyde. Increasing the electrolyte to 0.1 M HCl yielded more propylene glycol after 48 hours (6.6%) than 0.1 M H_2SO_4 (2.7% yield of propylene glycol) (11.1 mM lactic acid, 100 mA, and 70 °C).

We continued this work and performed a pair of experiments with 0.25 M betaine hydrochloride ($(CH_3)_3N^+CH_2COOH{\bullet}Cl^-$) in the presence of 0.3 M H_3PO_4 at both 100 °C and 130 °C, 1000 psi H_2, and 1 g dry 5% Ru/C. The results were compared to identical experiments using 0.25 M betaine ($(CH_3)_3N^+CH_2COO^-$ (chloride-free)) at 100 °C, 130 °C, and 150 °C. None of the desired product, choline chloride, was formed from betaine hydrochloride hydrogenation. The effect of a slight excess of HCl may be to inhibit the hydrogenation reaction. Figure 18 shows the hydrogenation reaction of betaine hydrochloride.

Results for chloride-free 0.25 M betaine ($(CH_3)_3N^+CH_2COO^-$) at the same conditions (130 °C) indicated 41% conversion and formation of 7% product, choline, after six hours. When the reaction was run at 150 °C the reaction was faster and yielded a conversion of 74% and 17% choline yield. As the temperature was increased, more conversion of the substrate was observed. At a reaction temperature of 100 °C there is minimal conversion and no product formation. The results for all three temperatures (100 °C, 130 °C, and 150 °C) are presented in Figure 19.

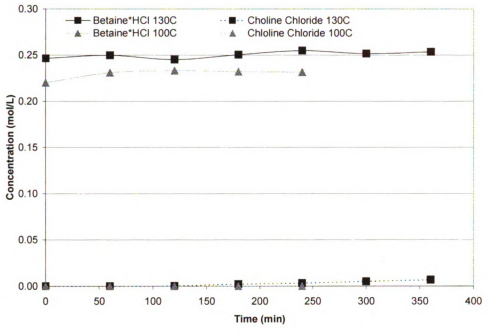

Figure 18. Hydrogenation of 0.25 M betaine hydrochloride (0.3 M H_3PO_4, H_2O, 100 °C and 130 °C, 1000 psi H_2, 1 g dry 5% Ru/C)

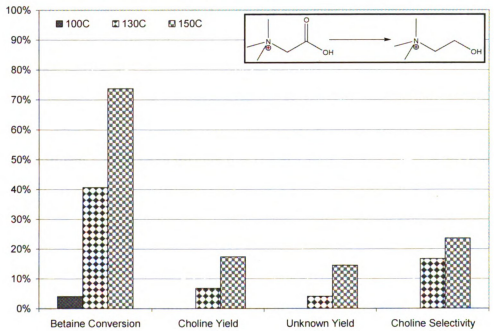

Figure 19. Hydrogenation of 0.25 M betaine after 6 hours (0.3 M H_3PO_4, H_2O, 100 °C, 130 °C, and 150 °C, 1000 psi H_2, 1 g dry 5% Ru/C)

When comparing the experiments using betaine hydrochloride and betaine at the same conditions, it appears that the presence of the chloride is inhibiting the hydrogenation reaction presumably due to the competitive interaction of the chloride with the catalyst surface.

There is an unknown peak that grew in at roughly the same rate as the choline. The unknown peak is most likely trimethyl amine. Due to the formation of the unknown peak in the experiment with 0.25 M betaine ($(CH_3)_3N^+CH_2COO^-$), an additional experiment was run in the absence of H_3PO_4 (150 °C, 1000 psi H_2, and 1 g dry 5% Ru/C) to evaluate whether the unknown peak was still formed. Results indicated no choline formation and no unknown peak formation after five hours. Part of the reason the unknown peak was not observed may be that if it is trimethylamine this good leaving group would be less stabilized in the absence of acid. No choline was formed because neutral betaine is in the zwitterionic form and hydrogenation of the carbonyl of the carboxylic acid will only occur if the carboxylic acid is protonated.

An experiment with 0.25 M glycine was run at 130 °C, 1000 psi H_2 in the presence of 0.3 M H_3PO_4 with 1 g dry 5% Ru/C in both the absence and presence of 0.3 M HCl. Addition of the HCl in proportion to the substrate was strongly inhibitory, cutting glycine conversion from 96% to 58% and ethanolamine yield from 80% to 25% after six hours. Figure 20 illustrates the results. In this experiment the amount of additional acid (0.3 M H_3PO_4 and 0.3 M HCl) is twice the amount (0.3 M H_3PO_4) used in our experiments with 0.25 M substrate and 1 g dry 5% Ru/C. Jere et al. examined the effect of excess H_3PO_4

and found a ~20% reduced alanine conversion (0.22 M alanine, 100 °C, 1000 psi H_2, and 1 g dry 5% Ru/C) with 0.6 M H_3PO_4 (as compared to 0.3 M H_3PO_4).[50] When further increasing the amount of H_3PO_4, the conversion continued to decrease slightly (~30% reduced conversion with 1.2 M H_3PO_4 as compared to 0.3 M H_3PO_4).

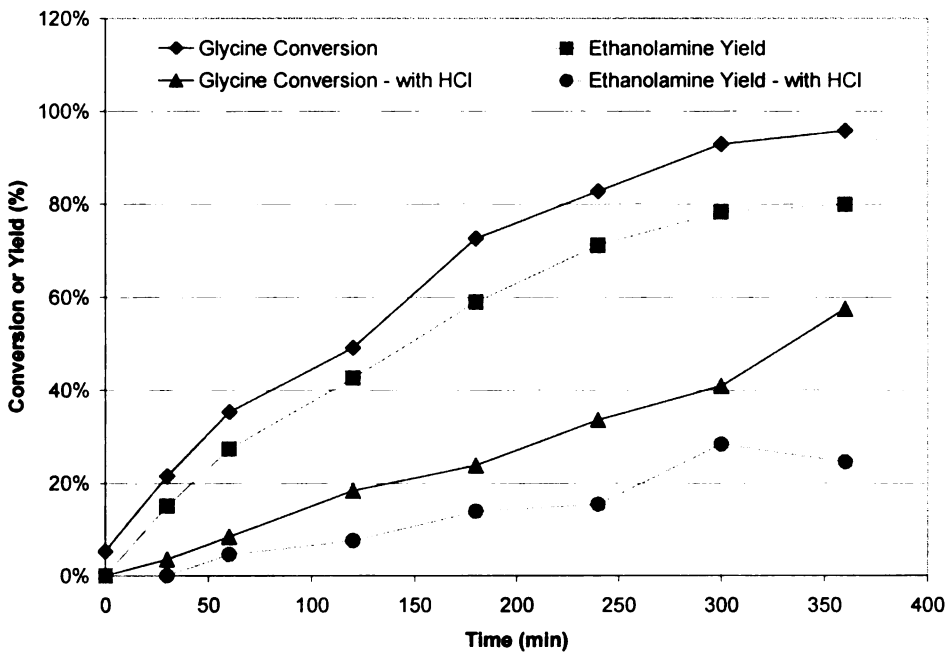

Figure 20. Hydrogenation of 0.25 M glycine in the absence and presence of 0.3 M HCl (0.3 M H_3PO_4, H_2O, 130 °C, 1000 psi H_2, 1 g dry 5% Ru/C)

An experiment was run with 0.125 M glycine at 130 °C with 1000 psi H_2 and slight excess equivalents of both H_3PO_4 and NaCl (0.15 M each) and 0.5 g dry 5% Ru/C to determine if NaCl had the same effect on the hydrogenation reaction. The same volume of solution was used (100 mL) so the substrate concentration was more dilute (not allowing a direct comparison). It appears that the HCl exerted a larger effect than NaCl but a direct comparison using the same substrate concentrations and catalyst amounts should be done. Figure 21 displays the conversion of glycine in the hydrogenation

reaction with no chloride (0.25 M glycine, 1 g dry 5% Ru/C, and 0.3 M H_3PO_4), with 0.3 M HCl (0.25 M glycine, 1 g dry 5% Ru/C, and 0.3 M H_3PO_4), and 0.125 M NaCl (0.125 M glycine, 0.5 g dry 5% Ru/C, and 0.15 M H_3PO_4). In the experiment with HCl, additional inhibition may be occurring due to the fact that HCl is a very strong acid (pKa ~ -4) and may be changing the sample media enough to slow the hydrogenation reaction.

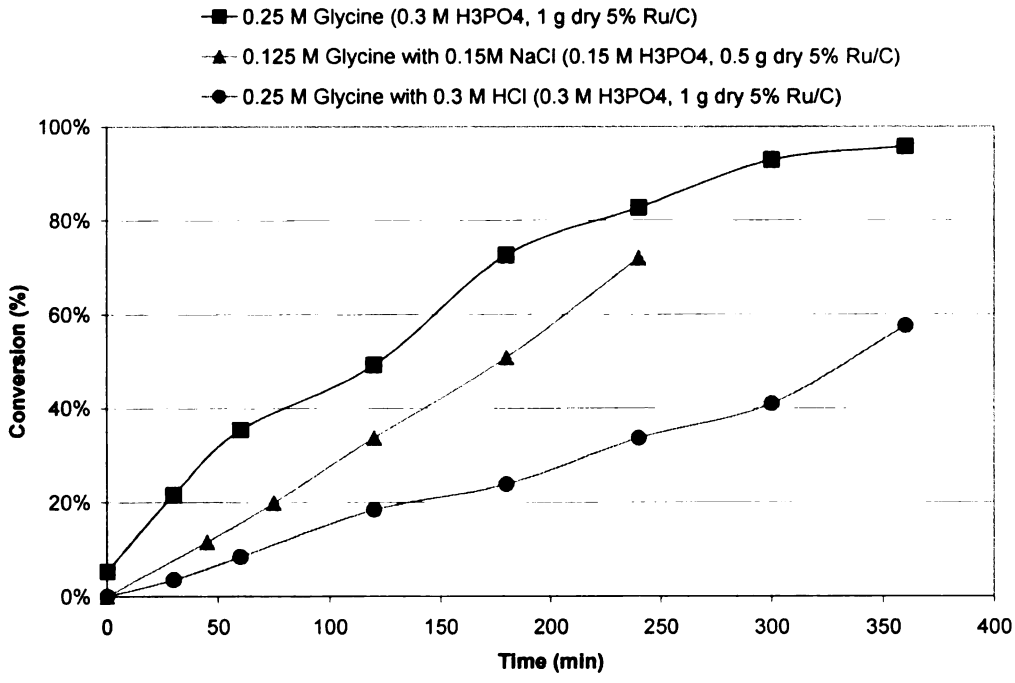

Figure 21. Hydrogenation of glycine alone and in the presence of NaCl or HCl (H_3PO_4, H_2O, 130 °C, 1000 psi H_2, 1 g dry 5% Ru/C)

In the hydrogenation experiments with amino acids, the role of the H_3PO_4 is to protonate the carboxylate, due to the preference of the amino acid to be in the zwitterionic form. The result is H_2PO4^-. In the experiment with both 0.3 M H_3PO_4 and 0.3 M HCl the HCl which is the stronger acid (pKa ~-4 as compared to ~2.15) is protonating the glycine carboxylate. Thus, H_3PO_4 is still in solution (as opposed to H_2PO4^-). The idea that perhaps it is the H_3PO_4 that is causing inhibition could be considered. However, in our

hydrogenation experiments with glycolic acid (discussed in section 4.4) we see no effect with the addition of an equimolar amount of H_3PO_4.

From the experiments with betaine and glycine, it is evident that the presence of chloride slows or completely inhibits (as in the case of betaine hydrochloride) the hydrogenation reaction. Chloride inhibition is also observed in the H/D exchange studies with betaine hydrochloride (which will be discussed next).

4.3.2 H/D Exchange Studies

As found in the hydrogenation experiments (Figure 18), betaine hydrochloride ($(CH_3)_3N^+CH_2COOH{\bullet}Cl^-$) was also unreactive toward H/D exchange. There was no measurable amount of exchange of the methylene or methyl hydrogens with deuterium. An experiment with 0.25 M betaine hydrochloride in D_2O was run at 100 °C with 1000 psi H_2 and 1 g dry 5% Ru/C. The results were compared with an experiment using 0.25 M betaine ($(CH_3)_3N^+CH_2COO^-$) at 130 °C. The experiments with betaine hydrochloride showed no deuterium incorporation on the methylene or methyl carbon sites (Figure 22).

This common inhibition by chloride could suggest that the hydrogenation and the H/D exchange catalyzing sites may be the same. But, we know from the experiment with betaine that the hydrogens on the methylene carbon undergo exchange with deuterium in the absence of catalyst due to the fixed cation promoting solution deprotonation (Figure 11, 130 °C). So, if the chloride was deactivating the catalyst it should only affect the

hydrogenation reaction. The reason for the chloride in betaine chloride inhibiting the H/D exchange reaction is still unknown.

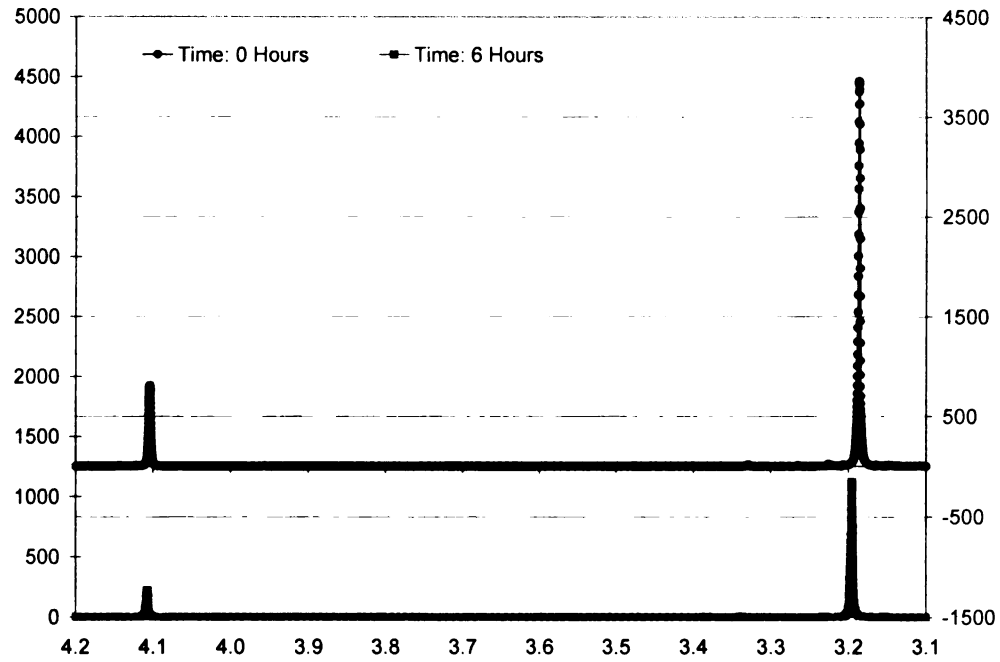

Figure 22. ^{1}H NMR of H/D exchange at the methyl (3.2 ppm) and methylene position (4.1 ppm) on 0.25 M betaine hydrochloride (D_2O, 100 °C, 1000 psi H_2, 1 g dry 5% Ru/C)

To try and push the H/D exchange reaction with betaine hydrochloride, an additional experiment was conducted at 130 °C and ran for 24 hours. During the course of the reaction, degradation of the betaine hydrochloride occurred yet still no observable H/D exchange.

In the experiment with 0.25 M betaine at 130 °C with 1000 psi H_2 and 1 g dry 5% Ru/C in D_2O exchange of hydrogen with deuterium is occurring at the methylene position albeit relatively slow. Kinetic rate data were determined and using the kinetic model described in Chapter 3, the fit of the methylene data can be observed in Figure 23. The

H_2O and HOD experimental (symbols) and fitted (line) data refers to the percent H in water and is on the right y-axis (secondary y-axis). The experimental (symbol) and fitted (line) concentration of CH_2 (referred to as AH_2), CHD (referred to as AHD), and CD_2 (referred to as AD_2) are on the left y-axis (primary y-axis).

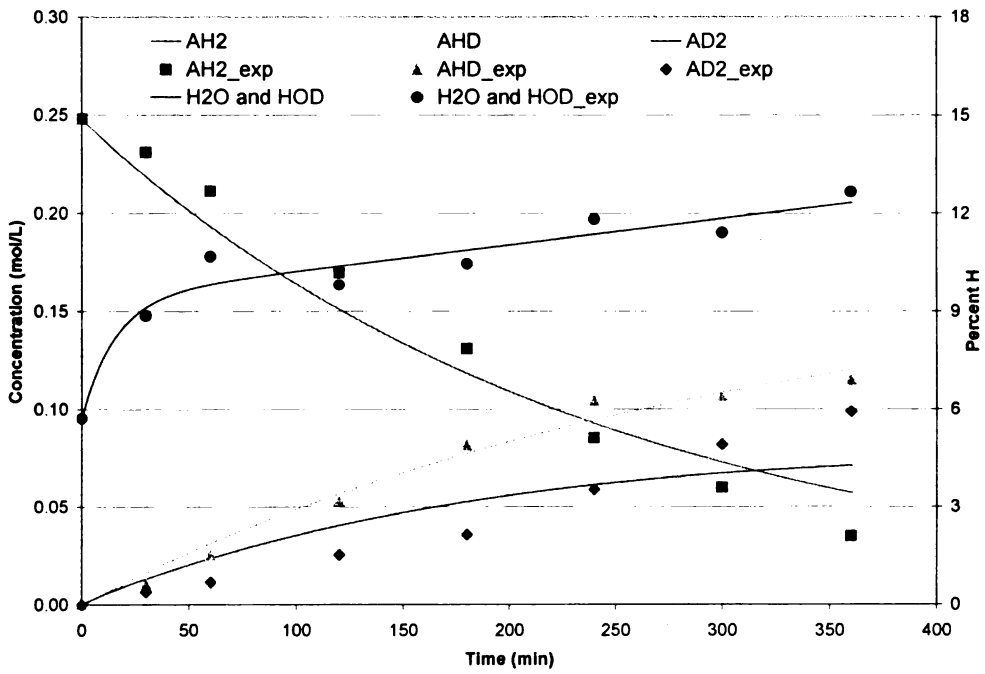

Figure 23. Fit of the kinetic rate data for 0.25 M betaine (D_2O, 130 °C, 1000 psi H_2, 1g dry 5% Ru/C)

The rate constants for H/D exchange on the methylene carbon are: $k_{1A} = 4.1x10^{-5}$, $k_{-1A} = 0$, $k_{2A} = 1.6x10^{-2}$, $k_{-2A} = 2.2x10^{-1}$ L/mol/min; and the sum of the squares error (SSE) = $1.9x10^{-3}$. At these low conversions, the back reaction rate constants are not likely to have much significance. A more detailed discussion considering the significance of the back reaction rate constants (k_{-1A}, k_{-2A}, k_{-1C}, k_{-2C}, and k_{-3C}) will be discussed in 4.7 (as well as H/D exchange of betaine ($(CH_3)_3N^+CH_2COO^-$)).

4.4 Effect of H_3PO_4

4.4.1 Hydrogenation Studies

In the case of the amino acids, a slight excess amount of H_3PO_4 was required to protonate the carboxylic acid. Glycine and the N-methylated glycines are zwitterionic in nature and thus the carboxylic acid functionality is dissociated unless the additional acid is added. The H_3PO_4 is only required for the hydrogenation of the amino acids, but was added to all hydrogenation experiments in order to be consistent. To determine the effect of the H_3PO_4 on substrates that were not zwitterionic in nature, glycolic acid was studied.

A pair of experiments with 0.25 M glycolic acid were conducted at 130 °C with 1000 psi H_2 in both the absence and presence of H_3PO_4 (0.3 M).

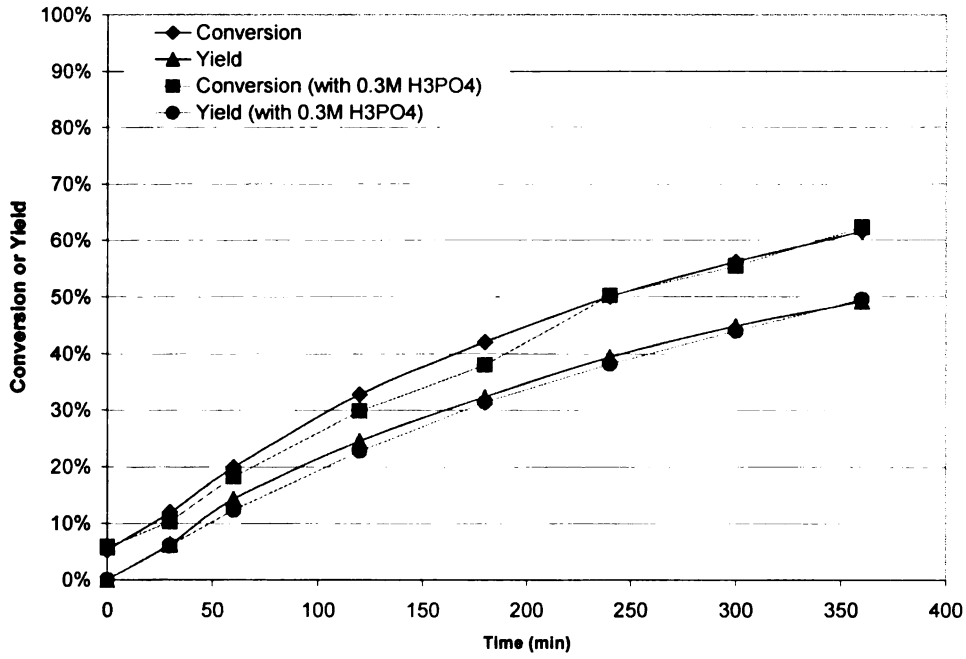

Figure 24. Hydrogenation of 0.25 M glycolic acid in the absence and presence of 0.3 M H_3PO_4 (H_2O, 130 °C, 1000 psi H_2, 1 g dry 5% Ru/C)

The addition of H_3PO_4 did not significantly affect the hydrogenation of glycolic acid to ethylene glycol. The conversion and yield for the pair of experiments were essentially the same (Figure 24).

A pair of experiments with 0.25 M glycine were conducted at 130 °C with 1000 psi H_2 in both the absence (Figure 25) and presence (Figure 26) of H_3PO_4. In the presence of H_3PO_4, a conversion of 83% and a yield of 71% ethanolamine were obtained after four hours of reaction time. However, in the absence of H_3PO_4 much lower conversion and yield values, both only 15% were obtained (Figure 27), presumably due to the amino acid being in the zwitterionic form a majority of the time.

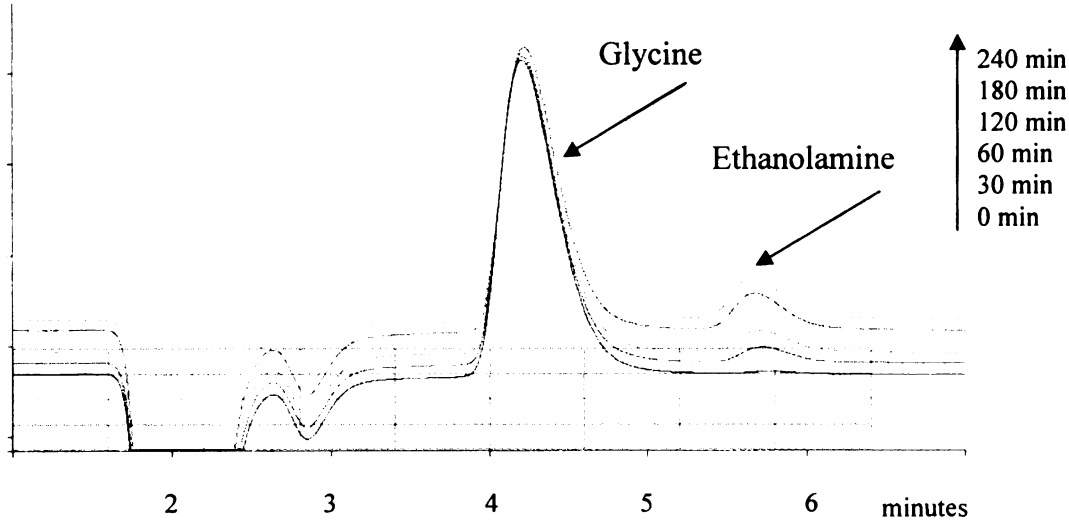

Figure 25. Hydrogenation of 0.25 M glycine (no H_3PO_4, H_2O, 130 °C, 1000 psi H_2, 1 g dry 5% Ru/C)

The H_3PO_4 is thought to protonate the carboxylic acid, allowing for the hydrogenation of glycine to form ethanolamine. In order to further determine whether or not the acid is competing with glycine for surface sites, H/D exchange studies can be done to see if the

presence of the additional acid slows or inhibits the H/D exchange. This is assuming that the hydrogenation and H/D exchange reactions are occurring on the same sites. The phosphoric acid is not necessary for H/D exchange and proved to be inhibitory (to be discussed next), but due to the need for the amino group to be free and electron donating.

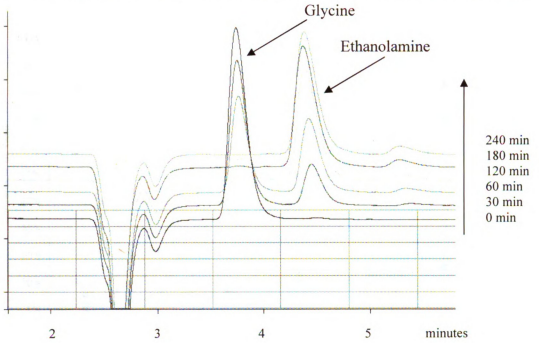

Figure 26. Hydrogenation of 0.25 M glycine (0.3 M H_3PO_4, H_2O, 130 °C, 1000 psi H_2, 1 g dry 5% Ru/C)

In the experiment with H_3PO_4 present, glycine is essentially fully converted after three hours of reaction (as opposed to almost no reaction in the case of no H_3PO_4 added). The retention times in the HPLC analyses of glycine and ethanolamine are slightly shifted due to the H_3PO_4. It is assumed that the H_3PO_4 is adsorbing on the same sites as the glycine. So, competitive adsorption of the H_3PO_4 and glycine should be considered. Peereboom et al. did find that compounds that are more hydrophilic tend to stay more in the bulk solution and are less competitive for the catalyst due to the hydrogen bonding ability with

the solvent water.[59] Competitive adsorption studies should be compared with the knowledge that H_3PO_4 was not significantly adsorbed on the Ru/C (Figure 17) and did not inhibit the hydrogenation of glycolic acid (Figure 24) to further determine whether the adsorption of H_3PO_4 on the catalyst should be included in the kinetic model.

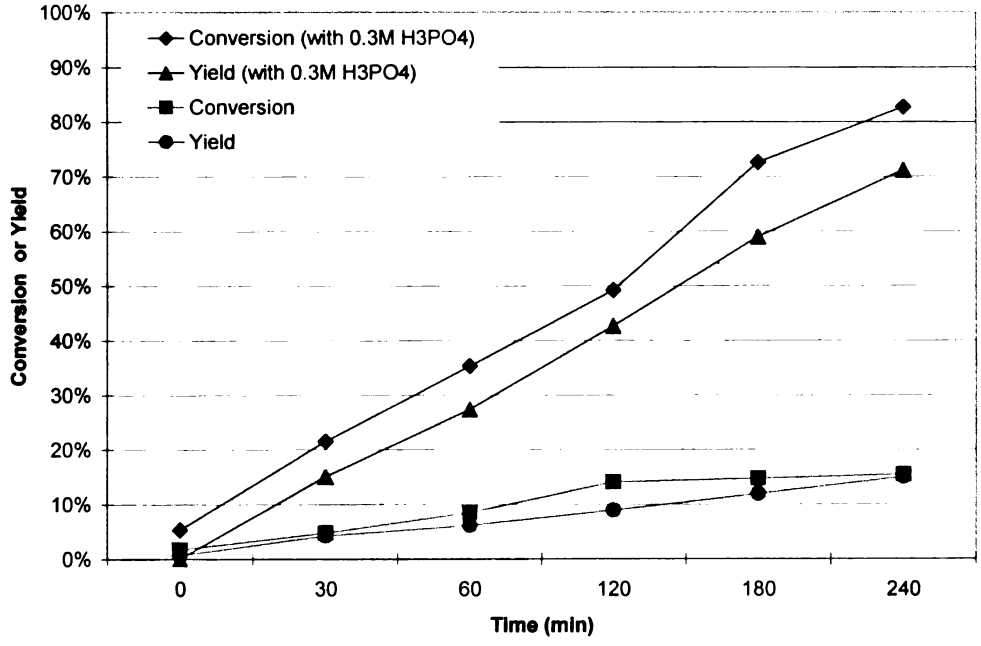

Figure 27. Hydrogenation of 0.25 M glycine in the absence and presence of 0.3 M H_3PO_4 (H_2O, 130 °C, 1000 psi H_2, 1 g dry 5% Ru/C)

Another approach to evaluating the potential effect of H_3PO_4 on the hydrogenation reaction would be to perform an experiment with equimolar amounts of glycine, lactic acid, and a slight excess of H_3PO_4. There were several competition experiments performed by members in our research group.[49,61,63] Results indicated that with equimolar amounts of alanine and lactic acid, the hydrogenation of alanine occurs but lactic acid is initially unreactive. One explanation for this may be that alanine binds stronger than lactic acid on the surface or has a greater affinity for the surface. But, a

second explanation may be that in the experiment with lactic acid and alanine, the lactic acid may serve to protonate the zwitterionic alanine resulting in deprotonation of the lactic acid thereby preventing the reduction. In the suggested experiment above, the H_3PO_4 would serve to protonate the alanine and allow a more direct comparison of alanine and lactic acid as well as evaluate the effect of H_3PO_4.

4.4.2 H/D Exchange Studies

Several experiments were conducted in the presence of H_3PO_4 to try and determine if the additional acid caused an effect on the H/D exchange reaction. One goal was to try and establish a link between the hydrogenation and H/D exchange studies. A pair of experiments with glycine and sarcosine were run at 50 °C to try and slow or eliminate the competing hydrogenation reaction and isolate the effect of H_3PO_4 on H/D exchange. Glycine (0.25 M) with 0.3 M H_3PO_4 at 50 °C with 1000 psi D_2 in D_2O was allowed to react for six hours. Results indicated a negligible amount of H/D exchange. Figure 28 shows the ^1H NMR at time zero and also at six hours. The yield of CHD and subsequently CD_2 was zero. We can compare these results to the identical experiment in which no H_3PO_4 was added (Figure 29).

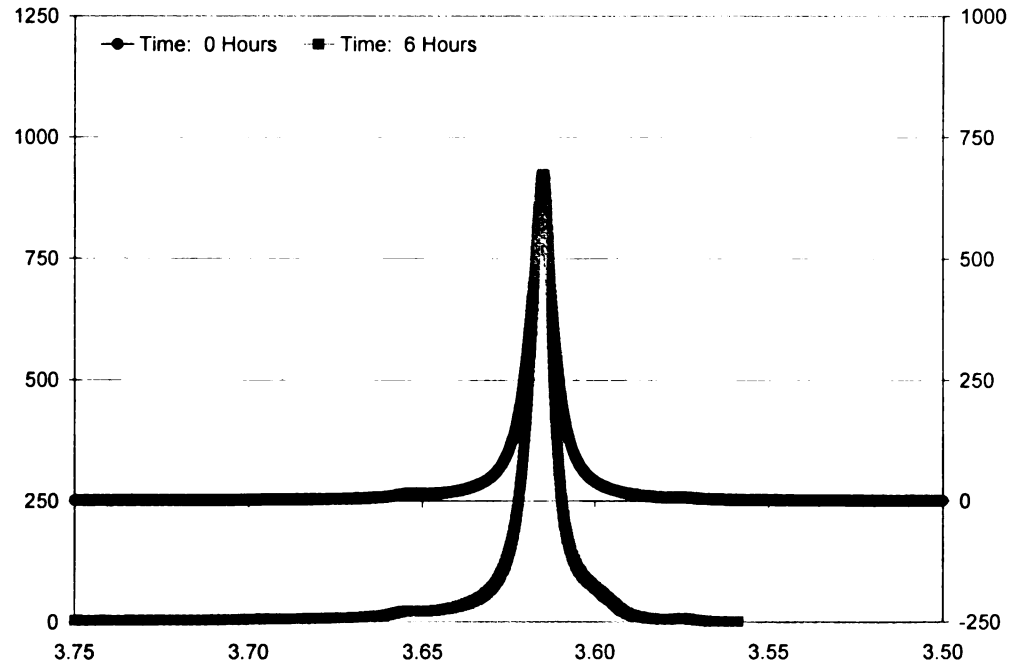

Figure 28. ^{1}H NMR of H/D exchange at the methylene position of 0.25 M glycine (0.3 M H_3PO_4; D_2O; 50 °C; 1000 psi D_2, 1 g dry 5% Ru/C)

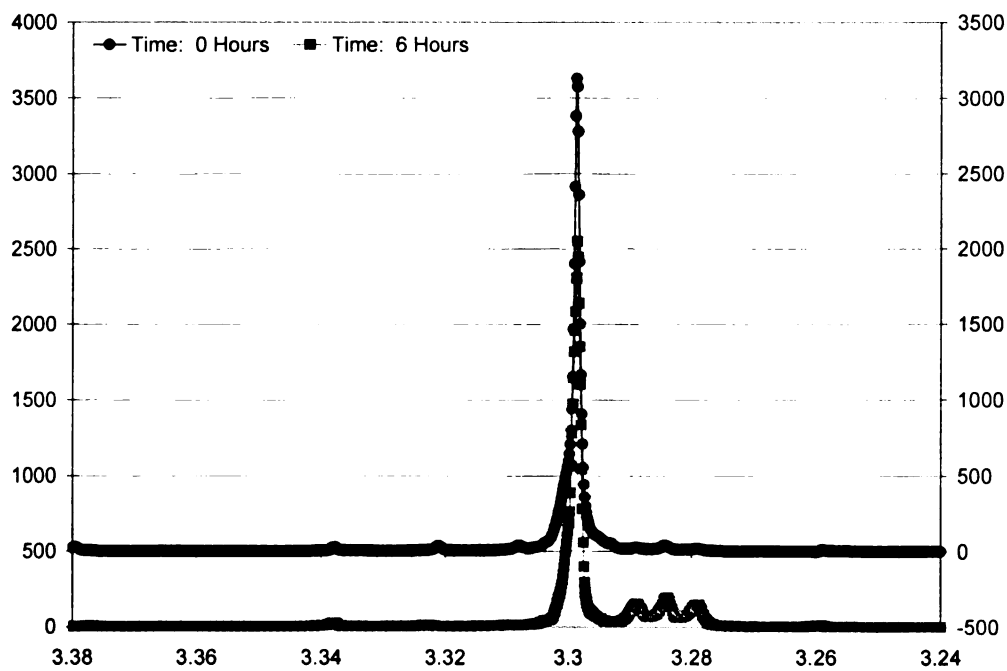

Figure 29. ^{1}H NMR of H/D exchange at the methylene position of 0.25 M glycine (D_2O; 50 °C; 1000 psi D_2, 1 g dry 5% Ru/C)

The concentration data for the experiment with H_3PO_4 showed essentially no H/D exchange at the methylene carbon on glycine (Figure 30). The concentration of CD_2 is not measured, but is the difference between the summed amount of AH_2 and AHD at time zero minus the summed amount of CH_2 and AHD at time t. Due, to some of the substrate being adsorbed on the surface ("lost") it may cause the calculated CD_2 to be slightly higher. However, in this experiment the amount "lost" was equal to less than 3% (it is reflected as the CD_2). The experimental percent H in water and the fitted line are also presented in Figure 30.

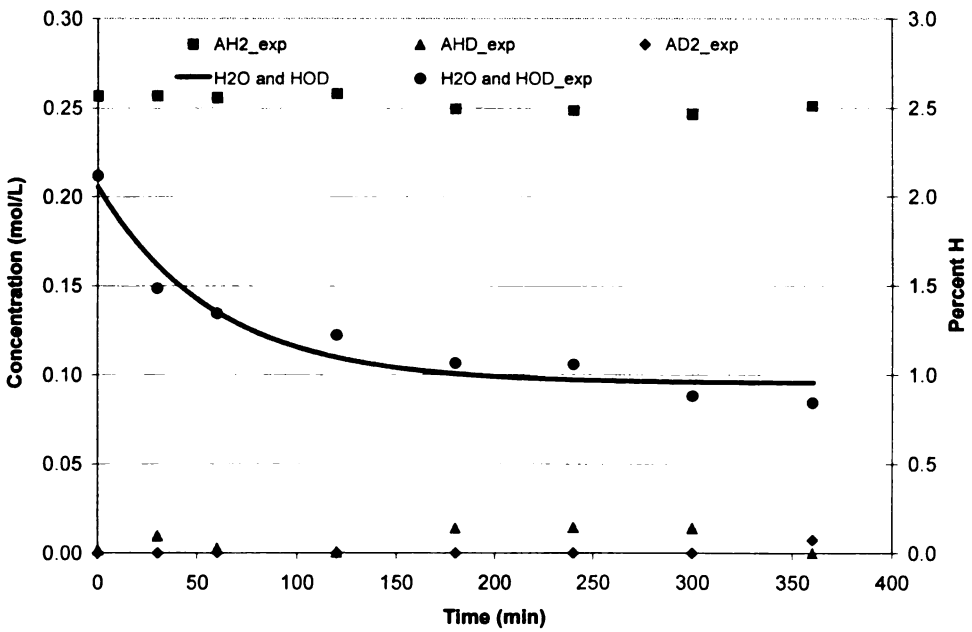

Figure 30. Concentration data for 0.25 M glycine (0.3 M H_3PO_4, D_2O, 50 °C, 1000 psi D_2, 1 g dry 5% Ru/C)

The catalytic H/D exchange of the amino acids is promoted by having an electron-rich C-H bond available for insertion by the catalyst. When the amino group is positively charged (as in the case with H_3PO_4 added), the C-H insertion by the catalyst is not as

likely to occur. This is also compounded by the fact that the experiment was run at such a low temperature (50 °C). A higher temperature reaction with sarcosine will be discussed later. The reason betaine (with a quartenary nitrogen) undergoes H/D exchange is because it is occurring non-catalytically through deprotonation of the α-carbon in solution.

The same experiment but with 0.25 M sarcosine was performed (0.3 M H_3PO_4, D_2O, 50 °C, 1000 psi D_2). Results again, as in the case of glycine, indicated a negligible amount of H/D exchange with H_3PO_4 added. Figure 31 shows the ^1H NMR at time zero and also at six hours. The yield of CHD and subsequently of CD_2 was zero. There was a small amount of conversion of the CH2 peak area (2.4%), but is presumably due to degradation of the substrate over six hours and experimental error. When calculating the amount "lost" from the difference between the time zero and at six hours for the methyl concentration, the percent lost was zero.

We can compare this reaction to the experiment (same conditions) in which no H_3PO_4 was added (Figure 32). The concentration data for the experiment with H_3PO_4 showed essentially no H/D exchange at the methylene carbon on sarcosine (Figure 33). The experimental percent H in water and the fitted line are also presented in Figure 33.

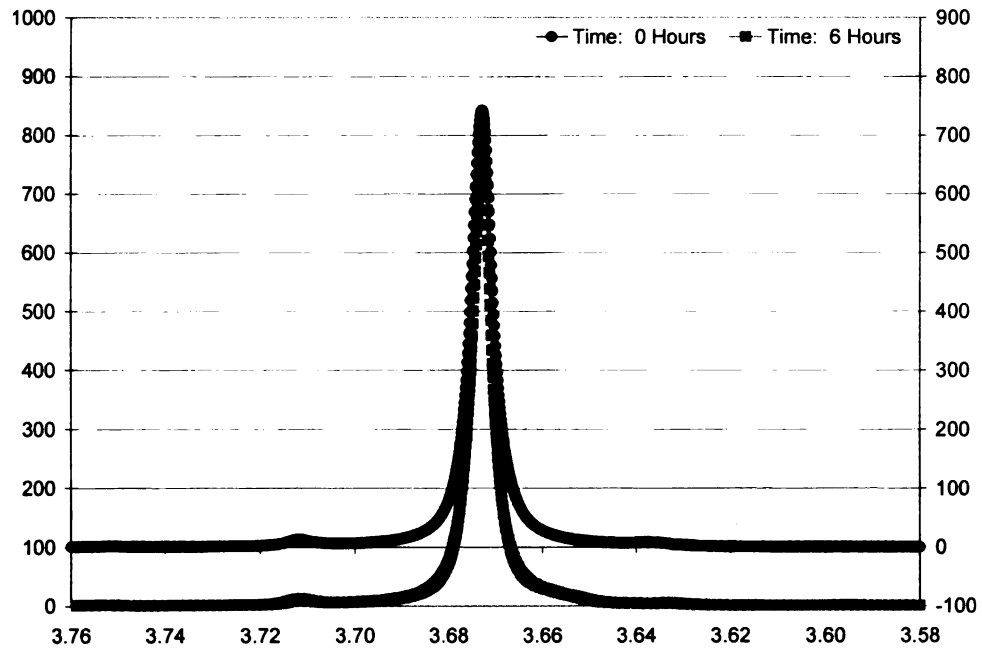

Figure 31. ^{1}H NMR of H/D exchange at the methylene position of 0.25 M sarcosine (0.3 M H_3PO_4, D_2O, 50 °C, 1000 psi D_2, 1 g dry 5% Ru/C)

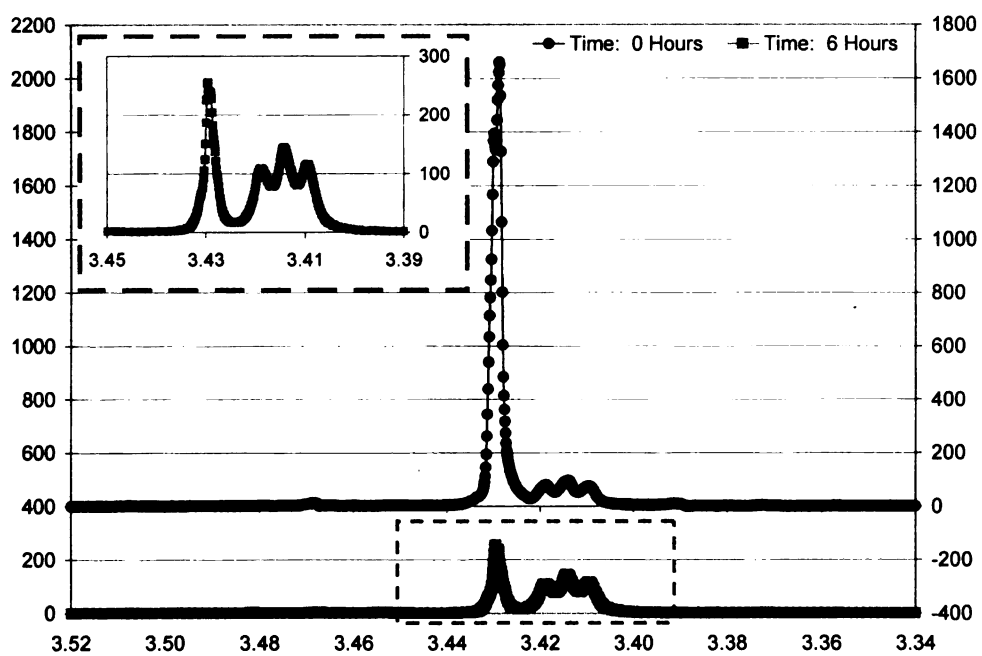

Figure 32. ^{1}H NMR of H/D exchange at the methylene position of 0.25 M sarcosine (D_2O, 50 °C, 1000 psi D_2, 1 g dry 5% Ru/C)

It is important to note that the amount "lost" after six hours with respect to time zero is small. This was confirmed in all experiments in which the desired reaction was not occurring. The catalyst and carbon adsorption studies indicated that up to 5-7% can be "lost" once the substrate is exposed to the catalyst. But, presumably this occurs immediately (at time zero) and does not increase with time. For the kinetic studies as well as conversion, yield, and selectivity the time zero concentration was used. It was assumed that the initial amount of substrate adsorbed on the carbon support does not eventually react but is degraded.

As discussed above, the ability for the amino acids to undergo H/D exchange is affected by protonation of the amino group. Thus, it would be of value to do a detailed pH study to measure the extent of protonation with increasing concentrations of H_3PO_4. Slight changes in pH could drastically change the H/D exchange reactivity. In addition, it could be suggested to explore the effect of added base on the H/D exchange reaction to evaluate whether it would increase reactivity.

We can also look at the rate of exchange on the methyl carbon (Figure 34). Again, there is essentially no H/D exchange occurring at the methyl position at these reaction conditions.

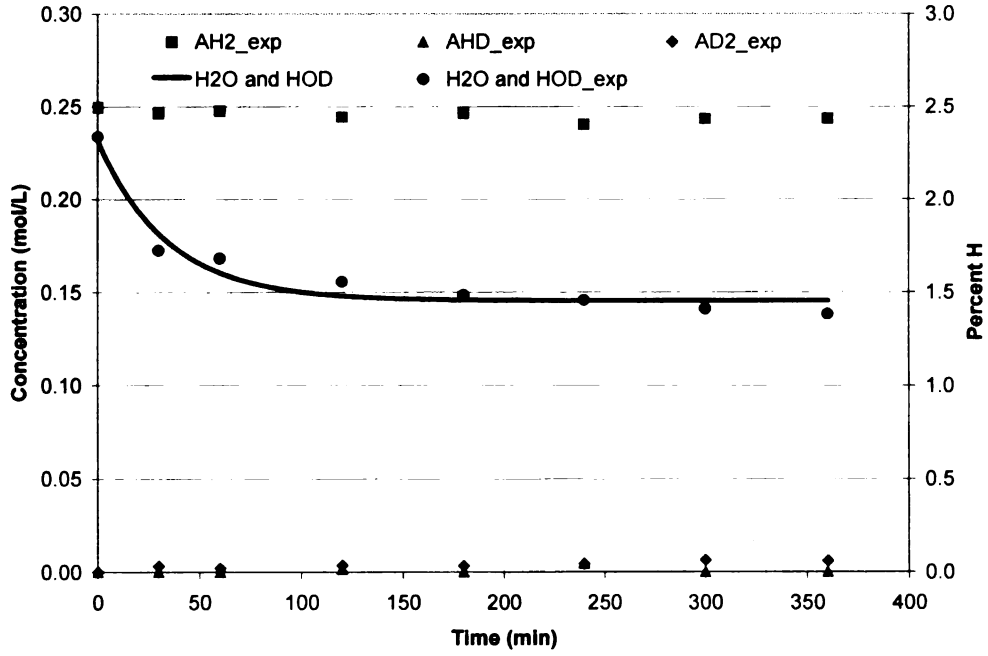

Figure 33. Concentration data for 0.25 M sarcosine (0.3 M H_3PO_4, D_2O, 50 °C, 1000 psi D_2, 1 g dry 5% Ru/C)

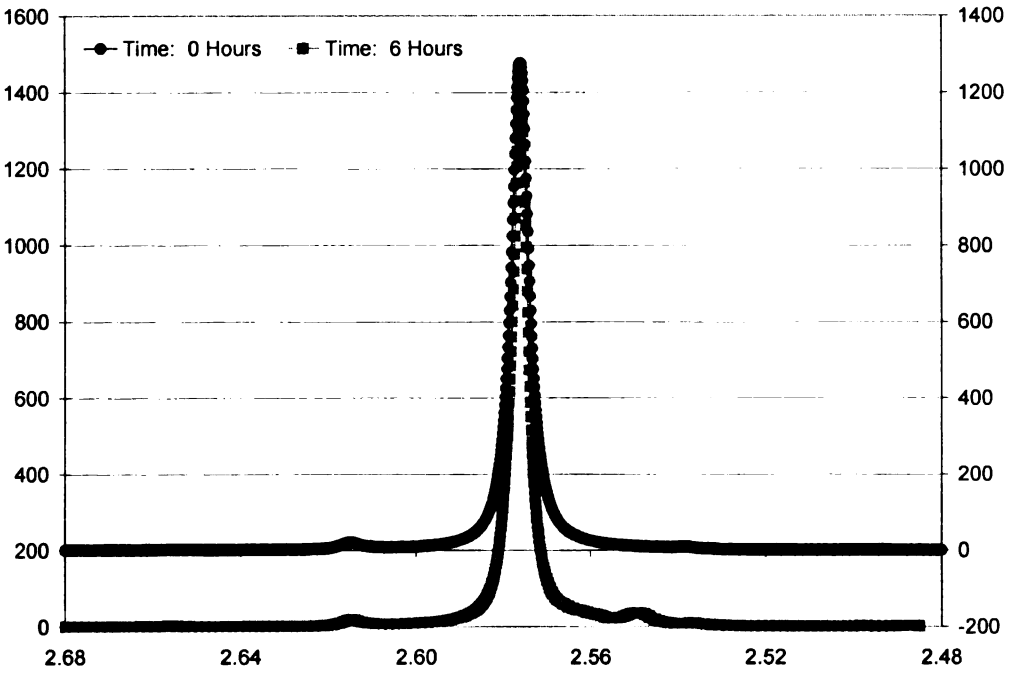

Figure 34. ^1H NMR of H/D exchange at the methyl position of 0.25 M sarcosine (0.3 M H_3PO_4, D_2O, 50 °C, 1000 psi D_2, 1 g dry 5% Ru/C)

Sarcosine is more reactive than glycine in the H/D exchange reactions, so a higher temperature, 70 °C, was also evaluated. It was desired to have some H/D exchange occurring so that the rate constants could be compared (absence and presence of H_3PO_4). In addition, higher temperatures promote dissociation and allow for more of the higher energy form (non-zwitterionic) to be present.

Figure 35 shows the ^1H NMR for the methylene carbon at time zero and after six hours for 0.25 M sarcosine with 0.3 M H_3PO_4 at 70 °C with 1000 psi D_2 in D_2O. A small amount of H/D exchange is occurring. H/D exchange is also observed at the methyl position. Figure 36 shows the ^1H NMR for the methyl carbon of sarcosine at time zero and after six hours.

The kinetics were determined using both kinetic models and the reaction data fit is shown below in Figure 37 and 38 (methylene and methyl). Again, by definition the rate constant k_{1A} should be twice that of k_{2A}. The model defines the rate constants on a per hydrogen basis and in the case of converting CH_2 to CHD there are two available hydrogens for exchange whereas in the conversion of CHD to CD_2 there is only one. The same theory is applied to the methyls in that the rate of k_{1C} should be 1.33 times that of k_{2C} and 1.67 times that of k_{3C}. This assumes there are no isotope effects (primary or secondary). This assumption as well as a detailed discussion on the rate constants will be included in section 4.7.

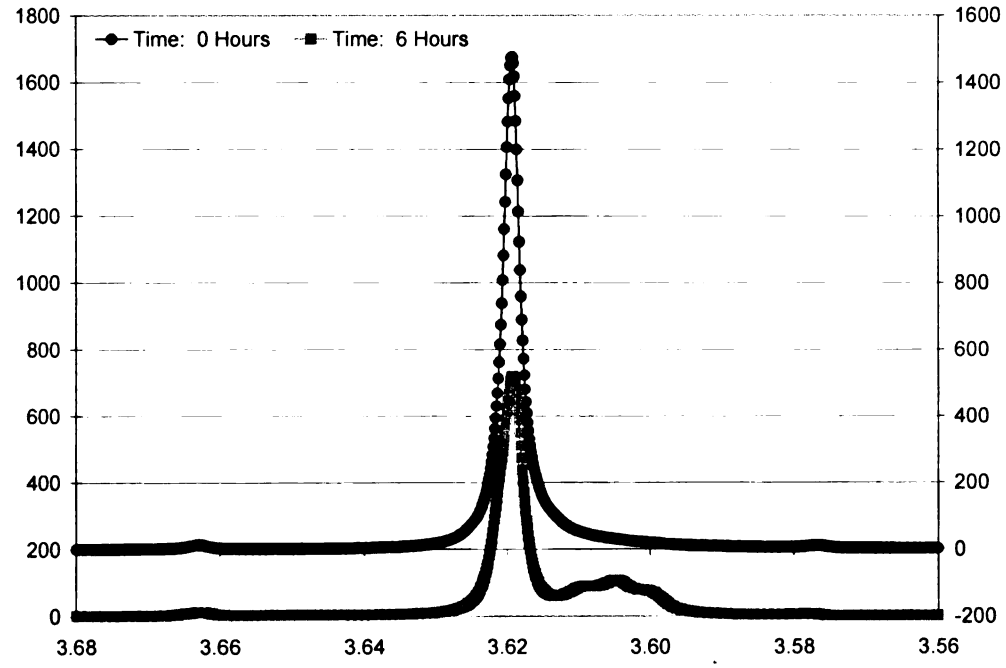

Figure 35. ^{1}H NMR of H/D exchange at the methylene position of 0.25 M sarcosine (0.3 M H_3PO_4, D_2O, 70 °C, 1000 psi D_2, 1 g dry 5% Ru/C)

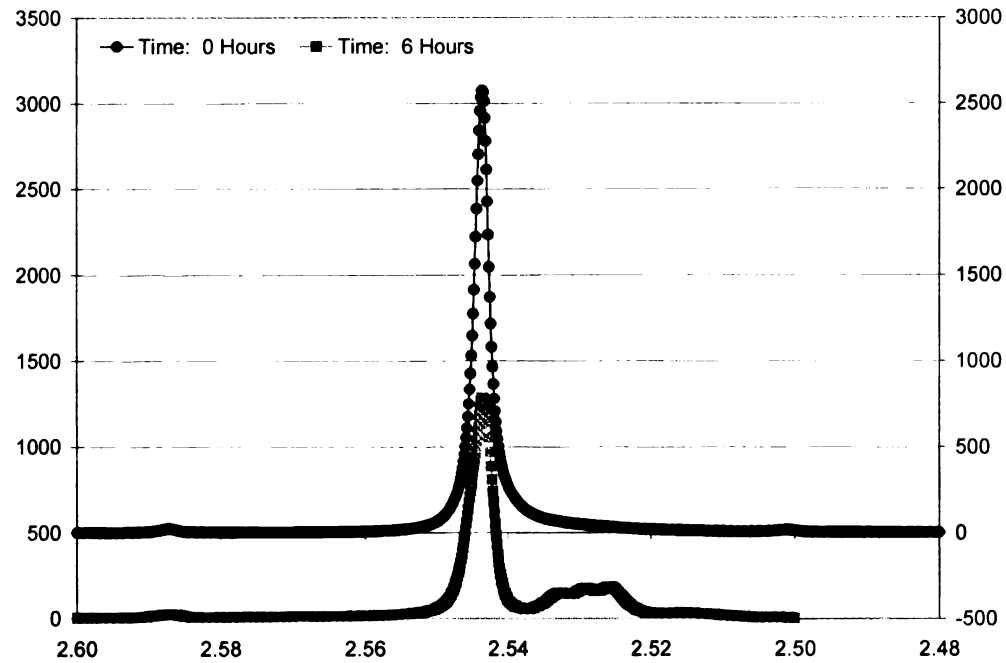

Figure 36. ^{1}H NMR of H/D exchange at the methyl position of 0.25 M sarcosine (0.3 M H_3PO_4, D_2O, 70 °C, 1000 psi D_2, 1 g dry 5% Ru/C)

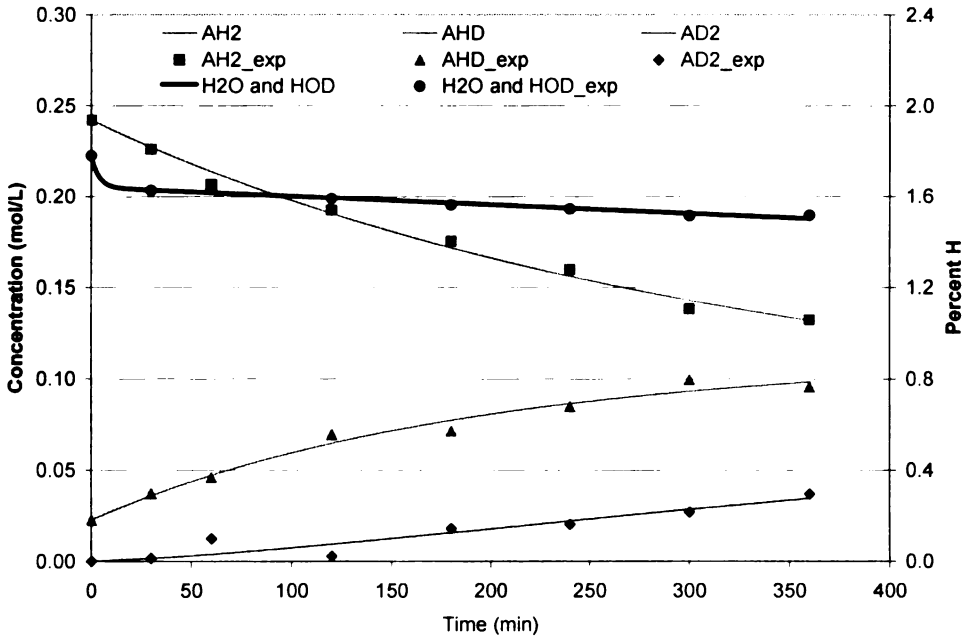

Figure 37. Fit of the kinetic rate data for 0.25 M sarcosine (0.3 M H_3PO_4, D_2O, 70 °C, 1000 psi D_2, 1 g dry 5% Ru/C)

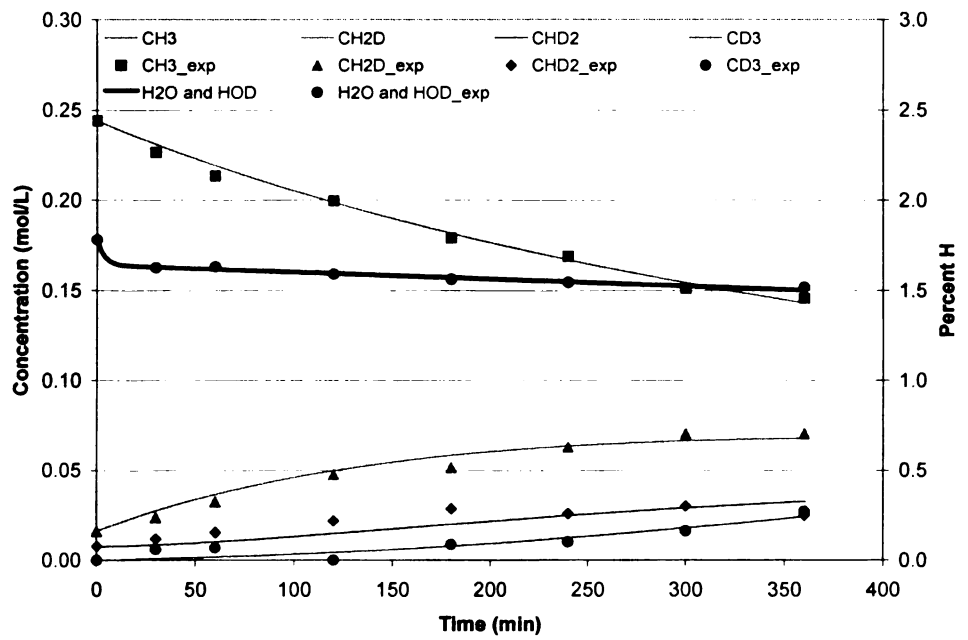

Figure 38. Fit of the kinetic rate data for 0.25 M sarcosine (0.3 M H_3PO_4, D_2O, 70 °C, 1000 psi D_2, 1 g dry 5% Ru/C)

The rates for H/D exchange on the methylene carbon are: $k_{1A} = 0.21x10^{-4}$, $k_{-1A} = 9.3x10^{-4}$, $k_{2A} = 0.18x10^{-4}$, and $k_{-2A} = 1.9x10^{-3}$ L/mol/min. The reaction rates for H/D exchange on the methyl carbon are $k_{1C} = 0.18x10^{-4}$, $k_{-1C} = 1.1x10^{-3}$, $k_{2C} = 0.30x10^{-4}$, $k_{-2C} = 1.2x10^{-2}$ $k_{3C} = 0.31x10^{-4}$, and $k_{-3C} = 0$ L/mol/min. We can compare the rate constant data for the experiment at 70 °C with 1000 psi D_2 in D_2O in both the absence and presence of 0.3 M H_3PO_4 (Figure 39).

Again at these low conversions, the back reaction rate constants do not have much significance. In addition, these experiments were conducted with 1000 psi D_2 and D_2O, so the available H in the water (which is in equilibrium with the surface) is only ~2%. Using a purely statistical approach and assuming the reaction has reached equilibrium the percent of CH_2 would be (0.02 x 0.02) 0.04%, CHD would be (0.98 x 0.02 + 0.02 x 0.98) 3.92%, and CD_2 would be (0.98 x 0.98) 96.04%. The large amount of deuterium available promotes the forward reactions to occur.

The rate constant results show that the rate of H/D exchange is significantly suppressed in the presence of H_3PO_4 (Figure 39). Again, this is presumably due to the amino group being protonated and not in the free form. The ratios for the forward rate constants for both the methylene and methyl carbon are not equal to the expected ratios (as discussed previously), indicating that isotope effects may be playing a role in the H/D exchange reaction. Kinetic model B (chapter 3) incorporates the possibility of primary and secondary isotope effects and will be explored in section 4.7.

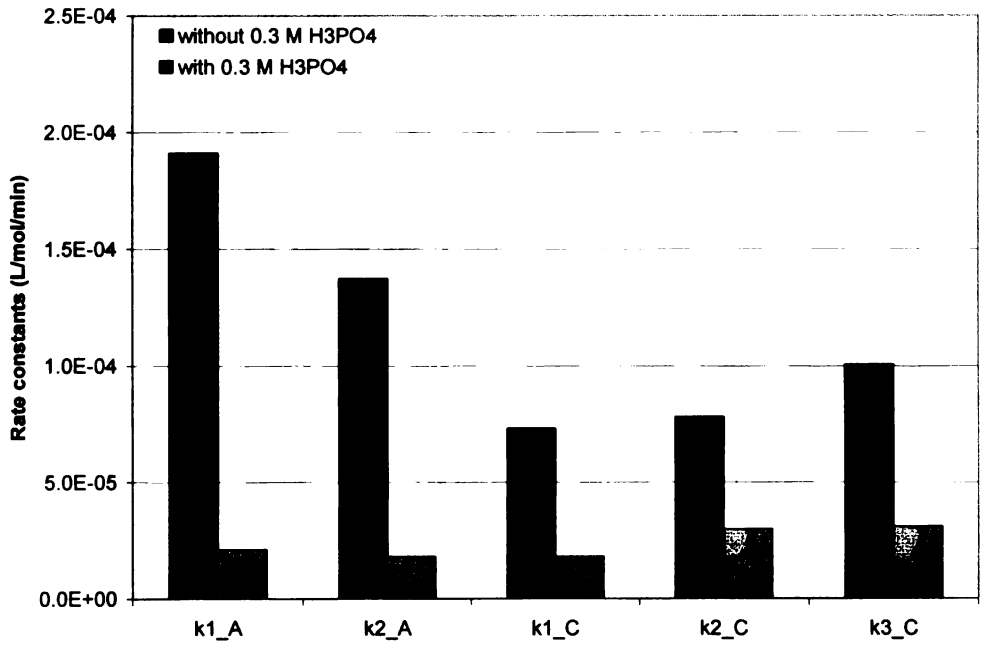

Figure 39. Rate constants for 0.25 M sarcosine in the absence and presence of 0.3 M H_3PO_4 (D_2O, 70 °C, 1000 psi D_2, 1 g dry 5% Ru/C)

An experiment was conducted with 0.25 M betaine ($(CH_3)_3N^+CH_2COO^-$) and 0.3 M H_3PO_4 at 100 °C with 1000 psi H_2 in D_2O. Results indicated that even with the H_3PO_4 present, H/D exchange is still occurring at the methylene carbon. The ^1H NMR of the methylene position on betaine is compared at time zero and at six hours of reaction time (Figure 40). The peak shape of the CHD (triplet) from the ^1H NMR for betaine was not as resolved as compared to most of the other experiments. In Figure 42 the inset shows the CHD peak after six hours. At six hours of reaction, 100% of the CH_2 had been converted.

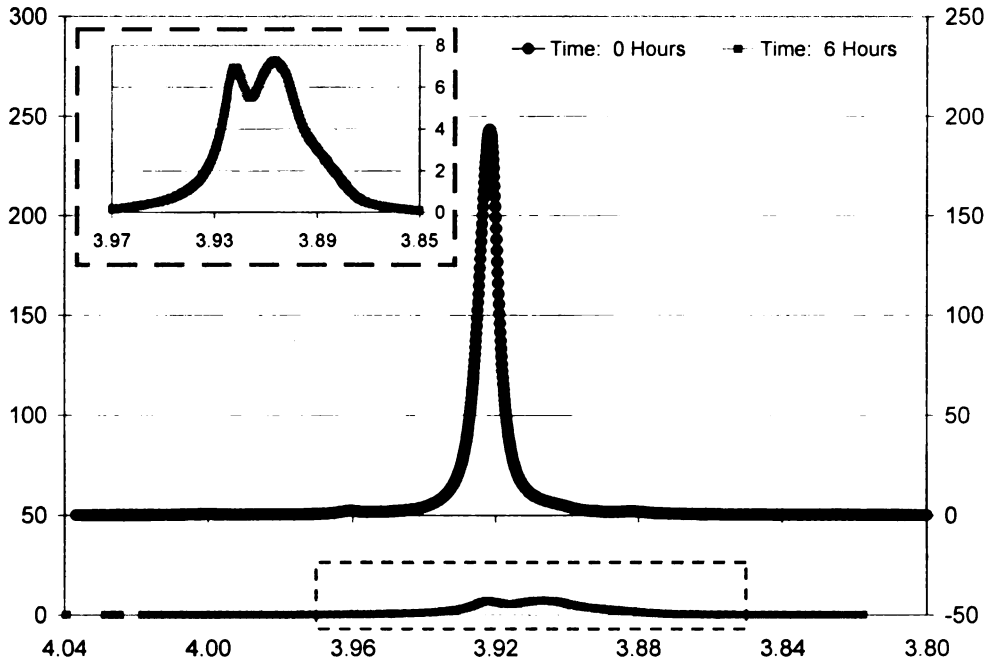

Figure 40. ^{1}H NMR of H/D exchange at the methylene position of 0.25 M betaine (0.3 M H_3PO_4, D_2O, 100 °C, 1000 psi H_2, 1 g dry 5% Ru/C)

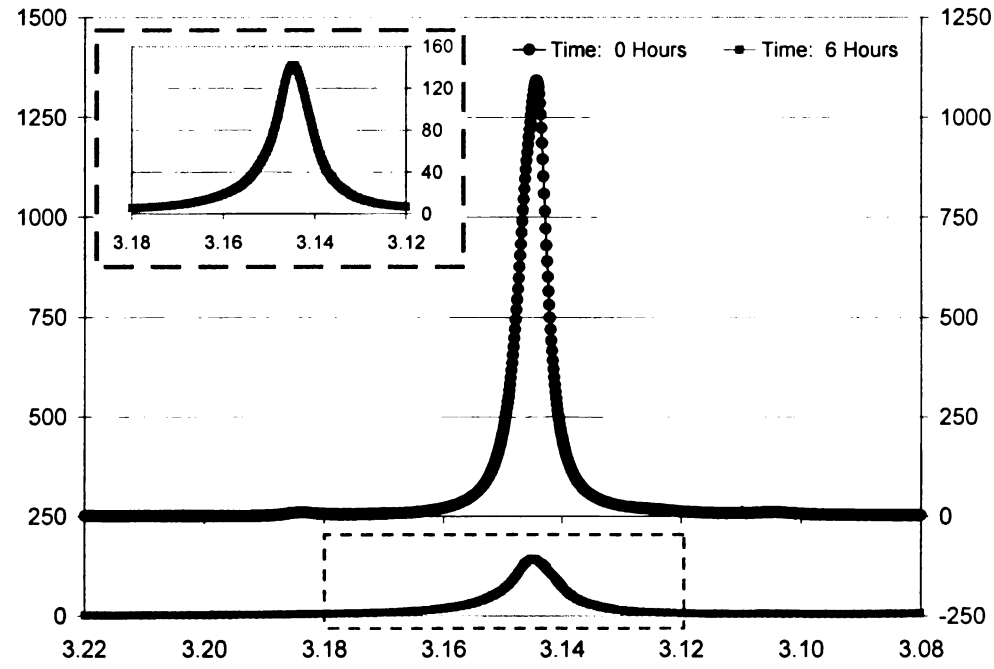

Figure 41. ^{1}H NMR of H/D exchange at the methyl position of 0.25 M betaine (0.3 M H_3PO_4, D_2O, 100 °C, 1000 psi H_2, 1 g dry 5% Ru/C)

This is not surprising considering that betaine exhibits H/D exchange at the methylene position even in the absence of catalyst. Thus, if the H_3PO_4 is competing for the catalyst it still should not inhibit the H/D exchange in betaine, as the exchange does not involve the catalyst. Consistent with this notion, H/D exchange was not observed at the N-methyl position of betaine. The ^1H NMR peak of the three methyls decreased in size over time due to the conversion of betaine to choline, but no H/D exchange occurred (Figure 41).

In this experiment the presence of choline was also detected over time. From HPLC analyses, a 38% yield of choline was obtained after 6 hours of reaction time. A conversion of 100% of the methylene carbon was measured after 6 hours, due to both hydrogenation and H/D exchange. Using the N-methyls as a reference for the amount of hydrogenation that occurred, roughly 55% of the N-methyl ^1H NMR peak was converted to choline. The HPLC analysis matched this, reporting 49% conversion after 6 hours.

For this experiment, the percent H in water was much variable. So, the [HOD] fit parameters were modified to better represent the actual data. A 4^{th} order polynomial was used to fit the aqueous hydrogen concentration. For all other experiments, equation 46 (Section 3.2.2) was used. The concentration data versus time and the fitted rate equations are presented in Figure 42. Betaine is undergoing uncatalyzed H/D exchange that does not appear to be inhibited by the H_3PO_4.

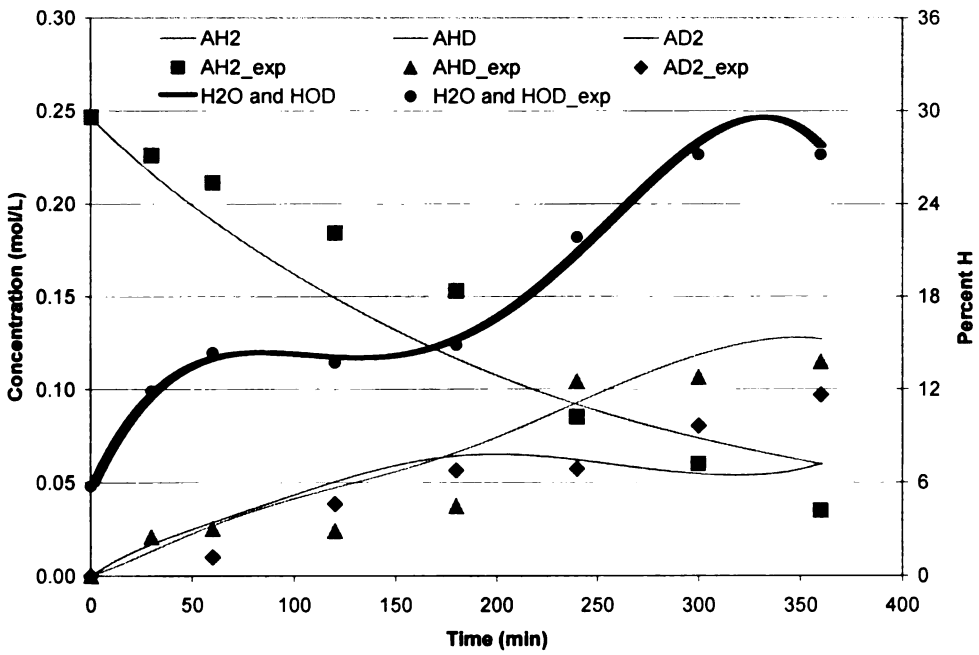

Figure 42. Fit of the kinetic rate data for 0.25 M betaine (0.3 M H_3PO_4, D_2O, 100 °C, 1000 psi H_2, 1 g dry 5% Ru/C)

The experiment with 0.25 M betaine in the absence of H_3PO_4 at 130 °C with 1000 psi H_2 and D_2O will be discussed further in section 4.7.

4.5 Solvent Effects on the Hydrogenation of Organic Acids

A key aspect involved in understanding the mechanisms controlling the catalytic hydrogenation of organic acids is the effect the solvent has on the hydrogenation. In catalytic hydrogenation of acids, it has been determined that catalyst and hydrogen are essential in order to convert the starting material. In addition it appears that the acids need to be in their protonated form. It is less clear what role, if any, the solvent plays in the overall catalytic hydrogenation scheme.

There are several advantages of using aqueous-phase conversion routes including: 1) most bio-based feedstocks are produced and handled in water solutions and 2) feed purity is less critical. However, the question of whether water is involved in the hydrogenation mechanism has not been answered. It has also been suggested that a more "organic" environment might favor conversion of the more polar amino and hydroxyl acids to their less polar alcohol reduction products. To examine this issue, an experiment was conducted in which no water was present. Glycolic acid (0.25 M) in dry tetrahydrofuran (THF) at 130 °C with 1000 psi H_2 revealed a suppressed hydrogenation reaction rate. The yield of ethylene glycol formed after six hours was about 14% compared with nearly 50% with water as the solvent. Though THF appeared to hinder the reaction some ethylene glycol was formed, indicating that the reaction did still occur. Additional experiments were conducted using ratios of 80/20 (v/v) water/THF and 20/80 (v/v) water/THF. From this series, it is clear that as the amount of organic solvent is increased the reaction is further suppressed (Figure 43).

To promote hydrogen solubility in water, high pressures are used (1000 psi H_2). In the case of THF as the solvent, the solubility of hydrogen was examined to determine if less hydrogen was present in these reactions.

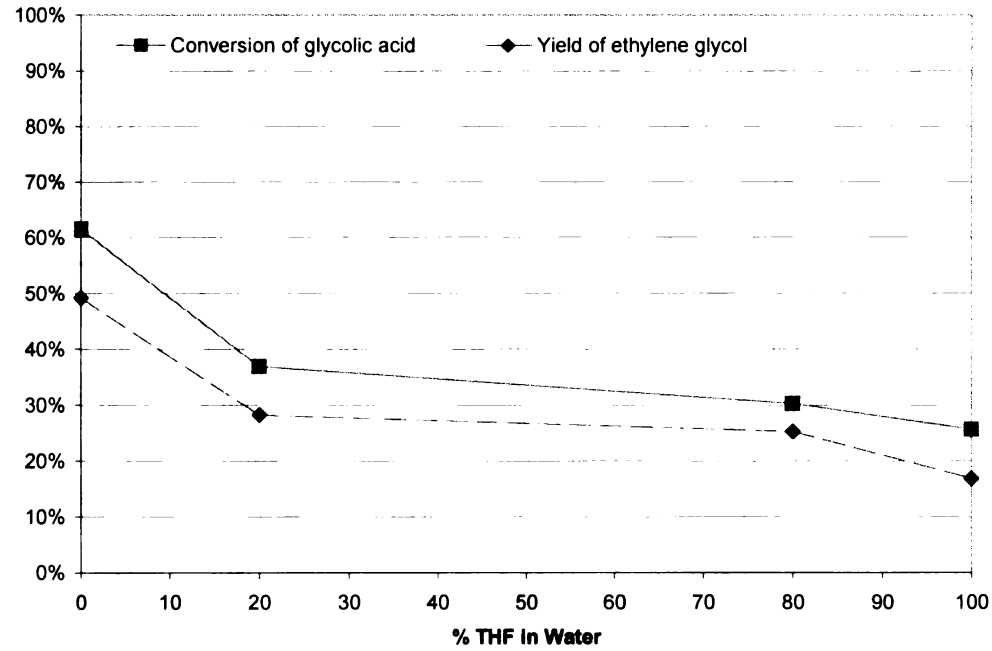

Figure 43. Hydrogenation of 0.25 M glycolic acid after 6 hours (THF/H_2O, 130 °C, 1000 psi H_2, 1 g dry 5% Ru/C)

In contemplating the role of the solvent, the various reactions in which it can participate need to be considered. From previous work in our group it was known that catalytic H/D exchange is possible between solvents and both the organic acids and the alcohol products. To understand whether hydrogenation and H/D exchange are occurring at the same sites on the surface THF was chosen as a solvent. An experiment with 0.25 M THF at 130 °C with 1000 psi H_2 in D_2O and 1 g dry 5% Ru/C was run and results indicated that THF readily undergoes H/D exchange at these conditions. The H/D exchange was observed at both C1 (83% α-CH_2 conversion) and C2 (42% β-CH_2 conversion) carbons. The ^1H NMRs for the methylene sites were difficult to convolute once the exchange started due to the overlap of the CH_2 and CHD peaks. So, the total amount of conversion was based on the disappearance of both CH_2 and CHD. If H/D

exchange and hydrogenation were occurring on distinct sites then the rate of hydrogenation should not be slowed as much in the presence of a solvent that predominantly undergoes H/D exchange. As mentioned above, the rate was significantly slowed as more THF was added, suggesting the sites may not be distinct and that there is competition at the surface.

Due to the α C-H activation present with the THF solvent, a solvent was chosen that was expected to be unreactive to H/D exchange or hydrogenation, namely *tert*-butanol. The results from 0.25 M glycolic acid hydrogenation in *tert*-butanol suggested that a competitive reaction is occurring involving the solvent on the catalyst surface, thereby possibly tying up the available sites for acid hydrogenation or perhaps simply excluding the water needed by the reaction. *tert*-Butanol in the presence of acid (0.25 M glycolic acid) at 130 °C with 1000 psi H_2 may also undergo selective dehydration to isobutylene.[64,65] Isobutene could undergo hydrogenation on the surface of the catalyst. No significant yield of ethylene glycol was detected. H/D exchange seemed unlikely in this context, but an experiment with neat *tert*-butanol and D_2 and D_2O was run to evaluate the amount of deuterium incorporation at the methyl groups of *tert*-butanol. After four hours, little H/D exchange was observed using ^1H NMR, eventhough there was some loss (~25%) of the CH_3 as assessed by the ^1H NMR (discussed further in section 4.7.2).

From previous research in our group and the work presented in this thesis, we know that alcohols can undergo C-H activation. But, we also know that, in general, they have less of an affinity for the Ru/C catalyst as compared to the organic acid substrates. So,

ethanol and ethylene glycol were both explored as solvents for the hydrogenation reaction of glycolic acid. Hydrogenation experiments with glycolic acid (0.25 M) in ethanol were run in both the absence and presence of H_3PO_4. The presence of H_3PO_4 promoted esterification (9%) at t=0 min, defined as the point where the reaction temperature reaches 130 °C and the H_2 pressure (1000 psi) is introduced. Figure 44 shows the HPLC chromatogram (mV versus time (min)) for glycolic acid in ethanol (with 0.3 M H_3PO_4) for the pre-reaction solution, time zero, and at 6 hours. In the absence of acid, the ester is not present until after 5 hours of reaction (Figure 45). However, there is some conversion of glycolic acid that is occurring over time. This may be due to the glycolic acid adsorbing into the catalyst. In either case, nearly the same amount of product, 8% of ethylene glycol, was formed. The conversion and yield over time is presented in Figure 46. This was an interesting result in that it also begs the question of whether the ester formed is able to undergo hydrogenation itself, albeit at a slower rate.

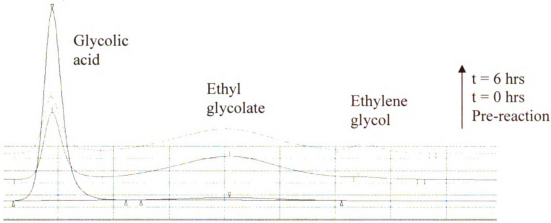

Figure 44. Hydrogenation of 0.25 M glycolic acid (0.3 M H_3PO_4, CH_3CH_2OH, 130 °C, 1000 psi H_2, 1 g dry 5% Ru/C)

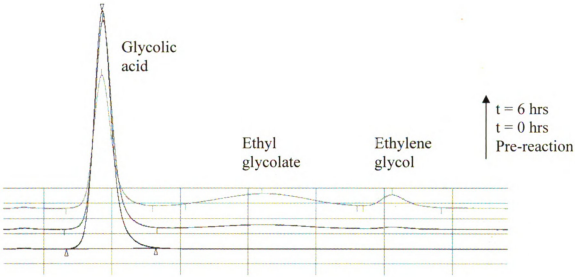

Figure 45. Hydrogenation of 0.25 M glycolic acid (CH_3CH_2OH, 130 °C, 1000 psi H_2, 1 g dry 5% Ru/C)

The literature suggests that esters undergo hydrogenation more rapidly than the corresponding acids with certain catalysts (Raney Ni, Copper/chromium oxide, rhenium

black). However, in the case of 100% ethanol there is little desired product formation. This result is not unexpected; early studies by Adkins (Raney Ni and Copper/chromium oxide) showed that esters hydrogenate poorly in the presence of free acids. Thus, the presence of both the organic acid and ester leads to competitive adsorption resulting in less desired product formation. If the ester formed does not undergo hydrogenation, less hydrogenation product is expected in the presence of acid due to more ester formed and depletion of free acid substrate available. However, these results indicate the same amount of ethylene glycol yield which suggests that some amount ester hydrogenation may be occurring (albeit small). In addition, in the presence of ethanol (and H_3PO_4) esterification is occurring faster than the hydrogenation of glycolic acid.

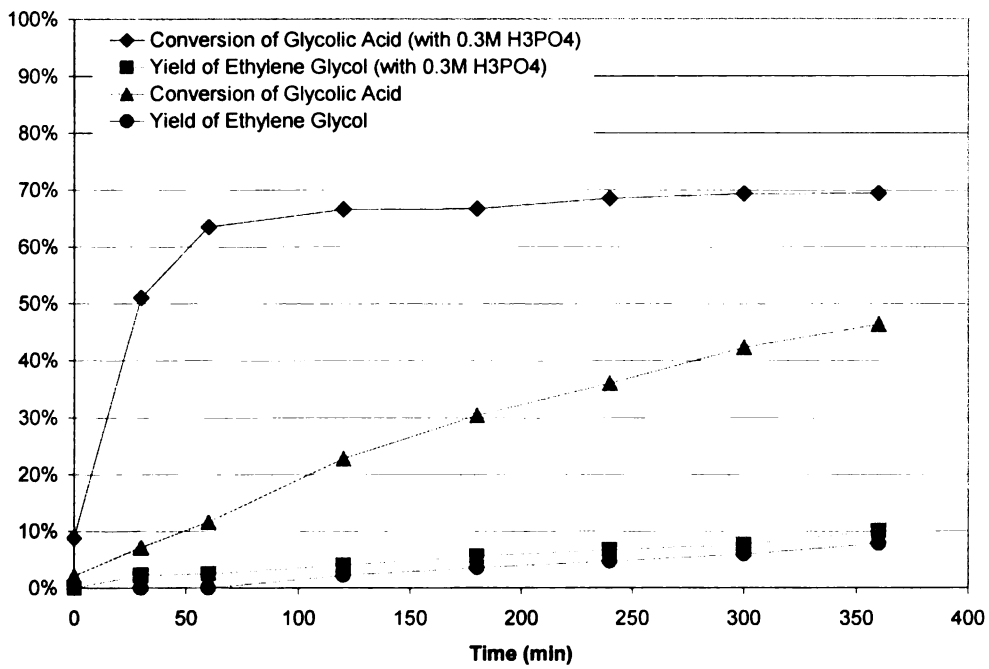

Figure 46. Hydrogenation of 0.25 M glycolic acid in the absence and presence of 0.3 M H_3PO_4 (CH_3CH_2OH, 130 °C, 1000 psi H_2, 1 g dry 5% Ru/C)

An experiment with 0.25 M ethyl lactate in water was exposed to the hydrogenation reaction conditions (130 °C; 1000 psi H_2). The ethyl lactate quickly hydrolyzed to form lactic acid. The lactic acid peak is overlapped by the ethyl lactate peak (Figure 47). The product propylene glycol was not observed until lactic acid was formed. However, the yield of propylene glycol at 6 hours was comparable to the yield using lactic acid as the substrate, nearly 72%.

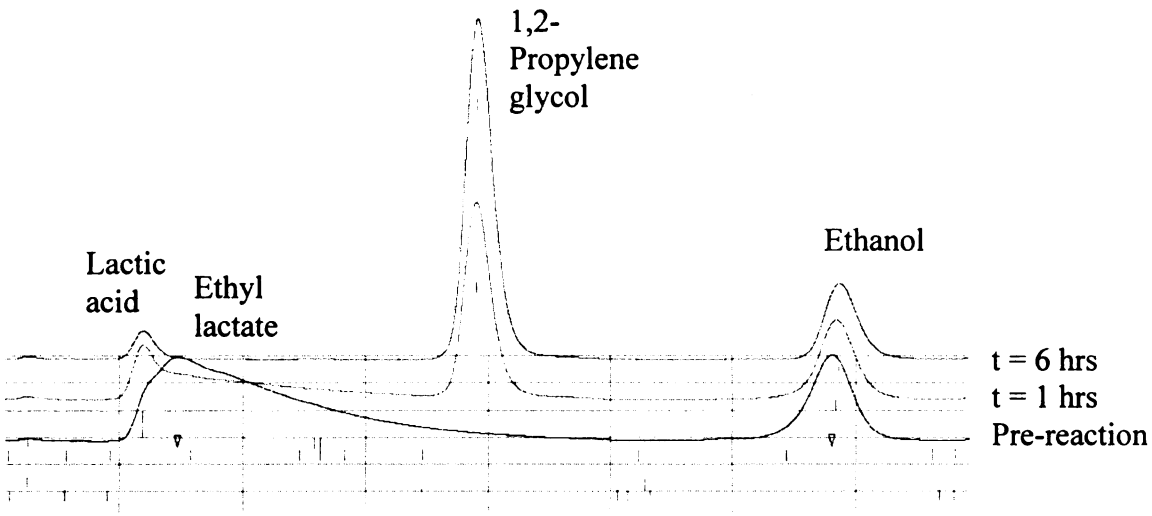

Figure 47. Hydrogenation of 0.25 M ethyl lactate (H_2O, 130 °C, 1000 psi H_2, 1 g dry 5% Ru/C)

This experiment suggests that the hydrolysis of ethyl lactate is faster than its hydrogenation, and that lactic acid hydrogenation is occurring with little hindrance from the ester or the product alcohol.

In the case of glycolic acid in ethanol, the hydrogenation is suppressed due to the solvent (solvent/catalyst interactions) and it appears that hydrogenation of ethyl glycolate is slow.

The reduced amount of hydrogenation observed with the ester be due to the ester functionality or may be more of a result of the overwhelming presence of the alcohol as the solvent. In the case of ethyl lactate in water, ethanol is formed as the ethyl lactate is hydrogenated. However, the amount of alcohol present is small compared with the solvent water and thus in this case the alcohol is not inhibiting the hydrogenation reaction.

An experiment that would help verify whether ester hydrogenation is possible is ethyl lactate in ethanol. However, as mentioned earlier, the solvent ethanol significantly suppresses the hydrogenation reaction and would presumably suppress it for an ester in the same way as it does for an acid. Our group has shown, using isotopic labeling experiments, that both glycerol and sorbitol exhibit rapid deuterium incorporation at C1 without reaction, suggesting reversible dehydrogenation on the metal surface as the first step in hydrogenolysis. This previous work sets a precedent for ethanol to undergo the same mechanism. Indeed, early qualitative studies by Kovacs et al. found deuterium incorporation at the 1-position of 1-propanol and 1,3-propanediol sites are very similar to the 1-position of ethanol.[53] The dehydrogenation/hydrogenation of ethanol is a possible reaction competing with the glycolic acid hydrogenation for catalyst sites.

Additional experiments using 0.25 M glycolic acid at 130 °C with 1000 psi H_2 in 80/20 (v/v) water/ethanol and 20/80 (v/v) water/ethanol mixtures were conducted and revealed that the yield of desired glycol continued to decrease as the organic solvent proportion was increased. However, net acid conversion was relatively the same (Figure 48) due to

increasing esterification and less reduction product formation as the solvent's ethanol fraction increased. The ethanol is known to undergo C-H activation and may be undergoing H/D exchange on the catalyst surface sites thereby reducing the amount of glycolic acid hydrogenation.

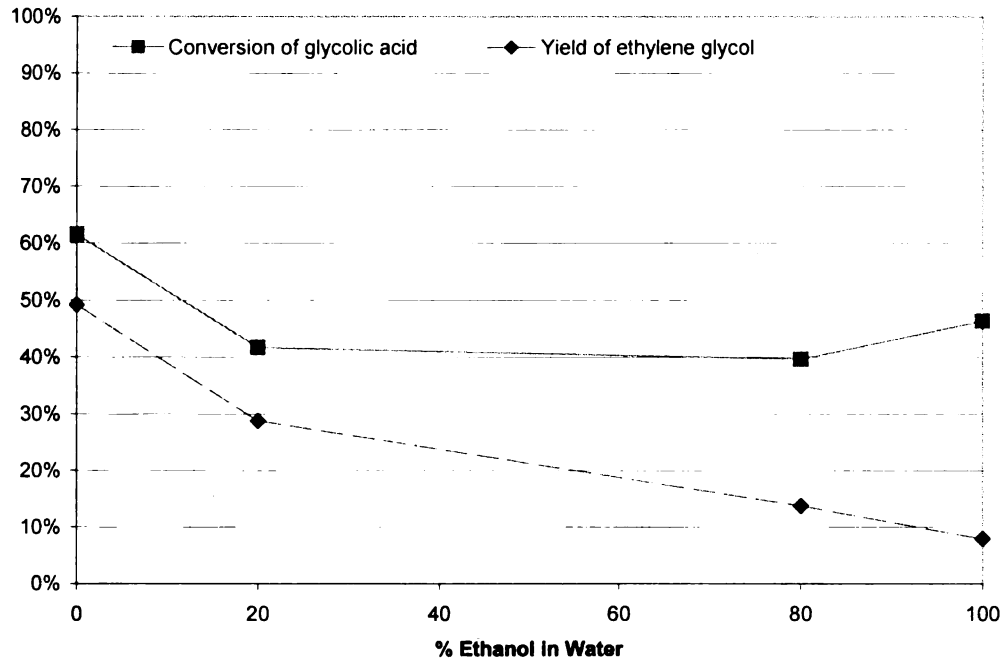

Figure 48. Hydrogenation of 0.25 M glycolic acid after 6 hours (CH_3CH_2OH/H_2O, 130 °C, 1000 psi H_2, 1 g dry 5% Ru/C)

Previous work in the Jackson/Miller group revealed that lactic acid had a higher surface affinity than propylene glycol.[66] These results were deduced from H/D exchange studies in which the rate of exchange and chirality loss in propylene glycol decreased as lactic acid was introduced to the system. Using this logic, ethylene glycol was chosen as a solvent. If glycolic acid has a higher affinity for the catalyst than ethylene glycol then some hydrogenation product might be expected. Studies of 0.25 M glycolic acid in ethylene glycol (130 °C; 1000 psi H_2) revealed that the dominant reaction occurring was

the esterification of the acid. The ester peak overlapped on the HPLC chromatogram with the glycolic acid peak and it was not possible to quantify the conversion of glycolic acid to the ester. Thus, the response factor was not determined for this suspected ester. Qualitatively, the amount of glycolic acid converted (based on manual integrations) and the amount of ester formed indicates that not much, if any hydrogenation product was formed. However, a small amount of ethanol was formed.

In the presence of hydridic hydrogens on the Ru surface, the mechanism to form ethanol as a side product from the degradation of ethylene glycol may involve a hydrogen from the surface displacing a water molecule.[67] To further examine the possible degradation of ethylene glycol a control experiment in which ethylene glycol alone is subjected to the reaction conditions should be run. However, we have seen ethanol formed after six hours in experiments with glycolic acid that resulted in high conversion (62%) yielding ethylene glycol (49%).

Up to this point, it seems apparent that the solvent may be occupying the surface and undergoing either H/D exchange or hydrogenation/dehydrogenation thereby competitively preventing the hydrogenation of the organic acid. If an organic acid is chosen as the solvent, then one would hypothesize that the product alcohol from the solvent would be formed. Glycolic acid has a much higher rate of reaction than acetic acid, 49% yield compared with 5% yield after six hours (H_2O, 130 °C; 1000 psi H_2, 1 g dry 5% Ru/C). This may be partly due to the difference in adsorption affinity as well as the activation due to the α-substituent.

From the present work, results with 0.25 M glycolic acid at 130 °C with 1000 psi H_2 in acetic acid as the solvent indicate that neither ethylene glycol nor ethanol is produced. The acetic acid forms esters with the glycolic acid's –OH side chain, and there is 0% yield of either alcohol products. If the solvent, acetic acid, were saturating the surface then some ethanol would be expected. However, the pKa of acetic acid is about 4.75 and it may be that the acid is reacting with the surface and causing deactivation of the catalyst due to the amount of acetic acid present in the system.

Though less reactive than lactic or glycolic acid, propanoic acid is more reactive and slightly less acidic (pKa = 4.85) than acetic acid. After six hours of reaction, nearly 13% of propanol is formed from 0.25 M propanoic acid (H_2O, 130 °C; 1000 psi H_2, 1 g dry 5% Ru/C). 0.25 M glycolic acid at 130 °C with 1000 psi H_2 in propanoic acid revealed about 3% propanol and detectable ester. Ethylene glycol elutes at the same time as the solvent propanoic acid and therefore could not be quantified, although 70% of the glycolic acid was converted after six hours. Some of the conversion may have yielded ethylene glycol and the ester of propanoic acid. Again, because there was hardly any propanoic acid hydrogenation product formed it begs the question of what reaction is taking place to prevent the acid hydrogenation.

Competitive adsorption is a key component in trying to understand these phenomena. Due to the fairly unreactive nature of the unsubstituted organic acids, it may be that the competitive reactions or esterification and self dimerization are enough to suppress the

hydrogenation of the propanoic acid. In order to further explore this, an experiment in which there is an equimolar amount of propanoic acid and glycolic acid in water was conducted. The hydrogenation of glycolic acid may be slightly suppressed if there is competitive adsorption with an equimolar amount of propanoic acid, but production of the alcohol products would be expected. In this case, the esterification and self dimerization are not expected to be dominant. Competition experiments will be discussed in section 4.8.

To summarize the solvent studies, it is evident that if the solvent is able to undergo reactions on the catalyst surface, these reactions compete with the organic acid hydrogenation. Solvent H/D exchange and hydrogenation/dehydrogenation, and catalyst deactivation (whether temporary or permanent) can almost completely stop the organic acid hydrogenation reaction. Thus, the water is playing an important role in the overall catalytic hydrogenation of organic acids in that it is not competing with the reaction. The water may be playing an additional role of assisting H_2 cleavage into hydrogen atoms on the surface. The potential role of water in the overall hydrogenation mechanism using 5% Ru/C will continue to be explored via detailed H/D exchange reactions and discussed later. Again, there are several advantages of aqueous phase processing. The nonvolatile organic acids can be converted without having to be esterified, as would be required for vapor-phase conversion. And energy costs associated with vaporizing and condensing process streams is reduced.

4.6 Organic Acid Hydrogenation Studies

4.6.1 Effect of the α-Substituent on the Hydrogenation Reaction

One of the key findings from the previous research done in the Jackson/Miller research group was that simple carboxylic acids such as propanoic acid and acetic acid are substantially more difficult to reduce than lactic acid and L-alanine. Thus, the presence of the heteroatomic side chains modify reactivity. Specifically, protonated alanine and lactic acid undergo aqueous-phase hydrogenation over a carbon-supported ruthenium catalyst ca. 10 and 3-5 times as fast as their unsubstituted analogue, propanoic acid. The present work explores the substituent effects on organic acids' reactivity and selectivity toward hydrogenation by comparing reduction rates over a wide range of electron-withdrawing, hydrogen-bonding, or sterically bulky vicinal substituents.

Several three-carbon and two-carbon organic acid substrates were chosen in order to evaluate the extent to which the α-substituent affects the hydrogenation rate. Substrates included the following α-substituents: -H, $-CH_3$, -OH, $-N^+H_3$, $-OCH_3$, $-N^+H_2CH_3$, $-N^+H(CH_3)_2$, $-N^+(CH_3)_3Cl^-$, $-N^+(CH_3)_3$. The experiments were conducted at 130 °C with 1000 psi H_2 using 1 gram of pre-reduced 5 wt% dry Ru/C with 0.25 M substrate and 0.3 M H_3PO_4 in water. Amino acids represent an attractive group of compounds for liquid-phase hydrogenation, both because of the diversity of substituents available and because of the recognized importance of optically active amino alcohol products as intermediates in pharmaceuticals.

Amino acids typically form dipolar ions in aqueous solution at their isoelectric point (pH ~5-7); the actual form is thus determined by the pH of the solution. The reason the H_3PO_4 was required (as discussed previously) for the successful hydrogenation of the amino acids was to protonate the zwitterionic carboxylic acid, thus enabling hydrogenation. In order to be consistent, the H_3PO_4 was added to all experiments.

Three carbon organic acid substrates:

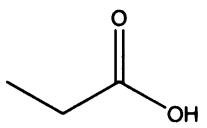

propanoic acid

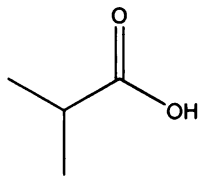

isobutyric acid

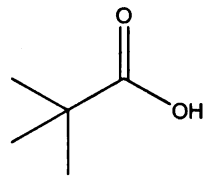

pivalic acid

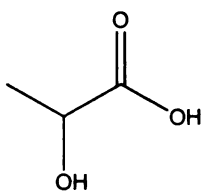

lactic acid

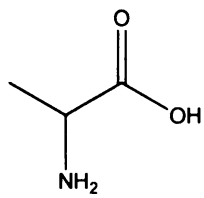

alanine

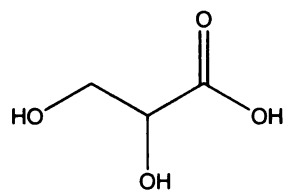

glyceric acid

Two carbon organic acid substrates:

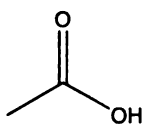

acetic acid

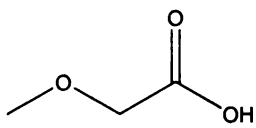

methoxyacetic acid

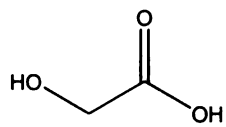

glycolic acid

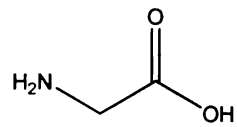

glycine

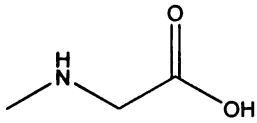

N-methylglycine

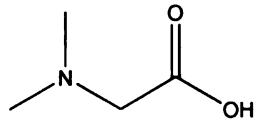

N,N-dimethylglycine

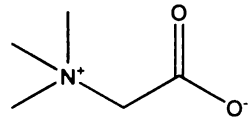

N,N,N-trimethylglycine (betaine)

Glycine and the N-methylated glycine series were protonated due to the presence of H_3PO_4. If additional acid is not present, they are in zwitterionic form. In addition, the hydrogenation of both betaine with and without the chloride counterion was compared.

A set of optimum reactor conditions was selected for this study based on previous work done by our research group.[25,48,49,50] The results are presented in the graphs (Figures 49 and 50) and table (Table 2) below. Table 2 presents the overall data after six hours of reaction time and details the conversion based on the initial concentration; selectivity, in units of mole product per mole reactant converted, and yield, in units of mole of product per mole of reactant fed. Carbon balances were calculated to account for most products (>90%).

Equation 62. Conversion of substrate in the hydrogenation reaction

$$= \left(\frac{\text{reactant moles consumed}}{\text{reactant moles fed}} \right)$$

Equation 63. Yield of desired product in the hydrogenation reaction

$$= \left(\frac{\text{product moles formed}}{\text{reactant moles fed}} \right)$$

Equation 64. Selectivity of desired product in the hydrogenation reaction

$$= \left(\frac{\text{product moles formed}}{\text{reactant moles consumed}} \right)$$

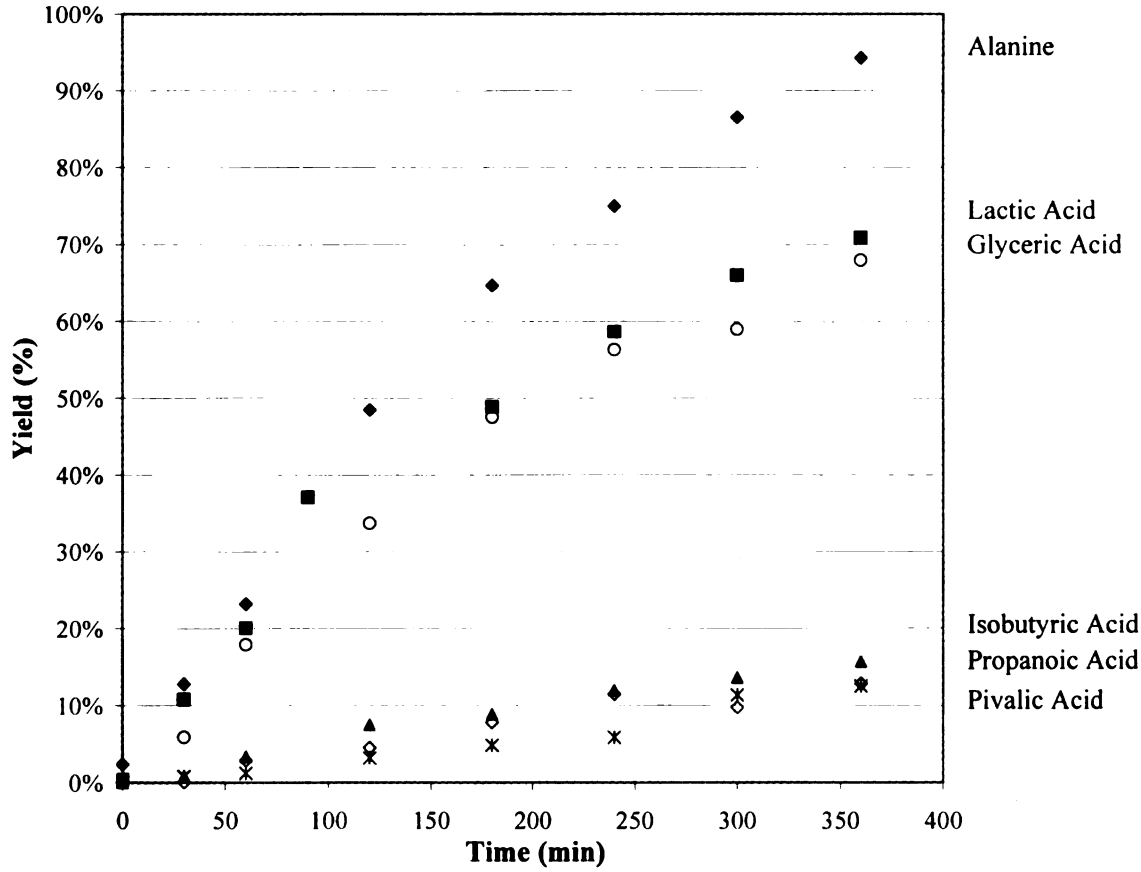

Figure 49. Hydrogenation of C_3 organic acids to alcohols (0.3 M H_3PO_4, H_2O, 130 °C, 1000 psi H_2, 1 g dry 5% Ru/C)

The various α-substituents were chosen in order to evaluate the effect of hydrogen bonding, electron withdrawing ability, and heteroatom coordination to the surface. In acid, the α-substituent if it is an amino group is presumably protonated. This allows for two types of hydrogen bonding. The hydrogen can interact with the hydridic hydrogens on the surface thereby increasing the reactivity by promoting interaction between the substrate and the catalyst surface. The other type of hydrogen bonding is intramolecular hydrogen bonding with the free electrons on the carbonyl oxygen, stabilizing the partial positive charge on the carbonyl carbon. In the case of the unsubstituted alkanoic acids

(acetic, propanoic, isobutyric, and pivalic acid) and the trimethylated amino species ($(CH_3)_3N^+CH_2COOH{\bullet}Cl^-$) the hydrogen bonding ability is eliminated and it was observed that they are very unreactive. In addition a comparison between glycolic acid and methoxyacetic acid indicates a reduced rate of hydrogenation in the case of the methoxy α-substituent. Thus, hydrogen bonding may be playing a role in accelerating the hydrogenation reaction.

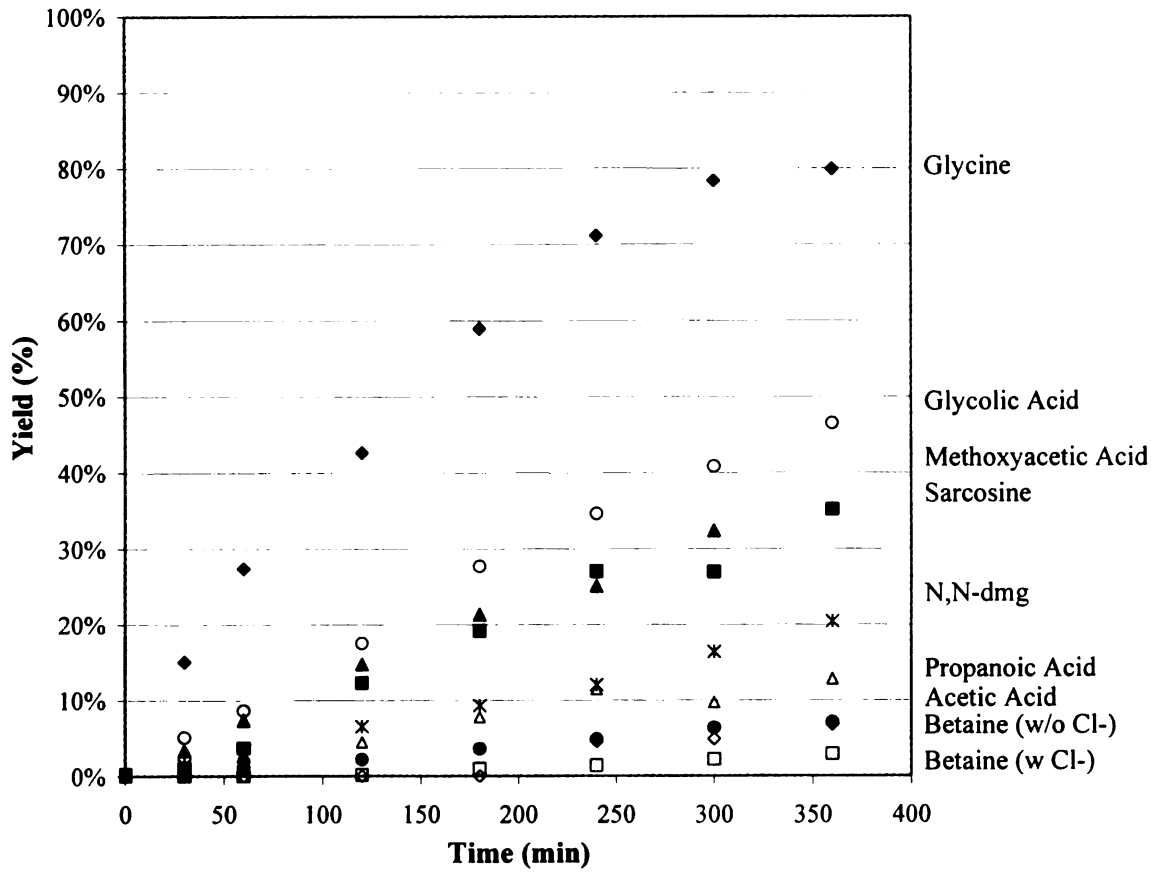

Figure 50. Hydrogenation of mostly C_2 organic acids to alcohols (0.3 M H_3PO_4, H_2O, 130 °C, 1000 psi H_2, 1 g dry 5% Ru/C)

It was observed that $(CH_3)_3N^+CH_2COOH{\bullet}Cl^-$ was not very reactive (<2% yield of choline chloride) and the extent to which the chloride counter-ion was playing a role was not

fully understood. So, betaine ($(CH_3)_3N^+CH_2COO^-$) was also run under the same conditions (0.3 M H_3PO_4, H_2O, 130 °C, 1000 psi H_2, 1 g dry 5% Ru/C). A conversion of 41% was obtained, but only 7% yield of the choline product of carboxylate reduction was achieved. Thus, the presence of the chloride counter-ion appears to be inhibiting the reaction. No other products were detected in the HPLC.

Table 2. Hydrogenation of C_3 and C_2 organic acids to alcohols after six hours (0.3 M H_3PO_4, H_2O, 130 °C, 1000 psi H_2, 1 g dry 5% Ru/C)

(Substrate) α-substituent	Conversion (%)	Yield (%)	Selectivity to Alcohol
(C3) N^+H_3	94	86	91
(C2) N^+H_3	96	80	83
(C3) OH	93	79	85
(C3) α,β $(OH)_2$	76	68	100
(C2) OH	56	47	82
*(C3) OCH_3	48	47	98
(C2) OCH_3	53	35	67
(C3) $N^+H_2(CH_3)$	37	35	96
(C3) $N^+H(CH_3)_2$	40	20	51
(C3) $(CH3)_2$	46	12	27
(C3) CH_3	39	16	40
(C2) CH_3 / (C3) H	33	13	39
(C3) $N^+(CH_3)_3$	41	7	17
(C2) H	19	7	37
(C3) $N^+(CH_3)_3Cl^-$	0	3	0

*Data from Norbert Varga's thesis (Michigan State University)

Looking at the low selectivities to the desired alcohol for the unsubstituted alkanoic acids, it is assumed that some of the by-products that are formed include methane, ethane, and propane.[48,49] Zhang et al. found that at temperatures below 170 °C these were the

typical by-products and at temperatures above 170 °C, degradation to 1-propanol, ethanol, and 2-propanol were observed.

4.6.2 Amino Acid Substrates

Additional experiments at temperatures of 100 °C and 150 °C were conducted with glycine and the N-methylated glycine series. The results for conversion, yield and selectivity are presented in Table 3. In general, the selectivity decreased at higher temperatures indicating increased degradation.

Table 3. Hydrogenation of glycine, sarcosine, N,N-dmg, and betaine at 100, 130, and 150 °C after six hours (0.3 M H_3PO_4, H_2O, X °C, 1000 psi H_2, 1g dry 5% Ru/C)

100 °C	Conversion (%)	Yield (%)	Selectivity
Glycine	31.4	28.2	89.8
Sarcosine	10.2	11.7	100
N,N-dimethylglycine	13.8	11.2	81.1
Betaine	4.1	0	0
130 °C	Conversion (%)	Yield (%)	Selectivity
Glycine	89.8	82.8	92.2
Sarcosine	40.5	30.4	75.1
N,N-dimethylglycine	29.4	18.6	63.2
Betaine	40.6	6.8	16.7
150 °C	Conversion (%)	Yield (%)	Selectivity
Glycine	98.5	79.9	81.1
Sarcosine	71.6	50.7	70.8
N,N-dimethylglycine	57.1	41.1	72.0
Betaine	73.7	17.4	23.6

The initial rates were calculated from plots of concentration (mol/L) versus time (min) and are reported in units of kmol/kg of cat/min (Table 4). The hydrogenation rate of reaction is reduced by a factor of ~3 as each methyl group is added. The activation

energy was calculated for each substrate and was 41, 56, and 50 kJ/mol for glycine, sarcosine, and N,N-dimethyglycine.

Table 4. Rates of reaction for hydrogenation of glycine, sarcosine, and N,N-dmg (0.3 M H_3PO_4, H_2O, 100, 130, and 150 °C, 1000 psi H_2, 1g dry 5% Ru/C)

	-Ri (kmol/kg of cat/s)*		
	100°C	130°C	150°C
Glycine	6.2	16.7	30.9
N-methylglycine	1.6	6.9	13.3
N,N-dimethylglycine	0.6	3.9	10.8
Betaine	0.0	0.0	0.0

*Rates are multiplied by 10^7

It is not clear whether the heteroatom at the α-position is adsorbing on the surface. There are a few different mechanisms to consider. It may be that the α-carbon adsorbs, or if the acidic proton on the heteroatom is able to dissociate, then a pi bond can be formed and interact with the surface. The ability to form this pi bond is only present in the hydroxy, amino, methylamino and di-methylamino substrates. In traditional C-H activation, it is the lone pair on the N that is active, so varying the amount of acid might lead to an understanding of how the C-H activation is affected. We know that for hydrogenation to occur, acid must be present to ensure the carboxylic acid is protonated. Looking at the amine species, the acid amount can be varied to slow or prevent hydrogenation. Jere et al. examined the effect of phosphoric acid concentration on conversion of 0.22 M alanine (100 °C and 1000 psi H_2).[50] The conversion was ~90% with 0.29 M H_3PO_4, ~65% with 0.14 M H_3PO_4, and 45% with 0.07 M H_3PO_4. H/D exchange will be exploited and discussed in section 4.7 to examine how the reactivity of each of the amine species is affected.

The methoxy substituent evidently benefits the reaction over the similar sized methyl substituent. From the data, it appears that the hydrogenation reaction is not as sensitive to sterics, with respect to a methyl group. In fact, the methylated substrate (isobutyric acid) appears to be slightly more reactive than the simple carboxylic acid substrates (propanoic acid, acetic acid). But, pivalic acid is about the same in reactivity as propanoic and acetic acid suggesting that at some point the addition of another methyl (as compared to isobutyric acid) may start to slow the reaction. In theory, the relatively bulky methoxy or methyl group may adversely influence the adsorption of the substrate on the catalyst surface as free rotation around the sigma bond between the C1 and C2 carbon is possible. The presence of a bulky substituent close to the sp^2 carbon of the carboxyl functionality could hinder the delivery of the hydride. However, this steric effect does not appear for the simple alkanoic acids.

The methylated amine species have provided more information on the sensitivity of the hydrogenation reaction to steric modifications at the α-amino position. Looking at the trend for $-N^+H_3$, $-N^+H_2CH_3$, $-N^+H(CH_3)_2$ the reactivity falls off by a factor of three as each hydrogen is replaced by a methyl. However, these replacements also represent changes in the amino groups' H-bonding abilities. To determine whether the addition of a methyl(s) is hindering the substrate interaction with the catalyst surface, H/D exchange studies can be done on this series. If less exchange is observed as methyl groups are added, it may support the decrease trend in reactivity, partly due to a steric effect.

In the hydrogenation of organic acids, electronics may be more important than sterics due to C-H activation. To understand the relative rates of C-H activation as well as gaining more mechanistic understanding of the reaction occurring at C2 in the organic acids, a series of substrates has been studied. Direct C-H activation has been observed with an ether (THF) and direct C-H activation or indirect (via dehydrogenation) C-H activation in terminal alcohols (ethanol, glycols) is commonplace with the heterogeneous Ru catalyst systems studied here. For future work, it is suggested that (S)-2-hydroxybutanol, (S)-2-methoxybutanol, and (S)-2-aminobutanol be evaluated because they are secondary alcohols (similar to the organic acid substrates). It would be interesting to measure the rate of deuterium incorporation at C2 as well as observe whether deuterium is incorporated at either C1 or C3 in the hydroxyl and amino substrates, indicating the enol and enamine intermediates. The rate of deuterium incorporation at C2 can be compared to the amount of deuterium incorporated at C2 of the corresponding acid. If deuterium is incorporated in (S)-2-methoxybutanol it may occur via direct α-C-H activation.

Another factor that is inevitably affecting the hydrogenation reaction is the adsorption affinity of each of the substrates. Competitive adsorption studies with the four amino species (N^+H_3, $N^+H_2CH_3$, $N^+H(CH_3)_2$, and $N^+(CH_3)_3)Cl^-$ should also be carried out to evaluate their relative adsorption affinity. If the trend follows their reactivity trend then a deeper understanding of the decreased reactivity can be realized. If they have similar adsorption affinities; however, it would suggest that the sterics or electronics are the controlling factors. Understanding the product distributions in the amino species and the reaction kinetics will help fill in details regarding their relative reactivities.

4.7 H/D Exchange Studies

4.7.1 Amino Acid Substrates

4.7.1.1 H/D Exchange at the Methylene Position

The catalytic hydrogenation of the methylated glycine amino acids to amino alcohols has been discussed. In general, amino alcohols can serve as building blocks for numerous products in pharmaceutical and fine chemical applications. Research conducted in the Jackson/Miller group by Jere et al. and Pimparkar et al. has shown the stereoretentive reduction of alanine, serine, and valine.[50,63] In an effort to build upon this research and probe the reactivity differences in hydrogenation of the methylated glycine series discuss above, H/D exchange studies were conducted on this series.

The amino acid substrates that were studied included glycine, N-methylglycine (sarcosine), N,N-dimethylglycine, betaine, and glycylglycine. Again, the rate equations (Chapter 3) can be used to calculate rate constants k_{1A}, k_{-1A}, k_{2A}, and k_{-2A}. The reactions described consider the back reactions (as opposed to the work by Frey et al.[26] and Richard et al.[28,29]). Although, the back reactions were not expected to have much significance, especially in the reactions with 1000 psi D_2 and D_2O. This will be discussed more as the individual experiments are considered.

An early experiment with 0.25 M glycine at 130 °C with 1000 psi H_2 and D_2O for two hours showed that the H/D exchange reaction occurred very quickly at this temperature. A CH_2 conversion of 99% was found and 18% and 80% (calculated) yield of CHD and CD_2, respectively. The ^1H NMR spectra taken of time zero and after two hours of

reaction time are compared in Figure 51. Conversion of CH_2 is already at 71% at time zero.

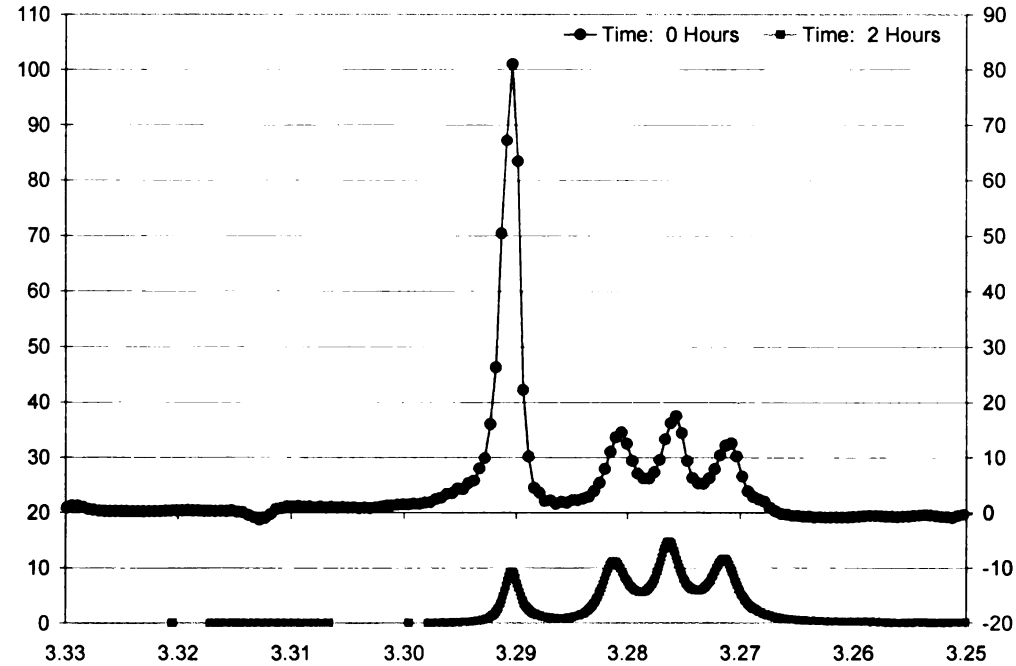

Figure 51. ^1H NMR of H/D exchange at the methylene position of 0.25 M glycine (D_2O, 130 °C, 1000 psi H_2, 1 g dry 5% Ru/C)

H/D Exchange Studies at 100 °C with 1000 psi H_2

In order to better understand and model the reaction rate kinetics, the reaction was subsequently run at lower temperatures (100, 90, 70 and 50 °C). An experiment with 0.25 M glycine at 100 °C with 1000 psi H_2 in D_2O was allowed to react for five hours, the singlet ^1H NMR peak representing the methylene (CH_2) position continued to decrease in size over time, the triplet peak representing CHD grew in reaching a maximum peak height at 60 minutes then started to decrease as the hydrogen at that position was further exchanged with deuterium. The stacked ^1H NMR spectra of time 0, 1, 2, 3, 4, and 5 hours of reaction time is compared in Figure 52.

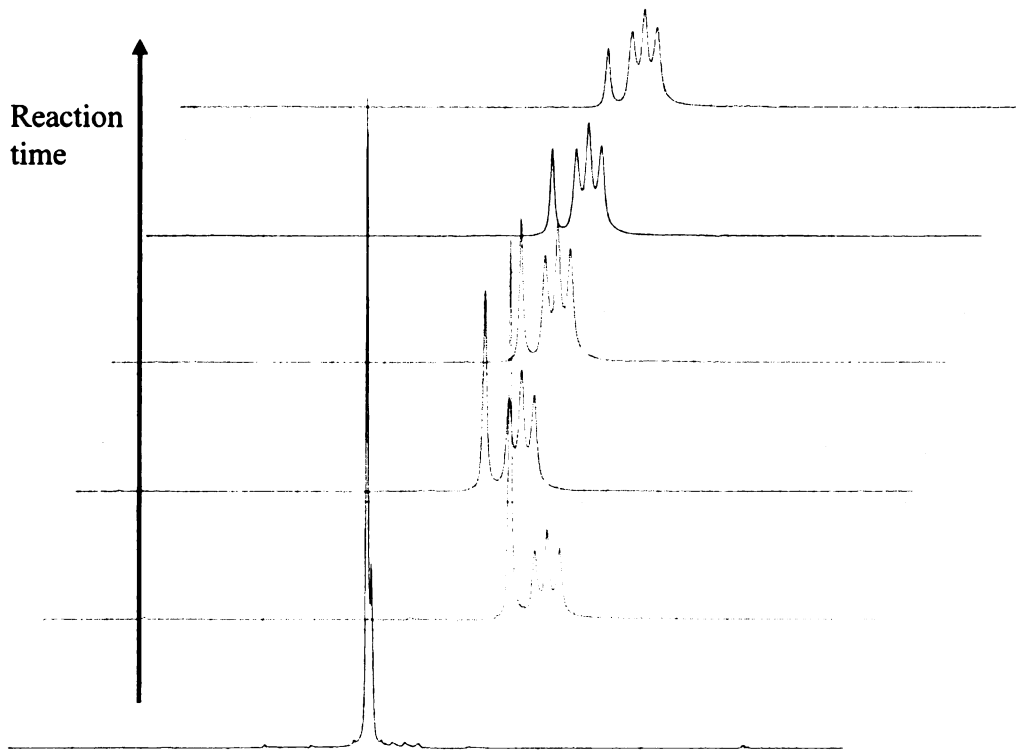

Figure 52. Stacked ^{1}H NMR of H/D exchange at the methylene position on 0.25 M glycine (D_2O, 100 °C, 1000 psi H_2, 1 g dry 5% Ru/C)

Figure 53 shows the experimental and fitted concentrations of CH_2, CHD, and CD_2 over time as determined by the equations in Chapter 3. The rate constants for H/D exchange on the methylene carbon are: $k_{1A} = 2.3x10^{-4}$, $k_{-1A} = 1.2x10^{-4}$, $k_{2A} = 1.2x10^{-4}$, $k_{-2A} = 3.2x10^{-4}$ L/mol/min and the sum of the squares error (SSE) = $3.9x10^{-5}$. The rate constants for glycine, sarcosine, and N,N-dimethylglycine at these reaction conditions (D_2O, 100 °C, 1000 psi H_2, 1 g dry 5% Ru/C) will be summarized after each experiment is discussed. The sum of the squares error (SSE) is minimized for AH_2 and AHD; thus it does not include AD_2 because AD_2 is not directly measured. The plotted points as shown

also represent residuals, differences between the known initial glycine concentration and the observable CH_2 and CHD amount.

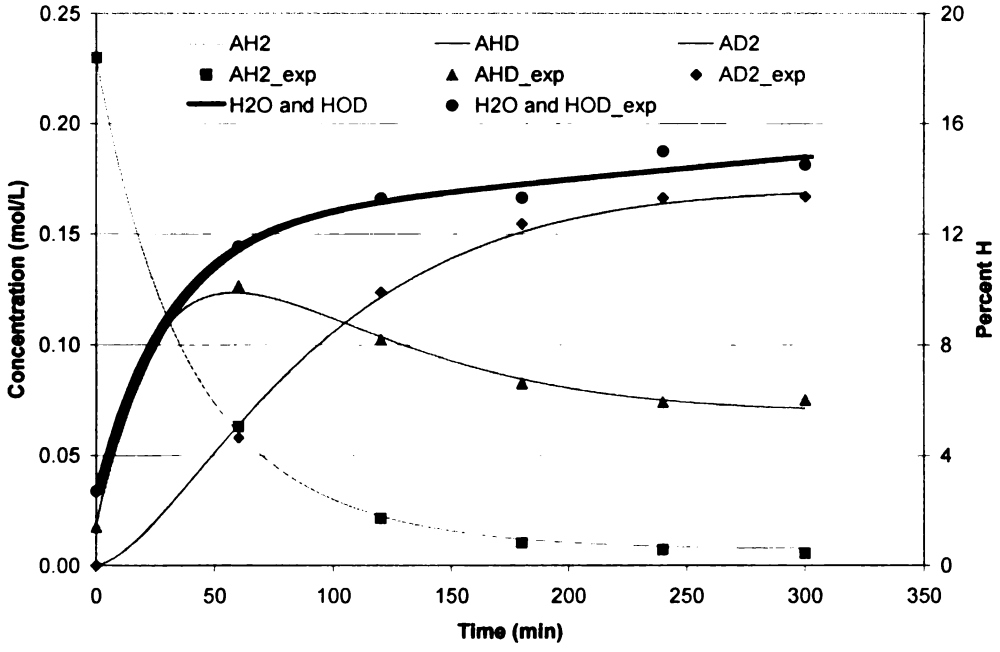

Figure 53. Fit of the kinetic rate data for 0.25 M glycine (D_2O, 100 °C, 1000 psi H_2, 1 g dry 5% Ru/C)

For this experiment, glycine reaches equilibrium at about 4 hours, thus the statistical equilibrium end points can be calculated and compared to the experimental data. The statistical concentrations of CH_2, CHD, and CD_2 based on the actual percent hydrogen in water at five hours (14.5%) and the concentration at time zero (0.23 M) are 0.0048, 0.057, and 0.168 M, respectively. The actual concentrations of CH_2, CHD, and CD_2 at five hours of reaction time are 0.0054, 0.075, and 0.166 M, respectively. Thus, the values are in good agreement.

The same experiment using sarcosine (N-methylglycine) was performed at 100 °C with 1000 psi H_2 and D_2O for six hours. The ^1H NMR spectra of time zero and after six hours of reaction are compared in Figure 54. Figure 55 shows the experimental and fitted concentrations of CH_2, CHD, and CD_2 over time as determined by the equations in Chapter 3. The kinetics were determined using the models described in Chapter 3. Using kinetic rate model A (Chapter 3.2.1) the rates for H/D exchange on the methylene carbon are: $k_{1A} = 1.6x10^{-4}$, $k_{-1A} = 0$, $k_{2A} = 1.6x10^{-4}$, $k_{-2A} = 2.6x10^{-4}$ L/mol/min and the sum of the squares error (SSE) = $4.5x10^{-3}$.

Again, we can compare the statistical equilibrium end points and the experimental data. The statistical concentrations of CH_2, CHD, and CD_2 based on the actual percent hydrogen in water at six hours (15.0%) and the concentration at time zero (0.24 M) are 0.0054, 0.062, and 0.176 M, respectively. The actual concentrations of CH_2, CHD, and CD_2 at six hours of reaction time are 0.004, 0.054, and 0.199 M, respectively.

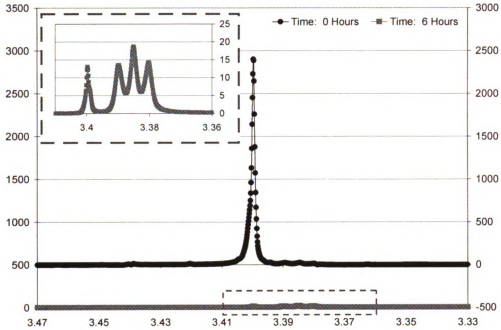

Figure 54. ^{1}H NMR of H/D exchange at the methylene position of 0.25 M sarcosine (D_2O, 100 °C, 1000 psi H_2, 1 g dry 5% Ru/C)

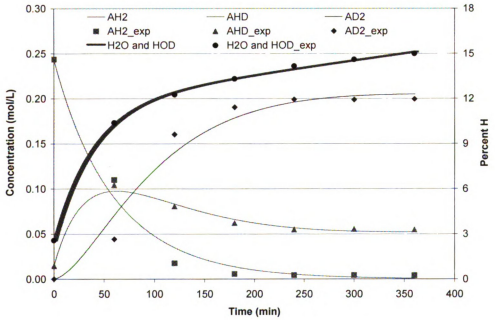

Figure 55. Fit of the kinetic rate data for 0.25 M sarcosine (D_2O, 100 °C, 1000 psi H_2, 1 g dry 5% Ru/C)

From the data, it appears the rate constants are too large or perhaps the fitted line should be starting at some time, t, after time zero. In experiments with 1000 psi H_2 and D_2O there may be two reasons for the apparent need for a time offset or something equivalent. The first reason is the slight delay in equilibrium between the liquid concentration and the amount of available hydrogen or deuterium on the catalyst surface. And in the beginning of the reaction, the amount of deuterium available on the surface is less so hydrogen exchange at this point may be occurring but with the hydrogen on the surface. The second reason may be a time delay due to the catalyst ramping up in activity. This will be discussed further.

The same experiment using N,N-dimethylglycine (N,N-dmg) was performed at 100 °C with 1000 psi H_2 and D_2O for six hours. The ^1H NMR of time zero and after six hours of reaction time is compared in Figure 56. Figure 57 shows the experimental and fitted concentrations of CH_2, CHD, and CD_2 over time as determined by the equations in Chapter 3. Using kinetic rate model A (Chapter 3.2.1) the rates for H/D exchange on the methylene carbon are: $k_{1A} = 7.1x10^{-5}$, $k_{-1A} = 0$, $k_{2A} = 6.4x10^{-5}$, $k_{-2A} = 1.6x10^{-4}$ L/mol/min and the sum of the squares error (SSE) = $2.5x10^{-3}$. Again, we can compare the statistical equilibrium end points and the experimental data. However, for the experiment with N,N-dimethylglycine the equilibrium is not reached at six hours. The statistical concentrations of CH_2, CHD, and CD_2 based on the actual percent hydrogen in water at six hours (15.3%) and the concentration at time zero (0.24 M) are 0.0057, 0.063, and 0.175 M, respectively. The actual concentrations of CH_2, CHD, and CD_2 at six hours of reaction time are 0.018, 0.084, and 0.142 M, respectively.

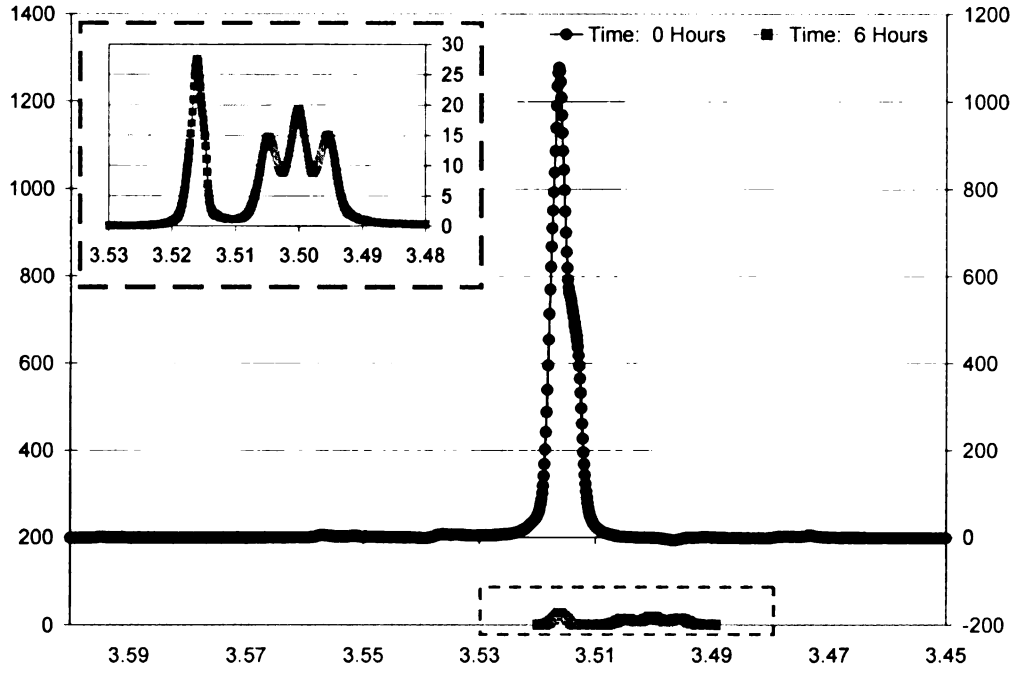

Figure 56. ^{1}H NMR of H/D exchange at the methylene position of 0.25 M N,N-dmg (D_2O, 100 °C, 1000 psi H_2, 1 g dry 5% Ru/C)

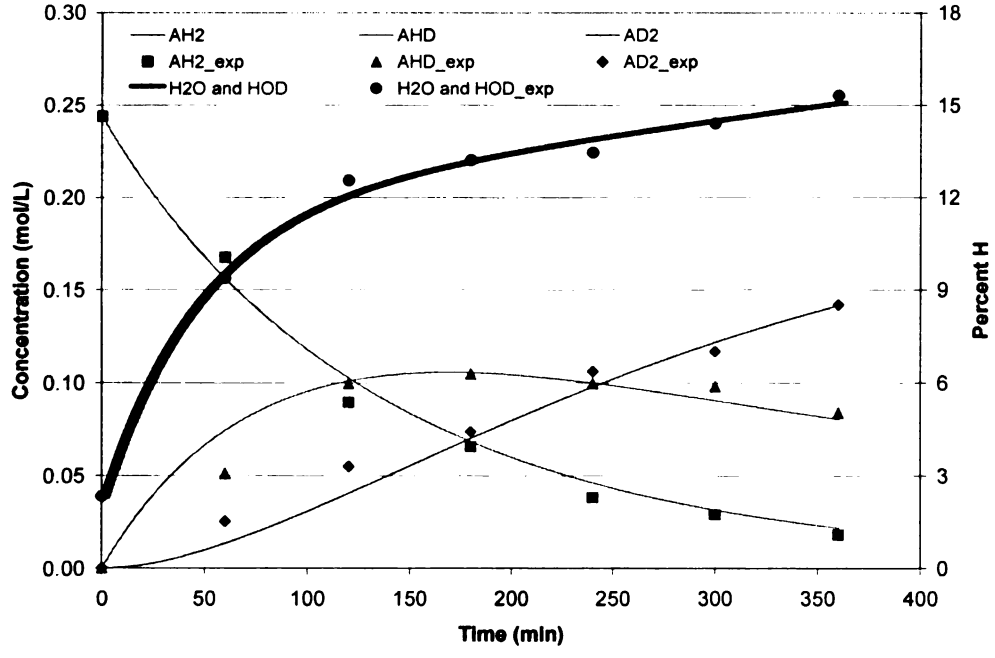

Figure 57. Fit of the kinetic rate data for 0.25 M N,N-dmg (D_2O, 100 °C, 1000 psi H_2, 1 g dry 5% Ru/C)

It is important to note, that we need to be skeptical of the rate constants for the back reactions (k_{-1A} and k_{-2A}, deuterium to hydrogen) because these rate constants depend so heavily on small variations in the "main event" of replacing the deuterium with hydrogen and its rate variation with time and how well we are modeling the aqueous [H] concentration. Unlike the hydrogen to deuterium exchanges, there is no initial rate behavior we can easily compare to the fitted constants, because deuterium to hydrogen only happens after substantial deuterium incorporation has occurred, and even then, it's a minor process because of the relatively low hydrogen concentration in the water. In addition, our water hydrogen and deuterium concentration versus time function is an empirical fit to fairly spread out data points and if it were off a bit, that could throw off the back reaction rate constants significantly. In order to partially address this, a more constrained model using essentially one k value for each site and then modified via isotope effect numbers was also explored.

A kinetic isotope effect is observed when the reaction rate is affected as one atom in a compound is replaced with its isotope. For the case of hydrogen and deuterium, the K_{IE} is expressed as $K_{IE}=k_H/k_D$. All of the H/D exchanges are assumed to be occurring through the same process, but now instead of four independent variables, the system is redefined and has three independent variables, k_{iA}, p_A, and s_A. As discussed in Chapter 3, k_{1A} is equal to $2*k_{iA}$ indicating that there are two hydrogens on the methylene carbon and subsequently two chances for H/D exchange. The equations for how the k_{1A}, etc rate constants could be effectively calculated from the k_{iA}, p_A, and s_A values are in Chapter 3 (equations 56 and 57). It was assumed p_A and s_A are independent.

Looking at the same three experiments glycine, sarcosine, and N,N-dimethylglycine at 100 °C with 1000 psi H_2 and D_2O the chemical equations which incorporate the kinetic isotope effects (6-variable kinetic model) were solved. For the forward reactions, the rate constants using both models are similar. For the back reactions the rate constants are somewhat different. Again we need to be skeptical of their meaning. When constraining the model to use only one rate constant, k_i and incorporating primary and secondary isotope effects, the rate constant for glycine is $k_{iA} = 1.2x10^{-4}$ L/mol/min and the isotope effects are $p_A = 0.76$ and $s_A = 0.98$. For sarcosine $k_{iA} = 0.82x10^{-4}$ L/mol/min, $p_A = 1.25$, and $s_A = 0.51$. For N,N-dimethylglycine $k_{iA} = 0.36x10^{-4}$ L/mol/min, $p_A = 2.12$, and $s_A = 0.69$.

The rate constants, k_i, for glycine, sarcosine, and N,N-dimethylglycine are about half of k_{1A} and k_{2A} that were calculated using the 10-variable model. This makes sense based on the fact that $k_{1A} = 2*k_{iA}$ and the k_{1A} as computed from both the 10 and 6-variable models are nearly the same. In addition, the fact that the k_{iA} values are similar to k_{2A} for sarcosine and N,N-dimethylglycine makes sense because $k_{2A} = k_{iA}/s_A$ and s_A for those two substrates is close to 0.5. For glycine, the secondary isotope effect is essentially one, so k_{iA} is essentially the same as k_{2A} and half the value of k_{1A}. It is important to note that it is the value of p_A that is most sensitive to the back processes, so the s_A values should be more reliable than the p_A values. For each N-methyl group added, the rate drops off by about one-third.

To further verify whether isotope effects are playing a role in the H/D exchange reaction at 100 °C with 1000 psi H_2 and D_2O, the primary and secondary isotope effects for the experiment with 0.25 M sarcosine were fixed to 1. The rate constants k_{iA} and k_{iC} were then solved. The newly solved rate constants k_{iA} and k_{iC} were equal to $1.1x10^{-4}$ and $0.51x10^{-4}$, respectively. These were compared to the original k_{iA} and k_{iC} which were equal to $0.82x10^{-4}$ L/mol/min and $0.40x10^{-4}$ L/mol/min, respectively. The quality of the fits indicated that when excluding the potential isotope effects, the rate constants are too large with respect to the experimental data.

Due to the knowledge of a delay in the available deuterium on the surface in the reactions with 1000 psi H_2 and D_2O a modified kinetic model was developed. In addition, the same set of experiments with glycine, sarcosine, and N,N-dimethylglycine were performed with 1000 psi D_2 (and otherwise identical conditions). The rate constants for these pairs of experiments should be the same. The comparison of these rate constants as well as the modified kinetic model will be discussed following the experimental results with 1000 psi D_2 (100 °C).

H/D Exchange Studies at 100 °C with 1000 psi D_2

As mentioned earlier, it is assumed that the equilibrium between the hydrogen/deuterium on the surface and the deuterium/hydrogen in the liquid at a temperature of 100 °C is fast with respect to the experimental data points. It is expected that the equilibrium is reached within the first hour. In the experiments with 1000 psi D_2 and D_2O there is only ~3% or less H in the solvent water and the gas is D_2, so the equilibrium is essentially reached at

time zero. In the experiments with 1000 psi H_2 and D_2O there is about ~15% H in the solvent water and the apparent delay in equilibrium needs to be addressed. The delay in equilibrium and its potential affect on the H/D reaction will be explored in this section.

The same three experiments were performed at 100 °C with 1000 psi D_2 and D_2O. For the experiment with 0.25 M glycine, the ^1H NMR spectra of time zero and after six hours of reaction time are compared in Figure 58. The singlet ^1H NMR peak representing the methylene (CH_2) position decreased continuously while the CHD triplet grew in over time, reaching a maximum peak height at sixty minutes of reaction time, and then decreasing as hydrogen at that position was further exchanged with deuterium (Figure 59). Figure 59 shows the experimental and fitted concentrations of CH_2, CHD, and CD_2 over time as determined by the equations in Chapter 3. The forward rate constants for the reaction with glycine at 1000 psi D_2 are fairly similar to those with 1000 psi H_2. The rates for H/D exchange on the methylene carbon are: $k_{1A} = 1.7x10^{-4}$, $k_{-1A} = 0$, $k_{2A} = 1.2x10^{-4}$, $k_{-2A} = 7.0x10^{-5}$ L/mol/min and the sum of the squares error (SSE) = $7.9x10^{-5}$.

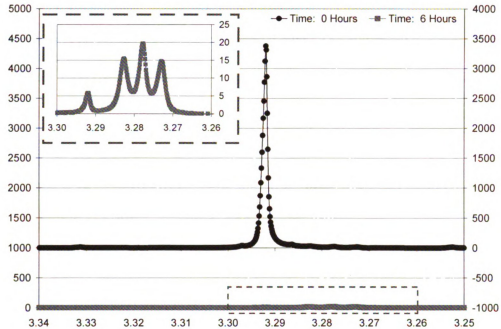

Figure 58. ^{1}H NMR of H/D exchange at the methylene position of 0.25 M glycine (D_2O, 100 °C, 1000 psi D_2, 1 g dry 5% Ru/C)

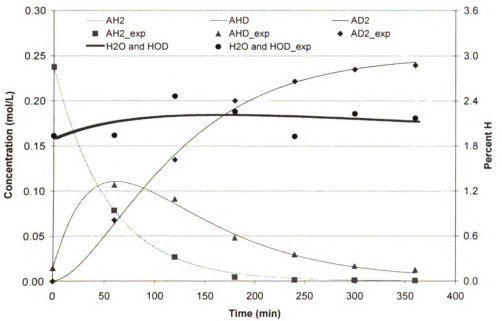

Figure 59. Fit of the kinetic rate data for 0.25 M glycine (D_2O, 100 °C, 1000 psi D_2, 1 g dry 5% Ru/C)

As in the experiments with 1000 psi H_2 and D_2O, we can compare the statistical equilibrium end points and the experimental data. The statistical concentrations of CH_2, CHD, and CD_2 based on the actual percent hydrogen in water at six hours (2.2%) and the concentration at time zero (0.24 M) are $1.1x10^{-4}$, 0.0101, and 0.227 M, respectively. The actual concentrations of CH_2, CHD, and CD_2 at six hours of reaction time are $4.7x10^{-4}$, 0.012, and 0.24 M, respectively. For this experiment, it appears that glycine has not quite yet reached the equilibrium at six hours.

The concentration of CHD at time zero was compared in the reactions with 1000 psi H_2 and with 1000 psi D_2. For both experimental conditions, the presence of AHD was noted. This suggests that even in the case with 1000 psi H_2, there is some deuterium available on the surface for exchange. In general, the experiments that were conducted in 1000 psi D_2 and D_2O resulted in larger concentrations of CHD at time zero.

The same experiment with 0.25 M sarcosine was performed at 100 °C with 1000 psi D_2 and D_2O for six hours. The ^1H NMR of time zero and after six hours of reaction time is compared in Figure 60. Figure 61 shows the experimental and fitted concentrations of CH_2, CHD, and CD_2 over time as determined by the equations in Chapter 3. The reaction of sarcosine started out quickly and the peak concentration of CHD occurred at about 60 minutes of reaction time but then rapidly fell off as the CD_2 grew in. The H/D exchange reaction rate constatns on the methylene carbon are: $k_{1A} = 2.8x10^{-4}$, $k_{-1A} = 6.9x10^{-4}$, $k_{2A} = 2.9x10^{-4}$, $k_{-2A} = 8.3x10^{-4}$ L/mol/min and the sum of the squares error (SSE) = $5.7x10^{-4}$.

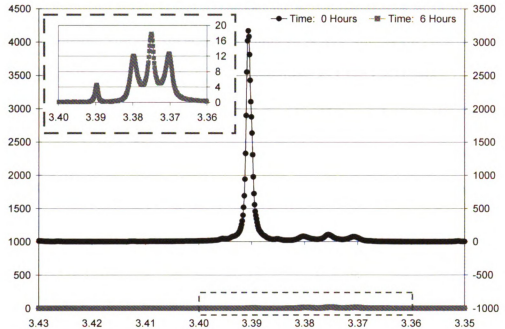

Figure 60. ^{1}H NMR of H/D exchange at the methylene position of 0.25 M sarcosine (D_2O, 100 °C, 1000 psi D_2, 1 g dry 5% Ru/C)

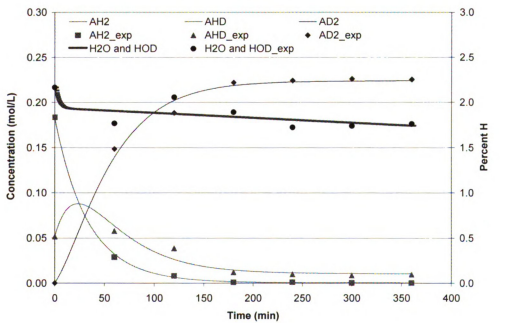

Figure 61. Fit of the kinetic rate data for 0.25 M sarcosine (D_2O, 100 °C, 1000 psi D_2, 1 g dry 5% Ru/C)

The experiment with sarcosine occurred very quickly, reaching an equilibrium at or before 4 hours. The statistical equilibrium end points were again compared to the experimental data. The statistical concentrations of CH_2, CHD, and CD_2 based on the actual percent hydrogen in water at six hours (1.95%) and the concentration at time zero (0.23 M) are $7.3x10^{-5}$, 0.0081, and 0.226 M, respectively. The actual concentrations of CH_2, CHD, and CD_2 at six hours of reaction time are $1.2x10^{-4}$, 0.009, and 0.225 M, respectively.

The same experiment using 0.25 M N,N-dimethylglycine was performed at 100 °C with 1000 psi D_2 and D_2O for six hours. The ^1H NMR of time zero and after six hours of reaction time is compared in Figure 62. Figure 63 shows the experimental and fitted concentrations of CH_2, CHD, and CD_2 over time as determined by the equations in Chapter 3. The reaction of N,N-dimethylglycine again started out quickly and the peak concentration of CHD occurred at about 60 minutes of reaction time but then rapidly fell off. The rate constants for H/D exchange on the methylene carbon are: $k_{1A} = 1.4x10^{-4}$, $k_{-1A} = 0$, $k_{2A} = 1.1x10^{-4}$, $k_{-2A} = 2.2x10^{-4}$ L/mol/min and the sum of the squares error (SSE) $= 6.3x10^{-4}$. The experiment with N,N-dimethylglycine was slower and did not reach equilibrium after six hours. The statistical equilibrium end points were again compared to the experimental data. The statistical concentrations of CH_2, CHD, and CD_2 based on the actual percent hydrogen in water at six hours (2.7%) and the concentration at time zero (0.20 M) are $1.5x10^{-4}$, 0.0105, and 0.188 M, respectively. The actual concentrations of CH_2, CHD, and CD_2 at six hours of reaction time are $5.3x10^{-4}$, 0.0114, and 0.187 M, respectively.

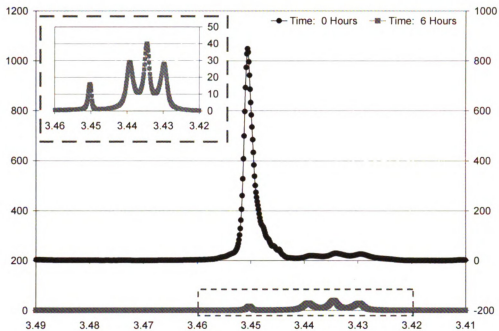

Figure 62. ^{1}H NMR of H/D exchange at the methylene position of 0.25 M N,N-dmg (D_2O, 100 °C, 1000 psi D_2, 1 g dry 5% Ru/C)

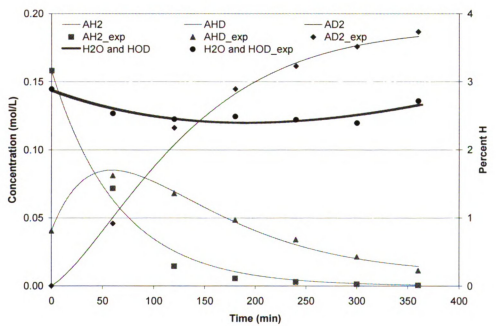

Figure 63. Fit of the kinetic rate data for 0.25 M N,N-dmg (D_2O, 100 °C, 1000 psi D_2, 1 g dry 5% Ru/C)

Figure 64 compares the rate constants for glycine, sarcosine, and N,N-dimethylglycine on the methylene carbon at 100 °C, 1000 psi D_2, and D_2O (reaction time = 6 hrs). For the first hydrogen exchanged, sarcosine reacts the most quickly and for glycine and N,N-dimethylglycine the rate falls off by roughly one-half. After the first hydrogen is replaced with deuterium the rate of exchanging the second hydrogen with deuterium is essentially the same for each compound as compared with the first hydrogen that is exchanged (k_{1A} compared to k_{2A}).

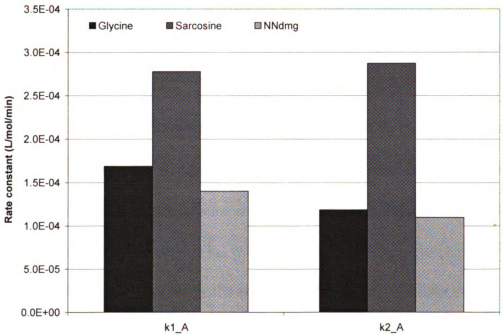

Figure 64. Rate constants for H/D exchange at the methylene carbon (D_2O, 100 °C, 1000 psi D_2, 1 g dry 5% Ru/C)

The sensitivity of the kinetic model to the back reactions is greatly reduced in the experiments conducted with 1000 psi D_2 and D_2O at 100 °C. To verify this, the kinetic model was modified and the back reaction rate constants were set to zero. So, the number of fitted variable was decreased from 10 to 5 (Model A). The fits were compared

and for the experiment with D_2, setting the back reaction rate constants to zero had essentially no effect.

Using the more constrained model (6-variable) the rate constants k_{1A}, k_{-1A}, k_{2A}, and k_{-2A} were compared to the computed rate constants obtained from using the 10-variable kinetic model. And, for the forward reactions the rate constants k_{1A} and k_{2A} are essentially identical using either model (as previously mentioned). For the experiments with 1000 psi D_2 (D_2O, 100 °C, 1 g dry 5% Ru/C) the calculated secondary isotope effects are comparable and less than one for glycine, sarcosine, and N,N-dimethylglycine (Figure 65). For glycine $k_{iA} = 0.84x10^{-4}$ L/mol/min, $p_A = 4.4$, and $s_A = 0.72$. For sarcosine $k_{iA} = 1.3x10^{-4}$ L/mol/min, $p_A = 0.76$, and $s_A = 0.46$. For N,N-dimethylglycine $k_{iA} = 0.71x10^{-4}$ L/mol/min, $p_A = 1.1$, and $s_A = 0.65$. The rate constants, k_i, for glycine, sarcosine, and N,N-dimethylglycine are roughly half of k_{1A} using the 10-variable model. Again this makes sense because k_{iA} is defined to be half of k_{1A}. And the k_{1A} from the 10- and 6-variable models are nearly the same. In addition, the secondary isotope effects, s_A, are between 0.5 and 0.7, thus the calculated k_{2A} from the 6-variable model are all about twice the value of k_{iA}. This is again similar to the values computed for k_{1A}.

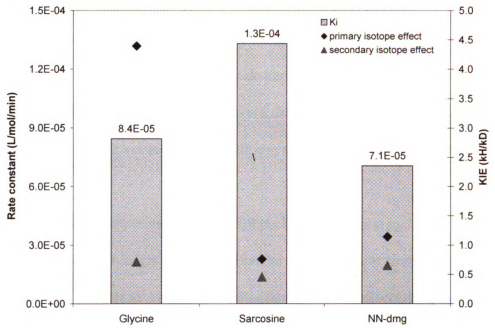

Figure 65. Kinetic rate constant and primary and secondary isotope effects for glycine, sarcosine, and N,N-dmg (D_2O, 100 °C, 1000 psi D_2, 1 g dry 5% Ru/C)

It is interesting to note that in the case of 1000 psi D_2 and D_2O the rate constants for glycine and N,N-dimethylglycine are comparable and both about one-third to one-half that of sarcosine.

Kinetic Model Modification – Linking experimental data (1000 psi H_2 and D_2)

The kinetic model for isotope exchange was varied to explore the effects of various assumptions with the intent of optimizing the fit to the experimental data. Experiments at 100 °C were discussed for glycine, sarcosine, and N,N-dimethylglycine with either 1000 psi H_2 or D_2 and D_2O as the solvent. The rate constants calculated for these pairs of experiments should, in theory, be the same. Using the kinetic model discussed above, the H/D exchange rate constants for the experiments with 1000 psi H_2 and D_2O appeared to

be too large. This is partly due to the fact that in the kinetic model the hydrogen or deuterium available for exchange with the substrate was assumed to be in equilibrium with the concentration of hydrogen or deuterium in the liquid. But from the experiments with H_2 and D_2O, it appears that there is a delay in the substrates' H/D exchange reaction due to the time it takes to reach equilibrium among liquid, gas, and surface hydrogens.

Note that for the experiments with 1000 psi D_2, the aqueous hydrogen concentration is almost an order of magnitude lower than the typical 15% or so that is observed with H_2 (Figure 67). This time evolution is important, but also reflects the gas/liquid exchange. The rate of exchange for the second hydrogen is essentially the same in both conditions (H_2 or D_2) which suggests an equilibrium is reached and at that point the reaction is not limited by the presence of available deuterium.

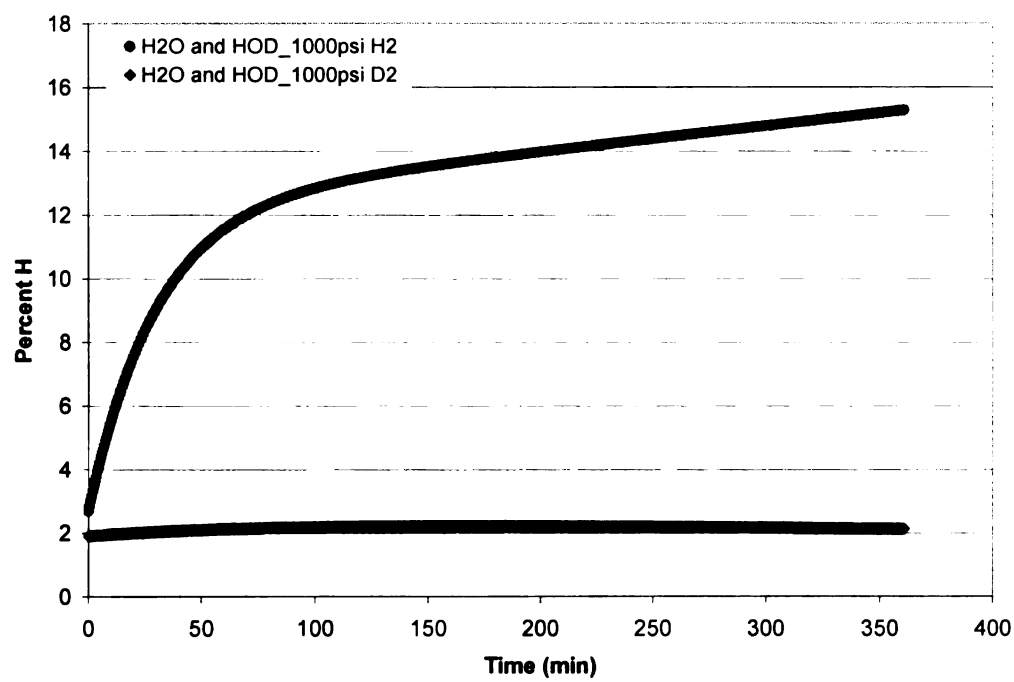

Figure 66. Percent H in D_2O with either 1000 psi H_2 or D_2

In terms of the delay of the deuterium available on the catalyst surface, this may be a result of not having deuterium available to get on the surface until there is enough HD formed. Scheme 30 shows the proposed mechanism for exchanging H and D between the various isotopomers of H_2, H_2O, and Ru-bound H atoms. Previous work in our research group has shown that a significant amount of HD is generated before D_2 is formed. According to this mechanism, it is not until HD is formed (in the experiments with H_2 and D_2O) that the catalyst surface is deuterated so that the substrate can start undergoing H/D exchange.

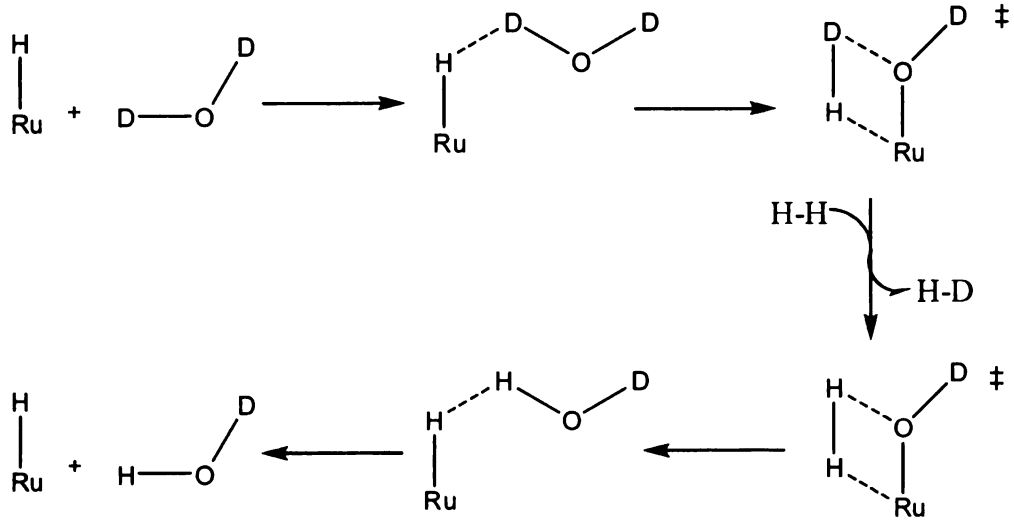

Scheme 30. Proposed mechanism for Ru/C catalyzed HD generation from H_2 and D_2O Note that exchange between H_2 and D_2O takes place without isotopic exchange on the Ru surface.

Various kinetic model modifications were employed to address this background equilibrium process. To start, the corresponding H_2, D_2O and D_2, D_2O experimental datasheets were linked and a common set of rate constants was defined. The hydrogen and deuterium available were defined by H_s and D_s (Chapter 3) as opposed to using the

liquid hydrogen and liquid deuterium concentrations. It would be ideal to assume that the total concentration in solution is in equilibrium with the surface, but since this can not be confirmed, it has to be treated simply in terms of rates. D_s is a variable and represents the fraction of total sites occupied by deuterium. For the experiments conducted with 1000 psi H_2, the initial H on the surface was assumed to be 111.11. This is because at time zero it is assumed that the amount of hydrogen on the surface is more similar to the gas (which in this case is H_2) than the aqueous D_2O. For the experiments conducted with 1000 psi D_2, the initial H on the surface was assumed to be equal to the amount of H measured in the liquid (usually less than 3%).

In addition, a catalyst turn-on function was included, as defined by:

1-(tdep_coeff)*exp(tdep_exp*t),

where tdep_coeff is constrained to range 0-1 and can describe the fact that part of the catalyst is fully active and there is a fraction that is not. This variable will ramp up to full activity on a timescale described by the tdep_exp variable, an effective rate constant for catalyst recovery.

Numerous fitting attempts were performed with the catalyst turn-on function included. The results for both the 10-variable model and the 6-variable model (both now with k_H as defined in Chapter 3) indicated that with tdep_coeff and tdep_exp there was little to no improvement of the fits. This finding is understandable in that much of the mathematical flexibility the turn-on function offers is quite similar to that conferred by the k_H variable.

The main focus was on using the 10- or 6-variable model with the addition of k_H (as defined by the equilibrium between the available hydrogen and deuterium on the surface and in the liquid). It is important to mention that we do not know the exact amount of available hydrogen and deuterium on the surface as it is not directly measured; only its ratio is truly meaningful. Table 5 presents the rate constants for glycine at 100 °C with 1000 psi H_2 or 1000 psi D_2 and the linked H_2 and D_2 results for the 10- or 6-variable model plus k_H. It also includes the rate constants derived from the kinetic model presented earlier in this thesis (based on the aqueous hydrogen and deuterium concentrations).

The rate constants for the case of D_2 and D_2O are not affected much by the kinetic model modification, due to the fact that this system essentially starts at equilibrium, so there is not a delay in building up available deuterium on the surface (as in the H_2, D_2O case). And k_H was calculated to be zero with this model, again indicating that for the experiments with D_2, the assumption of using the aqueous H and D concentrations in the kinetic model was adequate.

For the experiment with 1000 psi H_2 and D_2O, the experimental (symbols) and fitted (line) concentrations of CH_2 (referred to as AH_2), CHD (referred to as AHD), and CD_2 (referred to as AD_2) are presented in Figure 67. The fitted lines are a result of the 6-variable model plus k_H. This figure also shows the fitted (line) concentrations that resulted from linking the experiment conducted with H_2 with that with D_2 and solving for

one common set of rate constants. Figure 68 presents the analogous results from the experiment with 1000 psi D_2 and D_2O. Again, there is not much difference in the fits.

Table 5. Rate constants for glycine (100 °C, 1000 psi H_2 or D_2) using the original kinetic model, k10 + k_H, k6 + k_H

Rate Constant (L/mol/min)	Glycine 100 °C H_2		Glycine 100 °C D_2		Glycine 100 °C Linked H_2 and D_2
	k10	**k10 + kH**	**k10**	**k10 + kH**	**k10 + kH**
k1_A	2.3E-04	2.7E-03	1.7E-04	1.7E-04	**1.9E-04**
k-1_A	1.2E-04	1.8E-03	0.0	0.0	1.3E-05
k2_A	1.2E-04	1.4E-03	1.2E-04	1.2E-04	**1.2E-04**
k-2_A	3.2E-04	4.0E-03	7.0E-05	1.2E-04	3.1E-04
kH(10)		8.0E-05		5.6E-05	1.0E-02
	k6	**k6 + kH**	**k6**	**k6 + kH**	**k6 + kH**
ki_A	1.15E-04	2.20E-03	8.45E-05	8.49E-05	**9.88E-05**
p_A	0.76	0.69	4.39	2.36	0.80
s_A	0.98	2.10	0.72	0.71	0.81
kH(6)		8.20E-05		0.00E+00	8.22E-03

The apparent "blip" at the start of the curve fitting is a result from the initial H being defined as all hydrogen (111.11), so that there is essentially no forward rate occurring, k_{1A} but k_{-1A} can take CHD back to CH_2 (this is the same in the methyl case for sarcosine and N,N-dimethylglycine for k_{2A} and k_{-3A}). The rate constants and primary and secondary isotope effects were calculated and presented in Figure 69.

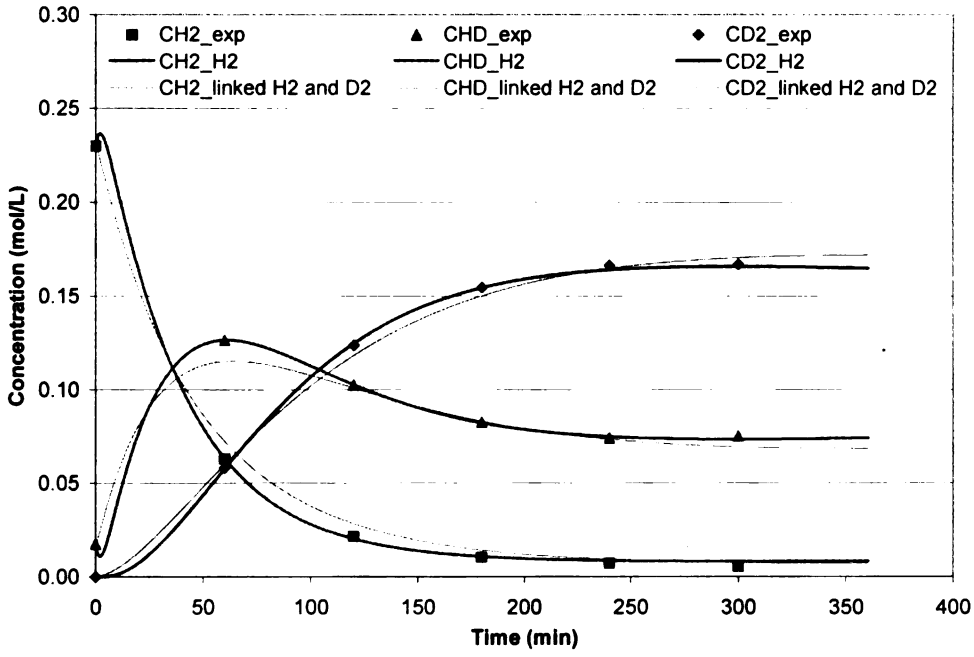

Figure 67. Fit of the kinetic rate data for 0.25 M glycine (D_2O, 100 °C, 1000 psi H_2 or linked H_2 and D_2, 1 g dry 5 % Ru/C)

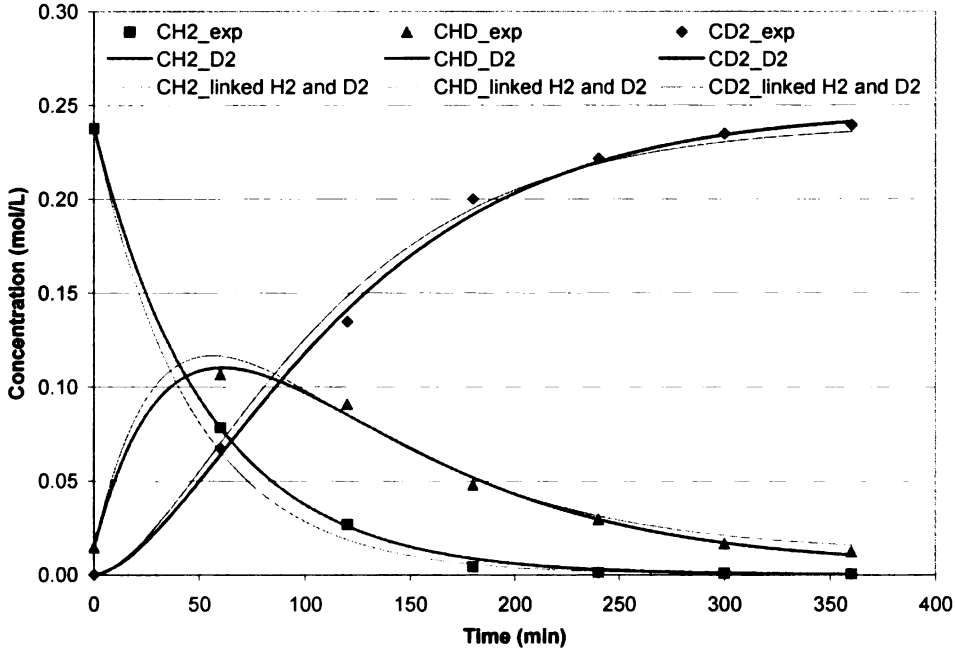

Figure 68. Fit of the kinetic rate data for 0.25 M glycine (D_2O, 100 °C, 1000 psi D_2 or linked H_2 and D_2, 1 g dry 5 % Ru/C)

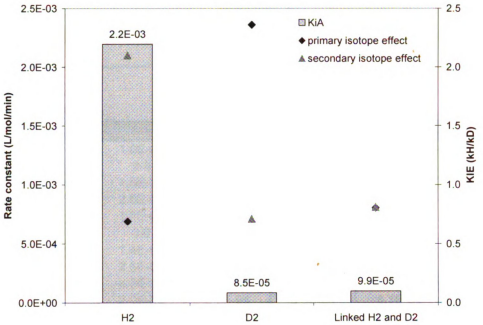

Figure 69. Kinetic rate constant and primary and secondary isotope effects for glycine with 1000 psi H_2 or 1000 psi D_2 or H_2 and D_2

Table 6 presents the rate constants for sarcosine at 100 °C with 1000 psi H_2 or 1000 psi D_2 and the linked H_2 and D_2 results for the 10- or 6-variable model plus k_H. It also includes the rate constants derived from the kinetic model presented in this discussion prior (based on the liquid hydrogen and deuterium concentrations).

Figures 70 and 71 are analogous to 67 and 68 (glycine) and show the experimental and fitted concentration data for the methylene carbon. The rate constants and primary and secondary isotope effects were calculated and presented in Figure 72.

Table 6. Rate constants for sarcosine (100 °C, 1000 psi H_2 or D_2) using the original kinetic model, k10 + k_H, k6 + k_H

Rate Constant (L/mol/min)	Sarcosine 100 °C H_2		Sarcosine 100 °C D_2		Sarcosine Linked Linked H2 and D2
	k10	**k10 + kH**	**k10**	**k10 + kH**	**k10 + kH**
k1_A	1.6E-04	4.6E-04	2.8E-04	3.0E-04	**2.7E-04**
k-1_A	0.0	1.3E-04	7.0E-04	9.4E-04	2.4E-05
k2_A	1.6E-04	9.5E-04	2.9E-04	3.2E-04	**2.9E-04**
k-2_A	2.6E-04	1.6E-03	8.3E-04	7.8E-04	5.3E-04
k1_C	1.1E-04	2.1E-04	1.6E-04	1.6E-04	**1.6E-04**
k-1_C	0.0	0.0	0.0	0.0	0.0
k2_C	1.4E-04	3.5E-04	1.9E-04	1.9E-04	**2.0E-04**
k-2_C	2.5E-06	4.0E-04	0.0	0.0	1.2E-04
k3_C	8.3E-05	2.2E-04	1.4E-04	1.5E-04	**1.3E-04**
k-3_C	2.0E-04	8.5E-04	8.5E-04	8.1E-04	4.7E-04
kH(10)		7.1E-05		5.2E-05	1.2E-04
	k6	**k6 + kH**	**k6**	**k6 + kH**	**k6 + kH**
ki_A	8.2E-05	2.9E-04	1.3E-04	1.4E-04	**1.5E-04**
p_A	1.25	1.34	0.76	0.80	1.08
s_A	0.51	0.16	0.46	0.44	0.49
ki_C	4.0E-05	9.4E-05	5.5E-05	5.6E-05	**5.8E-05**
p_C	0.71	0.75	0.45	0.49	0.82
s_C	0.47	0.40	0.59	0.59	0.63
kH(6)		6.3E-05		5.0E-05	1.3E-04

Comparing k_{iA} using the linked experimental data and that obtained in the case of 1000 psi D_2 and D_2O, the values are not much different. This is to be expected because the rate constants that are derived from the experiments with D_2 and D_2O are the "gold standard". Figures 70 and 71 compare the fitted concentration versus time data using the $k_6 + k_H$ rate constants as well as the linked H_2 and D_2 $k_6 + k_H$ rate constants. The fits are extremely close for both the individual data fit and the linked data fit. The results from the H/D exchange on the methyl carbon of sarcosine will be discussed in section 4.7.1.2.

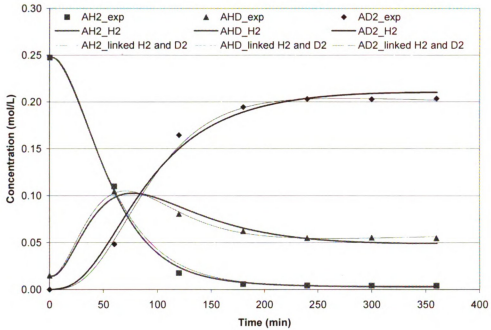

Figure 70. Fit of the kinetic rate data for 0.25 M sarcosine (D_2O, 100 °C, 1000 psi H_2 or linked H_2 and D_2, 1 g dry 5 % Ru/C)

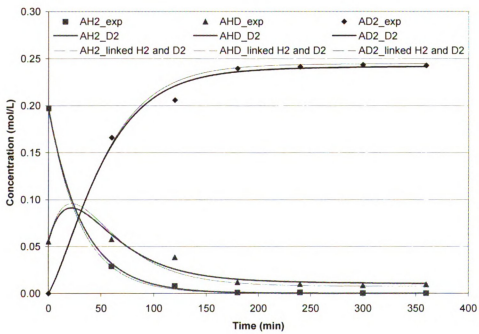

Figure 71. Fit of the kinetic rate data for 0.25 M sarcosine (D_2O, 100 °C, 1000 psi D_2 or linked H_2 and D_2, 1 g dry 5 % Ru/C)

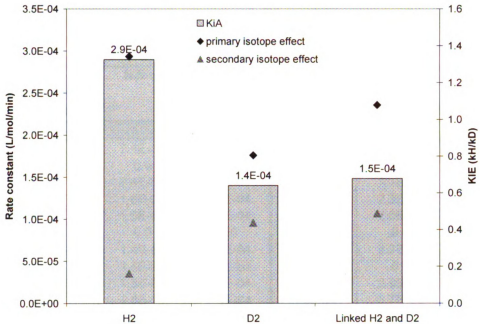

Figure 72. Kinetic rate constant and primary and secondary isotope effects for sarcosine with 1000 psi H_2 or 1000 psi D_2 or H_2 and D_2

The analogous data is presented below for N,N-dimethylglycine (Table 7, Figures 73-75).

The calculated fits for glycine, sarcosine, and N,N-dimethylglycine using the $k_6 + k_H$ kinetic model and linking the experimental data from the experiments with 1000 psi H_2 and D_2 were qualitatively very good and similar to the fits obtained when not linking the experimental data. This indicates that incorporating k_H into the kinetic model and using the initial hydrogen and deuterium on the surface (inferred) is the best approach for experiments conducted with 1000 psi H_2 and D_2O. The original kinetic model that does not include k_H is adequate for experiments with D_2 and D_2O.

Table 7. Rate constants for N,N-dimethylglycine (100 °C, 1000 psi H_2 or D_2) using the original kinetic model, k10 + k_H, k6 + k_H

Rate Constant (L/mol/min)	N,N-dimethylglycine 100 °C H_2		N,N-dimethylglycine 100 °C D_2		N,N-dmg Linked Linked H2 and D2
	k10	k10 + kH	k10	k10 + kH	k10 + kH
k1_A	7.1E-05	1.1E-04	1.4E-04	1.4E-04	**1.3E-04**
k-1_A	0.0	1.1E-04	0.0	0.0	5.1E-05
k2_A	6.4E-05	8.6E-05	1.1E-04	1.1E-04	**1.2E-04**
k-2_A	1.6E-04	3.1E-04	2.2E-04	2.3E-04	3.9E-04
k1_C	1.0E-04	1.4E-04	1.9E-04	2.0E-04	**2.0E-04**
k-1_C	0.0	0.0	0.0	0.0	0.0
k2_C	1.4E-04	1.8E-04	3.2E-04	3.2E-04	**2.7E-04**
k-2_C	1.8E-04	3.4E-04	0.0	0.0	4.8E-04
k3_C	1.5E-04	1.8E-04	2.8E-04	2.9E-04	**3.3E-04**
k-3_C	5.8E-04	7.5E-04	8.8E-04	8.7E-04	1.3E-03
kH(10)		1.5E-04		3.0E-05	7.9E-05
	k6	k6 + kH	k6	k6 + kH	k6 + kH
ki_A	3.6E-05	5.1E-05	7.1E-05	7.2E-05	**7.4E-05**
p_A	2.12	0.57	1.14	1.13	0.52
s_A	0.69	0.61	0.65	0.64	0.60
ki_C	3.5E-05	4.6E-05	6.9E-05	7.0E-05	**6.6E-05**
p_C	0.83	0.81	0.87	0.93	0.68
s_C	0.52	0.58	0.47	0.46	0.48
kH(6)		1.7E-04		3.2E-05	8.2E-05

The rate constants for glycine, sarcosine, and N,N-dimethylglycine at 100 °C (k_6 + k_H, linked H_2 and D_2) are $k_{iA} = 0.99x10^{-5}$, $1.5x10^{-4}$, and $0.74x10^{-4}$ L/mol/min, respectively. The trend in reactivity (sarcosine > glycine > N,N-dimethylglycine) does not match the reactivity observed in the hydrogenation of these same substrates (glycine > sarcosine > N,N-dimethylglycine). This may be due to the fact that for H/D exchange an electron-rich C-H bond promotes the reaction. Whereas, in the hydrogenation reaction, it is presumed that steric effects are playing more of a role. It is observed that for each N-methyl group added, the rate of the hydrogenation reaction falls by a factor of 3.

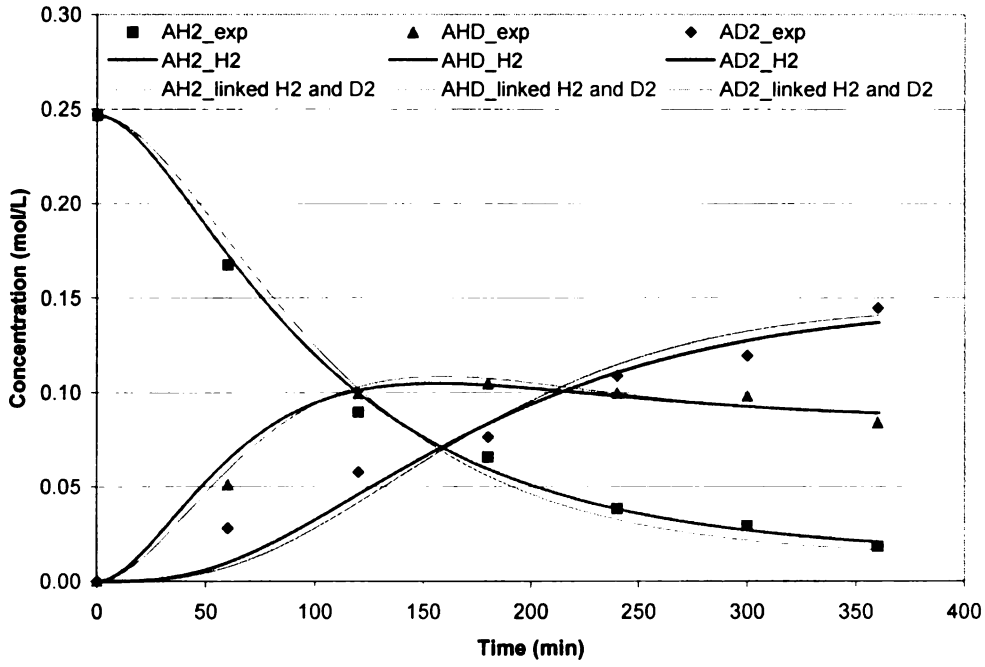

Figure 73. Fit of the kinetic rate data for 0.25 M N,N-dmg (D_2O, 100 °C, 1000 psi H_2 or linked H_2 and D_2, 1 g dry 5 % Ru/C)

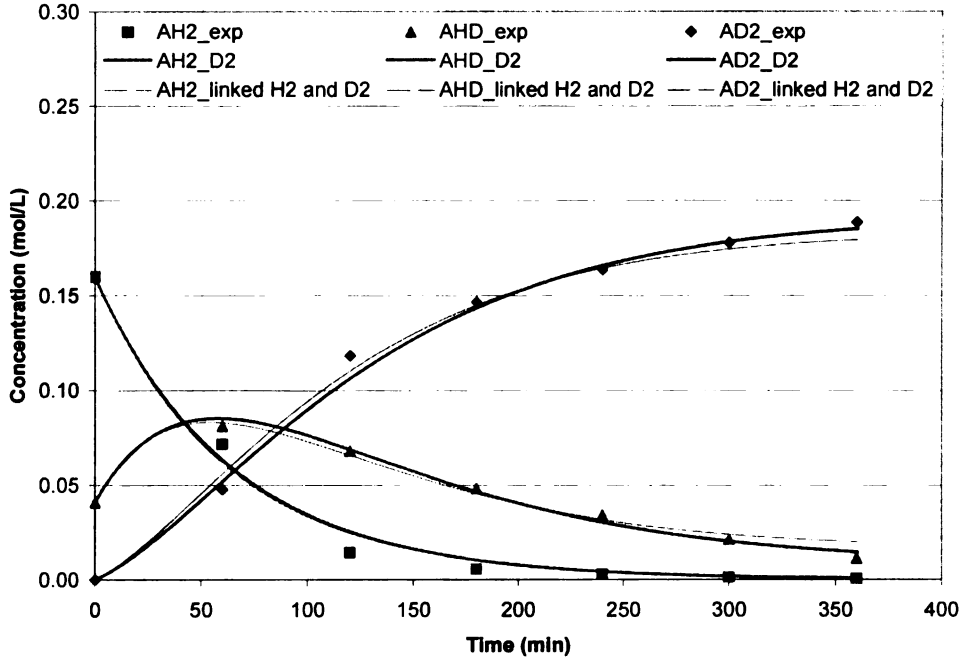

Figure 74. Fit of the kinetic rate data for 0.25 M N,N-dmg (D_2O, 100 °C, 1000 psi D_2 or linked H_2 and D_2, 1 g dry 5 % Ru/C)

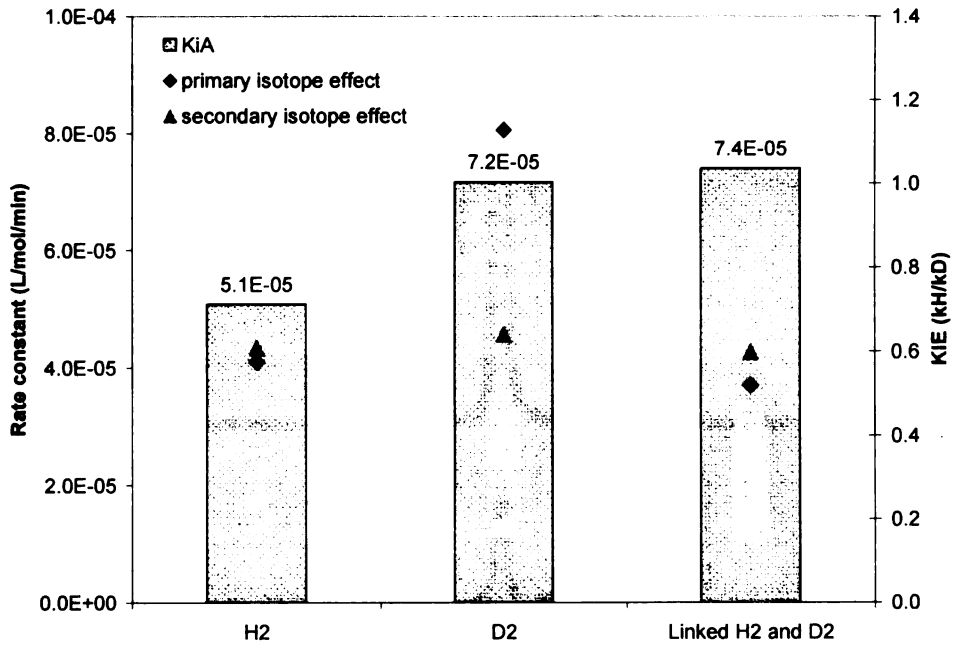

Figure 75. Kinetic rate constant and primary and secondary isotope effects for N,N-dmg with 1000 psi H_2 or 1000 psi D_2 or H_2 and D_2

H/D Exchange Studies at 70 °C with 1000 psi D_2

The reactions at 100 °C were occurring quickly reaching a maximum CHD concentration at sixty minutes. Therefore, the reaction temperature was reduced to 70 °C in order to obtain additional reaction rate data. The same three experiments were individually performed at 70 °C with 1000 psi D_2 and D_2O. For the experiment with glycine (0.25 M) the ^1H NMR of time 0.5 hours and 6 hours is compared in Figure 76. The singlet ^1H NMR peak representing the methylene (CH_2) position continued to decrease in size over time, while the CHD grew in, reaching a maximum peak height between 60 and 180 minutes of reaction time, and then started to decrease as the hydrogen at that position was further exchanged with deuterium (Figure 77).

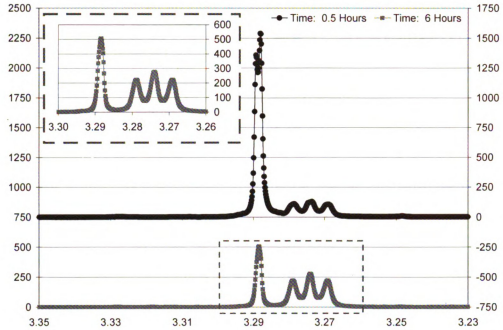

Figure 76. ^{1}H NMR of H/D exchange at the methylene position of 0.25 M glycine (D_2O, 70 °C, 1000 psi D_2, 1 g dry 5% Ru/C)

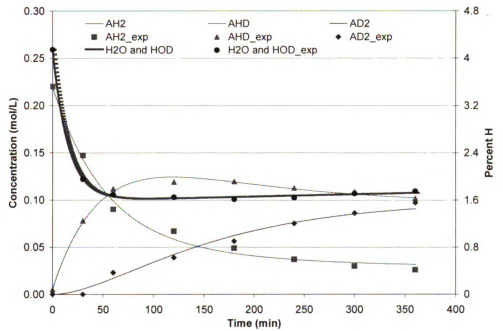

Figure 77. Fit of the kinetic rate data for 0.25 M glycine (D_2O, 70 °C, 1000 psi D_2, 1 g dry 5% Ru/C)

Figure 77 shows the experimental and fitted concentrations of CH_2, CHD, and CD_2 over time as determined by the equations in Chapter 3. The rate constants for H/D exchange at the methylene carbon are: $k_{1A} = 1.5x10^{-4}$, $k_{-1A} = 2.8x10^{-3}$, $k_{2A} = 4.1x10^{-5}$, $k_{-2A} = 2.5x10^{-3}$ L/mol/min and the sum of the squares error (SSE) = $2.9x10^{-4}$.

The same experiment using N-methylglycine (sarcosine) was performed at 70 °C with 1000 psi D_2 and D_2O. The ^1H NMR of time zero and after four hours of reaction time is compared in Figure 78. Figure 79 shows the experimental and fitted concentrations of CH_2, CHD, and CD_2 over time as determined by the equations in Chapter 3. A maximum concentration for CHD was realized in less than sixty minutes of reaction time. The rate constants for H/D exchange on the methylene carbon are: $k_{1A} = 1.9x10^{-4}$, $k_{-1A} = 0$, $k_{2A} = 1.4x10^{-4}$, $k_{-2A} = 1.2x10^{-3}$ L/mol/min and the sum of the squares error (SSE) = $6.4x10^{-4}$.

The same experiment using N,N-dimethylglycine was performed at 70 °C with 1000 psi D_2 and D_2O. The ^1H NMR of time zero and after four hours of reaction time is compared in Figure 80. Figure 81 shows the experimental and fitted concentrations of CH_2, CHD, and CD_2 over time as determined by the equations in Chapter 3. A maximum concentration for CHD was realized after about 180 minutes of reaction time and was much slower than either glycine or sarcosine at 70 °C. The rate constants for H/D exchange on the methylene carbon are: $k_{1A} = 1.3x10^{-5}$, $k_{-1A} = 0$, $k_{2A} = 2.2x10^{-5}$, $k_{-2A} = 0$ L/mol/min and the sum of the squares error (SSE) = $1.2x10^{-3}$.

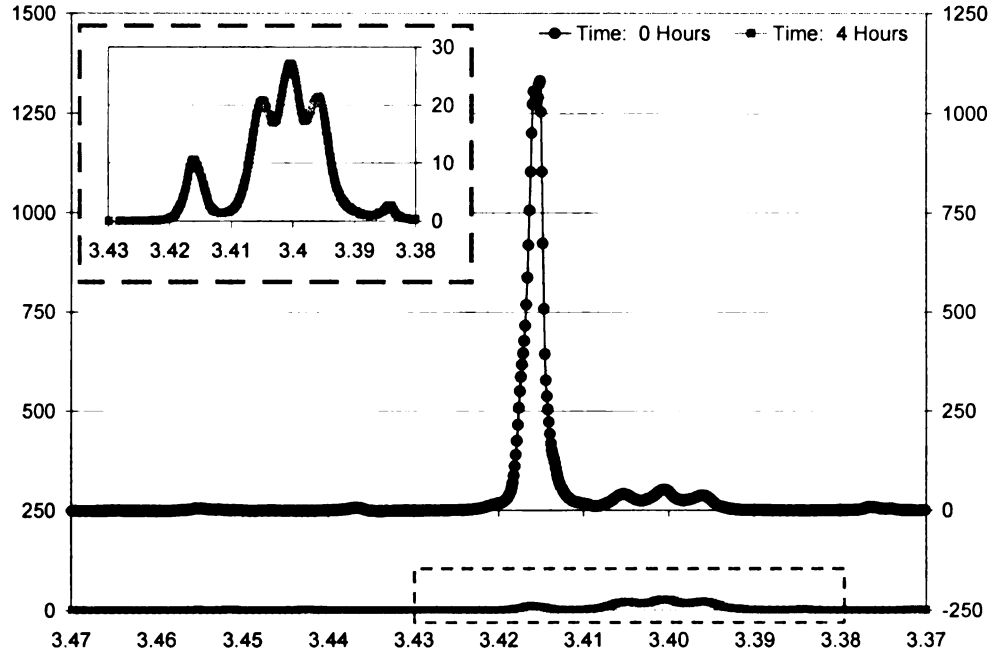

Figure 78. ^{1}H NMR of H/D exchange at the methylene position of 0.25 M sarcosine (D_2O, 70 °C, 1000 psi D_2, 1 g dry 5% Ru/C)

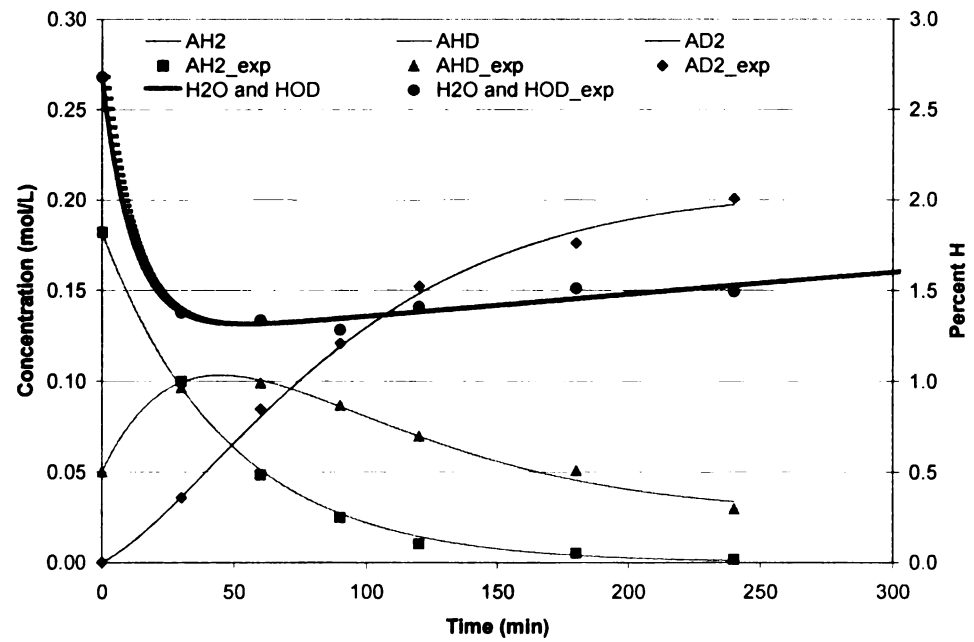

Figure 79. Fit of the kinetic rate data for 0.25 M sarcosine (D_2O, 70 °C, 1000 psi D_2, 1 g dry 5% Ru/C)

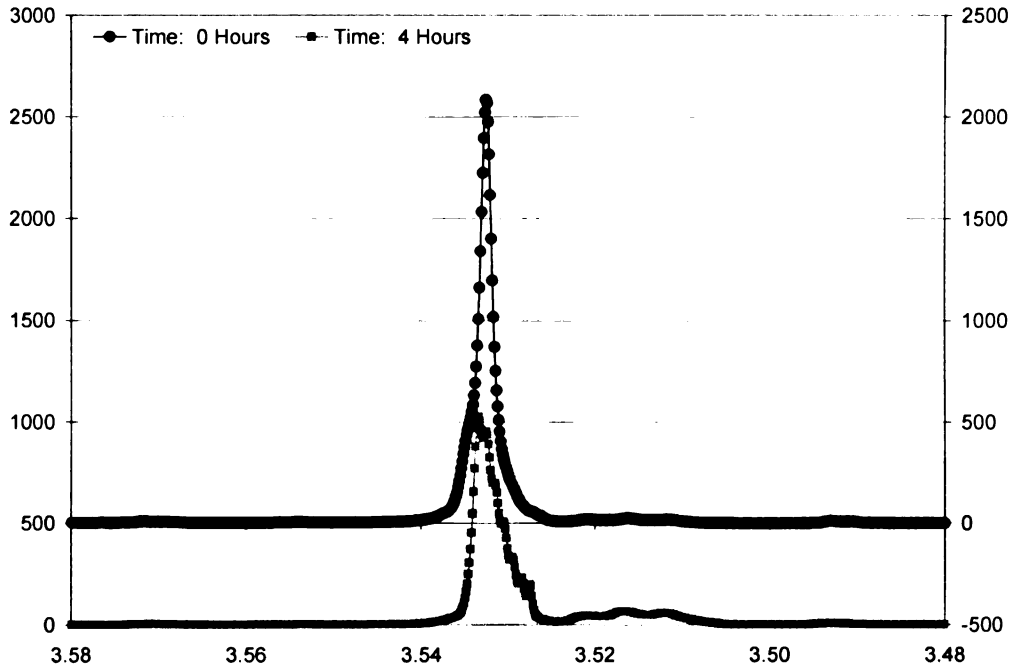

Figure 80. ^{1}H NMR of H/D exchange at the methylene position of 0.25 N,N-dmg (D_2O, 70 °C, 1000 psi D_2, 1 g dry 5% Ru/C)

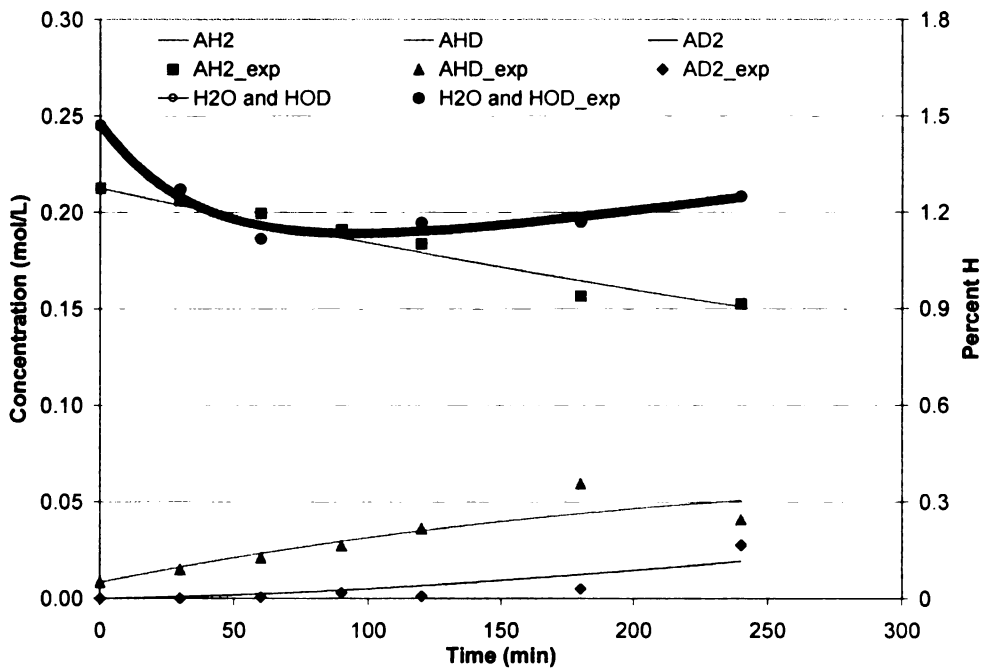

Figure 81. Fit of the kinetic rate data for 0.25 M N,N-dmg (D_2O, 70 °C, 1000 psi D_2, 1 g dry 5% Ru/C)

Figure 82 compares the rate constants for glycine, sarcosine, and N,N-dimethylglycine on the methylene carbon at 70 °C, 1000 psi D_2, and D_2O (reaction time = 6 hrs). For the first hydrogen exchanged, the rate constant, k_{1A}, for sarcosine is the largest, but is comparable to glycine. The k_{1A} rate for N,N-dimethylglycine is significantly less (more than a factor of ten) than the rate for either glycine or sarcosine. After the first hydrogen is replaced with deuterium the rate constants representing exchange of the second hydrogen with deuterium are less for both glycine and sarcosine but are comparable for N,N-dimethylglycine (k_{1A} compared to k_{2A}).

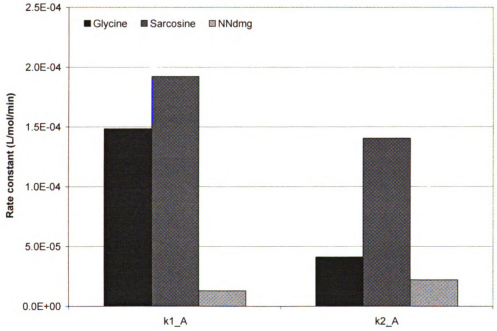

Figure 82. Rate constants for H/D exchange at the methylene carbon (D_2O, 70 °C, 1000 psi D_2, 1 g dry 5% Ru/C)

A comparison of rate constants for the temperatures 100 °C and 70 °C with 1000 psi D_2 for glycine, sarcosine, and N,N-dimethylglycine will be presented at the end of this section.

Using the more constrained model (6-variable) the rate constants k_{1A}, k_{-1A}, k_{2A}, and k_{-2A} were compared to the computed rate constants obtained from using the 10-variable kinetic model. And, for the forward reactions the rate constants k_{1A} and k_{2A} are essentially identical using either model (as mentioned previously). The rate constant and primary and secondary isotope effects were calculated for the experiments with 1000 psi D_2 (D_2O, 70 °C, 1 g dry 5% Ru/C) and for glycine $k_{iA} = 0.74x10^{-4}$, $p_A = 0.03$, and $s_A = 1.5$. For sarcosine $k_{iA} = 9.9x10^{-5}$ L/mol/min, $p_A = 0.24$, and $s_A = 0.72$. For N,N-dimethylglycine $k_{iA} = 5.9x10^{-6}$ L/mol/min, $p_A = 1.0$, and $s_A = 0.40$ (Figure 83). The rate constants, k_i, for glycine, sarcosine, and N,N-dimethylglycine are roughly half of k_{1A} using the 10-variable model. Again this makes sense because k_{iA} is defined to be half of k_{1A}. The secondary isotope effects, s_A, are between 0.4 and 1.5.

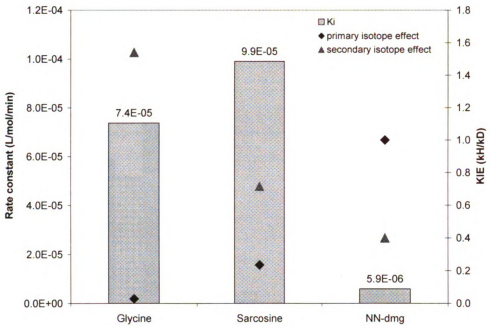

Figure 83. Kinetic rate constant and primary and secondary isotope effects for glycine, sarcosine, and N,N-dmg (D_2O, 70 °C, 1000 psi D_2, 1 g dry 5% Ru/C)

The rate constants for glycine, sarcosine, and N,N-dimethylglycine can be compared for the reactions at 100 °C and 70 °C with 1000 psi D_2. Additional experiments were conducted at 50 °C and 90 °C, but not for all three substrates. So, the individual substrates will be compared at each temperature at the end of this section.

The comparison data of the rate constants is in Figure 84. All of the rate constants are lower at 70 °C, which was expected.

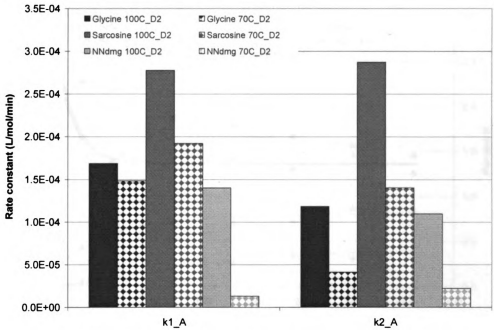

Figure 84. Rate constants for H/D exchange at the methylene carbon at 100 °C or 70 °C (D_2O, X °C, 1000 psi D_2, 1 g dry 5% Ru/C)

H/D Exchange Studies at 50 °C with 1000 psi D_2

The reaction temperature was lowered to 50 °C and the same experiments were individually performed using glycine and sarcosine with 1000 psi D_2 and D_2O. The substrate N,N-dimethylglycine was not evaluated at this temperature because of the low reactivity observed at 70 °C. The singlet ^1H NMR peak representing the methylene (CH_2) position continued to decrease in size over time, while the CHD grew in albeit slowly. This reaction was significantly slower than at 70 °C and 100 °C. Figure 85 shows the experimental and fitted concentrations of CH_2, CHD, and CD_2 over time as determined by the equations in Chapter 3. The rate constants for H/D exchange on the methylene carbon are: $k_{1A} = 5.5x10^{-5}$, $k_{-1A} = 8.1x10^{-3}$, $k_{2A} = 3.9x10^{-5}$, $k_{-2A} = 5.6x10^{-3}$ L/mol/min and the sum of the squares error (SSE) = $6.0x10^{-4}$.

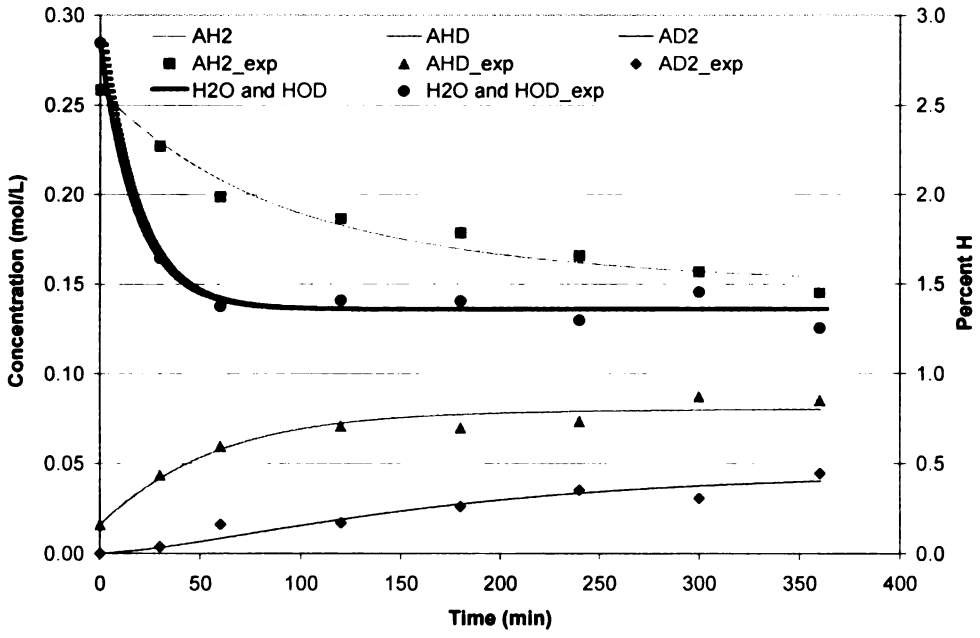

Figure 85. Fit of the kinetic rate data for 0.25 M glycine (D_2O, 50 °C, 1000 psi D_2, 1 g dry 5% Ru/C)

An experiment with sarcosine at the same conditions (D_2O, 50 °C, 1000 psi D_2, 1 g dry 5% Ru/C) was performed and results again showed a slower rate of H/D exchange. Figure 86 shows the experimental and fitted concentrations of CH_2, CHD, and CD_2 over time as determined by the equations in Chapter 3. The rate constants for H/D exchange on the methylene carbon are: $k_{1A} = 5.8 \times 10^{-5}$, $k_{-1A} = 6.4 \times 10^{-4}$, $k_{2A} = 4.3 \times 10^{-5}$, $k_{-2A} = 3.4 \times 10^{-3}$ L/mol/min and the sum of the squares error (SSE) = 4.9×10^{-4}.

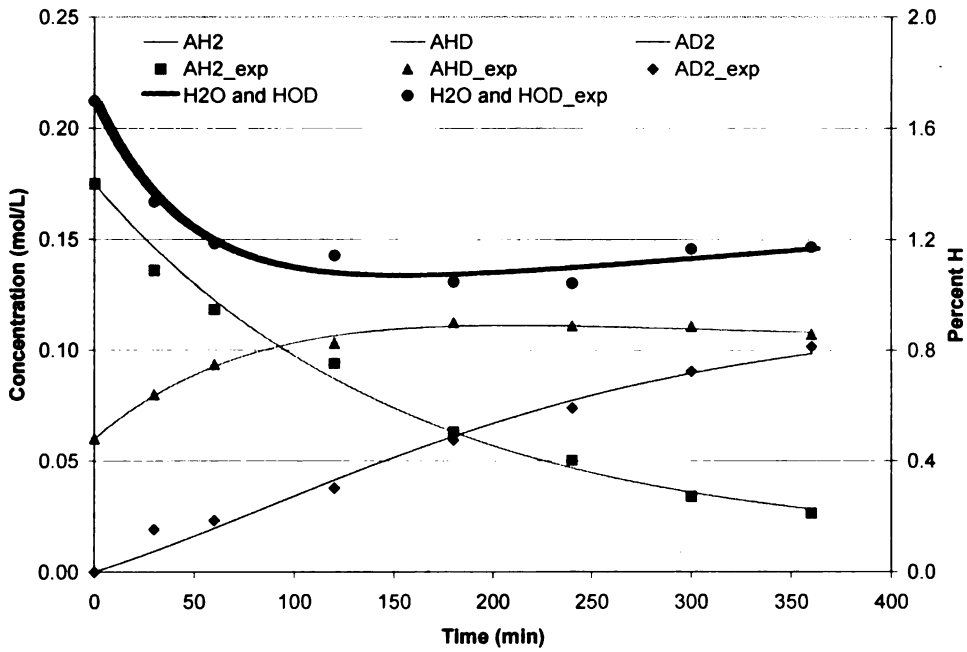

Figure 86. Fit of the kinetic rate data for 0.25 M sarcosine (D_2O, 50 °C, 1000 psi D_2, 1 g dry 5% Ru/C)

The kinetic rate constant for the H/D exchange on the methylene carbon will be compared to the rate constant for the H/D exchange on the methyl carbon at all three reaction temperatures in Figure 111.

In summary, we can compare the rate constants for glycine, sarcosine, and N,N-dimethylglycine at 100 °C, 70 °C and 50 °C with 1000 psi D_2. The rate constants at 100 °C were calculated from the linked H_2 and D_2 experimental data (and the kinetic model includes k_H). Using this set of data, activation energies were calculated. The E_A for the methylene carbon of glycine and sarcosine was 45 kJ/mol and 36 kJ/mol, respectively. The activation energy for N,N-dimethylglycine was calculated based on two

experimental points only, and was equal to 88 kJ/mol. Figure 87 presents k_{iA} for glycine, sarcosine, and N,N-dimethylglycine at 100, 70, and 50 °C.

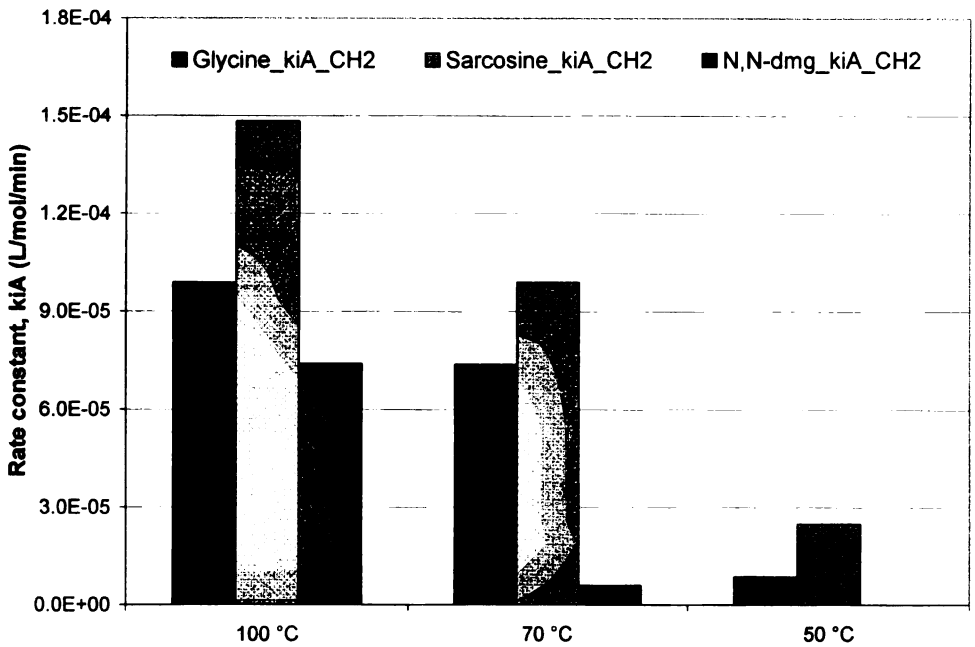

Figure 87. Kinetic rate constant for glycine, sarcosine, and N,N-dmg (D_2O, X °C, 1000 psi D_2, 1 g dry 5% Ru/C)

Again, it was observed that the rate constant for sarcosine is the largest and it falls off by about one-third for glycine and one-half for N,N-dimethylglycine at 100 °C. The same general trend is observed at lower temperatures.

The H/D exchange reaction is presumably promoted by having an electron-rich C-H bond. If the pKa's are examined for the three substrates (Table 8), the carboxylic acid of sarcosine is the most acidic and may result in sarcosine favoring the zwitterionic form more than glycine favoring the zwitterionic form. For H/D exchange to occur, the amino must be free, so this may suggest a slower rate for sarcosine than that of glycine. But,

sarcosine has a more electron-donating amino group as compared to that of glycine which would promote the H/D exchange reaction.

Table 8. pKa values for glycine, sarcosine, and N,N-dimethylglycine (25 °C)

Substrate	-NHx(CH_3)y(+)	-COOH
Glycine (x=3, y=0)	9.6	2.34
Sarcosine (x=2, y=1)	10.01	2.23
N,N-dimethylglycine (x=1, y=2)	9.8	2.08

Mass Transport Considerations

It was noticed that for the H/D reactions at 100 °C, the exchange is occurring quickly. So, a brief discussion on mass transport limitations is included. From our hydrogenation experiments it was determined that the overall rate of reaction was proportional to the catalyst loading (based on experiments with half and double the catalyst amount) and thus there are no external mass transport limitations in the system. This can be assumed to be true for the H/D exchange reactions as well. For our system with H_2 and D_2O, the reaction rate should be relatively insensitive to catalyst loading because the flux of H_2 from the gas to liquid would define the reaction rate. But, it is still possible to have internal mass transport limitations (even if the rate is proportional to the catalyst loading). This is because the catalyst will have the same rate per unit mass even if there are concentration gradients within the catalyst particles.

Internal mass transfer limitations occur when the Thiele modulus for the reaction is greater than 0.3. For an n-th order reaction, the Thiele modulus, Φ, is equal to

$L(k*C_o^{(n+1)/2}/D_e)^{0.5}$, where L = catalyst dimension (R/3 for a sphere), k = rate constant, C_o = bulk fluid concentration, and D_e = effective diffusivity of reactant in the catalyst. The H/D reactions are essentially second-order but will be treated as first-order in the D_2/D_2O case due to the large molar excess of deuterium. So, the equation is simplified to $\Phi = L(k/D_e)^{0.5}$. The effectiveness factor for intraparticle resistance is the ratio of the actual rate to the true kinetic rate. The rate constant in the equation for Φ is the true or intrinsic rate constant, which cannot be determined experimentally until we are sure there are no mass transfer limitations. It can be determined using the observable modulus. The effective diffusivity of glycine can be found from the Wilke-Chang equation. For the experiment with glycine at 70 °C in water, the diffusivity was equal to $3.5x10^{-5}$ cm^2/s.

The effective diffusivity in the catalyst pore takes into account the pore fraction, so $D_{eff,gly} = eps^2*D_{gly} = 1.2x10^{-9}$ m^2/s (based on eps = 0.59). The initial bulk concentration is 0.25 M = 0.25 $kmol/m^3$ but will vary throughout the reaction. To get the observable modulus, the rate of reaction $R_g = k*gly$ must be expressed in units mol gly/cm^3 catalyst/s (rate per unit catalyst volume). Using the data for the experiment with glycine with 1000 psi D_2 and 70 °C, the slope from the concentration (mol/L) versus time was multiplied by the volume of the reacting phase and dived by the volume of catalyst in the reactor (volume = mass catalyst/density of catalyst). For this experiment the rate equaled $5.3x10^{-3}$ $kmol/m^3*cat/s$.

The best way to assess the presence of mass transport is to use the observable modulus ($\eta^*\Phi^2 = R_g^*L^2/C_o/D_e$) and if this ($\eta^*\ \Phi^2$) is greater than about 0.3, then mass transport limitations in the catalyst particles during exchange need to be considered. For the experiment with glycine the observable modulus is equal to ($5.3x10^{-3}$ $kmol/m^3/s)^*(2.5x10^{-5}\ m^2)/(0.25\ kmol/m^3)/(1.2x10^{-9}\ m^2/s) = 0.01$. So, the conclusion is that there does not appear to be serious mass transfer consideration in the H/D exchange experiments. This is primarily because we are using such a small catalyst particle.

An additional experiment with 0.25 M glycine was performed at 90 °C with 1000 psi D_2 and D_2O. The singlet ^1H NMR peak representing the methylene (CH_2) position continued to decrease in size over time, while the CHD grew in, reaching a maximum peak height between 30 and 60 minutes of reaction time. Figure 88 shows the experimental and fitted concentrations of CH_2, CHD, and CD_2 over time as determined by the equations in Chapter 3. The rate constants for H/D exchange on the methylene carbon are: $k_{1A} = 1.9x10^{-4}$, $k_{-1A} = 1.0x10^{-5}$, $k_{2A} = 1.3x10^{-4}$, $k_{-2A} = 4.8x10^{-4}$ L/mol/min and the sum of the squares error (SSE) = $3.2x10^{-4}$.

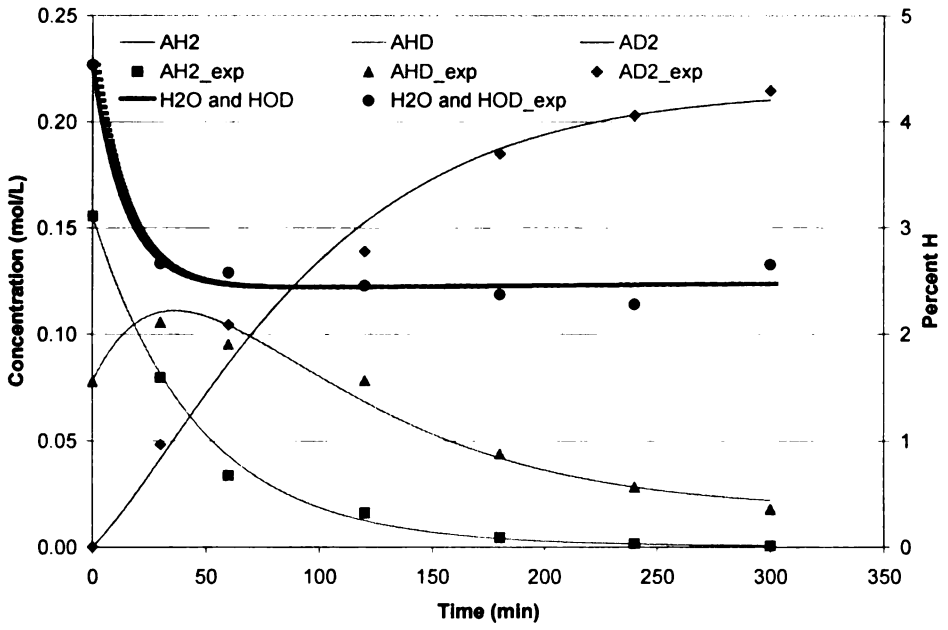

Figure 88. Fit of the kinetic rate data for 0.25 M glycine (D_2O, 90 °C, 1000 psi D_2, 1 g dry 5% Ru/C)

An experiment with 0.25 M betaine ($(CH_3)_3N^+CH_2COO^-$) at 130 °C was conducted to evaluate the extent of H/D exchange at the methylene position (Figure 12). Results at 130 °C with 1000 psi H_2 for six hours revealed 86% conversion of CH_2 to both CHD and CD_2. Figure 89 shows the experimental and fitted concentrations of CH_2, CHD, and CD_2 over time as determined by the equations in Chapter 3. The rate constants for H/D exchange on the methylene carbon are: $k_{1A} = 4.1x10^{-5}$, $k_{-1A} = 0$, $k_{2A} = 1.6x10^{-2}$, $k_{-2A} = 2.2x10^{-1}$ L/mol/min and the sum of the squares error (SSE) = $1.9x10^{-3}$.

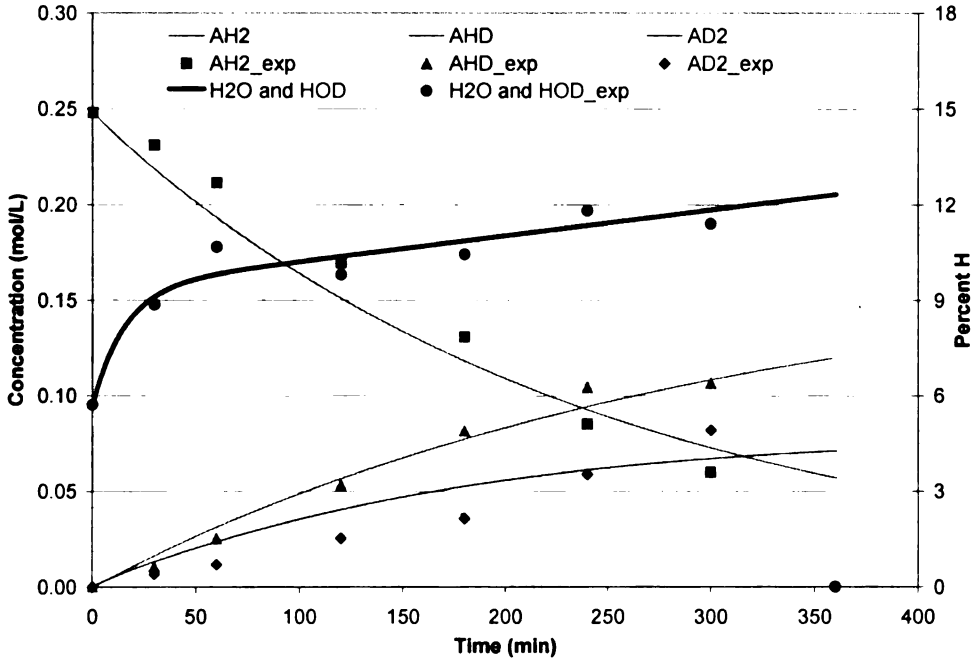

Figure 89. Fit of the kinetic rate data for 0.25 M betaine (D_2O, 130 °C, 1000 psi H_2, 1 g dry 5% Ru/C)

Isotopic exchange at the two methylene positions on glycylglycine was evaluated using 0.25 M glycylglycine at 100 °C with 1000 psi H_2 and D_2O. Position A, the more downfield ^1H NMR signal, exchanged much more rapidly than position B (Scheme 31).

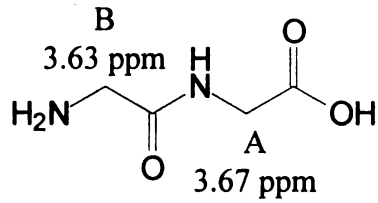

Scheme 31. ^1H NMR positions for the methylene hydrogens on glycylglycine

From the ^1H NMR results, it appeared as if both hydrogens at the methylene position exchanged at the same time, rather than step-wise. In most of the other isotopic exchange

experiments, the NMR results indicate the disappearance of the singlet and the appearance of the triplet over time. However, in this case the singlet (3.67 ppm) disappears quickly and without detectable triplet formation. The methylene position corresponding to the singlet at 3.63 ppm does appear to form CHD, as illustrated by the triplet formation.

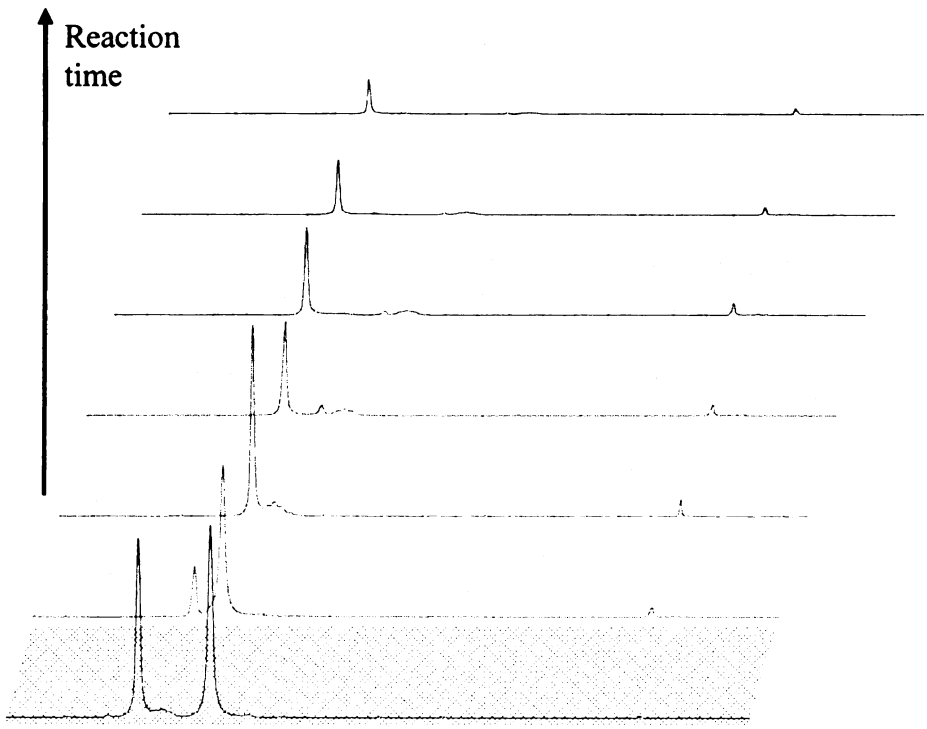

Figure 90. ^{1}H NMR of H/D exchange at the methylene positions of 0.25 glycylglycine (D_2O, 100 °C, 1000 psi H_2, 1 g dry 5% Ru/C

Again, the amount of triplet formed is quite small. Presumably much of the reason for the decrease in both 3.67 and 3.63 ppm methylenes is due to the formation of glycine. The results every hour over a six hour period are displayed in Figure 90. Hydrolyzed glycine is formed over time (3.36 ppm) and undergoes H/D exchange as it grows in (Figure 91).

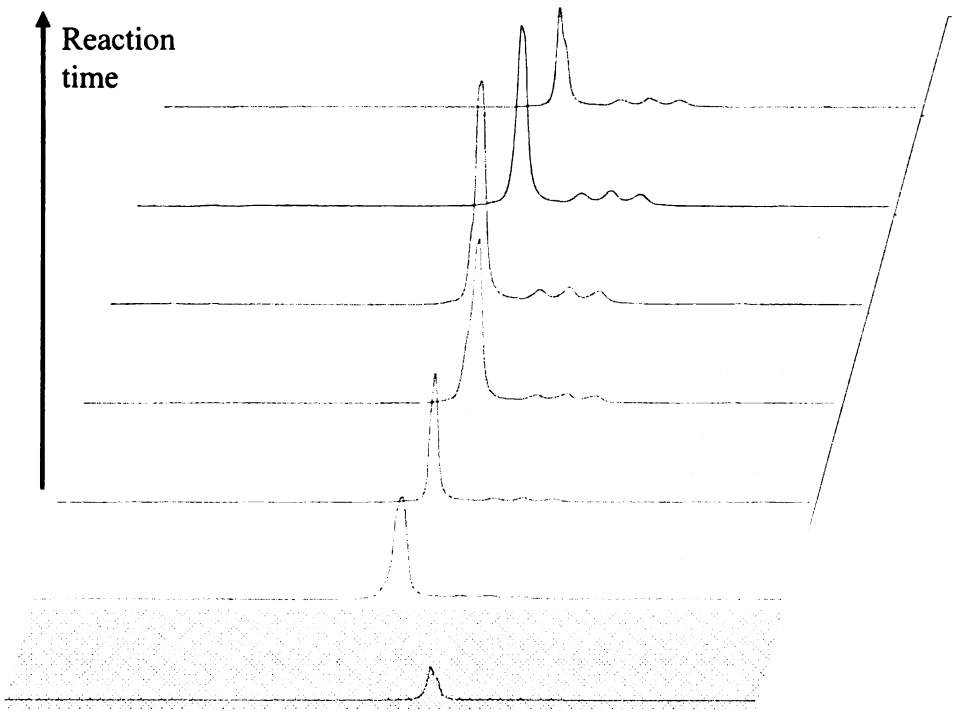

Figure 91. ^{1}H NMR of H/D exchange at the methylene position of hydrolyzed glycine from 0.25 M glyclglycine (D_2O, 100 °C, 1000 psi H_2, 1 g dry 5% Ru/C)

4.7.1.2 H/D Exchange at the N-Methyl Position

In this section H/D exchange at the N-methyl positions will be examined. At the end of this section a comparison will be made between the rate constants at the methylene and methyl carbons.

Again, the following chemical reactions (Chapter 3) can be used to calculate rate constants k_{1C}, k_{-1C}, k_{2C}, k_{-2C}, k_{3C}, and k_{-3C}. As mentioned in Chapter 3, the equilibrium between the hydrogens on the catalyst surface and the hydrogen concentration in the

liquid is not reached at time zero for the experiments with 1000 psi H_2 and D_2O, so the hydrogen concentration in the liquid is used.

The experiment describing the hydrogen-deuterium exchange on the methyl carbon is depicted by three reversible, consecutive first-order reactions (Chapter 3). The amino acid substrates which were studied included sarcosine (N-methylglycine), N,N-dimethylglycine, and betaine. An experiment with 0.25 M sarcosine at 100 °C with 1000 psi H_2 and D_2O was run for six hours. The singlet ^1H NMR peak representing the methyl (CH_3) position continued to decrease in size over time, while the triplet peak representing CH_2D grew in, reaching a maximum peak height at 120 minutes of reaction. A quintet peak representing CHD_2 grew in, reaching a maximum peak height at 180 minutes of reaction time. The ^1H NMR of time zero and after six hours of reaction time is compared in Figure 92. Figure 93 shows the experimental and fitted concentrations of CH_3, CH_2D, CHD_2 and CD_3 over time as determined by the equations in Chapter 3. The rate constants for H/D exchange on the methyl carbon are: $k_{1C} = 1.1x10^{-4}$, $k_{-1C} = 0$, $k_{2C} = 1.4x10^{-4}$, $k_{-2C} = 2.5x10^{-6}$, $k_{3C} = 8.3x10^{-5}$, and $k_{-3C} = 2.0x10^{-4}$ L/mol/min.

An experiment with 0.25 M N,N-dimethylglycine at 100 °C with 1000 psi H_2 and D_2O was run for six hours. The ^1H NMR of time zero and after six hours of reaction time is compared in Figure 94. Figure 95 shows the experimental and fitted concentrations of CH_3, CH_2D, CHD_2 and CD_3 over time as determined by the equations in Chapter 3. The rate constants for H/D exchange on the methyl carbon are: $k_{1C} = 1.0x10^{-4}$, $k_{-1C} = 0$, $k_{2C} = 1.4x10^{-4}$, $k_{-2C} = 1.8x10^{-4}$, $k_{3C} = 1.5x10^{-4}$, and $k_{-3C} = 5.8x10^{-4}$ L/mol/min.

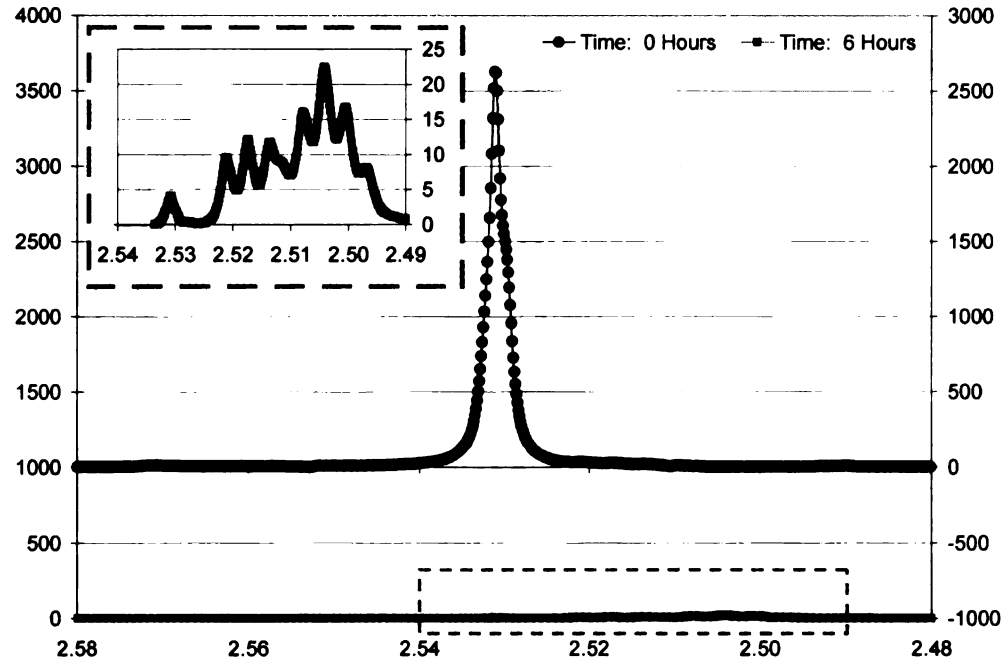

Figure 92. ^{1}H NMR of H/D exchange at the methyl position of 0.25 M sarcosine (D_2O, 100 °C, 1000 psi H_2, 1 g dry 5% Ru/C)

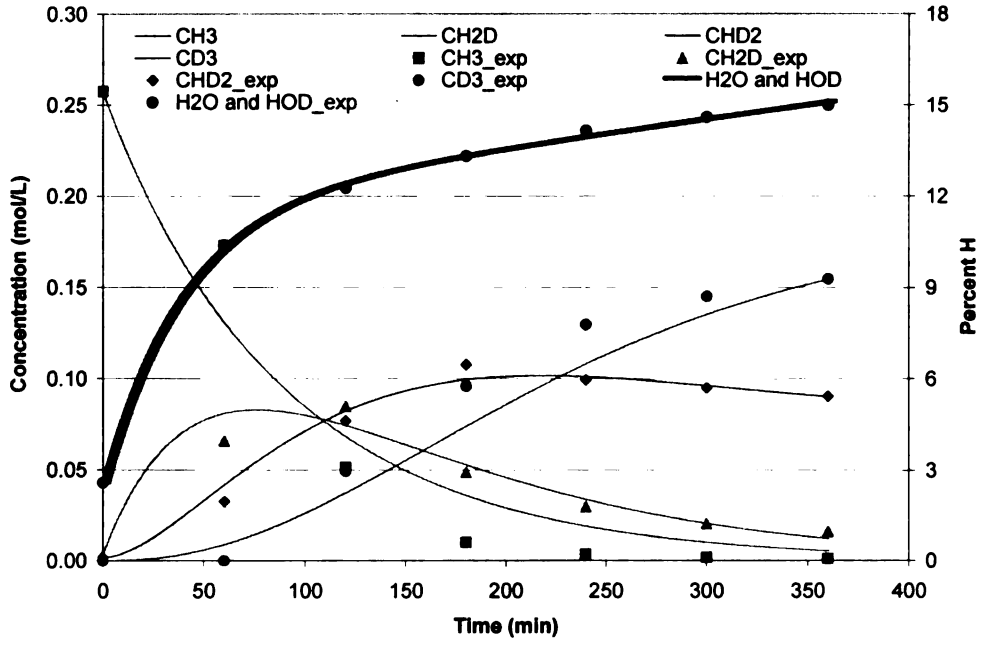

Figure 93. Fit of the kinetic rate data for 0.25 M sarcosine (D_2O, 100 °C, 1000 psi H_2, 1 g dry 5% Ru/C)

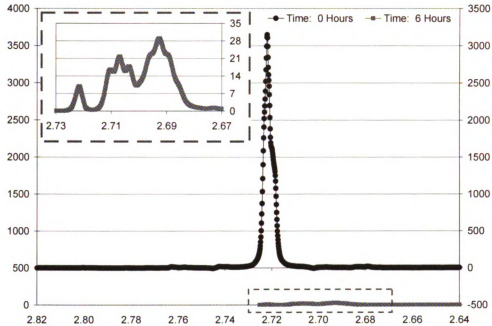

Figure 94. ^{1}H NMR of H/D exchange at the methyl position of 0.25 M N,N-dmg (D_2O, 100 °C, 1000 psi H_2, 1 g dry 5% Ru/C)

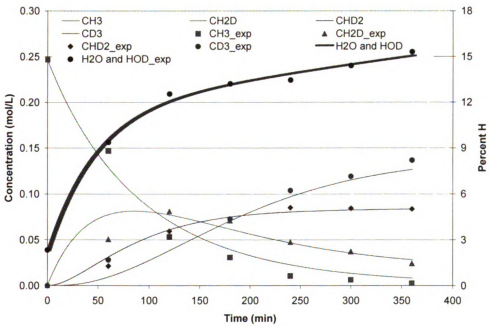

Figure 95. Fit of the kinetic rate data for 0.25 M N,N-dmg (D_2O, 100 °C, 1000 psi H_2, 1 g dry 5% Ru/C)

The same pair of experiments were performed at 100 °C but with 1000 psi D_2. An experiment with 0.25 M sarcosine was run for six hours. The ^1H NMR of time zero and after six hours of reaction time is compared in Figure 96. Figure 97 shows the experimental and fitted concentrations of CH_3, CH_2D, CHD_2 and CD_3 over time as determined by the equations in Chapter 3. The rate constants for H/D exchange on the methyl carbon are: $k_{1C} = 1.6x10^{-4}$, $k_{-1C} = 0$, $k_{2C} = 1.9x10^{-4}$, $k_{-2C} = 0$, $k_{3C} = 1.5x10^{-4}$, and $k_{3C} = 8.5x10^{-4}$ L/mol/min. The H/D exchange on the N-methyl of sarcosine was slower than the methylene (in general, for all conditions) and did not fully reach equilibrium after six hours. The statistical equilibrium end points were again compared to the experimental data (for the experiment with 1000 psi D_2). The statistical concentrations of CH_3, CH_2D, CHD_2 and CD_3 based on the actual percent hydrogen in water at six hours (1.76%) and the concentration at time zero (0.22 M) are $1.2x10^{-6}$, $2.0x10^{-4}$, 0.0113 and 0.210 M, respectively. The actual concentrations of CH_2, CHD, and CD_2 at six hours of reaction time are $2.1x10^{-4}$, $1.0x10^{-3}$, 0.027 and 0.22 M, respectively.

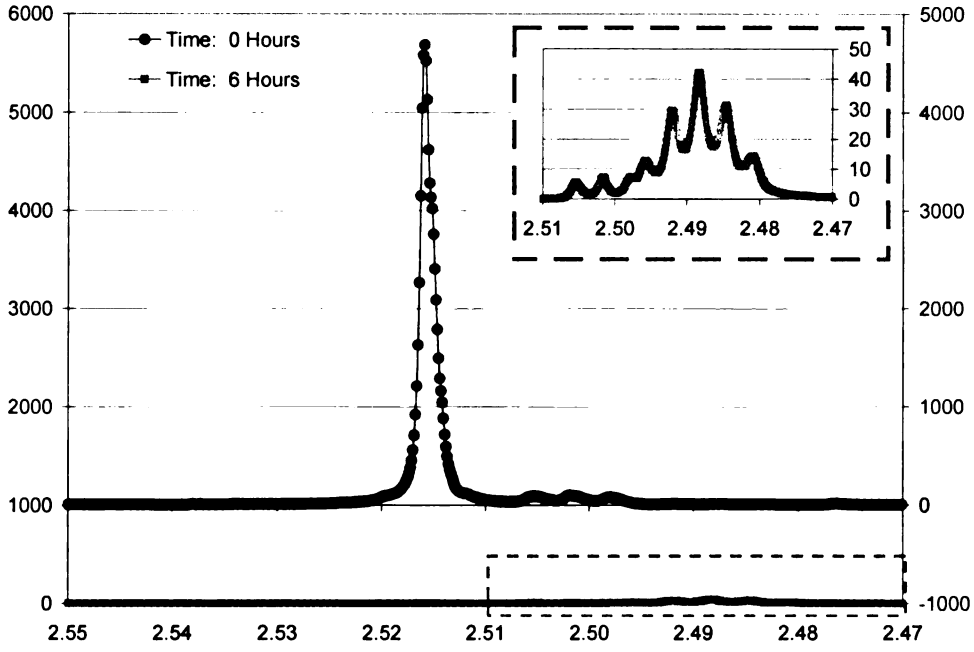

Figure 96. ^{1}H NMR of H/D exchange at the methyl position of 0.25 M sarcosine (D_2O, 100 °C, 1000 psi D_2, 1 g dry 5% Ru/C)

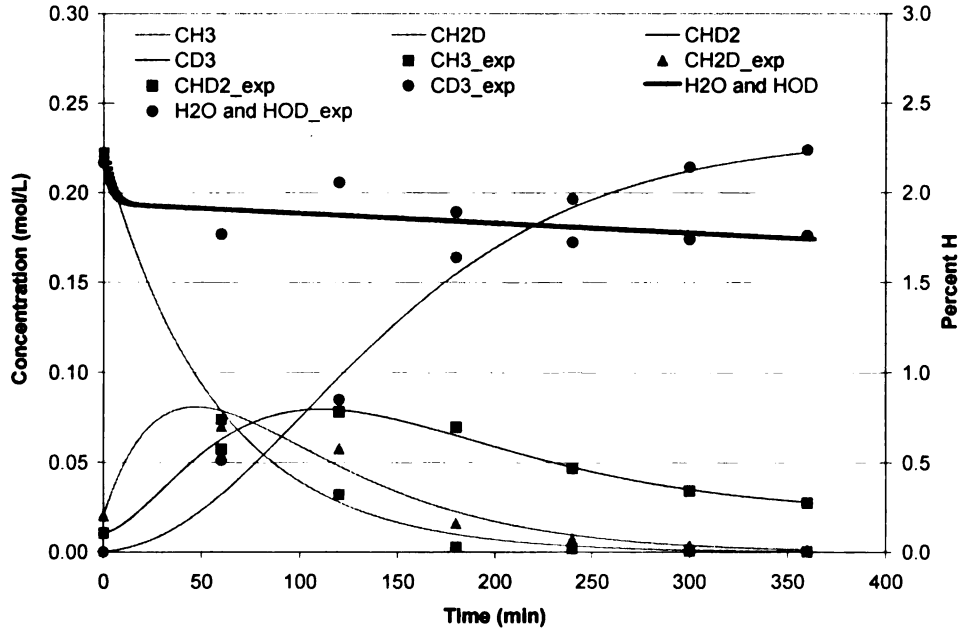

Figure 97. Fit of the kinetic rate data for 0.25 M sarcosine (D_2O, 100 °C, 1000 psi D_2, 1 g dry 5% Ru/C)

An experiment with 0.25 M N,N-dimethylglycine was run for six hours. The ^{1}H NMR of time zero and after six hours of reaction time is compared in Figure 98. Figure 99 shows the experimental and fitted concentrations of CH_3, CH_2D, CHD_2 and CD_3 over time as determined by the equations in Chapter 3. The rate constants for H/D exchange on the methyl carbon are: $k_{1C} = 1.9x10^{-4}$, $k_{-1C} = 0$, $k_{2C} = 3.2x10^{-4}$, $k_{-2C} = 0$, $k_{3C} = 2.8x10^{-4}$, and $k_{-3C} = 8.8x10^{-4}$ L/mol/min.

The H/D exchange on the N-methyl of N,N-dimethylglycine appeared to just approach equilibrium after six hours. The statistical equilibrium end points were again compared to the experimental data. The statistical concentrations of CH_3, CH_2D, CHD_2 and CD_3 based on the actual percent hydrogen in water at six hours (2.7%) and the concentration at time zero (0.15 M) are $2.9x10^{-6}$, $3.1x10^{-4}$, 0.011 and 0.134 M, respectively. The actual concentrations of CH_2, CHD, and CD_2 at six hours of reaction time are $6.7x10^{-6}$, $1.3x10^{-4}$, 0.0041 and 0.196 M, respectively.

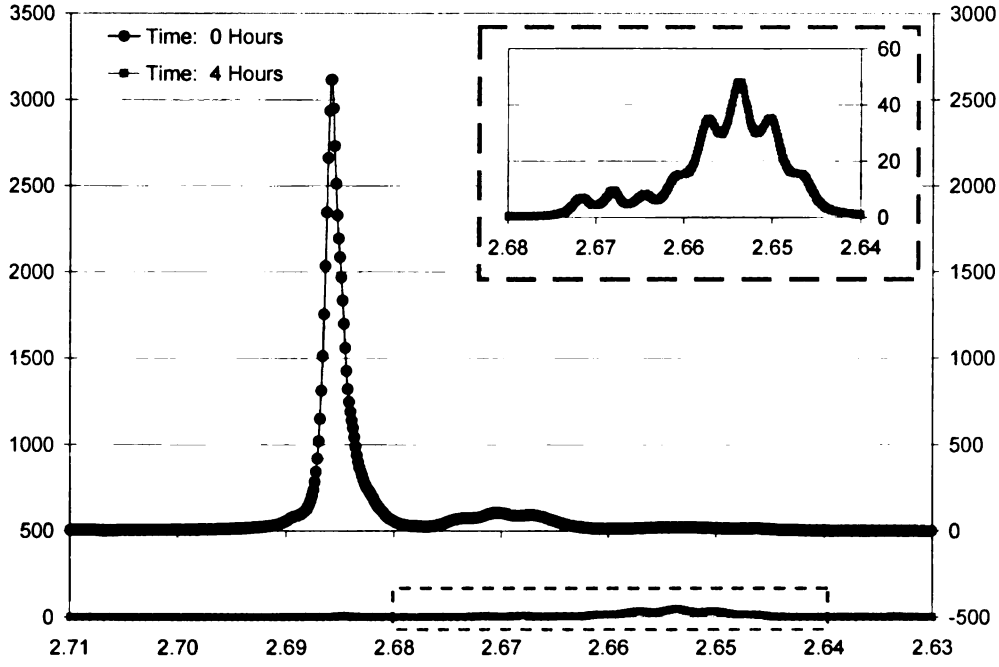

Figure 98. ^{1}H NMR of H/D exchange at the methyl position of 0.25 M N,N-dmg (D_2O, 100 °C, 1000 psi D_2, 1 g dry 5% Ru/C)

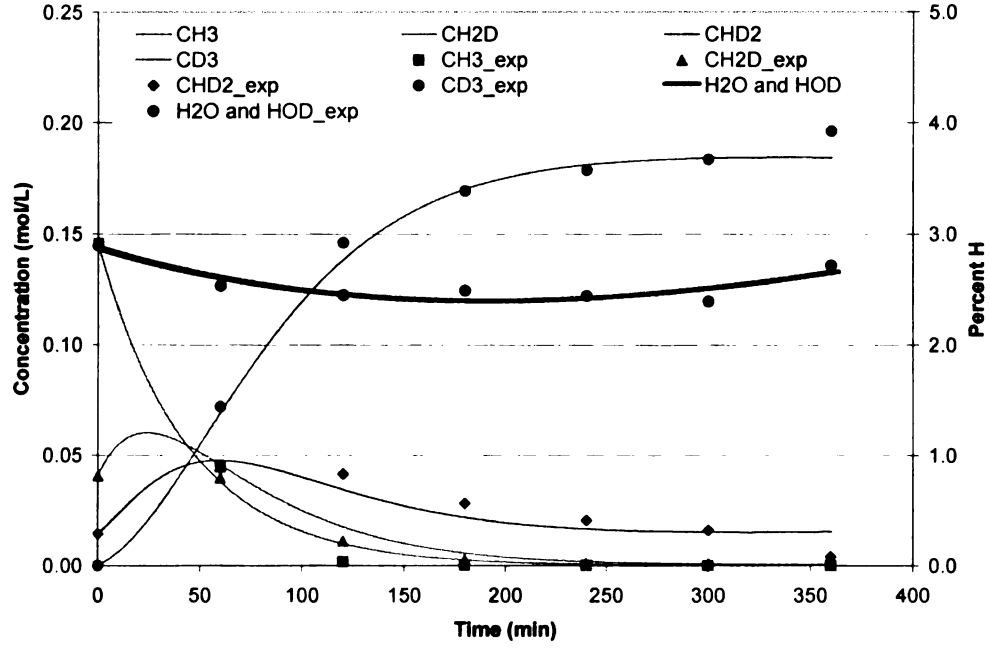

Figure 99. Fit of the kinetic rate data for 0.25 M N,N-dmg (D_2O, 100 °C, 1000 psi D_2, 1 g dry 5% Ru/C)

Again, as in the case of the methylene carbon, the kinetic model can be redefined using three independent variables, k_{ic}, p_C, and s_C instead of six. As discussed in Chapter 3, k_{1C} is equal to $3*k_{iC}$ indicating that there are three hydrogens on the methyl carbon and subsequently three opportunities for H/D exchange. The equations for how the k_{1C}, etc rate constants could be effectively calculated from the k_{ic}, p_C, and s_C values are discussed in Chapter 3. It was assumed p_C and s_C are independent.

For the reactions at 100 °C with 1000 psi H_2 one k (k_i) value for each site that is modified via an isotope effect was calculated. The results show that sarcosine and N,N-dimethylglycine the primary isotope effects are similar and about 0.7-0.8. For sarcosine $k_{iC} = 0.40x10^{-4}$ L/mol/min, $p_C = 0.71$, and $s_C = 0.47$. For N,N-dimethylglycine $k_{iC} = 0.35x10^{-4}$ L/mol/min, $p_C = 0.83$, and $s_C = 0.52$. The secondary isotope effects for sarcosine and N,N-dimethlyglycine are similar and equal to about 0.5. The trend for the rate constants, k_i, for sarcosine and N,N-dimethylglycine match well with k_{1C} using either the 10 or 6-variable model. The k_i values for both sarcosine are N,N-dimethylglycine are about 1/3rd that of k_{1C}, respectively. Again this makes sense based on the fact that k_{1C} is defined as being equal to $3*k_{iC}$.

For the reactions at 100 °C with 1000 psi D_2 one k (k_i) value for each site that is modified via an isotope effect was calculated. For sarcosine $k_{iC} = 0.55x10^{-4}$ L/mol/min, $p_C = 0.45$, and $s_C = 0.59$. For N,N-dimethylglycine $k_{iC} = 0.69x10^{-4}$ L/mol/min, $p_C = 0.87$, and $s_C = 0.47$. The secondary isotope effects for sarcosine and N,N-dimethlyglycine are similar

and equal to about 0.5. Again, the k_i values for both sarcosine are N,N-dimethylglycine are about 1/3rd that of k_{1C}, respectively.

As discussed in the H/D exchange on the methylene carbon section, the data from the experiments with 1000 psi H_2 and D_2 can be linked in order to define a common set of rate constants. Figure 100 presents the comparison of the kinetic fits using the $k_6 + k_H$ model with the data from the sarcosine experiment with 1000 psi H_2 and also from the linked data set (1000 psi H_2 and D_2). Figure 101 is the analogous plot showing the comparison of the kinetic fits with the data from the experiment with 1000 psi D_2 and also from the linked data set.

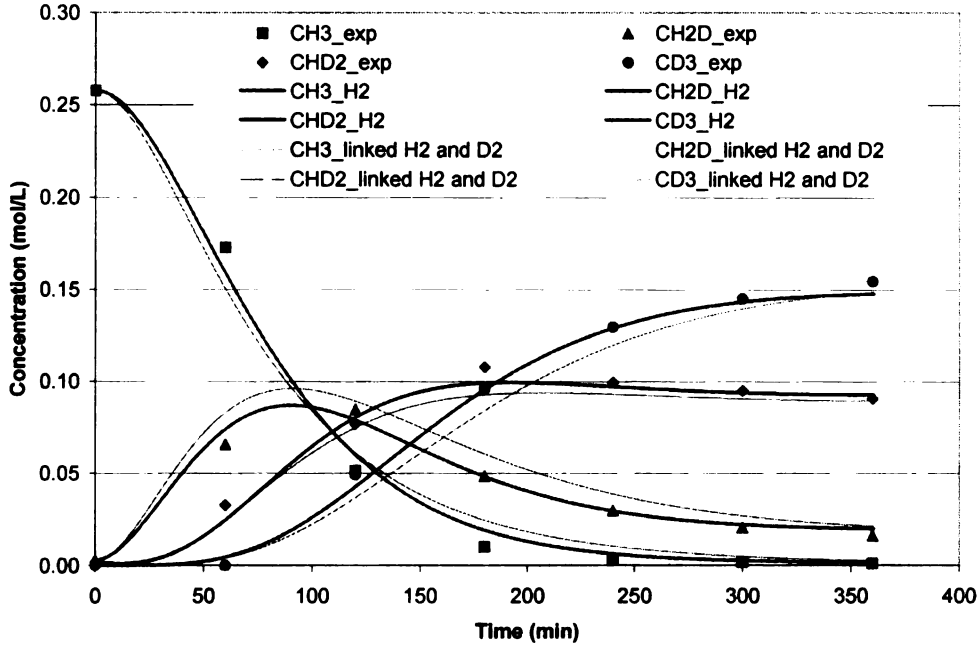

Figure 100. Fit of the kinetic rate data for 0.25 M sarcosine (D_2O, 100 °C, 1000 psi H_2 or linked H_2 and D_2, 1 g dry 5 % Ru/C)

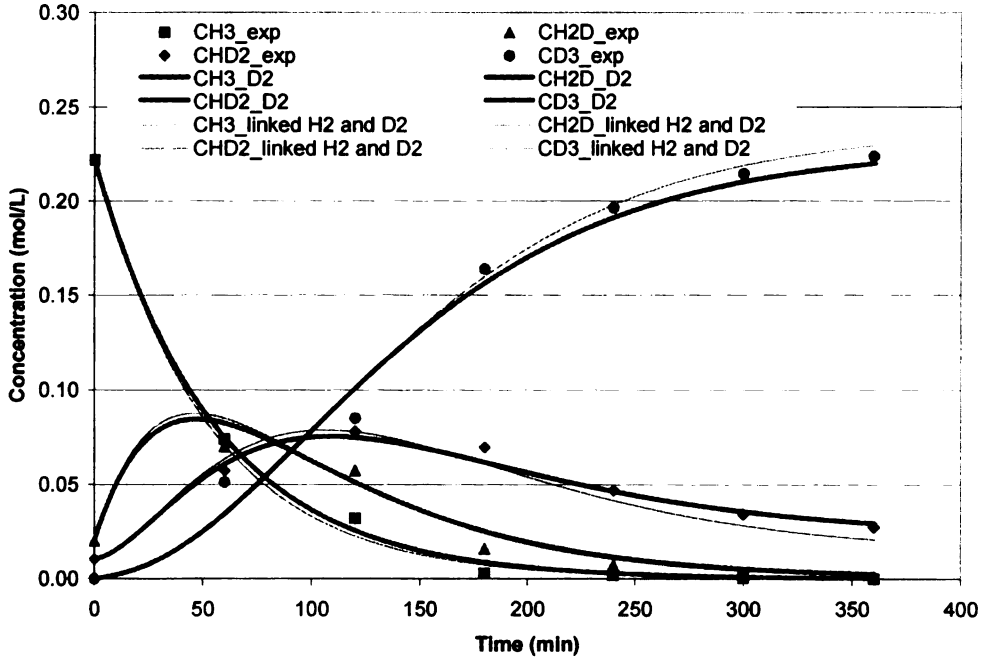

Figure 101. Fit of the kinetic rate data for 0.25 M sarcosine (D_2O, 100 °C, 1000 psi D_2 or linked H_2 and D_2, 1 g dry 5 % Ru/C)

The fits from the linked experimental data (1000 psi H_2 and D_2) is comparable to those from the individual experiments. For the experiment with 1000 psi H_2, the fit is slightly faster using the linked data. This result again gives credence to the common rate constants. Figure 102 shows the kinetic rate constant and primary and secondary isotope effects for the H/D exchange on the methyl carbon of sarcosine. The rate constants for the H/D exchange on the methyl are slower than those for the methylene ($k_{iA} = 1.5x10^{-4}$ versus $k_{iC} = 0.58x10^{-4}$ L/mol/min). The primary and secondary isotope effects are fairly close $p_A = 1.08$ versus $p_C = 0.82$ and $s_A = 0.49$ versus $s_C = 0.63$. Again, there is not much significance to the primary isotope effect because the back reaction is not occurring under these conditions.

Figures 103 through 105 present the results for N,N-dimethylglycine. The rate constants for H/D exchange on the methyl are slower than those for the methylene ($k_{iA} = 7.4x10^{-5}$ versus $k_{iC} = 6.6x10^{-5}$ L/mol/min). The primary and secondary isotope effects were compared for the methylene and methyl carbon. As with sarcosine, they are very close $p_A = 0.52$ versus $p_C = 0.68$ and $s_A = 0.60$ versus $s_C = 0.48$. The secondary isotope effects for both sarcosine and N,N-dimethylglycine at the methylene and methyl carbon are about 0.6 (note: glycine $s_A = 0.81$).

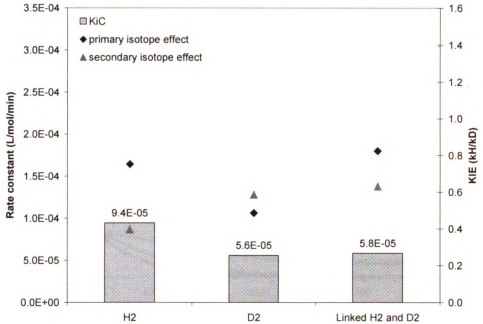

Figure 102. Kinetic rate constant and primary and secondary isotope effects for sarcosine with 1000 psi H_2 or 1000 psi D_2 or H_2 and D_2

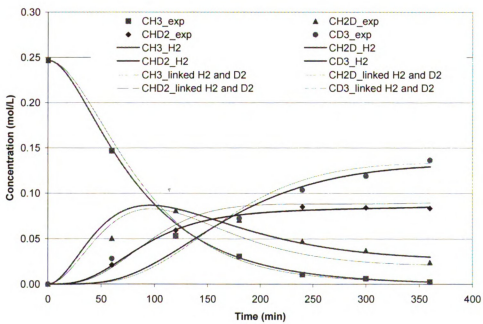

Figure 103. Fit of the kinetic rate data for 0.25 M N,N-dmg (D_2O, 100 °C, 1000 psi H_2 or linked H_2 and D_2, 1 g dry 5 % Ru/C)

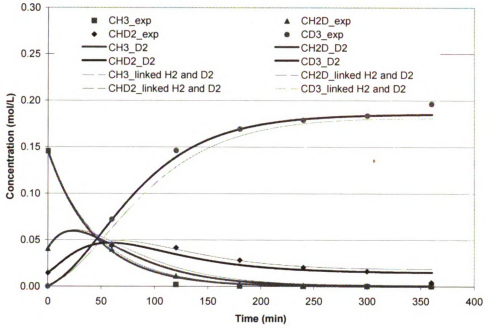

Figure 104. Fit of the kinetic rate data for 0.25 M N,N-dmg (D_2O, 100 °C, 1000 psi D_2 or linked H_2 and D_2, 1 g dry 5 % Ru/C)

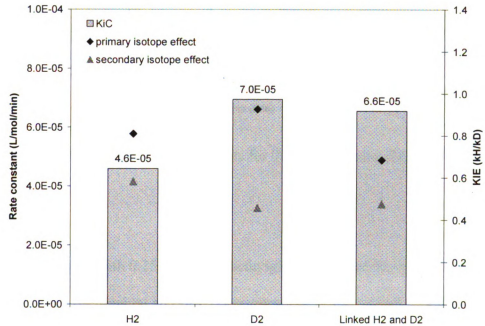

Figure 105. Kinetic rate constant and primary and secondary isotope effects for N,N-dmg with 1000 psi H_2 or 1000 psi D_2 or H_2 and D_2

A third pair of experiments was conducted at 70 °C with 1000 psi D_2 and D_2O. An experiment with 0.25 M sarcosine was run for four hours. Figure 106 shows the experimental and fitted concentrations of CH_3, CH_2D, CHD_2 and CD_3 over time as determined by the equations in Chapter 3. The rate constants for H/D exchange on the methyl carbon are: $k_{1C} = 7.4x10^{-5}$, $k_{-1C} = 0$, $k_{2C} = 9.4x10^{-5}$, $k_{-2C} = 2.1x10^{-3}$, $k_{3C} = 1.7x10^{-4}$, and $k_{-3C} = 6.0x10^{-3}$ L/mol/min.

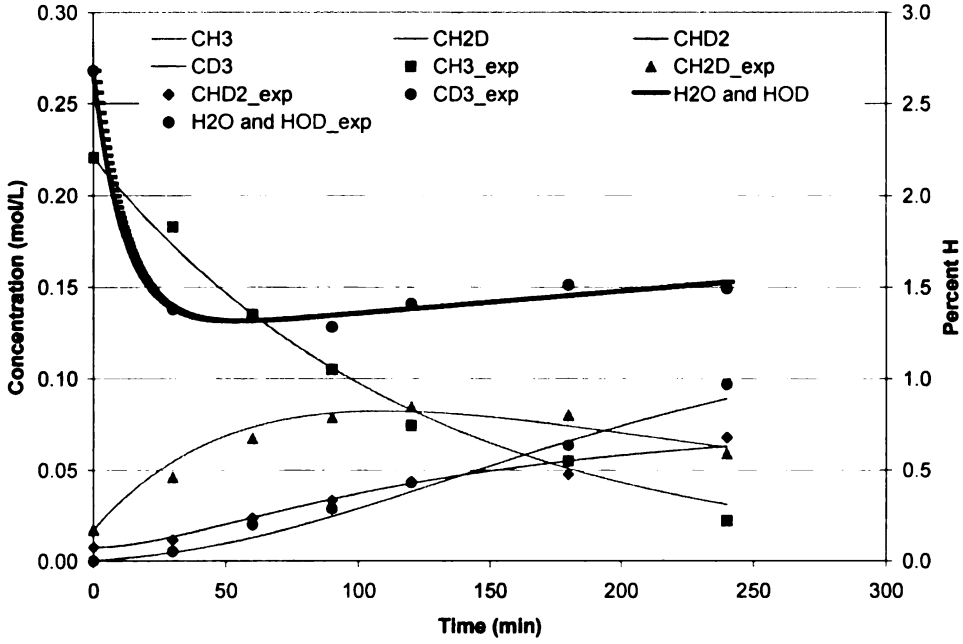

Figure 106. Fit of the kinetic rate data for 0.25 M sarcosine (D_2O, 70 °C, 1000 psi D_2, 1 g dry 5% Ru/C)

An experiment with 0.25 M N,N-dimethylglycine was run for four hours. Figure 107 shows the experimental and fitted concentrations of CH_3, CH_2D, CHD_2 and CD_3 over time as determined by the equations in Chapter 3. The rate constants for H/D exchange on the methyl carbon are: $k_{1C} = 3.0x10^{-5}$, $k_{-1C} = 0$, $k_{2C} = 1.1x10^{-4}$, $k_{-2C} = 1.1x10^{-2}$, $k_{3C} = 5.9x10^{-5}$, and $k_{-3C} = 0$ L/mol/min.

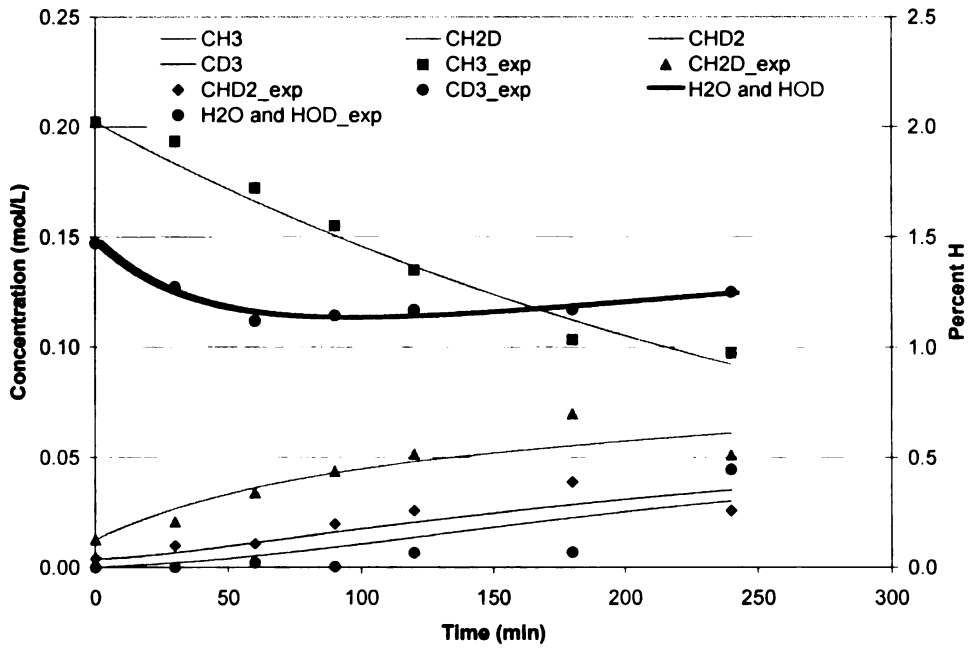

Figure 107. Fit of the kinetic rate data for 0.25 M N,N-dimethylglycine (D_2O, 70 °C, 1000 psi D_2, 1 g dry 5% Ru/C)

For the reactions at 70 °C in 1000 psi D_2 we calculated one k (k_i) value for each site that is modified via an isotope effect (Figure 108). The results show that for sarcosine and N,N-dimethylglycine the secondary isotope effects are both about 0.5 (similar to the experiments discussed above). For sarcosine $k_{iC} = 0.24 \times 10^{-4}$ L/mol/min, $p_C = 1.5$, and $s_C = 0.56$. For N,N-dimethylglycine $k_{iC} = 8.7 \times 10^{-6}$ L/mol/min, $p_C = 1.0$, and $s_C = 0.38$. Again, the k_i values for sarcosine and N,N-dimethylglycine are about one-third of their respective k_{IC}s.

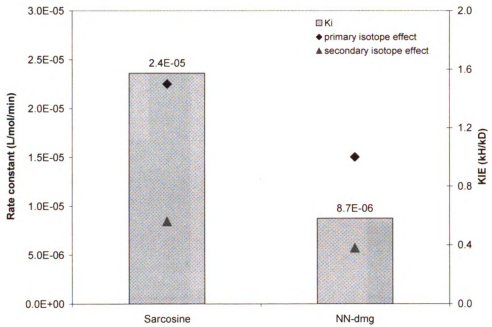

Figure 108. Kinetic rate constants and primary and secondary isotope effects for sarcosine and N,N-dimethylglycine; 70 °C, 1000 psi D_2

We can compare the reactions in 1000 psi D_2 at both 70 °C and 100 °C for the H/D exchange on the methylene carbon and N-methyls of sarcosine and N,N-dimethylglycine (Figure 109). Again for sarcosine the rate of exchange for the methylene hydrogens is slightly larger than for the methyl hydrogens. Whereas in the case of N,N-dimethylglycine, the methyl hydrogens exchange at a slightly faster rate than the methylene hydrogens. Again, this is partly due to the fact that with N,N-dimethylglycine there are twice as many N-methyl hydrogens available for H/D exchange. As seen previously, the rate constants calculated in the reaction at 70 °C are slower than the experiment with otherwise identical conditions at 100 °C.

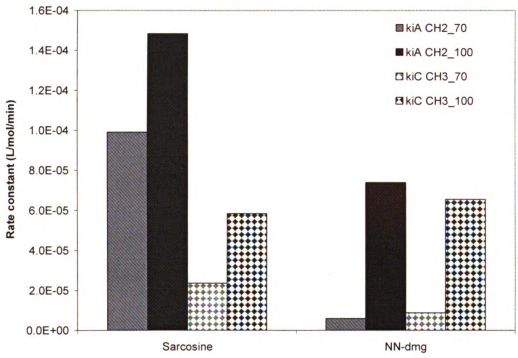

Figure 109. Rate constants for H/D exchange at 100 °C or 70 °C (D_2O, X °C, 1000 psi D_2, 1 g dry 5% Ru/C)

An additional experiment was done with sarcosine at 50 °C with 1000 psi D_2 and D_2O. Figure 110 shows the experimental and fitted concentrations of CH_3, CH_2D, CHD_2 and CD_3 over time as determined by the equations in Chapter 3. The rate constants for H/D exchange on the methyl carbon are: $k_{1C} = 1.6x10^{-5}$, $k_{-1C} = 3.1x10^{-5}$, $k_{2C} = 1.6x10^{-5}$, $k_{-2C} = 1.6x10^{-6}$, $k_{3C} = 3.2x10^{-5}$, and $k_{-3C} = 2.6x10^{-3}$ L/mol/min.

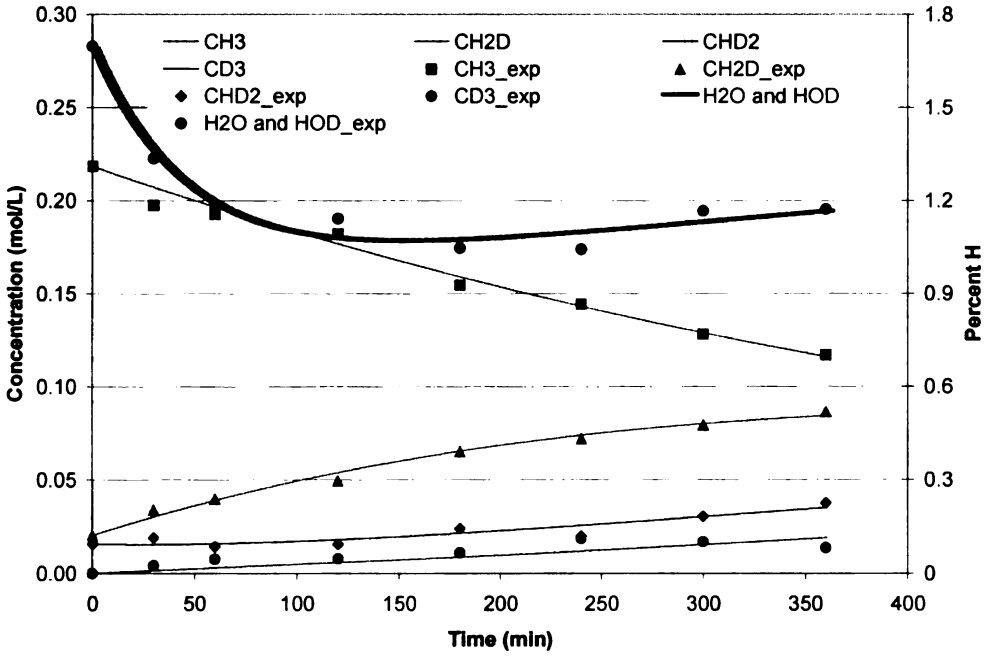

Figure 110. Fit of the kinetic rate data for 0.25 M sarcosine (D_2O, 50 °C, 1000 psi D_2, 1 g dry 5% Ru/C)

We can compare the rate constants for the H/D exchange at both the methylene carbon and the N-methyl carbons for the experiments with sarcosine at 100 °C, 70°C, 50 °C with 1000 psi D_2. Figure 111 compares k_{iA} and k_{iC}. The activation energy was calculated for this set of experiments and determined to be E_A = 67 kJ/mol (note the E_A for the H/D exchange on the methylene carbon was calculated to be 36 kJ/mol).

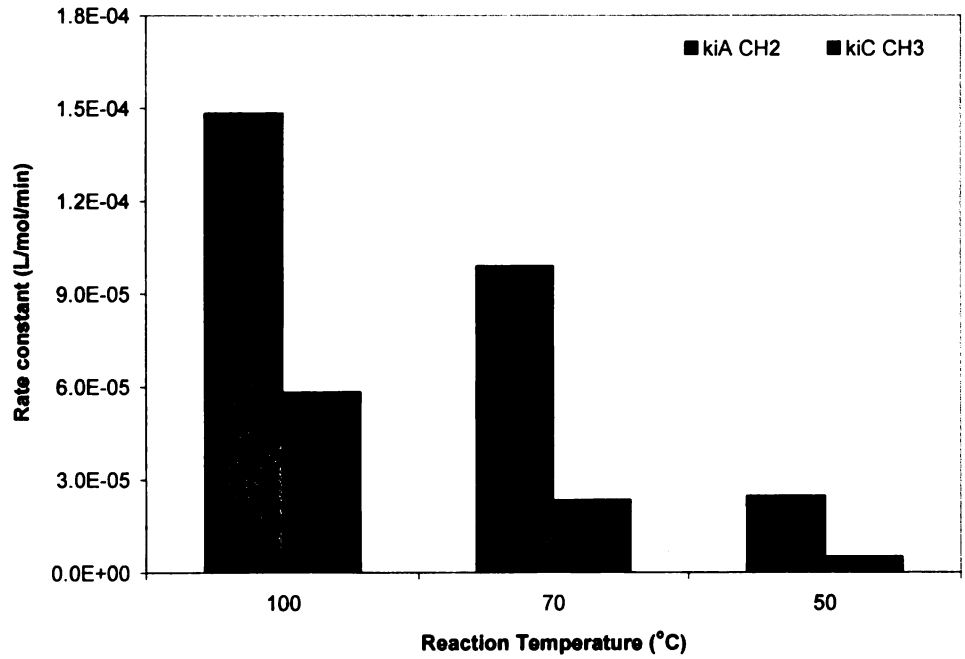

Figure 111. Rate constants for H/D exchange of sarcosine (D_2O, 50, 70, or 100 °C, 1000 psi H_2 or D_2, 1 g dry 5% Ru/C)

In summary, the kinetic rate constants from the 6-variable model can be compared for the three substrates at the reaction temperatures of 50, 70, and 100 °C (Table 9).

An experiment with 0.25 M betaine ($(CH_3)_3N^+CH_2COO^-$) at 130 °C was conducted to evaluate the extent of H/D exchange at the N-methyl positions. Results at 130 °C, 1000 psi H_2 for six hours reveal no H/D exchange at the N-methyl positions (Figure 112). The integration value for the N-methyls differed by about 6% comparing time zero and after six hours. This is within the expected value for adsorption onto the Ru catalyst.

Table 9. Summary of the rate kinetic rate constants and primary and secondary isotope effects for glycine, sarcosine, and N,N-dimethylglycine

Rate constant	Glycine 100 °C D_2	Sarcosine 100 °C D_2	N,N-dmg 100 °C D_2
k_{iA}	0.99	1.48	0.74
p_A	4.39	0.76	1.14
s_A	0.72	0.46	0.65
k_{iC}		0.58	0.66
p_C		0.45	0.87
s_C		0.59	0.47

Rate constant	Glycine 70 °C D_2	Sarcosine 70 °C D_2	N,N-dmg 70 °C D_2
k_{iA}	0.74	0.99	0.06
p_A	0.03	0.24	1.00
s_A	1.54	0.72	0.40
k_{iC}		0.24	0.09
p_C		1.50	1.00
s_C		0.56	0.38

Rate constant	Glycine 50 °C D_2	Sarcosine 50 °C D_2
k_{iA}	0.09	0.25
p_A	0.10	0.35
s_A	0.42	1.00
k_{iC}		0.05
p_C		1.00
s_C		0.70

All rate constants are multiplied by 10^4

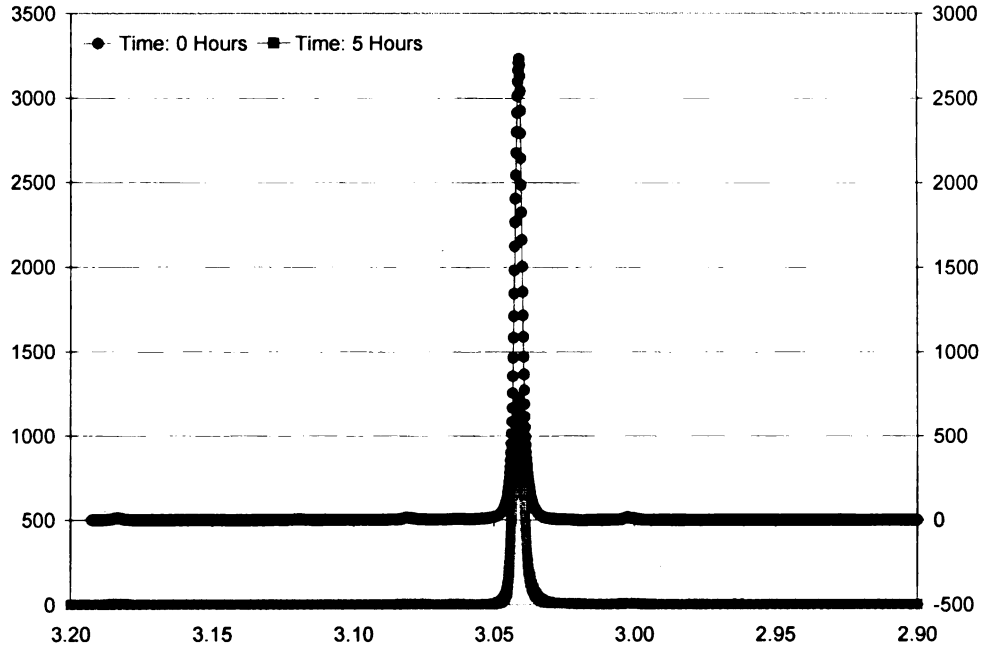

Figure 112. ^{1}H NMR of H/D exchange at the methyl position of 0.25 M betaine (D_2O, 130 °C, 1000 psi H_2, 1 g dry 5% Ru/C)

4.7.2 Other Substrates

Several additional substrates were examined. There were specific reasons for evaluating each of the substrates. Ethanolamine was chosen in order to determine whether the hydrogens on the methylene next to the oxygen or the methylene next to the nitrogen would exchange faster and it was hypothesized that the hydrogens on the methylene next to the oxygen would exchange faster. Using 0.25 M ethanolamine at 100 °C with 1000 psi H_2 and D_2O and 1 g dry 5% Ru/C for four hours, the hydrogens on the methylene adjacent to the oxygen exchanged more quickly than the hydrogens adjacent to the nitrogen (Scheme 32).

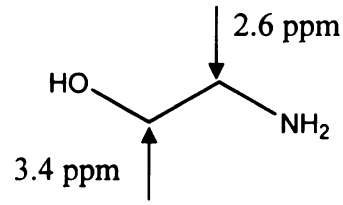

Scheme 32. ^{1}H NMR positions for the methylene hydrogens on ethanolamine

It was not possible to deconvolute the CH_2 from the CHD due to the fact that the splitting was overlapping. Thus, the concentrations are expressed as CH_2 plus CHD. The ^{1}H NMR of both the methylene next to the oxygen (Figure 113) and the methylene next to the nitrogen (Figure 114) are shown below.

After two hours of reaction time, the deuterium exchange at both positions reached equilibrium and was essentially identical (Figure 115). The concentrations expressed in Figure 115 are the sum of CH_2 and CHD.

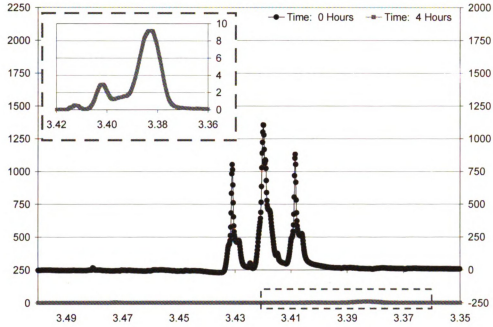

Figure 113. ^{1}H NMR of H/D exchange at the methylene position next to the –OH of 0.25 M ethanolamine (D_2O, 100 °C, 1000 psi H_2, 1 g dry 5% Ru/C)

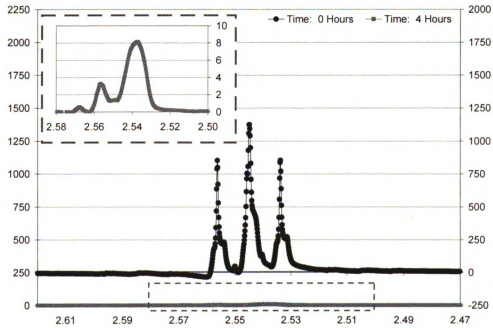

Figure 114. ^{1}H NMR of H/D exchange at the methylene position next to the –NH_2 of 0.25 M ethanolamine (D_2O, 100 °C, 1000 psi H_2, 1 g dry 5% Ru/C)

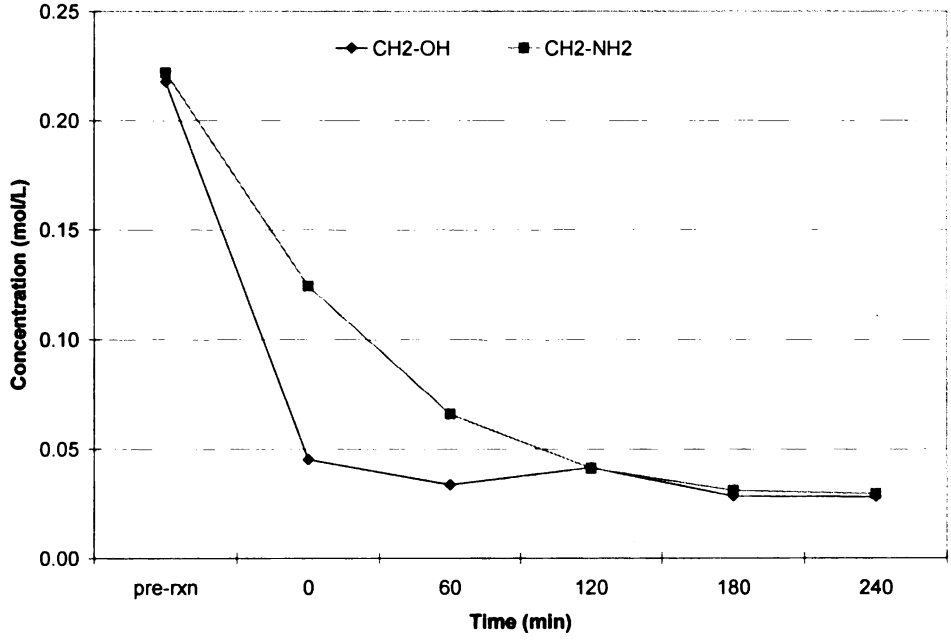

Figure 115. Concentration data for 0.25 M ethanolamine (D_2O, 100 °C, 1000 psi H_2, 1 g dry 5% Ru/C)

An experiment with 0.25 M glycolic acid at 100 °C with 1000 psi H_2 and D_2O was run for 6 hours. This experiment was conducted in order to evaluate the extent of H/D exchange at the methylene carbon. Results indicate that very little H/D exchange occurred at the methylene carbon and no measurable amount of CHD was observed. The concentration after six hours of reaction time was 0.23 M. However, the peak did become broader over the course of the reaction. Figure 116 compares one hour and after six hours of reaction. Glycolic acid will undergo hydrogenation under similar conditions, however, at 100 °C the hydrogenation rate is slowed significantly and no hydrogenation products were detected.

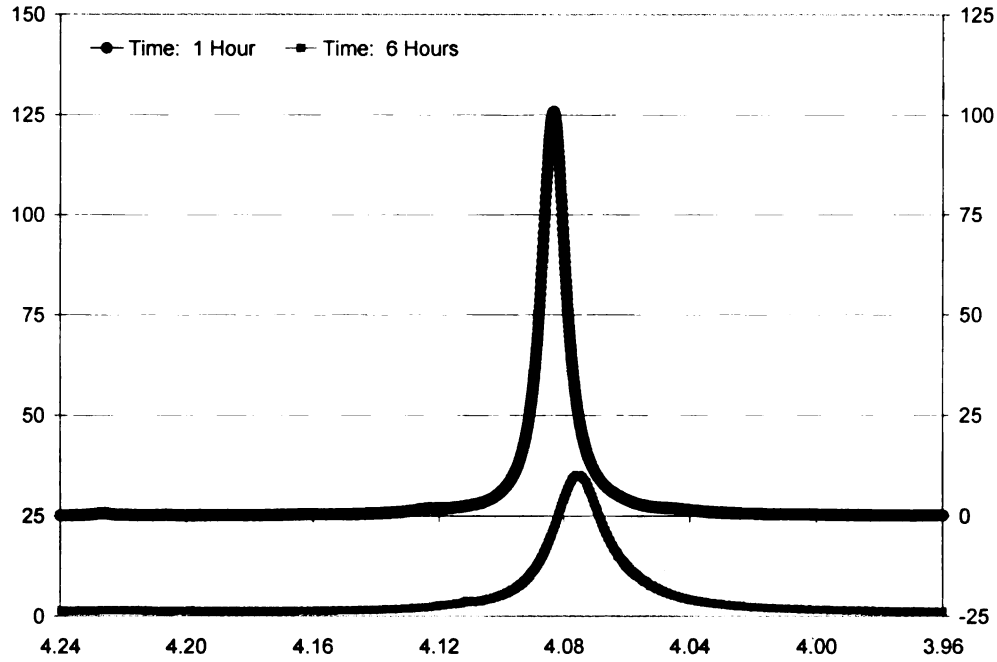

Figure 116. ^{1}H NMR of H/D exchange at the methylene position of 0.25 M glycolic acid (D_2O, 100 °C, 1000 psi H_2, 1 g dry 5% Ru/C)

An experiment with 0.25 M *tert*-butanol at 100 °C for with 1000 psi H_2 and D_2O for four hours was run to evaluate the extent of H/D exchange at the methyl carbons, although little was expected. Results indicate that little H/D exchange occurred at the methyl carbons and a nominal amount of CH_2D and CHD_2 was observed. The conversion after four hours of reaction time was 26%. However, the peak did become broader over the course of the reaction. Figure 117 compares one hour and after four hours of reaction. In the solvent study work *tert*-butanol was examined as a solvent and it was hypothesized that H/D exchange was not occurring on the methyl carbons due to an inability for C-H activation and this experiment confirmed this. However, there is still some solvent degradation and presumably the interaction with the solvent and the catalyst is preventing the substrate (in the hydrogenation experiments) reduction to the alcohol product.

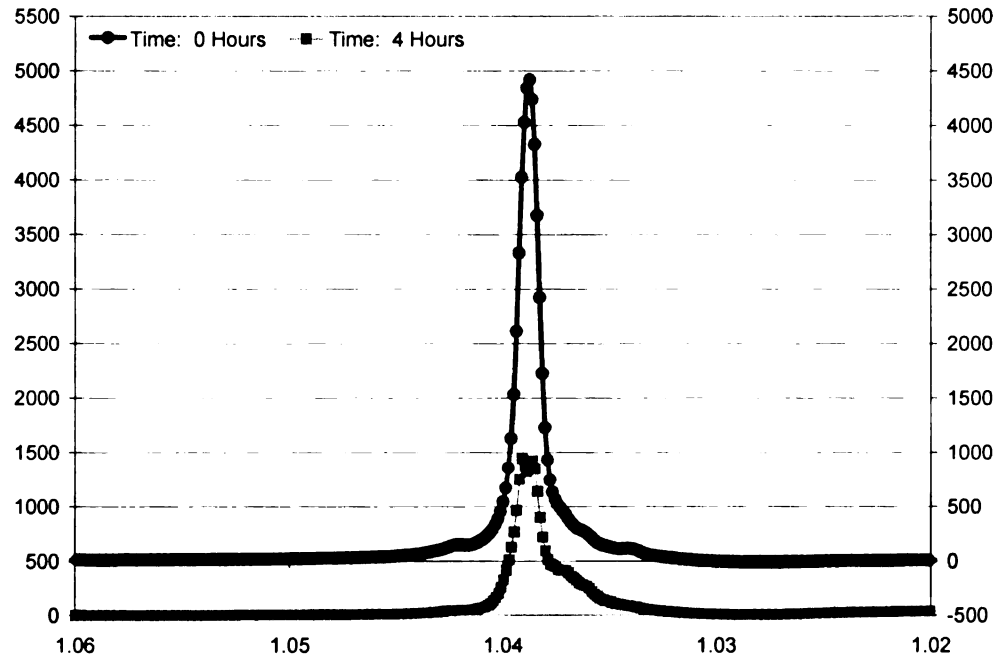

Figure 117. ^{1}H NMR of H/D exchange at the methyl positions of 0.25 M *tert*-butanol (D_2O, 100 °C, 1000 psi H_2, 1 g dry 5% Ru/C)

4.8 Competition Experiments

4.8.1 Hydrogenation Studies

Betaine hydrochloride did not undergo either hydrogenation or H/D exchange and it was not clear if the substrate was interacting with the surface and whether the chloride ion was poisoning or deactivating the surface. To evaluate the hypothesis that betaine hydrochloride was not interacting with the surface (possibly due to sterics) a competition experiment with glycine was conducted. Presumably, if betaine hydrochloride is not competing for the surface then the hydrogenation of glycine should be unaffected. However, if the chloride ion is reducing the efficiency of the catalyst, then the glycine hydrogenation rate would be affected.

Two competition experiments with betaine and glycine were performed. The first was hydrogenation of 0.25 M betaine hydrochloride, $(CH_3)_3N^+CH_2COOH{\bullet}Cl^-$ and 0.25 M glycine in the presence of 0.5 M H_3PO_4 at 130 °C with 1 g dry 5% Ru/C catalyst. The ratio of both the substrates and the additional acid to the catalyst was roughly double with respect to the baseline reaction of glycine alone. The results of the reaction compared with the baseline reaction are presented in Figure 118.

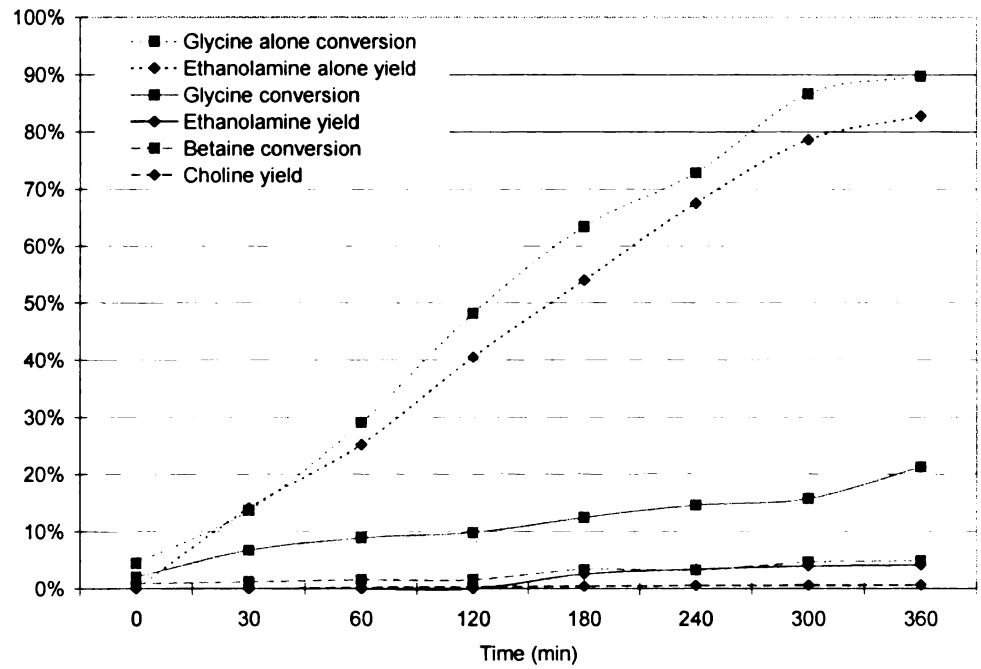

Figure 118. Hydrogenation of 0.25 M betaine hydrochloride and 0.25 M glycine (0.5 M H_3PO_4, H_2O, 130 °C, 1000 psi H_2, 1 g dry 5% Ru/C)

The conversion of glycine is significantly suppressed by the presence of betaine hydrochloride, however, the amount of substrate and additional acid present is double with respect to the amount of catalyst typically used. So, the increased substrate-to-catalyst ratio may have contributed partly to the reduced rate. In addition, chloride was

present as a complex with betaine. To examine the effect of the counter-ion chloride, an experiment without it was conducted.

The second experiment with glycine and betaine (chloride-free) was performed using 0.125 M of each and 0.3 M H_3PO_4. The results of 0.25 M glycine alone versus 0.125 M glycine and 0.125 M betaine are presented in Figure 119 (130 °C, 1000 psi H_2, 1 g dry 5% Ru/C). After six hours of reaction time, the conversion of glycine alone is 90% compared with 71% when in the presence of an equimolar amount of betaine. The yield of ethanolamine is 83% compared with 59% when in the presence of an equimolar amount of betaine. Thus, it appears that the betaine (chloride-free) is competing for surface reaction sites. This is consistent with the early findings that betaine will undergo hydrogenation at 100, 130, and 150 °C. So, it was expected that betaine would be reacting on the catalyst surface, thus a potential competitor to glycine.

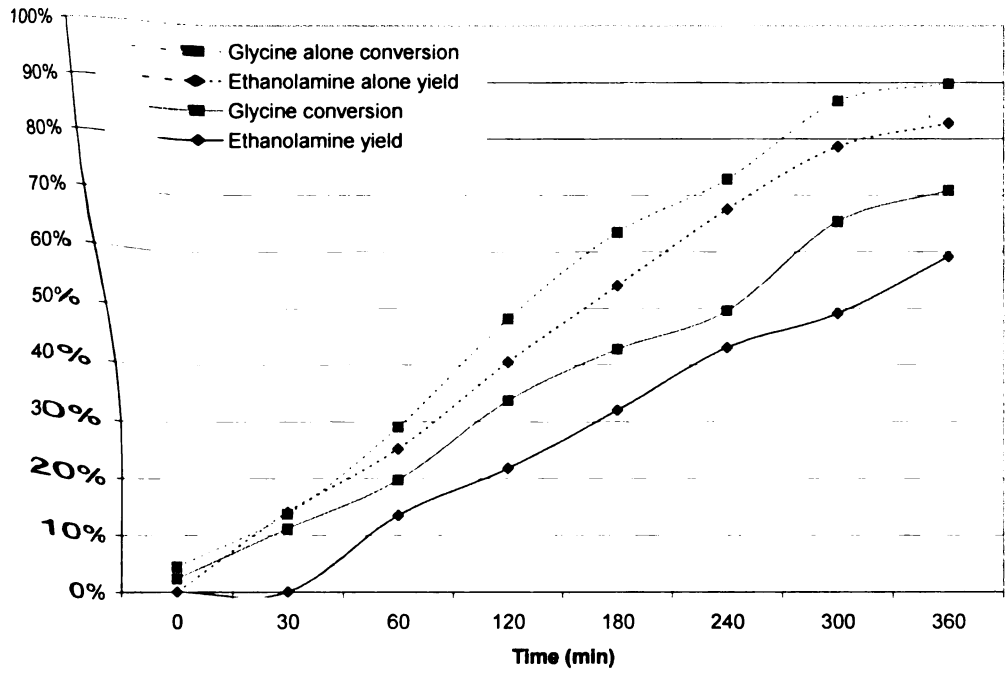

Figure 119. Hydrogenation of 0.25 M glycine alone and 0.125 M glycine and 0.125 M betaine (0.3 M H_3PO_4, H_2O, 130 °C, 1000 psi H_2, 1 g dry 5% Ru/C)

The results of betaine alone and betaine in the presence of an equimolar amount of glycine are presented below (Figure 120). Betaine is much less reactive than glycine so presence of glycine appears to have less of an effect on the betaine. The experiment with betaine hydrochloride resulted in a negligible amount of betaine hydrochloride conversion and the glycine conversion was reduced from 90% to 21%. Presumably this is mostly due to the presence of chloride and also partly to the substrate- and additional acid-to-catalyst ratio.

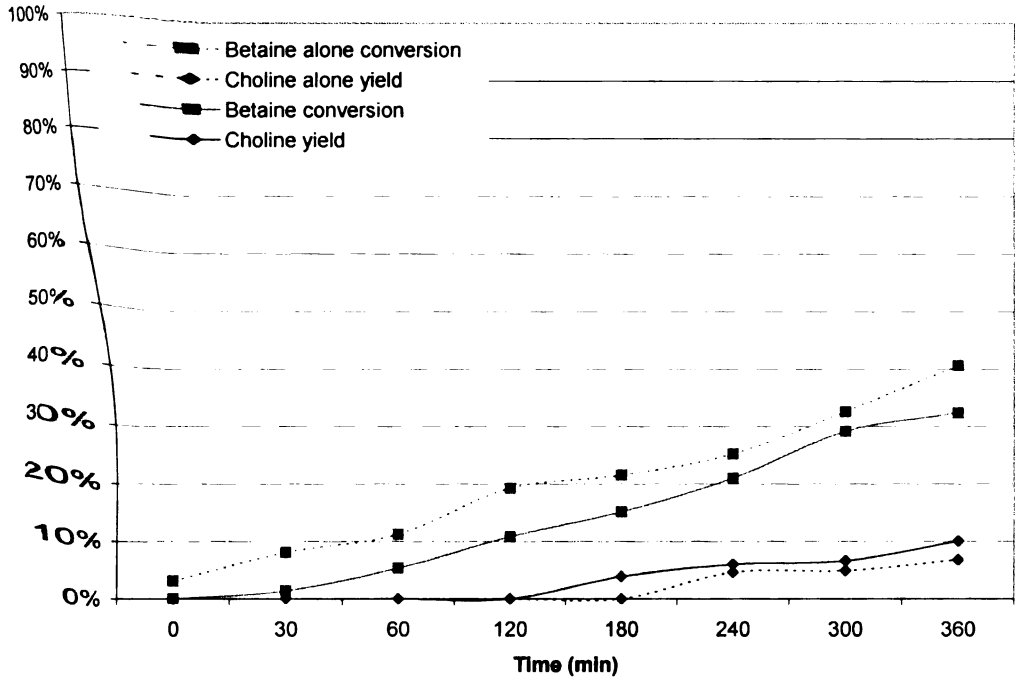

Figure 120. Hydrogenation of 0.25 M betaine alone and 0.125 M glycine and 0.125 M betaine (0.3 M H_3PO_4, H_2O, 130 °C, 1000 psi H_2, 1 g dry 5% Ru/C)

4.8.2 H/D Exchange Studies

A competition experiment was run with 0.25 M glycine and 0.25 M sarcosine at 100 °C with 1000 psi H_2 and D_2O. These results were compared to the results from the H/D exchange studies using the individual substrates. The experimental and fitted concentrations of CH_2, CHD, and CD_2 over time as determined by the equations in Chapter 3 are presented in Figures 121 (with respect to glycine alone) and 122 (with respect to sarcosine alone). When looking at the rate of H/D exchange for glycine at the methylene position, the rate is slightly suppressed in the competition experiment compared with the experiment of glycine alone.

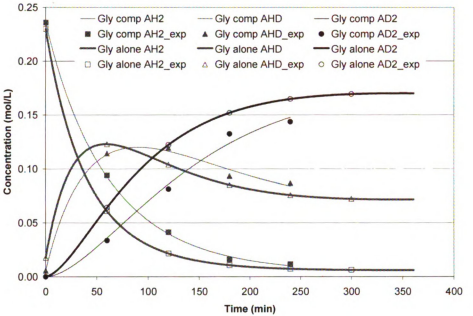

Figure 121. Fit of the kinetic rate data for 0.25 M glycine alone and 0.25 M glycine and 0.25 M sarcosine (D_2O, 100 °C, 1000 psi H_2, 1 g dry 5% Ru/C)

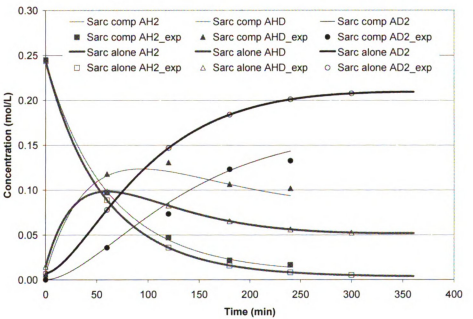

Figure 122. Fit of the kinetic rate data for 0.25 M sarcosine alone and 0.25 M glycine and 0.25 M sarcosine (D_2O, 100 °C, 1000 psi H_2, 1 g dry 5% Ru/C)

The conversion after 4 hours of reaction time is 97% in the experiment of glycine alone and 95% in the competition experiment. The yields of CHD and CD_2 after 4 hours of reaction time are 30% and 68% in the experiment of glycine alone and 35% and 59% in the competition experiment. However, the rate of H/D exchange for sarcosine at the methylene position appears to be much slower than in the experiment of sarcosine alone. The conversion after 4 hours of reaction time is 98% in the experiment of sarcosine alone and 94% in the competition experiment. The yields of CHD and CD_2 after 4 hours of reaction time are 21% and 75% in the experiment of sarcosine alone and 37% and 48% in the competition experiment.

The rate constants for glycine alone, sarcosine alone, and in the competition experiment are presented in Figure 123. The kinetics were determined using the models described in Chapter 3. The rate constants for H/D exchange on the methylene carbon of glycine in the competition experiment (and glycine alone) are: $k_{1A} = 1.6x10^{-4}$ L/mol/min; ($2.3x10^{-4}$), $k_{-1A} = 4.8x10^{-5}$ L/mol/min; ($1.2x10^{-4}$), $k_{2A} = 8.3x10^{-5}$ L/mol/min; ($1.2x10^{-4}$), $k_{-2A} = 1.6x10^{-4}$ L/mol/min; ($3.2x10^{-4}$). The rate constants are about 30% larger in the case of glycine alone for the exchange of both the first and second hydrogen.

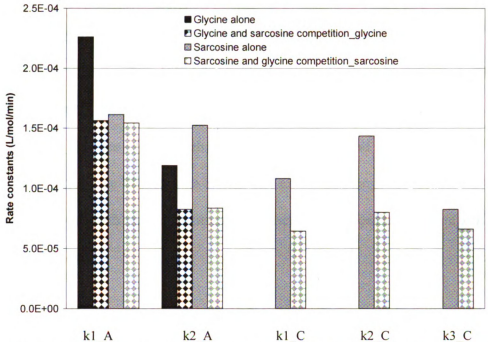

Figure 123. Rate constants for H/D exchange of 0.25 M glycine alone, 0.25 M sarcosine alone, 0.25 M glycine in the competition experiment, and 0.25 M sarcosine in the competition experiment (D_2O, 100 °C, 1000 psi H_2, 1 g dry 5% Ru/C)

The rates for H/D exchange on the methylene carbon of sarcosine in the competition experiment (and sarcosine alone) are: $k_{1A} = 1.5x10^{-4}$ L/mol/min; ($1.6x10^{-4}$), $k_{-1A} = 7.8x10^{-5}$ L/mol/min; ($1.4x10^{-5}$), $k_{2A} = 8.4x10^{-5}$ L/mol/min; ($1.5x10^{-4}$), $k_{-2A} = 2.3x10^{-4}$ L/mol/min; ($2.5x10^{-4}$). The rate of exchange for the first hydrogen for sarcosine alone or in the presence of glycine is the same. Although the rate of the second hydrogen being replaced with deuterium is roughly almost twice as fast in the case of sarcosine alone as compared to sarcosine plus glycine.

Again, using kinetic rate model A the rates for H/D exchange on the N-methyl carbon of sarcosine in the competition experiment (and sarcosine alone) are: $k_{1C} = 6.5x10^{-5}$

L/mol/min; ($1.1x10^{-4}$), $k_{-1C} = 4.9x10^{-6}$ L/mol/min; (0), $k_{2C} = 8.0x10^{-5}$ L/mol/min; ($1.4x10^{-4}$), $k_{-2C} = 3.2x10^{-4}$ L/mol/min; ($9.7x10^{-7}$), $k_{3C} = 6.6x10^{-5}$ L/mol/min; ($8.3x10^{-5}$), $k_{-3C} = 1.1x10^{-3}$ L/mol/min; ($2.0x10^{-4}$). These results again illustrate a slower rate of deuterium exchange on the methyl hydrogens of sarcosine in the presence of an equimolar amount of glycine. The rate of H/D exchange for both the first and second hydrogen are nearly 2x faster in the case of sarcosine alone. The rate of exchange for the third hydrogen is comparable for both the competition experiment and sarcosine alone but still quicker for sarcosine alone.

Chapter 5. SUMMARY

From the studies discussed it was confirmed that for hydrogenation of organic acids, the presence of hydrogen and catalyst (5% Ru/C) is required. Addition of equimolar H_3PO_4 resulted in a negligible effect on the hydrogenation reaction of glycolic acid, suggesting that phosphates, at least in protonated form, do not bind strongly to the catalyst. It was assumed that the additional acid would not affect the hydrogenation of the other substrates evaluated. However, from the competition experiments discussed in this paper as well as from the work by Chen, Jere, Peereboom, and Pimparkar et al. we know that the organic acid substrates have different binding affinities for the catalytic Ru particles and for the carbon support. Earlier amino acid reduction models included terms for H_3PO_4 competing with the same surface sites as the organic substrate. However, from the carbon adsorption studies it was found that H_3PO_4 has less of an adsorption affinity for the catalyst than the set of organic acids and alcohols examined, indicating that it is not in direct competition with the substrate for the actual hydrogenation sites on the catalyst.

For the H/D exchange control studies it was observed that non-catalytic H/D exchange does occur in the methylene positions of glycine, sarcosine and betaine. For sarcosine, about 30% of the methylene was monodeuterated after six hours at 130 °C. This result can be compared to a similar experiment run *with* catalyst (5% Ru/C) at the slightly lower temperature of 100 °C (both in 1000 psi H_2), where the methylene is ca. 30% monodeuterated after just one hour. Comparing rate constants, k_{1A} and k_{2A} for the two experiments, the control experiment had a $k_{1A} = 9.8 \times 10^{-6}$ and $k_{2A} = 0$ L/mol/min (i.e. CH_2

and CHD peaks accounted for all starting substrate), whereas the catalyzed but 30 °C cooler reaction was ca. 15 times faster, $k_{1A} = 1.6x10^{-4}$ and $k_{2A} = 1.5x10^{-4}$ L/mol/min. For betaine the measured concentrations of CH_2 and CHD are nearly identical in the experiment with or without catalyst (over 6 hours), showing little or no evidence of catalyzed exchange. H/D exchange in the absence of catalyst was not observed with glycine or choline bicarbonate (130 °C; 1000 psi H_2; D_2O).

Results from adsorption studies using 5% Ru/C illustrated that adsorption onto the catalyst is occurring and when the amount of catalyst is doubled, the amount of substrate lost to adsorption is also doubled. However, doubling the catalyst amount doubles the conversion rate for organic acid hydrogenations. Taken together, these facts indicate that the reaction is limited by the intrinsic kinetics and not by interphase mass transport. Peereboom et al. also confirmed and explored the adsorption of substrates on the catalyst surface and in the micropores. Results indicated that the less hydrophilic compounds have more of an affinity for the pores rather than the bulk solution and also the concentration of a substrate in the bulk solution could be very different from its concentration in the pores.

Comparing six substrates and their relative adsorption onto the carbon support, it was found that lactic acid (7% adsorbed) was absorbed more than any other substrate. The other substrates examined were butanol (5.7% adsorbed), glycolic acid (4.8% adsorbed), propylene glycol (3.4% adsorbed), phosphoric acid (1.0% adsorbed), and ethylene glycol (0.8% adsorbed). Experiments evaluating the effect of additional acid, H_3PO_4 have

shown no effect on the hydrogenation rate and this is partly due to the fact that it may have less of an adsorption affinity for the catalyst and is more hydrophilic than for instance, butanol. It may thus prefer the bulk solution over the micropores. The amount adsorbed on the carbon support was similar to the amount of substrate typically "lost" after being exposed to the catalyst (5% Ru/C) at time zero of the experiment.

The hydrogenation of betaine hydrochloride $(CH_3)_3N^+CH_2COOH{\bullet}Cl^-$ was compared to the hydrogenation of betaine $(CH_3)_3N^+CH_2COO^-$ (both experiments conducted with equimolar H_3PO_4). Results indicated that none of the desired alcohol product was formed using betaine hydrochloride. An experiment with 0.25 M glycine (130 °C, 0.3 M H_3PO_4, 1000 psi H_2) in both the presence and absence of 0.25 M HCl showed a conversion drop (83% to 34%) of more than half for the experiment with HCl. The effect of an equivalent amount of sodium chloride was also evaluated. The hydrogenation rate dropped from 83% to 72% indicating that again the chloride ion may be partially deactivating the catalyst, affecting the substrate, or competing with the surface. However, in this experiment half the amount of glycine, NaCl, and additional acid, H_3PO_4 was added compared with the experiment with HCl (for the same amount of catalyst). So, the reduction in the amount of total acids may have reduced the effect seen by the NaCl.

Additional insights arise from deuterium exchange studies comparing betaine hydrochloride $(CH_3)_3N^+CH_2COOH{\bullet}Cl^-$ and betaine $(CH_3)_3N^+CH_2COO^-$ substrates. In the former case, no deuterium was incorporated at either the methylene or methyl carbons. From the control experiments in which no catalyst was added, it was found that the same amount of deuterium incorporation was occurring in betaine in both in the presence and

absence of catalyst. This suggests that the lack of H/D exchange seen in the case of betaine hydrochloride is not due to a partially deactivated catalyst or competition by HCl for catalyst surface sites. The chloride ion in the solution appears to somehow inhibit methylene C-H activation in the bulk solution.

It was already noted that the presence of an equimolar amount of additional acid, H_3PO_4, does not reduce the hydrogenation rate of glycolic acid. The need for the additional acid is to ensure that the carboxylic acid functionality in glycine and the N-methylated glycines is protonated. These amino acids are zwitterionic in nature and thus the carboxylic acid functionality is dissociated unless the additional acid is present. For glycine, a yield of 15% is obtained in the absence of catalyst, compared with 83% conversion with additional acid. To determine if the additional acid slows the H/D exchange reaction, betaine was initially chosen due to its slower competing hydrogenation reaction. Results showed that both with and without the additional acid present the amount of H/D exchange on the methylene carbons were essentially the same. However, betaine undergoes non-catalytic H/D exchange. The k_{1A} values were 0.41×10^{-4} and 0.43×10^{-4} for the case of betaine (130 °C) and betaine with 0.3 M H_3PO_4 (100 °C), respectively. Presumably the rates should be different for the different temperatures, but at 100 °C with acid, some of the betaine is hydrogenated to form choline. After six hours a 38% yield of choline was detected by HPLC; thus, included in the H/D rates (methylene carbon) are both the exchange and also the conversion to choline. The yield of choline in this experiment is quite a bit higher than in the same conditions but at 130 °C. The

reason for this is that at higher temperatures more betaine degradation (presumably to trimethylamine and gases) is occurring.

Glycine and sarcosine were also run at 50 and 70 °C in the absence and presence of 0.3 M H_3PO_4 to evaluate the extent of H/D exchange. The rate of exchange was significantly decreased in the presence of H_3PO_4; presumably protonation of the amine makes the neighboring C-H bond less electron-rich and therefore less activated for C-H attack by Ru.

Various solvents were examined to explore their effects and the role of the water solvent in the hydrogenation reactions. The hydrogenation rate of glycolic acid was significantly depressed when using either dry THF or *tert*-butanol. Studies with THF indicate that it readily undergoes H/D exchange at both C1 (83% H replacement) and C2 (42% H replacement) positions over six hours. The fact that the H/D exchange reaction of THF slows glycolic acid hydrogenation supports the claim that the hydrogenation sites and H/D exchange sites are not distinct. Next, *tert*-butanol was tried based on the hypothesis that it would not undergo exchange or interact with the surface. Indeed, no exchange was observed in this solvent with or without added substrate, but neither was glycolic acid hydrogenated. Some loss of tert-butanol was seen, a finding likely due to dehydration of the solvent to isobutene and subsequent hydrogenation to isobutane.

The solvent ethanol was used for the experiments with glycolic acid both with and without additional acid, H_3PO_4. As expected, the acid promoted a significant amount of

esterification, but even in the case with no additional acid, the ester ethyl glycolate was still formed. In both experiments, only 8% of ethylene glycol was formed compared with 47% in the solvent water under otherwise identical conditions. The literature suggests that esters undergo hydrogenation with certain catalysts (Raney Ni, copper/chromium oxide, rhenium black) but that there is competition for the surface between the acids and the esters, reducing the amount of ester hydrogenation. But, in this case, slow or no ester hydrogenation occurs over 5% Ru/C . To examine this further, ethyl lactate was subjected to the usual aqueous hydrogenation conditions. It quickly hydrolyzed to lactic acid (100% at one hour). The product propylene glycol, was not observed until after lactic acid formed, again supporting the claim that the ester reacts slowly or not at all. This experiment's propylene glycol yield was nearly the same as with lactic acid itself, suggesting that in this case the lactic acid hydrogenation suffers little hindrance from the ester or dilute ethanol.

The results from the organic acid hydrogenation studies indicate that simple carboxylic acids such as propanoic acid and acetic acid are substantially more difficult to reduce than lactic acid and alanine. The various substrates were chosen in order to evaluate the effect of hydrogen bonding, electron withdrawing ability, and heteroatom coordination to the surface. Hydrogen bonding was determined to be a key player in accelerating the hydrogenation reaction. Reactions with the α-substituent $-N^+H_3$, -OH, $-OCH_3$, $-N^+H_2(CH_3)$, and $-N^+H(CH_3)_2$ were far more reactive than either the unsubstituted acetic acid or an α-substituent of $-CH_3$ or $-N^+(CH_3)_3$. Sterics were considered in the N-methylated glycine series ($-N^+H_3$, $-N^+H_2(CH_3)$, $-N^+H(CH_3)_2$, and $-N^+(CH_3)_3$) in that the

hydrogenation rate falls off by about 1/3 as each N-methyl group is added. However, there is a trend for hydrogenation in that the reactivity falls off by nearly half as a methyl is added. Also, when comparing the groups, -OH to a more bulky $-OCH_3$ or $-CH_3$, the substrates with the α-OH group (glycolic acid and lactic acid) are far more reactive. This may be partly due to a less bulky group but also due to electronics (-OH is more electron-withdrawing than $-OCH_3$) as compared to $-OCH_3$ or $-CH_3$. Considering the role of electronics, it was found that the substrate with α-OCH_3 is much more reactive than α-CH_3 (yield of desired product is 35% compared with 13%).

In an effort to build upon the above research and probe the reactivity differences in hydrogenation of the methylated glycine series, H/D exchange studies were performed. Reactions run in D_2O with either H_2 or D_2 and catalyst were effective at exchanging deuterium into the CH_2 and CH_3 sites of amino acids. The Ru catalyst also exchanges H (from H_2) for D (from D_2O) to form HOD and HD, independent of substrate. Analysis by internal standard-calibrated ^1H NMR allowed complete isotopomer-specific inventory of the H concentration in substrates and water. Simple sequential replacements of H by D were observed in the amino acids. Two kinetic models were developed to determine the rate constants for H/D exchange at both the methylene and methyl positions. Both included possible time delays due gas/liquid isotopic equilibration (k_H) and/or a catalyst induction (k_{turn_on}) period; ultimately the latter was discarded as redundant. The first model treated each isotope replacement step as a process unrelated to the others. Thus, between forward and reverse replacements in CH_2 and CH_3 sites and k_H, eleven rate constants were freely varied in the fitting. The second model used a single rate constant

for each site, further modified by primary and secondary isotope effect values, resulting in six values + k_H for this fitting. The latter, more economical and interpretive model gave fits nearly as good as those from the eleven-variable one.

The H/D exchange took place at lower temperatures (50-100 °C) than hydrogenation (100-150 °C) and therefore it was possible to study H/D exchange while minimizing the amount of competing hydrogenation reaction. Mapping out the optimal temperatures for both reactions allowed H/D exchange to be studied. Glycine, sarcosine, and N,N-dimethylglycine were run at 100 °C with 1000 psi H_2 or D_2 and the datasets from the pairs of experiments were linked in order to define a common set of rate constants. Experiments were also run at lower temperatures (70 and 50 °C). The rate constants for H/D exchange at the methylene and methyl carbons are summarized in Table 10.

Table 10. Summary of rate constants for glycine, sarcosine, and N,N-dimethylglycine

Rate constant (L/mol/min)	Glycine 100 °C D_2	Sarcosine 100 °C D_2	N,N-dmg 100 °C D_2	Glycine 70 °C D_2	Sarcosine 70 °C D_2	N,N-dmg 70 °C D_2	Glycine 50 °C D_2	Sarcosine 50 °C D_2
ki_CH_2	0.99	1.48	0.74	0.74	0.99	0.06	0.09	0.25
ki_CH_3		0.58	0.66		0.24	0.09		0.05

All rate constants are multiplied by 10^4

Somewhat surprisingly, H/D exchange rates decreased in the following order: sarcosine ($CH_3NH_2^+CH_2CO_2^-$) > glycine (CH_2 site) > N,N-dimethylglycine. This trend in reactivity does not match that observed in the hydrogenation of these same substrates (glycine > sarcosine > N,N-dimethyglycine. This may be due to the fact that for H/D exchange an

electron-rich C-H bond promotes the reaction, whereas in the hydrogenation reaction, it is presumed that steric effects play more of a role.

The H/D exchanges on the N-methyl(s) of both sarcosine and N,N-dimethylglycine were slower than on the methylene carbon (for all conditions) and in general did not fully reach equilibrium after six hours (Table 10) at 100 °C. In addition it was found that the H/D exchange occurs step-wise at both the methylene and methyl carbons (CH_2 to CHD to CD_2) and (CH_3 to CH_2D to CHD_2 to CD_3). Betaine was found to undergo non-catalytic H/D exchange at the methylene carbon. Glycine and sarcosine exhibited a small amount of H/D exchange in the absence of catalyst but only at higher temperatures (130 °C). With its fixed N^+ next door, the acidity of betaine's α-CH_2 is enhanced, increasing the rate of deprotonation, enol formation, and the resulting H/D exchange.

In summary, a detailed set of hydrogenation and H/D exchange experiments using a 5% ruthenium on carbon catalyst were conducted for several two- and three-carbon organic acid substrates and a kinetic model was developed for the H/D exchange. Simple alkanoic acids (acetic, propanoic, isobutyric) and betaine, quaternized glycine, are not very reactive. For the other methylated glycines, the rate of hydrogenation falls off by a factor of ca. three with each additional methyl, and reduction requires acid, as found earlier by Jere. Use of water as a reaction medium appears optimal. The H/D exchange studies indicated a different trend in reactivity for the methylated glycines (sarcosine > glycine > N,N-dimethylglycine) as compared to hydrogenation. The rate of H/D exchange appears to be promoted by an electron-rich C-H bond. The addition of H_3PO_4

significantly slows the H/D exchange while enabling the reduction, suggesting that the free amine is needed for the hydrogen replacement reaction.

Future projects could include additional probes of the roles of steric effects, pH more precisely defined, additional catalyst site inhibitors, and stereoelectronic aspects of control. For instance, to explore whether the electrons on the amine are coordinating with the catalyst surface, an experiment with a t-butyl-locked piperidine (chair conformer) with various N-alkyl groups could be run to determine the preference for H_{ax} versus H_{eq}. The results would help to map out the elements controlling C-H activation alpha to amine sites.

Chapter 6. REFERENCES

[1] Braun, B.; Charney, R.; Clarens, A; Farrugia, J.; Kitchens, C.; Lisowski, C.; Naistat, D.; O'Neil, A. J. Chem. Ed. *J. Chem. Ed.* **2006**, *83*, 1126

[2] British Petroleum, BP Statistical Review of World Energy, 2007

[3] Yang, M.; Somorjai, G.A. *J. Phys. Chem. B.* **2004**, *108*, 4405

[4] Jere, F. Ph.D. Dissertation, Michigan State University, 2003

[5] Antons, S. In *US Patent 5,731,479*; Bayer Aktiengesellschaft: USA, **1998**

[6] Antons, S. In *US Patent*; Bayer Aktiengesellschaft: USA, **2002**

[7] Carnahan, J.E.; Ford, T.A.; Gresham, W.F.; Grigsby, W.E.; Hager, G.F. *J. Am. Chem. Soc.* **1955**, *77*, 3766

[8] Behr, A.; Brehme, V. *Adv. Synth. Catal.* **2002**, *344*, 525

[9] Mao, B.W.; Cai, Z.Z; Huang, M.Y.; Jiang, Y.Y. *Polym. Adv. Technol.* **2003**, *14*, 278

[10] He, D.H.; Wakasa, N.; Fuchikami, T. *Tet. Lett.* **1995**, *36*, 1059

[11] Bowden, H.; Adkins, H. *J. Am. Chem. Soc.* **1934**, *56*, 689

[12] Adkins, H; Folkers, K. *J. Am. Chem. Soc.* **1932**, *54*, 1145-1154

[13] Adkins, H; Cramer, H.I. *J. Am. Chem. Soc.* **1930**, *52*, 4349

[14] Adkins, H.; Pavlic, A.A. *J. Am. Chem. Soc.* **1947**, *69*, 3039

[15] Adkins, H.; Billica, H.R. *J. Am. Chem. Soc.* **1948**, *70*, 3121

[16] Vaidya, P.D.; Mahajani, V.V. *Chem. Eng. Sci.* **2005**, *60*, 1881

[17] Sajiki, H.; Kurita, T.; Esaki, H.; Aoki, F.; Maegawa, T.; Hirota, K. *Org. Lett.* **2004**, *6*, 3521

[18] (a) Faller, J.W.; Smart, C.J. *Organometallics* **1989**, *8*, 602. (b) Heys, R. *J. Chem. Soc., Chem. Commun.* **1992**, 680. (c) Heys, J.R.; Shu, A.Y.L.; Senderoff, S.G.; Phillips, N.M. *J. Labelled Compd. Radiopharm.* **1993**, *33*, 431. (d) Lukey, C.A.; Long, M.A.; Garnett, J.L. *Aust. J.Chem.* **1995**, *48*, 79. (e) Hesk, D.; Das, P.R.; Evans, B. *J. Labelled Compd. Radiopharm.* **1995**, *36*, 497. (f) Chen, W.; Garnes, K.T.; Levinson, H.H.; Saunders, D.; Senderoff, S.G.; Shu, A.Y.L.; Villani, A.J.; Heys, JR. *J. Labelled Compd*

Radiopharm. **1997**, *39*, 291. (g) Klei, S.R.; Golden, J.T.; Tilley, T.D.; Bergman, R.G. *J.Am. Chem. Soc.* **2002**, *124*, 2092. (h) Skaddan, M.B.; Yung, C.M.; Bergman, R.G. *Org. Lett.* **2004**, *6*, 11

[19] (a) Hesk, D.; Jones, J.R.; Lockley, W.J.S. *J. Labelled Compd. Radiopharm.* **1990**, *28*, 1427. (b) Hesk, D.; Jones, J.R.; Lockley, W.J.S. *J. Pharm. Sci.* **1991**, *80*, 887. (c) Lenges, C.P.; White, P.S.; Brookhart, M. *J. Am. Chem. Soc.* **1999**, *121*, 4385

[20] (a) Weil, T.A.; Friedman, S.; Wender, I. *J. Org. Chem.* **1974**, *39*, 48. (b) Lenges, C.P.; Brookhart, M.; Grant, B.E. *J. Organomet. Chem.* **1997**, *528*, 199

[21] (a) Garnett, J.L.; Hodges, R.J. *J. Am. Chem.* **1967**, *89*, 4546. (b) Gol'dshleger, N.F.; Tyabin, M.B.; Shilov, A.E.; Shteinman, A. *A. Zh. Fiz. Khim.* **1969**, *43*, 1222. (c) Buncel, E.; Clement, O. *J. Chem. Soc., Perkin Trans. 2* **1995**, 1333

[22] (a) Ogasawara, M.; Saburi, M. *Organometallics* **1994**, *13*, 1911. (b) Collman, J.P.; Fish, H.T.; Wagenknecht, P.S.; Tyvoll, D.A.; Chng, L.-L.; Eberspacher, T.A.; Brauman, J.I.; Bacon, J.W.; Pignolet, L.H. *Inorg. Chem.* **1996**, *35*, 6746

[23] Perthuisot, C.; Fan, M.; Jones, W.D. *Organometallics* **1992**, *11*, 3622

[24] Sajiki, H.; Aoki, F.; Esaki, H.; Maegawa, T.; Hirota, K. *Org. Lett.*, **2004**, *6*, 1485

[25] Jere, F.T.; Miller, D.J.; Jackson, J.E. *Org. Lett.* **2003**, *5*, 527

[26] Halkides, C.J.; Frey, P.A.; Tobin, J.B. *J. Am. Chem. Soc.* **1993**, *115*, 3332

[27] Nibeilliu, M.E.; Malthouse, P.G. *Biochem. J.* **2004**, *381*, 847

[28] Rios, A.; Amyes, T.L.; Richard, J.P. *J. Am. Chem. Soc.* **2000**, *122*, 9373

[29] Rios, A.; Richard, J.P. *J. Am. Chem. Soc.* **1997**, *119*, 8375

[30] Cox, H.A.; Julian, R.R.; Lee, S.W.; Beauchamp, J.L. *J. Am. Chem. Soc.* **2004**, *126*, 6485

[31] Matsubara, S. Yokota, Y.; Oshima, K. *Chem. Lett.*, **2004**, *33*, 294

[32] Li, Z.; Li, C.J. *J. Am. Chem. Soc.* **2004**, *126*, 11810

[33] Li, Z.; Li, C.J. *Org. Lett.* **2004**, *6*, 4997

[34] Li, Z.; Li, C.J. *J. Am. Chem. Soc.* **2005**, *127*, 3672

[35] Alston II, W.C.; Haley, K.; Kanski, R.; Murray, C.J.; Pranata, J. *J. Am. Chem. Soc.* **1996**, *118*, 6562

[36] Broadbent, H.S., Campbell, G.C., Bartley, W.J., Johnson, J.H. *J Org. Chem.* **1959**, *24*, 1847-1854

[37] Antons, S.; Beitzke, B. *Chem. Abstr.* **1996**, *125*, 114175

[38] Studer, M.; Burkhardt, S.; Blaser, H.U. *Adv. Synth. Catal.* **2001**, *343*, 802

[39] Ruiz, A. Guerrero; Alarcón, M. Cerro; Valiente, A. Maroto; Ramos, I. Rodríguez *Carbon* **2005**, *43*, 2711

[40] Chemical Marketing Reporter, 1091-0110, 260 (11) (September 24, 2001) 30

[41] Chemical Marketing Reporter, 1092-0110, 265 (17) (April 26, 2004) 20 (4)

[42] Dasari, M.A.; Kiatsimkul, P.P.; Sutterlin, W.R.; Suppes, G.J. *Appl. Catal. A: Gen.* **2005**, *281*, 225

[43] Muller, P.; Rimmelin, P.; Hindermans, J.P.; Kieffer, R.; Kiennemann, A. Transformation of Sugar into Glycols on a 5% Ru/C Catalyst. *Stud. Surf. Sci. Catal.* **1991**, *59*, 237

[44] Lambert, J.B., Mazzola, E.P. Nuclear Magnetic Resonance Spectroscopy: An Introduction to Principles, Applications, and Experimental Methods

[45] Lambert, J.B., Greifenstein, L.G. *J. Am. Chem. Soc.* **1974**, *96*, 5120

[46] Gutowsky, H.S. *J. Chem. Phys.* **1959**, *31*, 1683f

[47] Pople, J.A. *Mol. Phys.* **1963**, *7*, 201

[48] Zhang, Z., Jackson, J.E., Miller, D.J. *Appl. Catal. A* **2001**, 89-98

[49] Zhang, Z., Jackson, J.E., Miller, D.J. *Ind. Eng. Chem. Res.* **2002**, *41*, 691-696

[50] Jere, F.T., Jackson, J.E., Miller, D.J *Ind. Eng. Chem. Res.* **2004**, *43*, 3297-3303

[51] Singh, U.K., Vannice, M.A. *Appl. Catal. A* **2001**, *213*, 1-24

[52] Pallassana, V.; Neurock, M. *J. Catal.* **2002**, *209*, 289-305

[53] Kovacs, D.G., Jackson, J.E., Miller, D.J. *Abstr Pap Am Chem. Soc.* **2001**, *221* U177-8

[54] Lahr, D.G., Shanks, B.H. *J. Catal.* **2005**, *232*, 386-394

[55] Lahr, D.G., Shanks, B.H. *Ind. Eng. Chem. Res.* **2003**, *42*, 5467-5472

[56] Kusunoki, Y., Miyazawa, T., Kunimori, K., Tomishige K. *Catal. Commun.* **2005**, *6*, 645-649

[57] Chaminand, J., Djakovitch, L., Gallezot, P., Marion, P., Pinel, C., Rosier, C. *Green Chem.* **2004**, *6*, 359-361

[58] Perosa, A., Tundo, P. *Ind. Eng. Chem. Res.* **2005**, *44*, 8535-8537

[59] Peereboom, L., Koenigsknecht, B., Hunter, M. Jackson, J.E., Miller, D.J. *Carbon* **2007**, *45*, 579-586

[60] Dalavoy, T.S., Jackson, J.E., Swain, G.M., Miller, D.J., Li, J., Lipkowski, J. J. Catal. 2007, 246, 15-28

[61] Chen, Y., Miller, D.J., Jackson, J.E. *Ind. Eng. Chem. Res.* **2007**, *46*, 3334-3340

[62] Zhang, Z., Jackson, J.E., Miller, D.J. *Bioresource Technology* **2008**, 5873-5880

[63] Pimparkar, K.P., Miller, D.J., Jackson, J.E. *Ind. Eng. Chem. Res.* **2008**, *47*, 7648-7653

[64] Knifton, J.F., Sanderson, J.R., and Stockton, M.E. *Catal. Lett.* **2001**, *73*, 55

[65] Abella, L.C., Gaspillo, P.D., Itoh, H., and Goto, S.J. *Chem. Eng. Jpn.* **1999**, *32*, 742

[66] W.B. Smith. *Tetrahedron* **2002**, *58*, 2091